Fakultät für Chemie

Two Sides of the Same Silicon Particle

Toward the Synthesis of Two-Sided "Janus" Silicon Nanocrystals and other Functionalization Methods

Marc Julian Kloberg

Vollständiger Abdruck der von der Fakultät für Chemie der Technischen Universität München zur Erlangung des akademischen Grades eines

Doktors der Naturwissenschaften

genehmigten Dissertation.

Vorsitzender	Prof. Dr. Ulrich K. Heiz
Prüfende der Dissertation	1. Prof. Dr. Dr. h. c. Bernhard Rieger
	2. Prof. Dr. Tom Nilges
	3. Prof. Dr. Jonathan Veinot

Die Dissertation wurde am 12.04.2021 bei der Technischen Universität München eingereicht und durch die Fakultät für Chemie am 01.06.2021 angenommen.

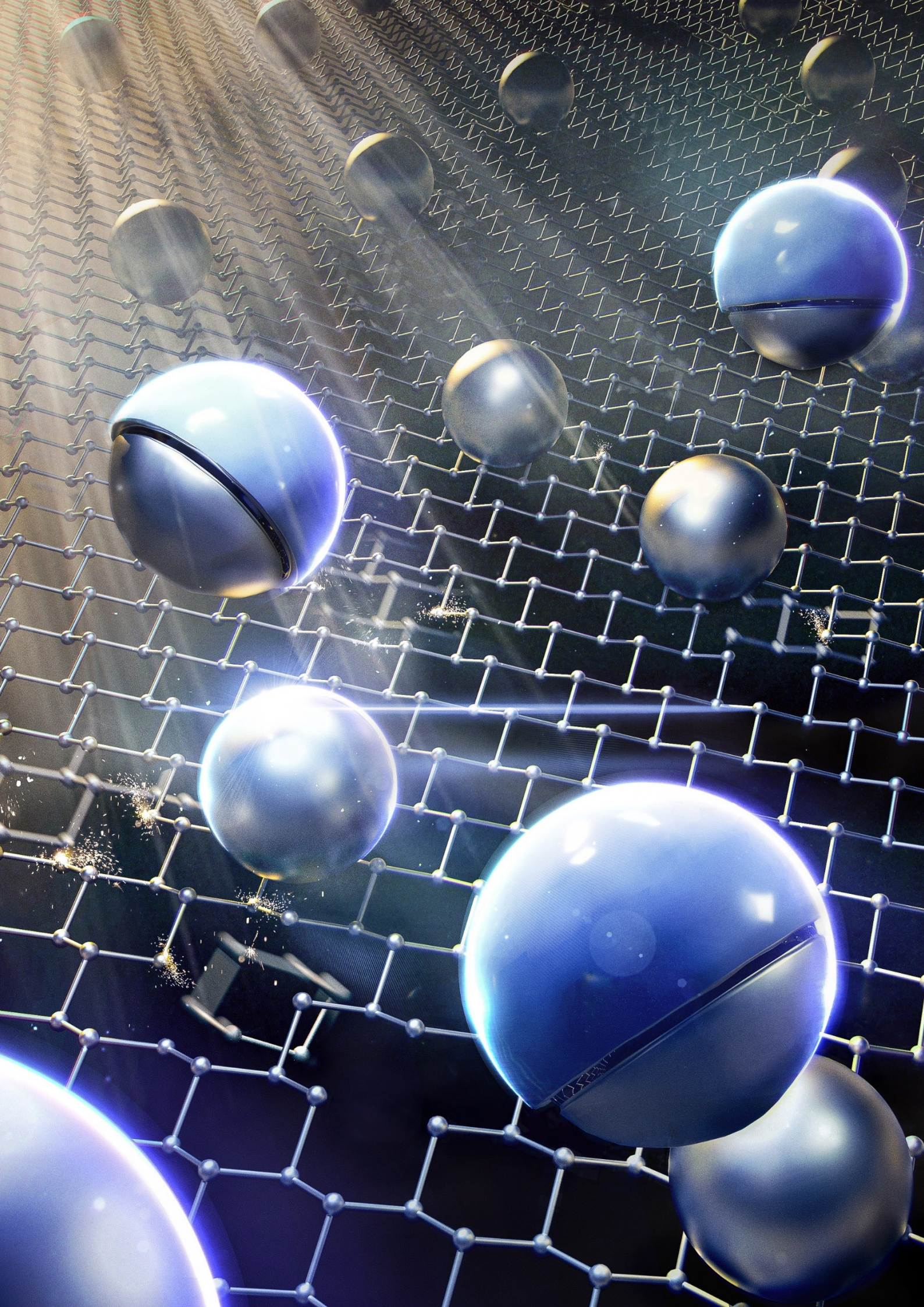

“To succeed, planning alone is insufficient. One must improvise as well.”

— Isaac Asimov, from *Foundation*

Acknowledgement

First and foremost I want to thank my supervisor *Prof. Dr. Bernhard Rieger* for giving me the opportunity to pursue a doctorate at his chair and giving me the freedom and trust to choose my own research projects. My sincere gratitude also goes to my co-supervisor *Prof. Dr. Jonathan G. C. Veinot* who has guided me throughout my thesis and wholeheartedly welcomed me into his group during my research stays at the University of Alberta; even making me an honorary member. Furthermore I give a sincere thanks to my mentor *Dr. Matthias Ludwig* who advised me throughout the progression of my thesis and helped me see the big picture. Many thanks to *Dr. Carsten Troll, Leah Veinot, Katia Rodewald, Annette Bauer* and *Dr. Sergei Vagin* for always being available and helping in all organizational matters.

Thank you to all members of the WACKER-Chair for creating a wonderful and friendly atmosphere to work in. I enjoyed coming into the lab every day and I offer my sincere apologies for the occasional smell.

I would like to give a big thanks to my collaboration partners, *Dr. Haoyang "Emmett" Yu, Felix Eckmann, Dr. Tassilo Restle, I Teng "Emily" Cheong, Dr. Alina Lyuleeva-Husemann* and *Josef Mock*. Thank you for all of your contributions. I am so lucky to work with people I can call friends. My students *Jinyu Liu*, *Monika Wenisch, Sebastian Auffarths*, *Lucas Stieglitz* and my Master student *Elisabeth Groß* all deserve a round of applause for having the patience to deal with me as their supervisor. I thank you for the time we've spent together. An honorable mention goes to the TGA-wizard (you know who you are).

I am extremely grateful to my former colleagues and friends *Dr. Arzu Angı* (am I still 23?) and *Dr. Tobias Helbich* (where's Tobi?), who guided me through my Master's thesis and pushed me to continue my research as a doctoral student and join the family of the *Alberta Technical University of Munich Graduate School for Hybrid Functional Materials (ATUMS)*. Speaking of which, my thanks goes to all members, past and present, for being so welcoming, offering valuable input and just being an awesome community to be part of. I am convinced I would not have continued with a doctorate had it not been for the ATUMS program. The biggest regret I have is that I was not able to spend more time at the University of Alberta (hindsight is 2020).

I thank my Canadian brethren for all of the good times while I was staying in Edmonton: *Matthew Roy* and *Benjamin Rehl* (for valuable tea-room discussions), *Ryan Kisslinger*, *Jedd, Troitsky* and *Stretch (*I still remember the Alum house Wifi-Password), *Alyxandra Thiessen, Maryam Aghajamali* and *Regina Sinelnikov* (I miss our lunches), *Emmett* and *Christian* (who brought my photography skills to a new level), *David Purschke* (sandwiches) and of course *Ian Watson* and *Jocelyn Sinclair* (I don't think I know anyone more welcoming).

Thank you to all of my friends and fellow students who helped me pull through my Bachelor and Master studies. *Ryan*, *Insu*, *Jacob, David, Michi*, *Bruno and Jarek,* I'm looking at you. Our "homework sharing" policy was indispensable.

To my close friends *Matti, Carlos, Fabi* and *Tom*: You have shaped who I am today, so if I do anything foolish, it's your fault. In all seriousness, thank you for all the laughs, the torment and everything in between; you're the best.

Of course, this would not be complete without thanking my family. So, *Kim*, thanks for keeping it real. *Mom* and *Papa*, thank you for all the support, unconditional love and always believing in me, no matter what. I love you! This thesis would not have been possible without you.

Abstract

This thesis encompasses multiple research projects focusing on the surface-modification — *functionalization* — of zero- and two-dimensional silicon nanomaterials: *silicon nanocrystals* and *silicon nanosheets*. These silicon nanomaterials exhibit unique properties due their nanostructured composition. Silicon nanocrystals are incredibly small, while silicon nanosheets are atomically thin. Owing to their small size, these unique materials exhibit optoelectronic properties that are not found in bulk silicon. Due to the relatively large surface of the nanomaterials, different chemical groups on the surface can have profound impacts on the properties and thus applications of these materials. As such, the modification of the surface comprises a fundamental aspect of silicon nanomaterial research.

The herein presented work describes newly developed concepts and methods to introduce unique surface groups to the surface of these nanomaterials. Starting from the development of a simple hydrosilylation initiator (*trityl salts*), the research progresses toward extending the silicon-silicon framework of the silicon nanomaterials by introducing reactive silicon substrates — *silanes* and *siliranes.* Unfortunately, these methods were found to be ineffective and the incorporation of these molecules proceeds slowly or not at all. Interesting observations were made when silicon nanocrystals were functionalized with *dichalcogenides*. Depending on the employed reagent, a shift in photoluminescence or an increased brightness is observed. These initial observations were developed into a full-fledged functionalization method that produces silicon nanocrystals with two-fold quantum yields when compared to conventionally functionalized ones.

Finally, in a serendipitous discovery, *surface-anisotropic "Janus" silicon nanocrystals* were synthesized in a synergistic reaction network between silicon nanocrystals and silicon nanosheets. The synthesis pathway was extensively developed and the challenges of verifying the anisotropic character of the nanoparticles addressed through a variety of different characterization strategies. The titular research project establishes a whole new class of materials — *Janus Silicon Nanocrystals* — which broadens the possibilities for future research, greatly extending the library of functional silicon nanoparticles and possible applications.

Table of Contents

1 List of Acronyms

4-DDB	4-decyldiazobenzene tetrafluoroborate
AFM	atomic force microscopy
AIBN	azobisisobutyronitrile
ATR	attenuated total reflection
BCF	tris(pentafluorophenyl)borane
BP	benzoyl peroxide
ClDMVS	chloro(dimethyl)vinyl silane
DCB	1,4-dichlorobenzene
DLS	dynamic light scattering
EDX	energy dispersive X-ray
EELS	electron energy loss spectroscopy
EtOH	ethanol
FEP	fluoroethylene propylene
FPT	freeze-pump-thaw
FTIR	Fourier-transform infrared
HR-TEM	high resolution transmission electron microscopy
IR	infrared
m/z	Mass to charge ratio
MeCN	acetonitrile
MeOH	methanol

*n*Bu	*n*-butyl
NMP	N-methyl-2-pyrrolidone
NMR	nuclear magnetic resonance
-Ph	phenyl
PL	photoluminescence
*p*Si	porous silicon
QY	quantum yield
RA	roughness average
RMS	roughness mean square
SAM	self-assembled monolayer
SEM	secondary electron microscopy
SiNC	silicon Nanocrystals
SiNS	silicon nanosheets
TEM	transmission electron microscopy
TGA	thermogravimetric analysis
TGA-MS	thermogravimetric analysis mass spectrometry
THF	tetrahydrofuran
TLC	thin layer chromatography
TMVS	trimethylvinylsilane
UPS	ultraviolet photoelectron spectroscopy
UV	ultraviolet

1 Introduction

Silicon. Without a doubt, one of the most important materials of the current era. While the first transistor was based on germanium, silicon is the material that enabled the widespread adoption of computers and propelled humanity into the information age.

The silicon-based microelectronics industry has advanced to the point that we are now reaching the limit of what is possible with our current technology. The transistor is so small, that quantum effects limit the capability of these devices. Molecular interactions, that are negligible in the bulk (e.g. van der Waals forces, interfacial tension), become increasingly relevant as sizes become smaller. These phenomena are what that the famous Nobel laureate Richard Feynman described in his lecture *There's Plenty of Room at the Bottom: An Invitation to Enter a New Field of Physics* in 1959. In his talk, he envisioned nanoscale machines that manipulate atoms precisely how we want them and talked about tiny surgical robots – a concept that was developed into the film *Fantastic Voyage* a few years later. Although credited with the concept of *nanotechnology*, historians are unsure whether he inspired actual research in the field.

The scientific field of nanotechnology only came into existence much later in the 1970s and 80s, propelled by the invention of the scanning tunneling microscope (STM) and the discovery of fullerenes in 1985 as well as the development of the atomic force microscope (AFM) in 1986. These discoveries brought to light the potential of *nanomaterials* — materials, that exhibit at least one external dimension lower than 100 nm — and that, due to their small size, exhibit properties and behaviors strange to their parent material. These sub 100 nm materials had already been visually observed in the early 20th century and were even used, albeit unintentionally, throughout history as artistic additives. Due to their unique optical characteristics, they were used in pigments or ceramic glazes, called "*luster*". Even Michael Faraday worked on what he called "*Ruby Gold*", a solution of gold that exhibits different colors under certain lighting conditions. He recognized the effect to be due to the small size of particles — now known to be gold nanoparticles.[1]

While one side of the application of nanomaterials focuses on enhanced "bulk" properties: strength, reduced friction, aesthetics, thermal- and electrical conductivity, the other side focuses on more "nano" properties, e.g. bandgap engineering, quantum effects and optoelectronics. Most applications of nanomaterials only use the properties of the nanomaterial in bulk: titania nanoparticles in sunscreen, silver nanoparticles as disinfectants or MoS_2 nanosheets as lubricants in suspension components. These applications, however,

do not take advantage of the unique properties that nanomaterials offer due their intrinsic nanostructured nature. For example, due to their conjugated and one atom thick structure, graphene and carbon nanotubes are predicted to exhibit extremely high electron mobility, even competing with metals.[2] Inorganic nanoparticles such as colloidal gold exhibit an effect called *localized surface plasmon resonance*, which is dependent on the surrounding chemical environment and thus makes it an interesting material for sensing applications (this is also what Michael Faraday observed). And in semiconductor nanocrystalline particles, excitations are confined to such small dimensions that remarkable effects occur, most notably *fluorescence.*

This is where silicon becomes relevant once more. At first, the study of nanostructured silicon was thought of as the next step towards the ever increasing miniaturization of our silicon-based computers, however, now having reached a 7 nm transistor size, the use of silicon nanomaterials — that aren't actually significantly smaller (~3 nm) — does not seem like a viable alternative. Fortunately, silicon nanomaterials show interesting properties and immense potential in their own right.

As a semiconductive material, nanostructured silicon has received significant attention due to the unique effects that occur at the nanoscale, but do not occur in bulk. Being an *indirect, small band gap* semiconductor, bulk silicon does not (and cannot) luminesce and thus applications in optoelectronic devices remained elusive. The discovery of nanostructured luminescent silicon has thus propelled the idea of new and exciting applications of silicon and their integration into the pre-existing silicon-based microelectronics industry.[3] Fabrication of so-called on-chip devices has seen numerous research reports and the study of silicon-based nanomaterials remains an intense research field. One of their unique-selling-points, as opposed to other nanomaterials, is the possibility of altering their surface chemistry, which can influence or enhance the underlying properties and help the integration into optoelectronic devices. Improved batteries, tunable emission and selective sensors are only some examples of properties and applications achieved by surface modification. Therefore, the study of the surface chemistry of silicon nanomaterials is one of the fundamental aspects of silicon nanomaterial research.

While we are a long way away from technologies resembling the visions of Feynman, Asimov and the-like, advances in nanomaterial research has seen significant strides over the past decades and still holds promise in future technologies.

2 Theoretical Background

2.1 Silicon Nanocrystals and Silicon Quantum Dots

2.1.1 Discovery and Synthesis of Silicon Nanocrystals

When it comes to nanomaterials, their synthesis can usually be summarized into two key concepts: Top-down and bottom-up.

Top-down approaches rely on pre-existing nanostructures that are in some way 'trapped' in a larger material. A popular example is the synthesis of graphene by mechanical exfoliation of graphite with adhesive tape. The nano graphene structure is present in graphite and merely needs to be extracted. Ball-milling or laser ablation are some other examples of top-down synthesis methods. On the other side, bottom-up approaches directly synthesize the material from scratch. Synthesis of gold nanoparticles through reduction of chloroauric acid or the pyrolysis of a precursor gas are prominent examples widely employed in the field of nanotechnology.

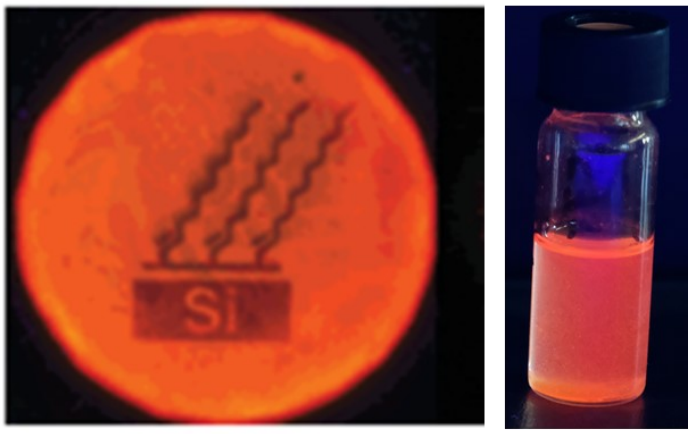

Figure 2.1–1. Pictures of the visible red/orange photoluminescence of porous silicon (left) and colloidal silicon nanocrystals (right). Adapted with permission from Buriak, J. M. Organometallic chemistry on silicon and germanium surfaces. *Chemical Reviews* **2002**, *102* (5), 1271–1308. Copyright (2021) American Chemical Society.

In similar fashion, the synthesis of silicon nanocrystals can be categorized in such a way. In fact, the initial discovery of silicon nanocrystals falls into the category of top-down. Canham produced a material now called porous silicon (*p*Si) through the electrochemical etching of silicon wafers in a HF acid electrolyte and observed red photoluminescence; one of the first examples of observed quantum confinement in silicon (**Figure 2.1–1** left).[3] He later discovered that this emission stems from crystallites as small as 3 nm that he observed in transmission electron microscopy (TEM).[4] One year later, Kavanagh, Sailor, and coworkers were able to isolate these nanocrystallites from porous silicon, forming the first colloidal

suspension of free-standing silicon nanocrystals (**Figure 2.1–1** right).[5] These initial reports triggered research in silicon nanocrystals and have since led to the growth of the research field. While bottom-up approaches are great for discovering new materials, structures, and producing the initial "prototypes" they usually lack precise control over composition, size and size distributions. Further improvements were made by adjusting the parameters of the *p*Si-method[6] and other top-down approaches such as laser ablation[7] and ball-milling[8, 9] can improve yields and quality, but still lack precise size control, especially when compared to bottom-up approaches.[10]

While top-down synthesis relies on the existence of the target structure, bottom-up produces the nanomaterial from a simple starting material, with the desired target structure in mind. The example mentioned earlier – the discovery of fullerenes – can be thought of as a bottom-up approach. Fullerenes are found in soot, so can be synthesized by burning organic matter. However, the target structure is only achieved serendipitously with many byproducts. This example highlights the challenges of nanomaterial synthesis. Next to realizing the desired silicon nanocrystal structure, other attributes need to be considered such as the selectivity, desired shape, size and size-distribution, as well as the purity and quality of the final material. Bottom-up approaches offer significantly better control over the resulting final material and have the potential for high yields that can be scaled up for industrial purposes.

Here, gas-phase methods have shown to be promising candidates as they also exhibit high yields and very high throughputs. They typically rely on the gas-phase reduction of a silane precursor in the presence of an energy source.[11] Notable examples are the aerosol reactor,[12] laser pyrolysis[13] and non-thermal plasma synthesis.[14] By adjusting the reaction/reactor parameters and starting silane (i.e. halogenation) the size and resulting surface-reactivity can be adjusted.[15] This allows tuning of the resulting optoelectronic properties and these methods have shown that the resulting materials have excellent quantum yields, due their high purity.[16] Unfortunately, the size distribution is still relatively large (± 20%) – increasing with decreasing particle size[17] – and only through size-selection methods can narrower distributions and small sizes be achieved that are small enough to allow for optoelectronic applications.[16, 10] Recently, the group of Kortshagen developed an all-aerosol-approach using a non-thermal plasma to synthesize, functionalize and anneal silicon nanocrystals in one gas stream (**Figure 2.1–2**). This approach is able to produce SiNCs in high yields with size-distributions and quantum yields comparable to those produced by solid state methods, however, particles with emissions below 750 nm could not be achieved as of yet.[18]

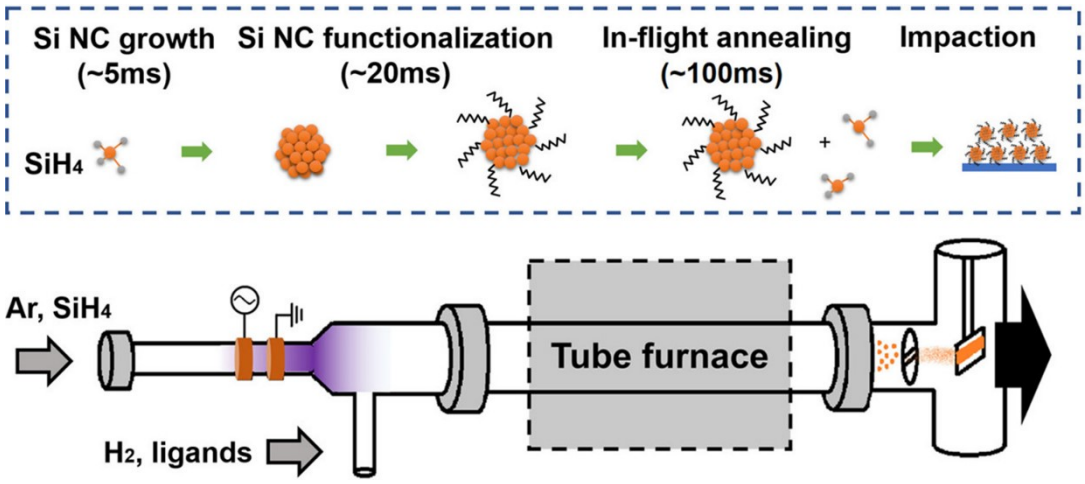

Figure 2.1–2. Experimental setup of the all-aerosol-phase non-thermal plasma synthesis of functionalized SiNCs developed by Li and Kortshagen. Reprinted with permission from Li, Z.; Kortshagen, U. R. Aerosol-Phase Synthesis and Processing of Luminescent Silicon Nanocrystals. *Chem. Mater.* **2019**, *31* (20), 8451–8458. Copyright (2021) American Chemical Society.

In comparison, metal chalcogenide quantum dots achieve very low size distributions and size control in simple solution synthesis methods.[19] Solution phase methods are also known for silicon nanocrystals, but are much more complex. Reduction of halosilanes with $NaBH_4$ or the Zintl phase reduction are prominent examples.[20, 21] The advantage of solution phase methods are the high yields, the precise control of surface chemistry and the possibility of modifying the surface in a one-pot reaction.[22] Through microwave assistance[23] or the use of a supercritical solvent,[24] improvements to the methods were achieved. However, the solution methods still lack precise size control and have problems with impurities that impact the final optoelectronic properties, limiting their overall application. Most notably, almost all solution-based methods result in silicon nanoparticles that exhibit blue luminescence with nanosecond excited state lifetimes, a phenomenon that is attributed to surface-state or defect based emission (see chapter 2.1.2 *Properties of Silicon Nanocrystals*).[25]

The highest quantum yields, narrowest size-distributions and good optoelectronic properties are achieved with solid phase methods relying on the thermal disproportionation of a silicon oxide rich matrix. In 1993 Hayashi *et al.* first reported the synthesis of luminescent silicon clusters in an annealed thin-film of SiO_x.[26] Later, the group of Veinot developed a method for producing silicon nanocrystals from electronic grade hydrogen silsesquioxane (HSQ)[27, 28] and improved the method by using a synthesized sol-gel polymer of silicon oxide.[29] The method produces silicon nanocrystals embedded in a silicon dioxide matrix, from which the nanocrystals are liberated by HF acid etching. The thermal disproportionation allows precise control over the mean diameter of the silicon nanocrystals by adjusting the

processing temperature and results in particles with narrow size-distributions (± 12 %); without the need for size-sorting techniques. Particle sizes can be tuned from hundreds of nanometers, down to the quantum confined regime, i.e. < 5 nm. The method requires only simple laboratory techniques and mainly employs commercially available precursors.[30]

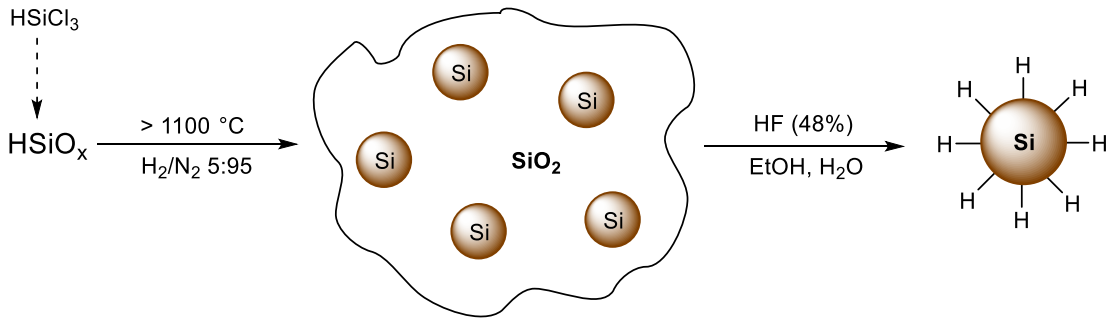

Scheme 2.1-1. Thermal disproportionation of a polymeric silicon oxide resulting in SiNCs embedded in a silicon dioxide matrix, from which they are liberated by HF acid etching.

While gas-phase methods may offer higher throughputs and higher conversion of the starting materials, the quality of silicon nanocrystals obtained from the HSQ method make them better suited for optoelectronic applications and laboratory scale research. As such, this method was used to synthesize silicon nanocrystals throughout this work.

2.1.2 Properties of Silicon Nanocrystals

The properties of a bulk material start to change when the confining dimensions reach the nanoscale (< 100 nm). For semiconductor materials this is even more evident as the dimensions become lower than their Bohr exciton radius (4.5 nm for silicon).[31] At this point crystalline semiconductors become so-called quantum dots.

A quantum dot is a material, which shows evidence of quantum confinement effects. Quantum confinement occurs when a material reaches the dimensions of its Bohr exciton radius. Within the LCAO model (linear combination of atomic orbitals) and in a bulk material, the energy difference between the energy states of each individual atom is so minute that they are considered to form so-called *bands* (valence, conduction band). When the dimension of the bulk material reaches the nanoscale, the energy differences between the energy states become larger and the energy states become discrete. Therefore, as the size of the particle becomes smaller, the band-gap increases (**Figure 2.1–3**).[32] From a quantum mechanics point of view, a generated exciton (i.e. electron-hole pair) confined in dimensions smaller than its radius behaves like a *particle in a box*.[33] As the confining dimensions decrease, the energy of the allowed states increase, thus widening the band gap of the material.

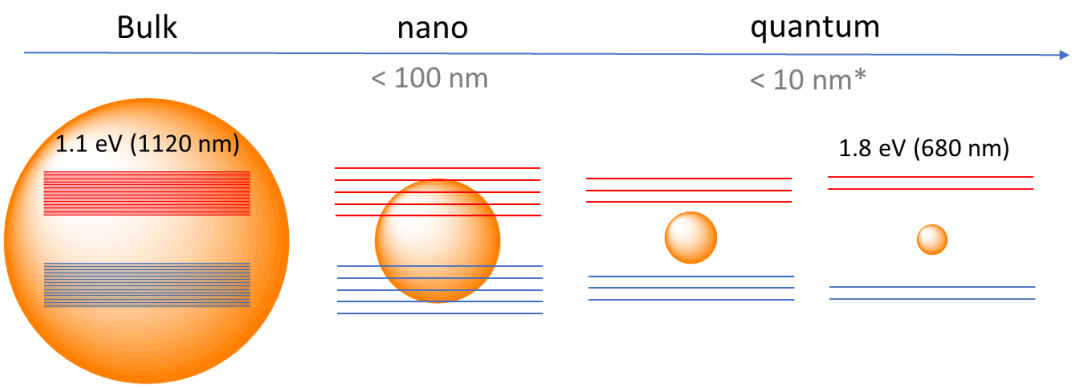

Figure 2.1–3. Illustration of the discretization of energy states and widening of the band gap as the dimension of the material shrinks. Values refer to silicon.

Bulk silicon does not show any optoelectronic properties, due to its (relatively) small and indirect band gap. As the dimension of the silicon crystallite decreases toward its Bohr exciton radius (~4.5 nm)[31], the band gap widens and the nanocrystals exhibit photoluminescence (PL) in the visible spectrum.[3] As quantum confinement dictates the optical behavior of the crystallite, silicon nanocrystals with sizes lower than 5 nm are considered quantum dots. Observations of the optoelectronic properties of silicon nanocrystals with different sizes have indeed shown a distinct correlation between the PL emission maxima and the nanocrystal size.[34] However, for the higher energy emissions (i.e. lower wavelengths; < 600 nm) the excited state lifetimes were frequently found to be in the regime of nanoseconds while the lower energy emissions (i.e. higher wavelengths; > 600 nm) had lifetimes in the range of microseconds.[35, 36] The long lifetime observations are attributed to the indirect nature of the band gap and are consistent with quantum confinement models,[37–39] while the nanosecond lifetime observations remained a topic of ongoing debate. Recently, reports revealed that the short lived lifetimes are attributed to surface-state emissions and defects that arise from surface ligands or oxidation; a generally undesired trait[34, 40–42]. In addition, the photoluminescence behavior observed for nanosecond lifetime samples showed short lifetimes irrespective of their size, while the long-lived emissions follow the size-dependent trend, as is predicted by quantum confinement models.[43–46]

This size-PL correlation, however, was and still is inconsistent between various reports, especially between different research groups, and does not always correlate to predictions made by the effective mass approximation (**Figure 2.1–5**).[47–49, 46, 43, 44] One could easily attribute these incongruences to the different synthesis methods, such as HSQ disproportionation vs. non-thermal plasma synthesis, or to the differing methods used to determine the nanocrystal diameters. However, the precise origin remained unclear. With the assumption that the PL stems from the quantum confinement of excitons within the crystalline

core of the nanoparticle, then the same crystal size must report the same PL emission maxima, regardless of synthesis method.

Recently, Thiessen, Ha, and coworkers determined through solid-state nmR measurements that the actual structure of silicon nanocrystals consists of a core-, subsurface- and surface species (**Figure 2.1–4**).[50] A critical size junction of 9 nm was determined, below which the identification of the core species becomes difficult and the surface structure dominates. Above 6 nm the core of the silicon nanocrystals exhibits chemical shifts similar to those of crystalline bulk silicon, as is in agreement with quantum confinement models. These structural properties have profound implications toward the optoelectronic properties of silicon nanocrystals, since the core is mainly attributed to the photoluminescence characteristics.

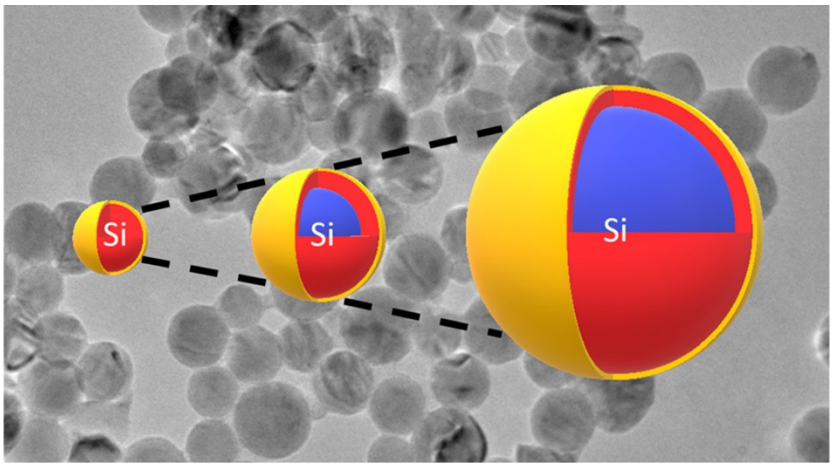

Figure 2.1–4. Illustration of the core-, subsurface-, and surface species found in different sizes of silicon nanocrystals. Reprinted (adapted) with permission from Thiessen, A. N.; Ha, M.; Hooper, R. W.; Yu, H.; Oliynyk, A. O.; Veinot, J. G. C.; Michaelis, V. K. Silicon Nanoparticles: Are They Crystalline from the Core to the Surface? *Chem. Mater.* **2019**, *31* (3), 678–688. Copyright (2021) American Chemical Society.

Later work by the same author used this knowledge to address the issue of incongruencies of size and photoluminescence (**Figure 2.1–5**).[43] The discrepancies are most notable at sizes below 4 nm,[46] a regime where the nature of the subsurface species becomes less precise.[50] Thiessen found that the size-PL correlation is much more accurate when considering crystallite size, which can be determined by X-ray diffraction techniques (XRD).[43] In general, TEM is used as the preferred method for determining size and size-distributions of silicon nanocrystals by many research groups. However, 3 nm SiNCs, as determined by TEM, only have a 1.2 nm crystallite size, as determined by XRD, which is found to fit much better to PL data with the predictions made by effective mass approximation.[43, 47] For larger particles (> 6 nm, TEM) the correlation between size and PL is a much better fit, as the surface and subsurface species (i.e. amorphous layer) is much thinner and does not contribute much to the overall size.[43, 50, 46] The problem that X-ray diffraction techniques pose, is that the sizes

are volume-averaged and not number-averaged as TEM techniques are. As such, the size-determination of polydisperse particles becomes inaccurate, which explains the reported differences in size-PL correlations, as different research groups use different synthesis techniques, which in turn results in varying polydispersities and crystallite sizes.[44, 43, 46]

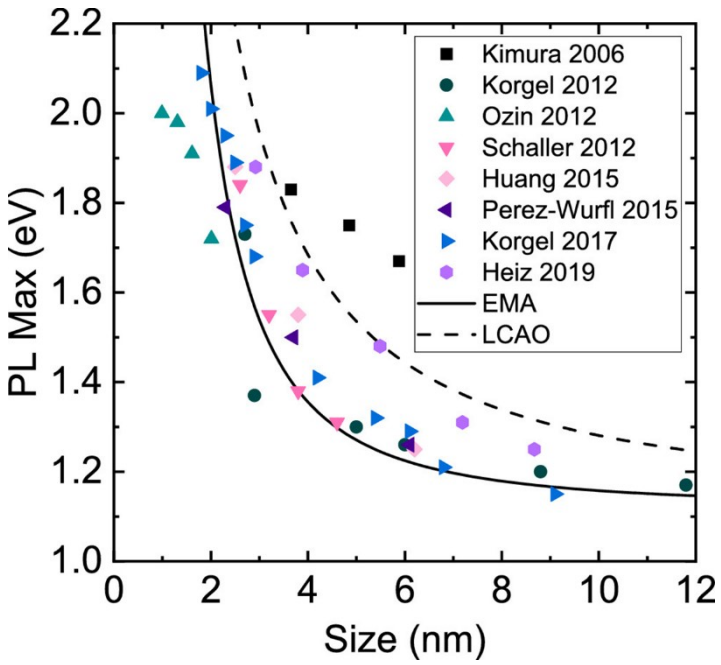

Figure 2.1–5. Summary of the literature data showing the relationship between silicon quantum dot peak PL emission and the particle dimension. Reprinted with permission from Thiessen, A. N.; Zhang, L.; Oliynyk, A. O.; Yu, H.; O'Connor, K. M.; Meldrum, A.; Veinot, J. G. C. A Tale of Seemingly "Identical" Silicon Quantum Dot Families: Structural Insight into Silicon Quantum Dot Photoluminescence. *Chem. Mater.* **2020**, *32* (16), 6838–6846. Copyright (2021) American Chemical Society.

2.1.3 Surface Chemistry of Silicon Nanocrystals

One of the fundamental aspects of silicon nanocrystals is the reactive surface that results from most synthesis methods. On one hand this makes SiNCs sensitive to oxidation and moisture, but on the other it offers a platform for modification, allowing the design of SiNCs with specific properties. The intrinsic properties of the SiQDs, i.e. the photoluminescence and conductivity, can be influenced by the surface group and their interaction with the environment can be tailored to suit the needs of a given application.[34] Capping with unpolar organic groups can stabilize particles and prevent degradation, while hydrophilic groups can render them water-soluble, a prerequisite for biological applications. Many of the published reports concerning the surface modification of silicon nanocrystals have taken inspiration from other silicon surfaces, such as porous silicon, silicon wafers and nanocrystalline silicon. Pioneering work by Buriak,[51] Sailor,[52] Linford and Chidsey,[53, 54] among others, has helped broaden the scope and laid the foundation for the development of functionalization methods for SiNCs.

Instead of focusing on the commonly employed methods and techniques used for functionalizing silicon nanocrystals, this chapter gives a brief summary and will highlight some interesting research articles that focus on unique approaches to surface-modification as well as surface-ligands that can impart unique properties and behaviors to silicon nanocrystals. For comprehensive reviews on the topic of silicon nanocrystal surface modification, see the fantastic works by Buriak[51], Dasog and Kehrle,[25] Cheng and Gooding,[55] and Veinot.[11]

2.1.3.1 Summary of Common Functionalization Approaches

The functionalization methods of silicon nanocrystals are based upon the reactive surface that results from any given functionalization method. While some methods directly produce functionalized SiNCs, most methods will result in either hydrogen- or halogen-termination.

For the latter, the extremely reactive surface lends itself to various functionalization approaches including reactions with nucleophiles – alcohols[21] and amines[56] – as well as Grignard[57] or organolithium reagents.[58] The drawback of these methods does not lie in the functionalization approach, but rather the quality of particles that result in halogen surface termination. These methods frequently produce blue-emitting SiNCs, which has been attributed to surface-state or defect emissions with no evidence for the desired size-dependent core emission.[25, 34] Even when core-emission particles are halogenated via chlorination or bromination, the SiNCs exhibit nanosecond lifetimes, indicating a coherence between the halogen surface and surface-state emissions.[25, 59]

Hydride-terminated particles produced by laser/plasma pyrolysis or solid-state disproportionation show much more promising optoelectronic properties (see chapter 2.1.1: *Discovery and Synthesis of Silicon Nanocrystals*). Their derivatization is commonly achieved via the well-established hydrosilylation reaction, which produces a robust Si-C linkage, which hinders oxidation while permitting the attachment of distal functional groups (depending on the hydrosilylation method). Thermal hydrosilylation is the most straightforward approach, but requires high-boiling alkenes and has been shown to produce oligomers, instead of monolayer coverage.[60, 25] The UV-initiated hydrosilylation was proposed as a versatile alternative, but further investigations revealed a size-dependent reactivity, only permitting particles with sizes lower than 5 nm.[61, 62] This limitation is proposed to be due to the exciton-mediated mechanism, which relies on the generation of excitons to initiate the reaction, only possible in luminescent SiNCs.[63] Room (or low) temperature hydrosilylations that use chemical initiators have emerged as size-independent, versatile (i.e. large substrate scope) and mild approaches to silicon nanocrystal functionalization. Apart from Lewis-acid initiated hydrosilylation[64, 65] most methods generate radicals through decomposition (AIBN,[66] benzoyl

peroxide,[66] PCl_5,[67] XeF_2[68]) or generate radicals through interaction with the nanomaterial surface (diazonium salts,[69] iodonium salts[70]). These radicals then generate surface silicon radicals which can react with the desired unsaturated substrate. Mechanistically speaking the hydrosilylation of silicon nanocrystals boil down to two main pathways: the exciton-mediated hydrosilylation (**Scheme 2.1-2**a)[63] and the direct radical initiation hydrosilylation (Scheme 1b, c).

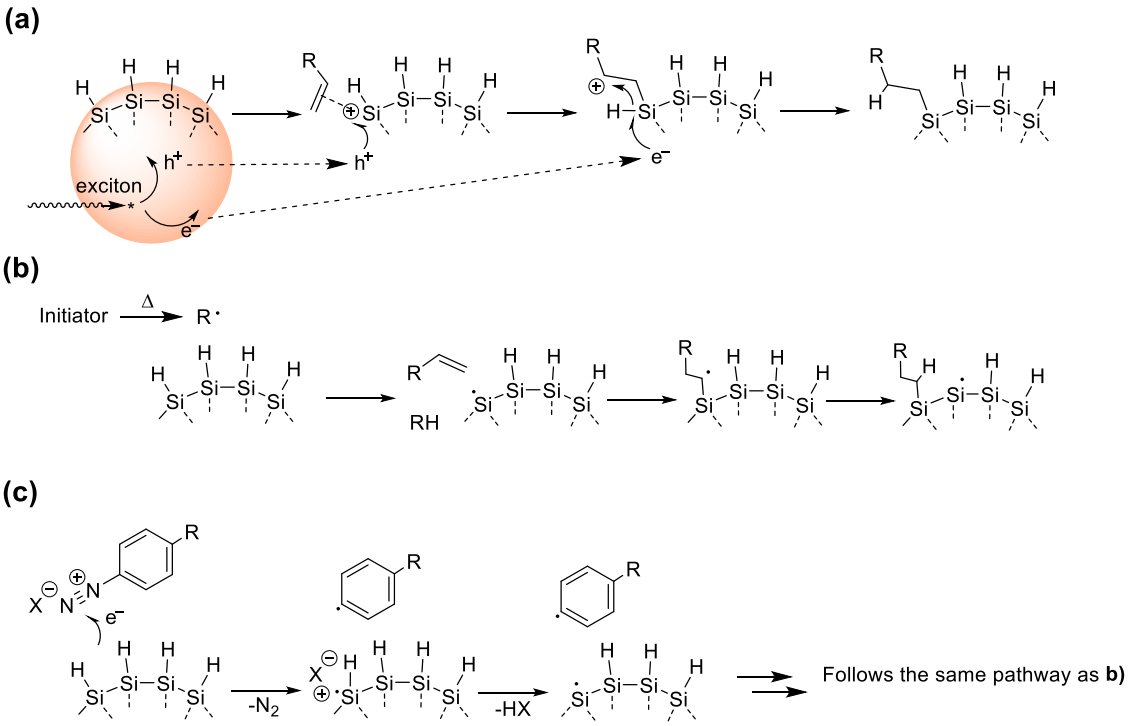

Scheme 2.1-2. Mechanisms of SiNC hydrosilylations following the (a) exciton-mediated mechanism, (b) direct radical initiation and (c) initiation with diazonium compounds. Based on mechanisms from refs [51, 69, 63].

2.1.3.2 Selected Highlights of the Surface Functionalization of Silicon Nanocrystals

The hydrosilylation with silicon nanocrystals is a versatile approach to introduce a variety of substrates with different functional groups. However, some substrates remain incompatible, especially ones that possess an acidic proton or have large steric demand.[70, 69] In addition, the requirement of a double bond limits the potential scope of substrates. To address this, Höhlein and coworkers developed a post-functionalization method that uses a chlorosilane moiety as a reactive precursor for further derivatization.[71] Using the established 4-DDB initiated hydrosilylation, the silicon nanocrystal surface is functionalized with chlorodimethylvinylsilane (ClDMVS), which allows subsequent reaction with nucleophiles or Grignard reagents. In contrast to the direct chlorination with PCl_5, the reaction proceeds efficiently with minimal oxidation and the optoelectronic properties of the SiNCs remain unaffected. In this fashion, the group of Paola Ceroni was able to introduce challenging

groups such as amines[72] and water-soluble PEG units.[73] Such a post-functionalization approach has been proposed previously and uses hexadiene to introduce a distal alkene group that can be further modified via the *thiol-ene* reaction. This approach, however, leaves questions as to whether cross-linking occurs due to the hydrosilylation of both alkenyl moieties.[74]

A completely unique approach was developed by Zhukhovitskiy and coworkers, who used N-heterocyclic carbenes (NHC) as functional substrates to insert into Si-H bonds.[75] They demonstrated the feasibility using model molecular silanes and applied the developed method to both Si(111) wafers and silicon nanocrystals; synthesized by the HSQ disproportionation method. The use of carbenes is not unprecedented for Si-H surfaces, as in-situ generated dichlorocarbene was applied to Si(111) wafers, and transition metal-catalyzed carbene insertion was shown for porous silicon.[76] These methods, however, use metal substrates or catalysts, which have detrimental effects on the optoelectronic properties of SiNCs.[77] The benefits of the persistent carbene method lie with the customizability of the NHCs and the precision and control the reaction could permit.[75] The effect of nitrogen on SiNCs is well established[34] and the NHC method allows the insertion of nitrogen species close to the silicon surface with only one carbon spacer. As the authors state, this could permit through-bond/-space electronic coupling between the functional group and the surface.[75] Unfortunately, the authors do not explore these optoelectronic effects on SiNCs and the provided infrared spectra suggest only minor carbene insertion along with significant oxidation. While the method remains in the early stages, it provides an interesting starting point for further investigations.

Surface groups can impart unique properties on silicon nanocrystals, often combining characteristic behaviors of organic substrates and the inorganic nanoparticles. Kehrle *et al.* demonstrated this by grafting a thermoresponsive polymer from the surface of silicon nanocrystals; the resulting LCST (lower critical solution temperature) is transferred to the nanomaterial (**Figure 2.1–6**).[78] In another example, the switchable hydrophilicity of amidine groups is added to silicon nanocrystals, which allows the control of the solubility by altering the CO_2 concentration in solution.[79] Upon sparging with CO_2, the SiNCs become water-soluble and transfer to the water phase, while sparging with argon moves them back into the toluene phase (**Figure 2.1–6**).

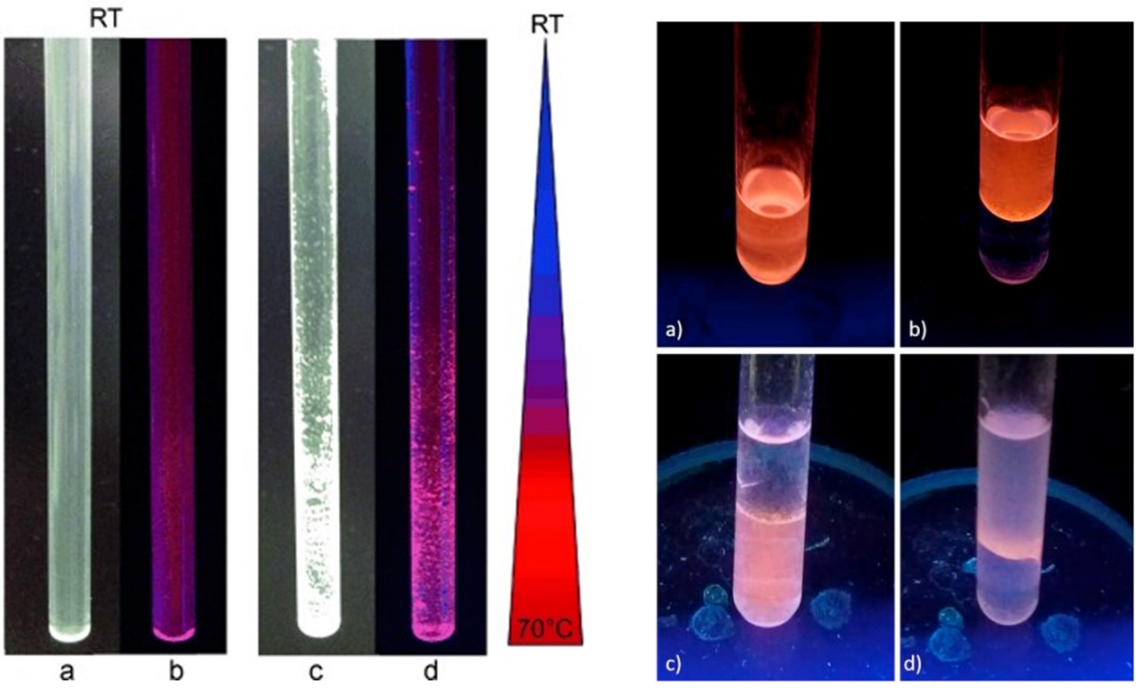

Figure 2.1–6. Pictures of silicon nanocrystal dispersions highlighting unique solvation behaviors. Left images depict the LCST behavior of PDEVP-functionalized SiNCs and the right pictures illustrate the switchable hydrophilicity of amidine-functionalized SiNCs. Reprinted with permission from Kehrle, J.; Höhlein, I. M. D.; Yang, Z.; Jochem, A.-R.; Helbich, T.; Kraus, T.; Veinot, J. G. C.; Rieger, B. Thermoresponsive and photoluminescent hybrid silicon nanoparticles by surface-initiated group transfer polymerization of diethyl vinylphosphonate. *Angewandte Chemie - International Edition* **2014**, *53* (46), 12494–12497 and Thiessen, A. N.; Purkait, T. K.; Faramus, A.; Veinot, J. G. C. Lewis Acid Protection:A Method Toward Synthesizing Phase Transferable Luminescent Silicon Nanocrystals. *Phys. Status Solidi A* **2018**, *215* (7), 1700620. Copyright (2021) Jon Wiley & Sons.

The synthesis of water-soluble particles has been an ongoing challenge for silicon nanocrystals; especially if the water-solubility is to be achieved via surface groups. Direct solution synthesis of water-soluble silicon nanoparticles is well established, however, this is usually achieved via an oxide layer and the nanoparticles exhibit less-desirable optoelectronic properties: low quantum yields and the size-independent blue photoluminescence originating from surface states and/or -defects.[80, 81] Similar behavior is also observed for water-soluble (allyl)amine functionalized silicon nanocrystals that exhibit short nanosecond lifetimes, which indicate surface state/defect emissions.[82–84] The chlorination of SiNCs using PCl_5 and subsequent post-functionalization with sugars was able to produce water-soluble SiNCs, but also resulted in the undesired blue-emission.[85] For applications that require water-solubility, the long-lifetime red core-emission is typically desired.[61] Water-solubility with high-quality SiNCs can be achieved with polymer grafting of poly(methyl methacrylate)[86] or with diethylvinylphosphonate,[78] however, solubility derived from monolayer surface groups has been difficult to achieve. Some success is observed for SiNCs functionalized with unsaturated carboxylic acids, but the resulting material requires additional purification procedures,

including dialysis and filtration, lowering the overall yield significantly.[87] Finally, Islam *et al.* was able to achieve water-solubility by using mixed-surface chemistry, introducing two functional groups that render the SiNCs amphiphilic, i.e. soluble in both hydrophilic and hydrophobic solvents (**Figure 2.1–7**).[88] The procedure uses a straightforward thermal hydrosilylation approach and produces silicon nanocrystals exhibiting desirable optoelectronic properties, including red core-emission and long excited state lifetimes.

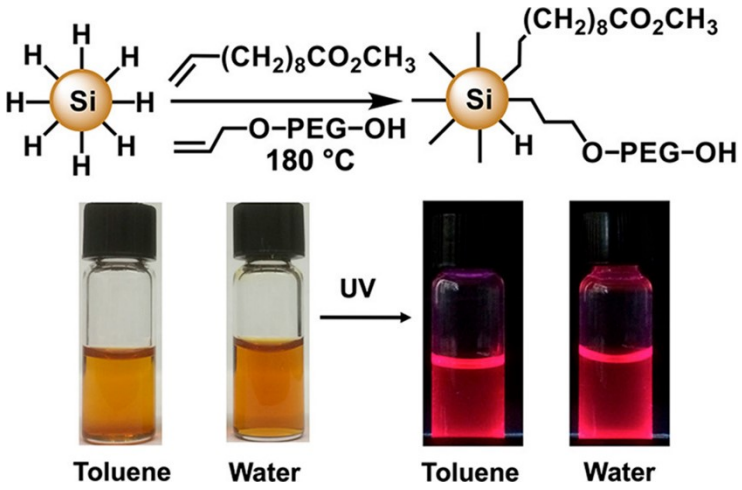

Figure 2.1–7. Synthesis strategy for obtaining amphiphilic silicon nanocrystals. Pictures depict the solubility of the resulting particles in toluene and water. Reprinted with permission from Islam, M. A.; Sinelnikov, R.; Howlader, M. A.; Faramus, A.; Veinot, J. G. C. Mixed Surface Chemistry:An Approach to Highly Luminescent Biocompatible Amphiphilic Silicon Nanocrystals. *Chem. Mater.* **2018**, *30* (24), 8925–8931. Copyright (2021) American Chemical Society.

2.1.4 Applications of Silicon Nanocrystals

The applications of silicon nanocrystals or more specifically, silicon quantum dots, still remain in prototype stages.[25] Numerous proof of concepts have been developed ranging from the fields of microelectronics to biological imaging.[89] Most of the applications take advantage of the unique optoelectronic properties of the silicon quantum dots as well as the unique surface chemistry.

The most obvious application of this light-emitting material is to use them in light-emitting devices. The tunability of the photoluminescence could allow the preparation of various colored LEDs. For other quantum dots this has already found commercial application as the photo-emissive layer in television screens – known as QLED TVs. The advantage is the sharp emission of the quantum dot layer, achieving a wider color gamut and thus more accurate and brilliant colors. Currently, Cd-based quantum dots are mainly employed, but concerns about their toxicity have already introduced restrictions in some jurisdictions.[90] Silicon quantum dots could arise as a non-toxic,[91] earth abundant alternative for next-generation devices.[92] Adjusting the photoluminescence emission, increasing efficiency and narrowing

the emitted wavelengths are challenges that still need addressing before any commercial applications can be realized.[93] As an optoelectronic material, silicon nanocrystals have also shown potential in energy applications.[94] The high affinity of silicon for lithium promises immense capacities in batteries, but the accompanied volume expansion limits any commercial application.[95] The increased surface to volume ratio in nanostructured silicon could provide a means to alleviate the issue.[96] In hybrid composites of silicon nanocrystals and polymers, significant strides have been made. These materials exhibit high capacities while still providing high cyclability. The SiNCs provide sites for Li intercalation, while the surrounding polymer provides a matrix to allow the nanostructure to expand into.[97] In other related energy applications, silicon nanocrystals have been used to improve efficiencies of solar cells. The SiNCs act as so-called *luminescent solar concentrators*. These convert incident light into wavelengths that can be absorbed by the underlying solar cell. The surface of the SiNCs is key in this application, as the SiNCs need to be well dispersed in the transparent polymer matrix, thus avoiding energy deficient scattering due to agglomeration.[98] In addition, the surface groups can be used to tune the LSCs behavior and increase the overall efficiency.[99]

The visible photoluminescence of silicon nanocrystals can also be used to fabricate simple sensors.[100] Because the photoluminescence is strongly dependent on surface groups and the surrounding chemical- and physical environment, changes in these can induce changes in the optoelectronic behavior, thus providing a simple feedback mechanism. The significant advantage that SiNCs offer when compared to other QDs is the possibility of adding surface groups with substrate targeting abilities (just like enzymes or antibodies). The surface groups can provide an interaction interface, while the silicon nanocrystals provide the feedback to indicate changes.[101]

The optoelectronic properties of silicon nanocrystals also make them uniquely qualified for biological imaging, in addition to their biocompatibility.[91, 102] Quantum dots, in general, have been intensively investigated to replace dyes in biological imaging, due to higher brightness and stability toward photobleaching.[103] The near-IR emission of SiNCs is of particular interest as this spectral region is able to maximally penetrate tissue without absorption by hemoglobin, allowing for deep-tissue imaging.[104] However, the near-UV excitation of SiNCs lies outside of this physiological window, thus hindering their current widespread implementation. This problem has been addressed by a multitude of reports, suggesting the use of two-photon absorption to shift the PL excitation to near-IR regions.[105–107] The long excited state lifetimes of SiNCs, attributed to the indirect bandgap of silicon, gives a significant advantage over other QDs in biological imaging. The autofluorescence of

endogenous biological species exhibit short lifetimes (~2 ns)[108] and can thus be separated from the SiNC emission through time-gated imaging.[73, 109]

Currently, the focus of surface chemistry in relation to biological applications lies upon rendering the silicon nanocrystals water-soluble and physiologically stable. Various strategies, including simply attaching hydrophilic functional groups,[88, 73] to polymer composites,[110, 86] and micelle- and lipid encapsulation[111, 112, 106] have all proven successful. However, the potential of the reactive surface has not been fully taken advantage of, as it can also be used to attach functional molecules that could impart additional desired properties, such as cell-targeting through specific functional groups, enzymes or proteins,[113–115] complementary fluorescence mechanisms with dyes,[107] and possibly drug-delivery and applications in theranostics.[112] Since SiNCs first use as fluorescent tags back in 2004,[86] many reports have been published discussing their applicability. Comprehensive reviews on this topic are found in refs [55, 20, 109, 116].

This chapter only briefly touched upon a few applications and developments of silicon nanocrystals, but there are many more that were not discussed. For more information and detailed descriptions and examples, refer to references [109, 94, 55, 89].

2.2 Silicon Nanosheets

In this chapter a brief summary of the state of the art for two-dimensional silicon nanosheets is given. While not as detailed as the chapter on silicon nanocrystals, silicon nanosheets are an important part of this thesis. For more detailed reports on the topics of history, synthesis and properties many comprehensive reviews have been published.[117–122]

2.2.1 Discovery, Synthesis and Structural Elucidation

With the discovery of luminescent silicon materials in the 1990s a surge of interest toward the topic of silicon nanomaterials emerged. In fact, two-dimensional silicon had already been well known since the 1860s, but until that point had remained in the background. Nanomaterials are categorized according to their nanoscale dimensions – or more precisely, the dimensions not in the nanoscale (< 100 nm). Silicon nanosheets fall into the two-dimensional category. They exhibit lateral sizes in the micro regime, while their thickness lies on the atomic scale. This two-dimensionality imparts some unique properties that can also be found in other 2D materials; properties such as mechanical strength, flexibility, optical transparency and unique (opto)electronic behavior.[123] Silicon nanosheets can be thought of as the silicon equivalent of graphene. They also exhibit a hexagonal honeycomb lattice structure, but in contrast to graphene are not planar, but rather buckled. Just as cyclohexane is buckled and benzene is planar due to the different hybridizations of carbon (i.e. sp^3 vs sp^2), the buckling arises due to the mixed hybridization of the silicon framework. The larger interatomic distance between silicon atoms prevents the formation of strong π-bonds and only the p_z orbitals are able to overlap slightly, resulting in a mixed sp^2-sp^3 hybridization.[124] This hybridization leads to the slightly buckled honeycomb framework of the silicon nanosheets (**Figure 2.2–1**).[125–127]

There is much ambiguity to the term “silicon nanosheets”, because there are multiple structures that constitute this overarching term. The just-described material is the ‘true’ graphene analog and is called *silicene*. Silicene is inherently unstable and can only be synthesized epitaxially, i.e. grown on pre-existing substrates. It exhibits some unique properties such as a massless Dirac-cone state[128] and conduction along the edges. As such, it is a promising material in next-generation devices, such as the 2D topological insulator.[119]

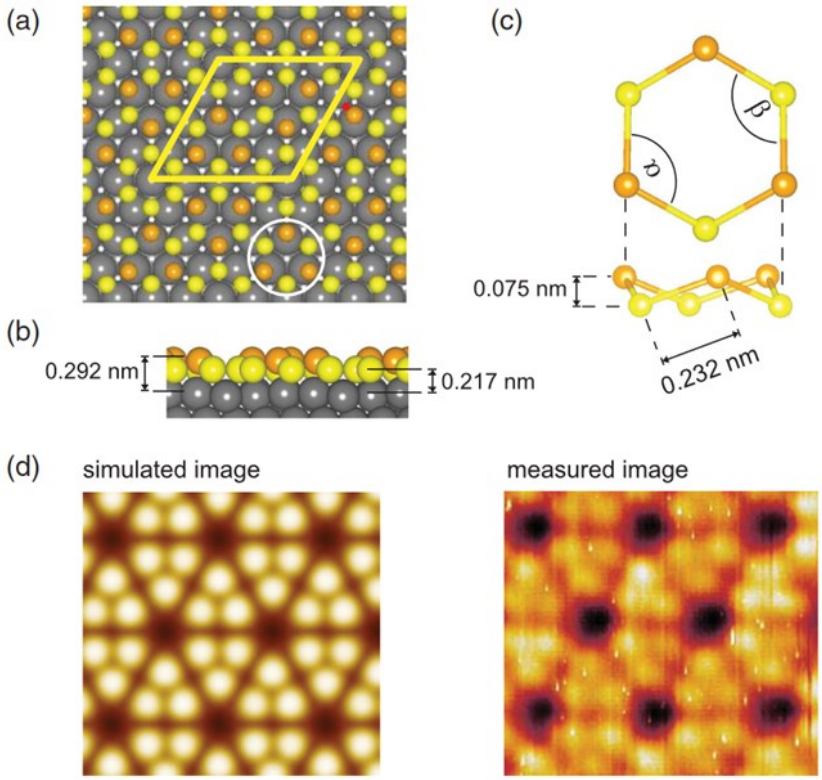

Figure 2.2–1. DFT results for the silicene on Ag(111). (a) Top view of the fully relaxed atomic geometries of the model for silicene on the Ag(111) surface from Fig.3. (b) Side view of (a).c) Enlarged image of the hexagonal silicene ring indicated by the white circle in (a). (d) Simulated STM image (left) for the structure shown in (a). The simulated image exhibits the same structural features as those observed in the experimental STM image (right), i.e., a hexagonal arrangement of the triangular structure around dark centers. Reprinted figure with permission from Vogt, P.; Padova, P. de; Quaresima, C.; Avila, J.; Frantzeskakis, E.; Asensio, M. C.; Resta, A.; Ealet, B.; Le Lay, G. Silicene: compelling experimental evidence for graphene like two-dimensional silicon. *Phys. Rev. Lett.* **2012**, *108* (15), 155501. Copyright (2021) by the American Physical Society.

The stable and free-standing form of silicene – which is the focus in this thesis – is obtained by filling the fourth valence of the silicon atoms with a covalently bound ligand, thus filling the p_z orbital, removing π-bonding and thereby increasing the buckling of the silicon framework.[119] As the framework is now fully sp^3-hybridized the material is called *silicane* (derived from graphene (sp^2) vs. graphane (sp^3)). In its simplest form, silicane is produced by hydrogenating silicene. However, silicane can also be synthesized from the chemical exfoliation of calcium disilicide, a Zintl phase, which consists of polyanionic $[Si]_n$ layers with intercalated calcium ions. The composition of the resulting material is highly dependent on the employed reaction conditions. Varying the exfoliation temperature or -reagents leads to different surface ligands. The first isolation of this graphane-analog occurred in the 1860s by *Friedrich Wöhler* who noted its graphite-like morphology and characteristic yellow luster. He determined the stoichiometry to be either $Si_8H_4O_6$ or $Si_6H_3O_4$ and saw the material as

noteworthy, because he saw it as example of an organic-like structure, wherein silicon replaces carbon.[129] In 1921, *Hans Kautsky* attempted to synthesize the same compound but under more "controlled" conditions. He proposed a structure for the resulting material consisting of six-membered Si-rings interconnected by oxygen bridges, with the fourth valence of the silicon atoms saturated by hydrogen (**Scheme 2.2-1** left).[130] This came to be known as "*Kautsky siloxene*". Only 120 years after its first isolation could the exact structure be determined. Through X-ray diffraction, *Weiss et al.* determined that the as-prepared "*Wöhler Siloxene*" consists of a puckered honeycomb lattice of silicon 6-membered rings terminated with alternating hydrogen and hydroxyl groups above and below the silicon plane (**Scheme 2.2-1** right).[131] The structure reported by *Kautsky* has not been observed by X-ray diffraction experiments and some reports show that the as-prepared "*Kautsky-siloxene*" actually consists of multiple substances.[132, 133]

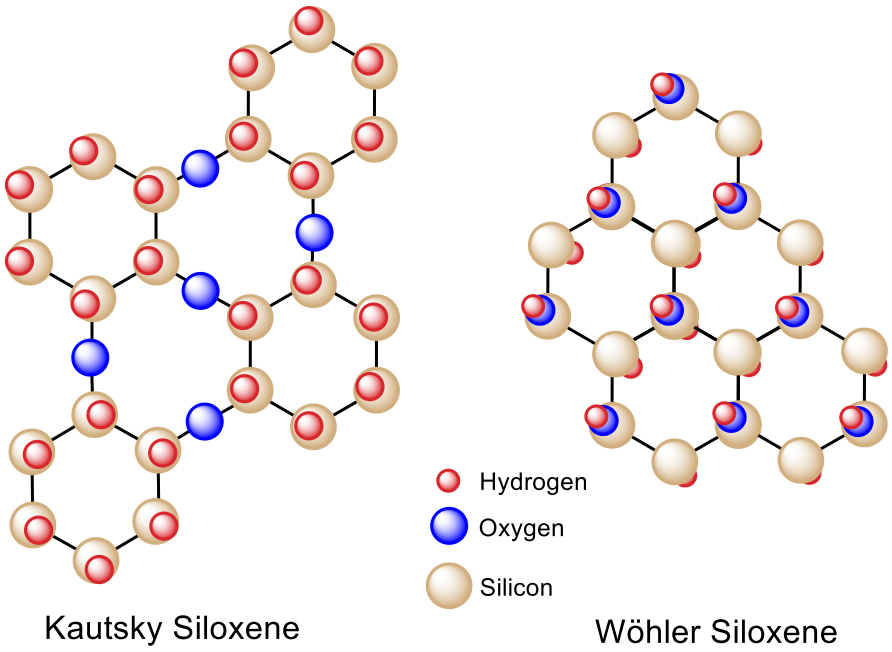

Scheme 2.2-1. Schematic illustrations of the proposed structures of Kautsky- and Wöhler siloxene.

Attempts to synthesize a non-oxygenated from of siloxene were pursued by Dahn *et al.* in 1993. The authors successfully exfoliated siloxene from $CaSi_2$ at 0 °C and subsequently washed the sample with hydrofluoric acid.[133] The acid removes the oxides from the sample, resulting in what the authors called *layered polysilane*, the silicon-equivalent to graphite. Later, the group of *Matsu-ura* designed a new recipe for the synthesis of layered polysilane: conducting the reaction at -30 °C in aqueous HCl under inert atmosphere, which resulted in a much lower incorporation of oxygen.[134, 135] Nevertheless, in every report concerning the synthesis of layered polysilane oxygen is always incorporated to a small degree, even when

the sample is rinsed with HF. To this date, no method has been able to definitively synthesize a completely oxygen-free sample of these silicon nanosheets.[117]

In summary of these discoveries, the synthesis of free-standing silicane and its derivatives can be summarized in the following. The Zintl phase calcium disilicide is exfoliated with concentrated hydrochloric acid. When conducted at 0 °C or above, *Wöhler siloxene* is formed. At temperatures below -25 °C the purely hydrogenated *silicane* (or *layered polysilane)* is formed and when conducted in alcoholic hydrochloric acid, alkoxy-terminations are introduced (**Scheme 2.2-2**).[131]

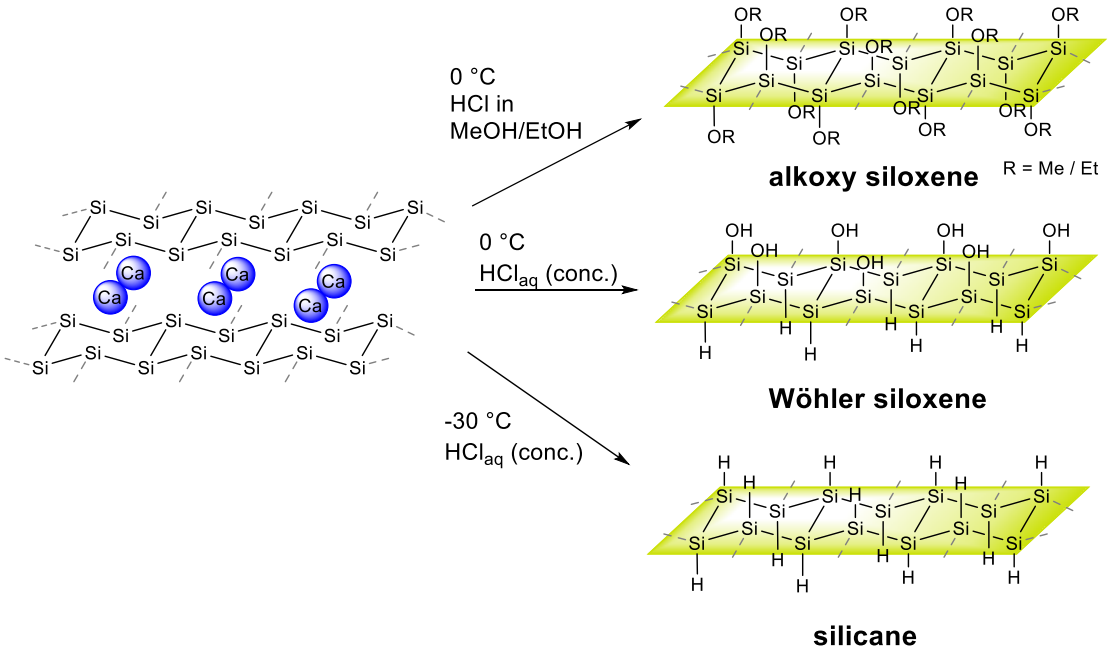

Scheme 2.2-2. Summary of the different silicon nanosheets obtainable from the Zintl phase calcium disilicide.

2.2.2 Properties of Silicon Nanosheets

Even though 2D silicon (siloxene) has been known for over 150 years, research has mainly been focused on its bulk chemistry (i.e. in powdered form) and structural properties. With the advent of porous silicon and the observations that the luminescence properties stem from nanocrystalline silicon structures within, focus has shifted toward the optoelectronic characterization of these nanostructures and their integration into microelectronics. Some authors have even suggested that the luminescence properties of the seminal porous silicon is due to annealed siloxene structures, which exhibit similar optoelectronic characteristics.[136–138]

The characteristic properties of silicane and its derivatives stem from the extended Si-Si framework. Resonance interactions between the sp^3 orbitals of adjoining Si atoms result in a σ-conjugated system with electron delocalization throughout the entire Si-backbone.[139, 140] Silicanes exhibit strong absorptions in the UV-Vis region, which are ascribed to the σ-σ* transition of this conjugated system; silicanes are thus semiconducting, exhibit an indirect band gap and show photoluminescence (**Figure 2.2–2**).[141, 119] The photoluminescence that silicanes exhibit still remains a topic of ongoing debate. It has mostly been attributed to quantum confinement of charge carriers to the planar silicon framework,[142] but recent data suggests that the photoluminescence is strongly dependent on the surface ligands.[143, 144]

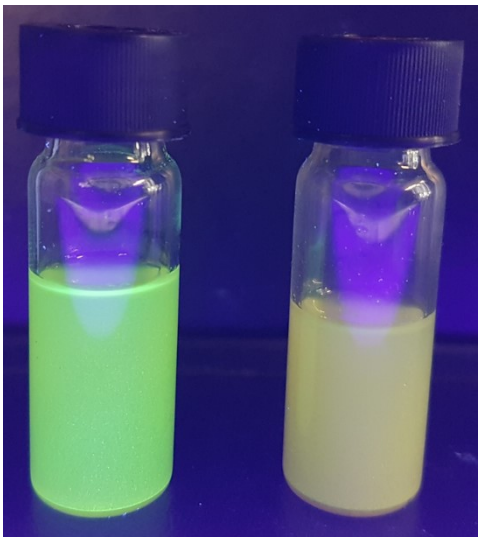

Figure 2.2–2. Picture of modified SiNSs in solution showing photoluminescence (left) and no photoluminescence (right) due to prolonged exposure to UV light.

One of the key issues that is plaguing applications of SiNSs is the degradation observed during UV illumination (**Figure 2.2–2** right). A simple explanation goes back to the σ-conjugation of the silicon material. UV irradiation promotes electrons from the bonding σ-orbitals to the anti-bonding σ*-orbitals, weakening the Si-Si bonds. This leads to a rearrangement of surface-bound oxygen atoms into the silicon framework, thus removing the σ-conjugation.[145, 146] Parallels to thin amorphous-silicon films can be made, which exhibit the so-called Staebler-Wronski effect – a loss of photoconductivity under prolonged irradiation.[147] The exact cause for this effect is still unknown, but many theories suggest that the loss comes from the generation of dangling bonds.[148] A dependance on the hydrogen content was determined, and the authors suggested a mechanism in which the rearrangement of Si-H into a Si-Si bond leads to the formation of a new Si-H and a dangling bond.[147]

2.2.3 Surface Modification of Silicon Nanosheets

The ligand-dependent observations of UV-degradation and photoluminescence highlight the importance of surface chemistry for silicon nanosheets. Surface ligands can also induce strain or change the bond lengths of the silicon framework, thus influencing the underlying optoelectronic properties.[117] In addition, without proper surface-termination, silicanes are extremely prone to oxidation due to the oxophilicity of silicon, the reactivity of Si-H and the high surface area that the material exhibits. As such, silicanes are frequently modified with organic groups after synthesis to protect the material from degradation (**Figure 2.2–3**).[149] The introduction of functional groups can also enhance the interaction of the material with its surroundings, which leads to enhanced properties or increased device performance.[150, 149] Since the synthesis of silicane results in a Si-H surface, many of the functionalization methods are based on parallels made with other Si-H terminated materials, especially other Si(111) H-terminated surfaces.[51] Hydrosilylation is the most commonly used and a versatile and straightforward approach, which has been extensively developed for silicanes with a variety of initiators, including Lewis-acids,[151] heat,[152] AIBN,[149] iodonium salts,[70] and Pt catalysts.[153] Some other functionalization methods include the formation of Si-N bonds through amination[153] or the use of Grignard reagents.[122] Unfortunately, none of these methods are able to produce complete coverage of the nanosheet surface, with Si-H bonds as well as oxidation still remaining. This may be one of the reasons why no changes in optoelectronic behavior have been reported. One of the only reports with almost complete surface coverage is shown for the related 2D material germanane, where the authors exfoliated the germanium nanosheets from $CaGe_2$ with MeI instead of HCl. In this case an increased band-gap was observed.[154]

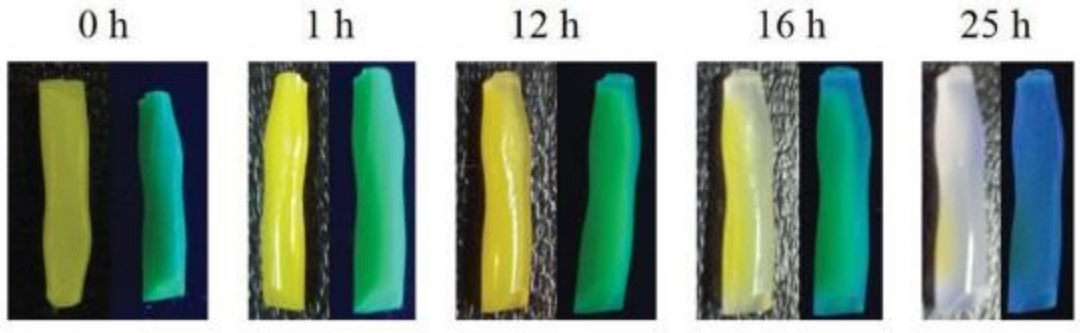

Figure 2.2–3. UV degradation of a silicon nanosheet polystyrene composite after prolonged exposure. Reprinted with permission from(1) Lyuleeva, A.; Helbich, T.; Rieger, B.; Lugli, P. Polymer-silicon nanosheet composites: bridging the way to optoelectronic applications. *J. Phys. D: Appl. Phys.* **2017**, *50* (13), 135106. Copyright (2021) Jon Wiley & Sons.

2.2.4 Applications of Silicon Nanosheets

The applications of silicon nanosheets remain limited to prototypes and to proof of concepts. The aforementioned silicene has been used to build a transistor, establishing the possibility of fabricating silicene on-chip devices.[155] With the chemical tunability of silicane, different surface groups can be used to fabricate different sensors[156] or transistors.[157] Functional groups improve the stability of the nanomaterial and allow the use of straightforward preparation techniques, such as solution-processing, spin-coating or extrusion.[149] It was even shown that the attached functional group can have a profound effect on device performance. Lyuleeva, Holzmueller and coworkers found that in a P3HT transistor, grafted hexylthiophene groups on SiNSs enhance the interaction between the matrix, leading to an overall increase in transistor performance.[150] Another notable example of surface group influence is shown by the photocurrent generation when conjugated groups are attached to the surface.[139]

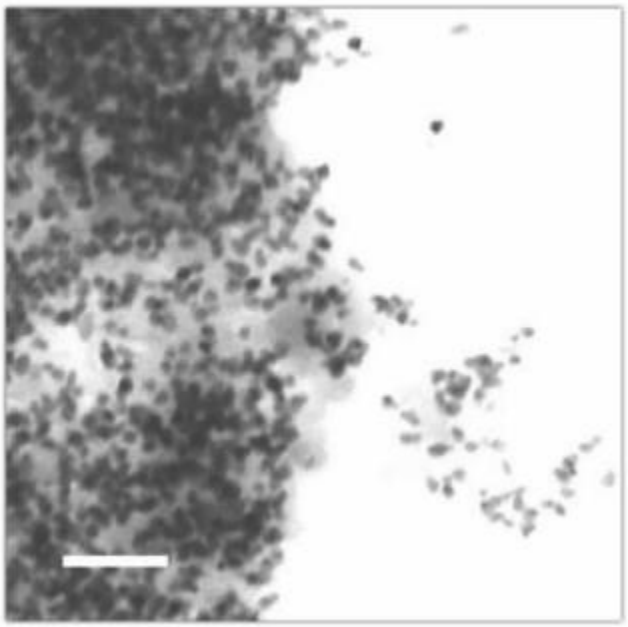

Figure 2.2–4. TEM image of Pd decorated silicon nanosheets used for the catalytic CO_2 reduction. Reprinted by permission from Springer Nature, Qian, C.; Sun, W.; Hung, D. L. H.; Qiu, C.; Makaremi, M.; Hari Kumar, S. G.; Wan, L.; Ghoussoub, M.; Wood, T. E.; Xia, M.; Tountas, A. A.; Li, Y. F.; Wang, L.; Dong, Y.; Gourevich, I.; Singh, C. V.; Ozin, G. A. Catalytic CO_2 reduction by palladium-decorated silicon–hydride nanosheets. *Nat Catal* **2019**, *2* (1), 46–54. Copyright 2021.

More recently, silicon nanosheets have garnered interest in catalytic applications. The large surface area can increase reaction efficiency and provides a platform as a high-surface area substrate. The reduction potential of the Si-H surface even allows for a simple synthesis of metal-decorated nanosheets, that have shown promise in CO_2 reduction and could prove useful in many other catalytic applications (**Figure 2.2–4**).[158, 159] The SiNSs act as a hydrogen-

donor/reductant as well as a solution-suspendable solid-state substrate providing the surface for reactions to occur. The high surface area of the SiNSs as well as the high affinity of silicon for lithium ions has also made them a contender for battery materials.[160–162] The detrimental volume-expansion of silicon when combined with lithium is addressed by synthesizing hybrid materials of SiNSs with carbon, providing good capacities with increased cyclability.[163–165]

Even though silicon nanosheets were first discovered in the 19th century, research into their aspects as a nanomaterial and their related properties only gained significant attention over the recent years with the emergence of the carbon-equivalent graphene. The library of publications regarding silicon nanosheets is much smaller than that of other silicon-based nanomaterials, i.e. silicon nanocrystals and porous silicon. Regardless, silicon nanosheets show great promise as an optoelectronic material and prototypes have shown the viability of using silicon nanosheets in a variety of applications.

2.3 Janus Particles

While Janus particles were not part of the initial topic of this thesis, over time they became an integral part. As such, fundamental aspects of Janus particles are discussed in this chapter.

Janus particles are colloidal particles that exhibit different physical or chemical properties on different sides. Just like their molecular counterparts – amphiphiles – they are anisotropic. The term Janus particle was first used by Pierre-Gilles de Gennes in his Nobel prize lecture in 1991 and is a reference to the Roman god of duality, often depicted as having two faces.[166] Janus particles can be sub-divided into two different categories: compartmentalized and surface-modified Janus particles. Compartmentalized Janus particles are synthesized from the ground up, thus their composition is anisotropic, whereas surface-modified Janus particles start as isotropic particles and are rendered anisotropic on the surface through functionalization. The anisotropy gives Janus particles unique properties that are not observed in the isotropic counterparts; properties such as surface-activity, movement, and self-assembly, to name a few.[167–170] They are a promising class of materials with many potential applications including microelectronics[171] biological/medical applications,[172] sensors, coatings[173] and self-propelled carriers or probes.[174]

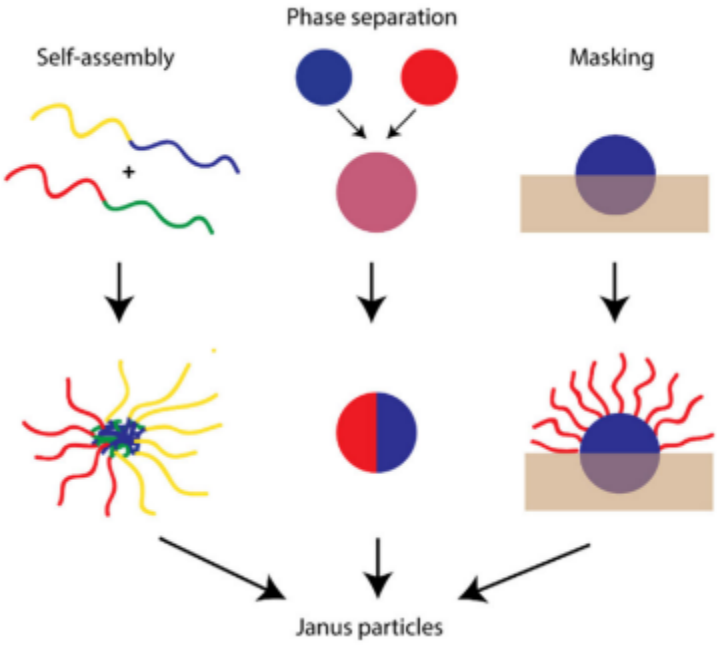

Figure 2.3–1. Illustration of the three main pathways to obtain Janus particles. Self-assembly of block copolymers (left), phase separation (middle) and masking (right). Reprinted by permission from Springer Nature, Poggi, E.; Gohy, J.-F. Janus particles: From synthesis to application. *Colloid Polym Sci* **2017**, *295* (11), 2083–2108. Copyright 2021.

2.3.1 Synthesis of Janus Particles

There are three main strategies to synthesize Janus nanoparticles: self-assembly, masking and phase separation (**Figure 2.3–1**).[175] While self-assembly and phase separation result in compartmentalized Janus particles, masking produces surface-anisotropic particles.

2.3.1.1 Compartmentalized Particles

Because the focus of this work lies upon surface functionalization, the synthetic strategies of compartmentalized Janus particles are only touched upon briefly. For comprehensive reviews on the topic refer to refs [176, 177, 175, 178].

The main strategy to obtain compartmentalized is to combine two immiscible substances and subsequently induce their phase separation to create an anisotropic particle (**Figure 2.3–1**). One of the simplest methods is to combine two different homopolymers in an emulsion of organic solvent and water. Slow evaporation of the solvent then causes the phase separation of the polymers in the droplet, forming asymmetric homopolymer domains inside the micrometer-sized particle.[179] Unfortunately, this method is somewhat unpredictable as it is strongly dependent on the reaction conditions, chosen polymers, and additives, such as surfactants. Techniques that rely on physical forces instead of chemically induced arrangements are co-jetting techniques, such as microfluidic co-flow[180] and

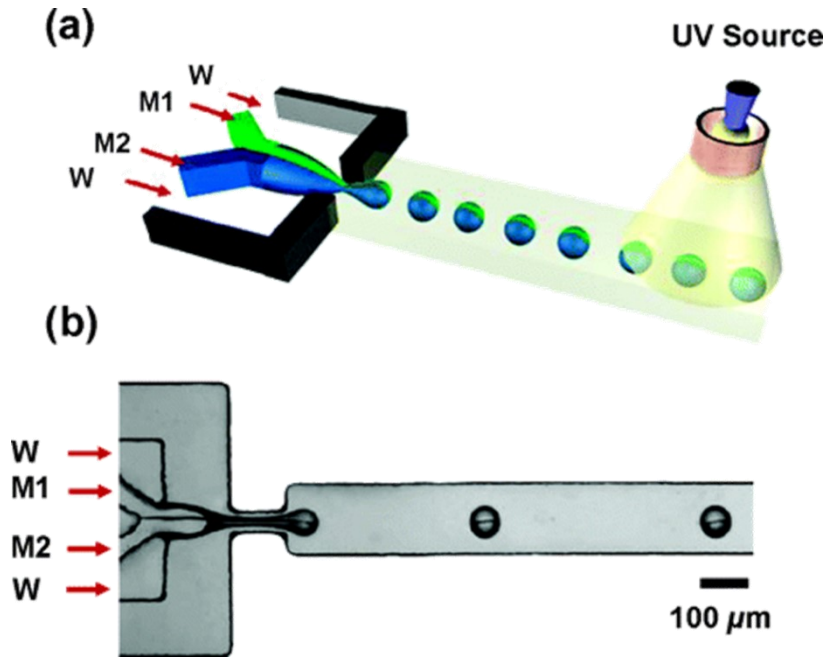

Figure 2.3–2. (a) Schematic of generation of Janus droplets from immiscible monomers M1 and M2, emulsified in an aqueous solution of W. The droplets are irradiated with UV light in the downstream channel. (b) Optical microscopy image of formation of Janus droplets. Reprinted with permission from Nie, Z.; Li, W.; Seo, M.; Xu, S.; Kumacheva, E. Janus and ternary particles generated by microfluidic synthesis: design, synthesis, and self-assembly. *J. Am. Chem. Soc.* **2006**, *128* (29), 9408–9412. Copyright (2021) American Chemical Society.

electrohydrodynamic co-jetting.[181] By combining streams of two different substances, single emulsion droplets are formed which are then solidified through polymerization or cross-linking, producing large quantities of micrometer-sized Janus particles (**Figure 2.3–2**).

A different approach, that is also able to produce smaller sized Janus particles (sub 5 nm) is the selective nucleation or seeded growth strategy. Using this method various inorganic Janus particles with different combinations can be synthesized, such as metal/metal oxide, metal/ metal sulfide or hetero-dimer CTVL001c13efb9cb81e4fcfb762afd87ebbea26[182][182][183, 184, 182] Soft Janus particles, i.e. comprising two different polymers, can also be realized in this fashion: first a polymer seed particle is synthesized – usually through emulsion polymerization – then it is swollen by a different monomer causing phase separation, whereupon the second monomer is polymerized forming a second lobe on the particle.[185–187] Through selection of appropriate monomers, functionalities can be introduced that allow subsequent modification.[188, 189] This versatile method is able to produce soft Janus particles with sizes ranging from the sub 100 nm region up to few micrometers. Hybrid systems of inorganic and polymer components are also easily synthesized using seeded growth.[190] Through combination of polystyrene (PS) beads on colloidal gold, Ohnuma and co-workers were able to realize asymmetric gold-PS particles, with each PS bead only containing a single gold particle on its surface (**Figure 2.3–3**).[191]

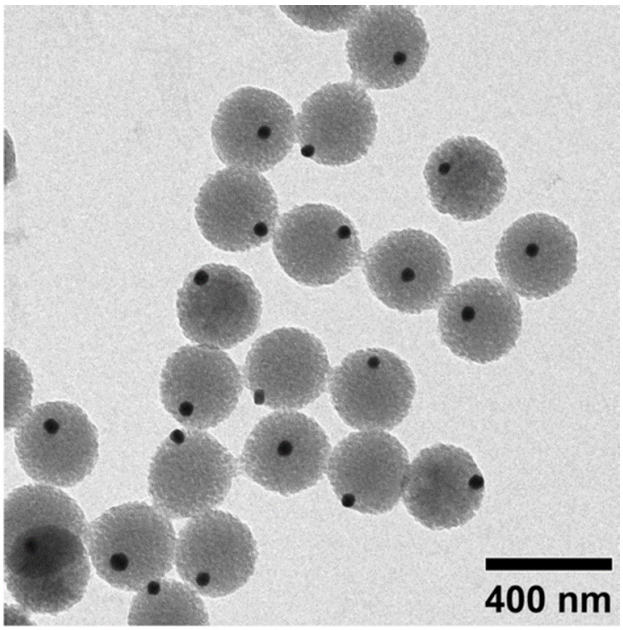

Figure 2.3–3. TEM image of gold/polystyrene Janus particles. Reprinted with permission from Ohnuma, A.; Cho, E. C.; Camargo, P. H. C.; Au, L.; Ohtani, B.; Xia, Y. A facile synthesis of asymmetric hybrid colloidal particles. *J. Am. Chem. Soc.* **2009**, *131* (4), 1352–1353. Copyright (2021) American Chemical Society.

For soft Janus particles the above techniques can almost exclusively produce sizes in the micrometer regime. To produce them on the nanometer-scale, self-assembly is used. With appropriate compositions, block copolymers with segments displaying different properties can self-assemble into Janus nanoparticles.[192, 174] Parameters such as molecular weight, temperature, concentration and pH all have effects on the self-assembly behavior; on the one hand allowing precise tuning of the resulting nanoparticle, on the other complicating the process. Once the Janus structure is formed, it needs to be "locked" in place, since self-disassembly is also possible.[193, 194] Typically, tri-block polymers are used because of their unique bulk morphology, which even allow the synthesis of different Janus superstructures, including Janus particles,[193] Janus cylinders[195] and Janus discs (**Figure 2.3–4**).[194]

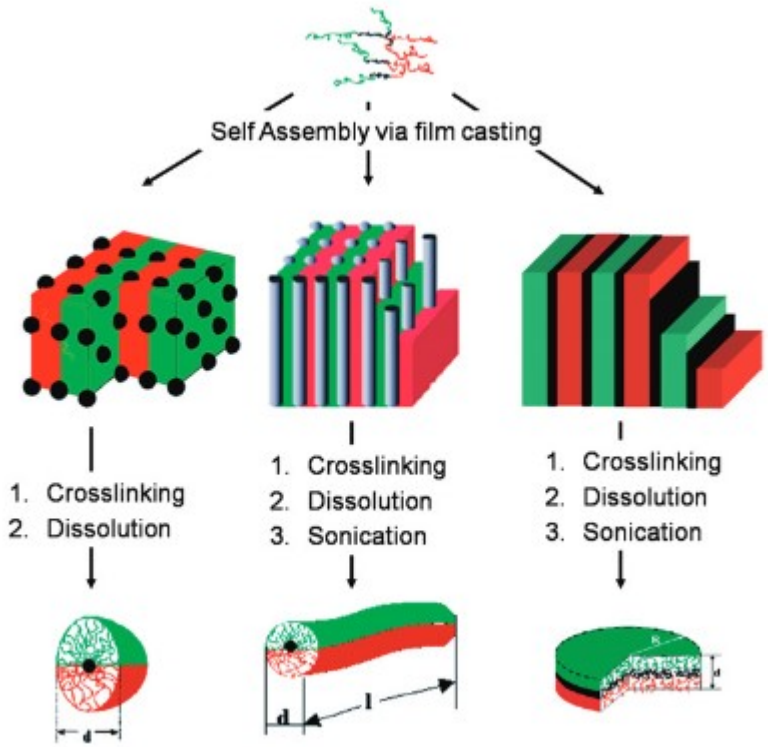

Figure 2.3–4. Different Janus morphologies obtainable through the self-assembly and cross-linking of different terpolymers. Used with permission of Royal Society of Chemistry, from Walther, A.; Müller, A. H. E. Janus particles. *Soft Matter* **2008**, *4* (4), 663–668. Copyright 2021; permission conveyed through Copyright Clearance Center, Inc.

2.3.1.2 Surface-modified Janus Particles

Next to compartmentalized Janus particles, surface-modified Janus particles exhibit similar properties, as the surface dictates most of the chemical and/or interaction behavior of colloidal particles. The advantage of anisotropic surface-modification techniques is the possibility to render any existing isotropic (nano)particle anisotropic.

The most straightforward strategy to obtain surface-modified Janus particles is to mask or protect one side of a particle and functionalize the other. The simplest approach would be to immobilize an isotropic particle on an interface or substrate and functionalize the exposed side. “Janus beads” were first reported in the 1980s by *Veyssié* and coworkers who used the oil/water interface to render one side of commercially available glass beads hydrophobic and the other hydrophilic.[196] In general, interfaces of two phases, such as air-liquid (Langmuir-Blodgett),[197] liquid-liquid,[198] air-solid,[199] and solid-liquid,[200] are able to produce a large variety of Janus particles of different sizes and surface compositions. Especially the deposition of particles on flat solid substrates offers many possibilities due to diverse deposition techniques (physisorption,[201] covalent attachment,[202] embedding[203]), the variety of (nano)particles that can be deposited (silica,[204] metallic,[205] polymers[206]) and the variety of employable functionalization techniques.[175]

These interface techniques can reliably render Janus particles with different sizes, but suffer from low yield, as only a single layer of particles can be functionalized at a time, thus being limited by the amount of available surface area. This problem was addressed through the use of emulsions, which vastly increase the amount of available surface.[167, 207] Specifically, *Pickering emulsions* – emulsions stabilized by solid particles – were first utilized by Granick *et al.* to produce large quantities of Janus silica particles.[200] By emulsifying molten wax in water, silica particles adsorbed at the interface and were locked in place by solidifying the wax at lower temperatures, forming so-called colloidosomes (**Figure 2.3–5**). This procedure has multiple advantages. First it allows the use of filtration as a recovery technique and second, the solidified wax locks the particles in place, preventing rotation during the modification step – a crucial measure to avoid homogenization. Dissolution of the wax in an organic solvent then allows subsequent modification of the previously “protected” side of the particles. Addressing some drawbacks of the solution-based modifications, the authors extended this concept to use chemical vapor deposition to modify the silica surface, improving the overall yield and quality of Janus particles.[208] Other authors later used the wax emulsion technique to produce Janus particles of different compositions, such as titania[209] and Iron oxide particles[210].

While Pickering emulsions – and emulsions in general – are able to produce large quantities of Janus particles, the technique suffers from a few drawbacks. The most obvious one is that the to-be-functionalized particles are exposed to water. If the desired particles are sensitive to oxidation or hydrolysis, this technique is not viable. A further limitation to the number of viable particles, is the actual formation of the Pickering emulsion, requiring that the particles’ surface energy be between that of the two interfaces.[211] Additionally, if the particles

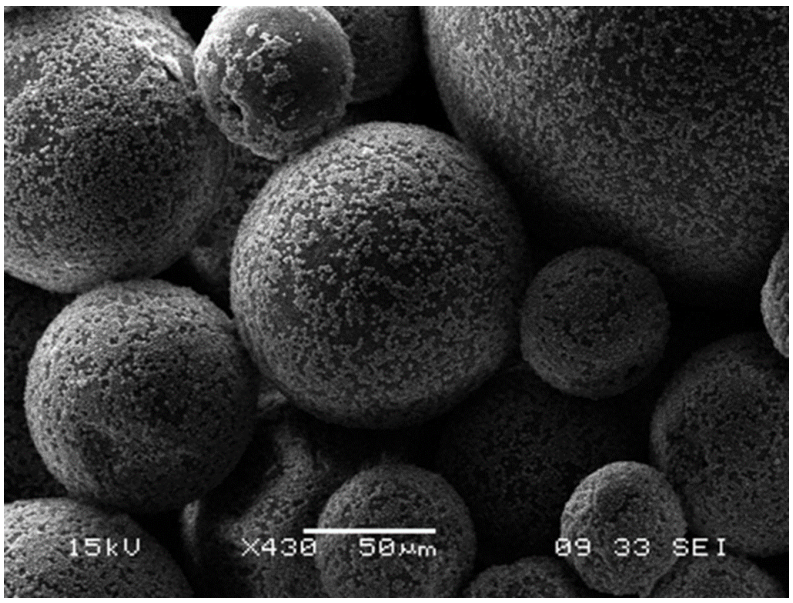

Figure 2.3–5. Colloidosome of silica particles on emulsified molten wax. Reprinted (adapted) with permission from Hong, L.; Jiang, S.; Granick, S. Simple method to produce Janus colloidal particles in large quantity. *Langmuir : the ACS journal of surfaces and colloids* **2006**, *22* (23), 9495–9499. Copyright (2021) American Chemical Society.

do not exhibit sufficient affinity to the interface, desorption and rotation can occur. This is not always the case, and can be addressed with the use of surfactants.[212] The method is also limited in the number of possible modification reactions, either due to solvent restrictions, the necessity of volatile reagents (in the CVD method) and most significantly, due to the requirement of low temperatures to prevent melting of the wax. Local heating in exothermic reactions also needs to be considered. While not as consequential, the diffusion of the modifying reagents in the two phases can also influence the quality of the resulting Janus particles.[177]

Using the Pickering emulsion in wax technique to produce particles in the nanoscale (sub 10 nm) is also uniquely challenging. Not only do the previously mentioned drawbacks increase in significance with smaller particle size, but because nanoparticles are so small, wrinkles in the wax droplet can cause difficulties. The adsorption energy of the small nanoparticles coincides closely with thermal energy, which can cause particle rotation and most notably, assembly of particle multi-layers.[176] This is detrimental to the technique as this would result in a mixture of anisotropic and isotropic particles once they are released from the interface. There are some methods to address this challenge. In what the authors call a “limited coalescence process”, they were able to adjust the hydrophobicity of sub 100 nm silica particles by using CTAB as a surfactant. Depending on the amount used, the authors were even able to adjust the penetration depth of the silica particles, thus allowing precise control over the Janus balance.[213] Other known practices to form stable Pickering emulsions with

nanoparticles include the physisorption of THF,[210] the use of ATRP[214] or using thermal shock.[215]

The liquid-solid interface, mentioned at the beginning of this chapter, is a much more viable approach for the synthesis of Janus particles in the nanoscale. By depositing (or forming) a monolayer of the desired nanoparticles on a solid substrate, many more functionalization approaches are imaginable, such as vapor deposition, solution chemistry, plasma etching, etc. and isn't limited by the choice of solvents and reactants or the necessity of surfactants, as is the case for Pickering emulsions. It should also be possible to modify both sides of the particle by releasing the nanoparticles after the first functionalization, thus exposing the other side. One such method was achieved by using a glass substrate to deposit an array of silica nanospheres and subsequently evaporate a metal film on the exposed sides.[216]

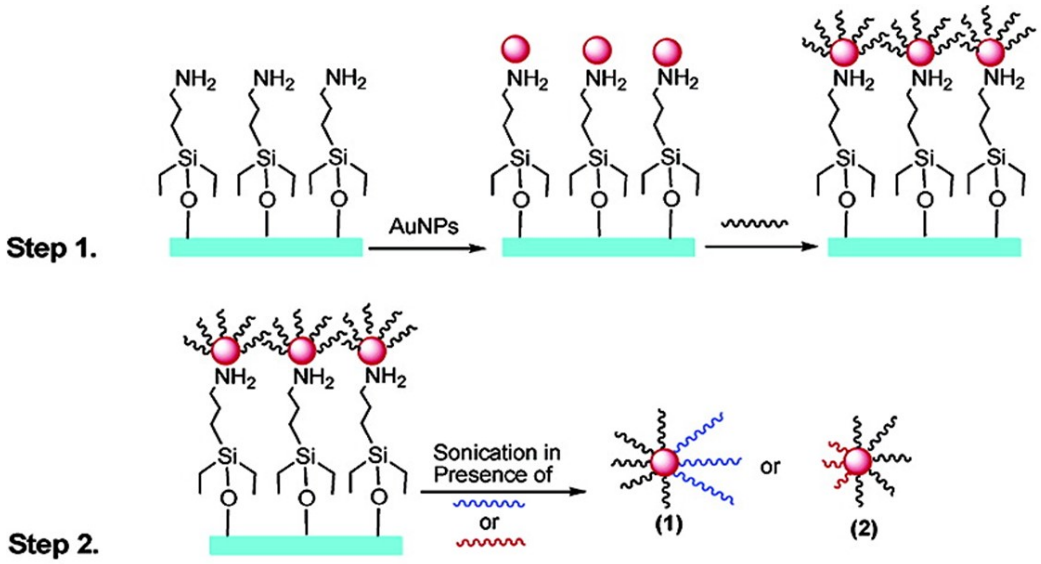

Figure 2.3–6. Synthesis of Janus gold nanoparticles on a silanized glass surface. Adapted with permission from Sardar, R.; Heap, T. B.; Shumaker-Parry, J. S. Versatile solid phase synthesis of gold nanoparticle dimers using an asymmetric functionalization approach. *J. Am. Chem. Soc.* **2007**, (*1297*), 5356–5357. Copyright (2021) American Chemical Society.

The obvious limitation of this method is the formation of the nanoparticles' monolayer on the substrate, which can only be achieved with clever design, due to the possible formation of multi-layers. With large enough particles, careful evaporation of the solvent suffices but for nanoparticles, selective chemical bonding to the substrate is usually used, such as thiol groups for gold nanoparticles or acid groups for noble metal nanoparticles. For example, a silanized glass surface with appropriate functional groups is able to immobilize metal nanoparticles for subsequent asymmetric functionalization (**Figure 2.3–6**).[217]

The problem with these large flat substrates is the inherently small surface available for functionalization. In an ingenious approach, the group of Li used micrometer-sized polymer single crystals suspended in solution as a “quasi-solid” interface.[218, 219] This vastly increases the available surface area and thus possible yield of Janus nanoparticles. Briefly summarized, end-group functionalized polymer chains are crystallized to form a micrometer-sized lamella, exposing the end groups to the crystal surface (**Figure 2.3–7**). Nanoparticles are then immobilized onto the surface through physical or chemical adsorption and then functionalized using solution chemistry. The polymer single crystal can then be dissolved thus releasing the nanoparticles and forming the second functional group. By adapting the end groups of the polymer, the adherence to different nanoparticles can be adjusted. The authors were thus able to synthesize a variety of Janus nanoparticles, including magnetic nanoparticles[220], AuNP of different sizes[221] and silica nanoparticles[220].

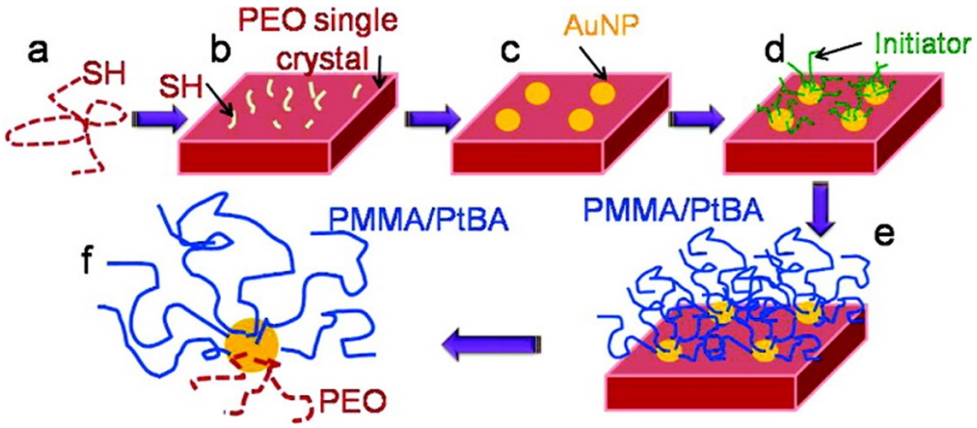

Figure 2.3–7. Polymer functionalized Janus AuNPs by depositing on a polymer single crystal and subsequent dissolution. Reprinted with permission from Wang, B.; Li, B.; Zhao, B.; Li, C. Y. Amphiphilic Janus gold nanoparticles via combining "solid-state grafting-to" and "grafting-from" methods. *Journal of the American Chemical Society* **2008**, *130* (35), 11594–11595. Copyright (2021) American Chemical Society.

While this polymer single crystal approach solves many of the previously mentioned problems, its strength is also its weakness. Since the polymer single crystals form the second functional group of the particle, they cannot be adapted to the desired end-properties but rather need to be adapted to the reaction protocol (functional end-group, solubility, single-crystal formation). Therefore, at least one of the functional groups is predetermined. In addition, because it is imperative that the polymer single crystal not dissolve during the deposition, the other functional group must usually be of competing solubility. Therefore, two functional groups with similar functionality (such as long organic groups) cannot be introduced simultaneously.

2.3.2 Proving Anisotropy

When it comes to proving the anisotropic character of particles, the process is not as trivial as demonstrating two different compositions or two different surface groups. While techniques such as FTIR, TGA, XPS, EDX, elemental analysis etc. are great at identifying different surface groups, they only show an average of the whole sample and cannot distinguish between two differently functionalized sides of a particle.

For colloidal Janus particles, imaging has become the norm. Secondary electron microscopy (SEM), transmission electron microscopy (TEM) and atomic force microscopy (AFM) are great at visually demonstrating composition, as the forces used to translate the measurement into an image correlate to the composition of the sample. While electron microscopy images contrast the electron density of the imaged elements, AFM contrasts the difference in adhesion forces. For compartmentalized Janus particles, SEM and TEM are straightforward tools, as long as the elements have differing contrasts. In such images it is easy to see the two different halves or "patches" of other elements (**Figure 2.3–8a**).[222, 201] For non-inorganic Janus (nano)particles, i.e. polymeric ones, AFM is a good tool, because TEM and SEM cannot differentiate between different polymers, since they are mainly composed of carbon. Thus there is no visible contrast difference. With AFM the image contrast depends on the adhesion forces and thus different polymers can show different AFM contrast.

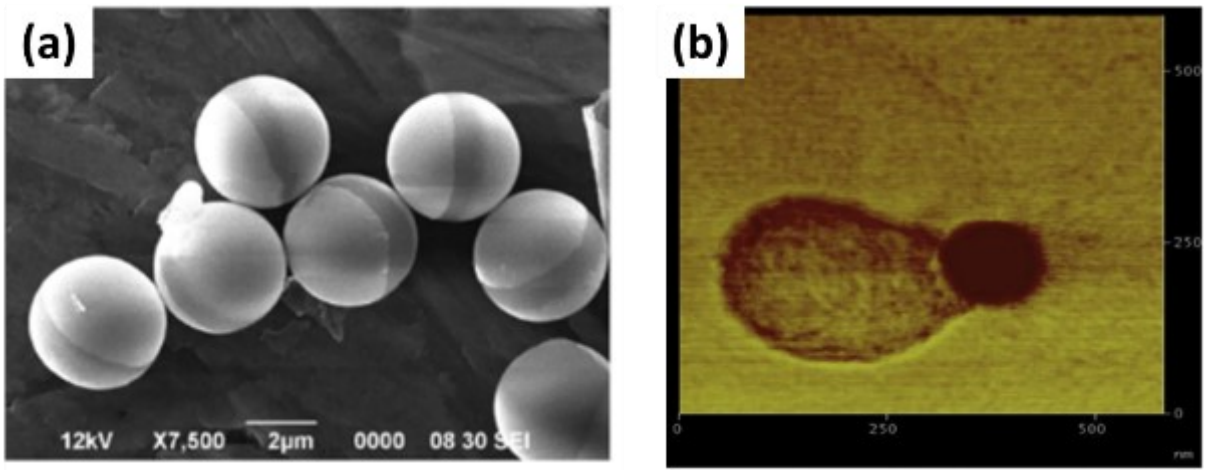

Figure 2.3–8. Images depicting proof of anisotropy through (a) SEM image of inorganic Janus particles showing different contrasts and (b) polymer lobe grown from one side of a Janus particle. Reprinted with permission from Ye, S.; Carroll, R. L. Design and fabrication of bimetallic colloidal "Janus" particles. *ACS applied materials & interfaces* **2010**, *2* (3), 616–620 and Mendez-Gonzalez, D.; Alonso-Cristobal, P.; Lopez-Cabarcos, E.; Rubio-Retama, J. Multi-responsive hybrid Janus nanoparticles: Surface functionalization through solvent physisorption. *European Polymer Journal* **2016**, *75*, 363–370. Copyright (2021) American Chemical Society and copyright (2021) with permission from Elsevier.

The task of proving anisotropy becomes more challenging when dealing with surface-anisotropic Janus particles. TEM and SEM images of lone Janus particles will not show any clear difference to isotropic particles, due to the uniform composition of the particles with the only differences present in the surface groups. On the scale of the particle, these surface group differences are minute and cannot be picked up via electron microscopy. Therefore, many reports rely on purposefully inducing a strong difference between the two surface groups. For instance, if one of the surface groups is a polymer, it is possible to deliberately increase the polymer size (e.g. by extending polymerization time), creating a large polymer-lobe that can be imaged with AFM (**Figure 2.3–8**).[210] Other strategies include the attachment of fluorescent dyes that can be used to illuminate only one side of the Janus particle.[200]

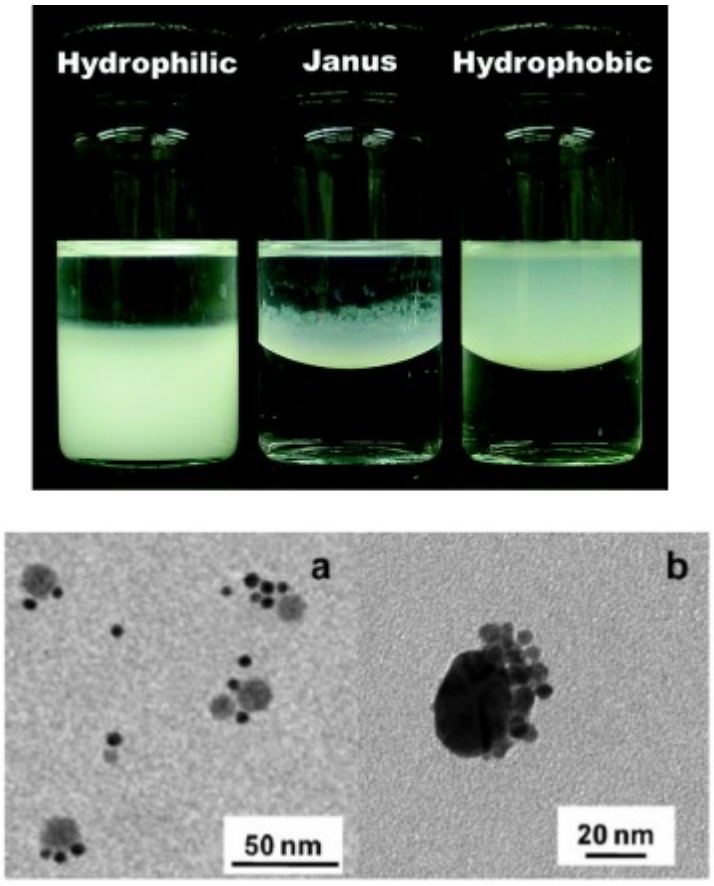

Figure 2.3–9. Examples of techniques used to prove anisotropy of surface-anisotropic Janus particles. Aggregation behavior of amphiphilic particles (top) or nanoparticle decoration (bottom). Reprinted with permission from Jiang, S.; Schultz, M. J.; Chen, Q.; Moore, J. S.; Granick, S. Solvent-free synthesis of Janus colloidal particles. *Langmuir : the ACS journal of surfaces and colloids* **2008**, *24* (18), 10073–10077 and Wang, B.; Li, B.; Ferrier, R. C. M.; Li, C. Y. Polymer single crystal templated janus nanoparticles. *Macromolecular rapid communications* **2010**, *31* (2), 169–175. Copyright (2021) with permission by American Chemical Society and Jon Wiley & Sons.

However, these methods are mostly limited to Janus particles with sizes over 100 nm. For truly nanoscale Janus nanoparticles more indirect strategies are used. For example, if an appropriate functional group is present the Janus nanoparticles are decorated with metal nanoparticles, increasing the contrast in electron microscopy images and demonstrating the location of the complementary functional groups.[167, 213] By looking at the pattern of assembly, the Janus nature can be inferred (**Figure 2.3–9** bottom). When the Janus nanoparticles are amphiphilic many authors resort to looking at the aggregation of the nanoparticles at the interface of two immiscible solvents. While isotropic particles prefer their respective solvents, amphiphilic ones will preferentially arrange at the interface (**Figure 2.3–9**).[167, 208, 215, 213] Taking this approach one step further, some authors use the formation of micelles[209] and even the micelle-dependent UV/Vis absorptions as evidence for Janus nanoparticles.[214, 205] If the appropriate functional end-group can be attached to one side of the Janus nanoparticle, cluster formation with isotropic particles can be directly observed with TEM.[221, 218]

In general, when it comes to nanoscale Janus particles, the surface anisotropy is often not directly observed, but rather is inferred from their chemical or physical behavior. It is a prime example of the difficulties and challenges associated with nanomaterial characterization.

3 Motivation and Guideline

At the beginning of this thesis no single tangible goal was conceptualized. Rather the topic of the thesis was to find new and improved methods for the *Functionalization of Zero- and Two-Dimensional Silicon Nanomaterials* (previous title). Only over time and with the success and failures of various research projects did the thesis finally develop the titular topic *— Two Sides of the Same Particle: Toward the Synthesis of Two-Sided "Janus" Silicon Nanocrystals and other Functionalization Methods.*

As outlined in detail in the previous chapters, the surface chemistry and surface groups of the zero- and two-dimensional nanomaterials play a crucial role in guiding their properties and applications. While their remarkable inherent properties, such as the tunable band gap, are due to the nanostructured nature of the material, surface functionalization can influence or enhance these properties and give rise to new applications. Furthermore, silicon nanomaterials without functionalization are incredibly susceptible to oxidation, hydrolysis and photodegradation. In light of these insights, the surface chemistry of these unique silicon nanomaterials is one of their fundamental research aspects and was chosen as the focus point of this thesis.

Because the surface chemistry of silicon nanomaterials constitutes such a broad range of topics and research possibilities, this thesis is subdivided into smaller research projects. Each project features an introduction to the topic, research results and their discussion, as well as a summary and outlook of the results and insights gained throughout the project. The projects are described in chronological order of their conception, but much of the work was conducted in parallel. A final conclusion at the end of this work gives a brief summary of the various research projects, but more details are found within each project chapter.

The topics covered in this thesis start with a simple research project developing a new initiator (*trityl salts*) for hydrosilylation reactions and moved from there to finding new methods of forming more complex hetero-atom linkages with the silicon surface (*silanes*, *siliranes*, *dichalcogenides*). Finally, in a serendipitous discovery during a previous research project, the thesis culminates in the synthesis of the very first *surface-anisotropic "Janus" silicon nanocrystals.*

4 Projects

4.1 Trityl Salt Initiated Hydrosilylation

4.1.1 Introduction

As outlined in chapter 2.1: *Silicon Nanocrystals and Silicon Quantum Dots*, the functionalization of SiNCs is one of the main focus areas of silicon nanomaterial research. Here, finding new and improved methods for introducing functional groups offers the possibility of discovering new properties through introduction of yet unknown functional groups or improving upon the existing functionalization methods, increasing surface coverage or offering an extended substrate scope.[25]

Salts of the triphenylmethyl cation are known to active the Si-H bond in molecular silanes through the abstraction of the hydride group, forming what is known as a silylium ion.[223] Compared to the carbon counterpart, the carbenium ion, the silylium ion is not able to stabilize the resulting positive charge as well and thus, is much more reactive.[224] Any present impurities, solvents or even the counterions of the trityl salt are susceptible to electrophilic attack by the silylium ion.[224] Many functionalization methods concerning silicon surfaces imply that the mechanism proceeds through radical cation intermediates, either through activation by an initiation agent, such as AIBN or a diazonium salt,[66, 69] or through the generation of a reactive exciton through UV-irradiation.[62, 63] Because of their ability to abstract hydrides, it is reasonable to assume that trityl salts are able to produce the reactive cation intermediate on the Si-H surface of SiNCs and subsequently react with a variety of substrates. Such a behavior was shown for molecular silanes[225] and in fact, Buriak and coworkers were able to show exactly such a behavior on porous silicon, showing that the triphenyl cation can be used to initiate the hydrosilylation of a variety of alkenes.[226]

In a similar approach, this concept is extended to the hydrosilylation with silicon nanocrystals. Trityl salts offer the advantages of commercial availability, solubility in non-halogenated organic solvents and a potential for good functional group tolerance, due to the formation of an intermediate cation instead of a cation radical. Previous functionalization methods developed within our group – the diazonium salt- and diaryliodonium salt-induced hydrosilylation – were not able to functionalize SiNCs with substrates containing acidic protons, i.e. alcohols and carboxylic acids.[70, 69] The stability of trityl salts against acids could allow their functionalization using this approach.

4.1.2 Results and Discussion

4.1.2.1 Proof of Concept

The initial reaction to examine the proof of concept for the hydrosilylation with SiNCs used 1-dodecene as the model substrate and trityl hexafluorophosphate as the initiator. The reaction was carried out at room temperature for approximately two hours. The initially turbid dispersion turned clear after 1 hour; a qualitative indicator of successful functional group attachment.[60] Work-up of the resulting suspension was carried out through multiple precipitation and centrifugation cycles. Briefly, the suspension of functionalized SiNCs was precipitated in a 1:1 mixture of MeOH and EtOH. The suspension is centrifuged, and the residue dispersed in a minimal amount of toluene. After precipitation via addition of an anti-solvent (MeOH, EtOH) the residue is re-dispersed and the cycle repeated two more times to yield purified dodecyl-functionalized SiNCs.

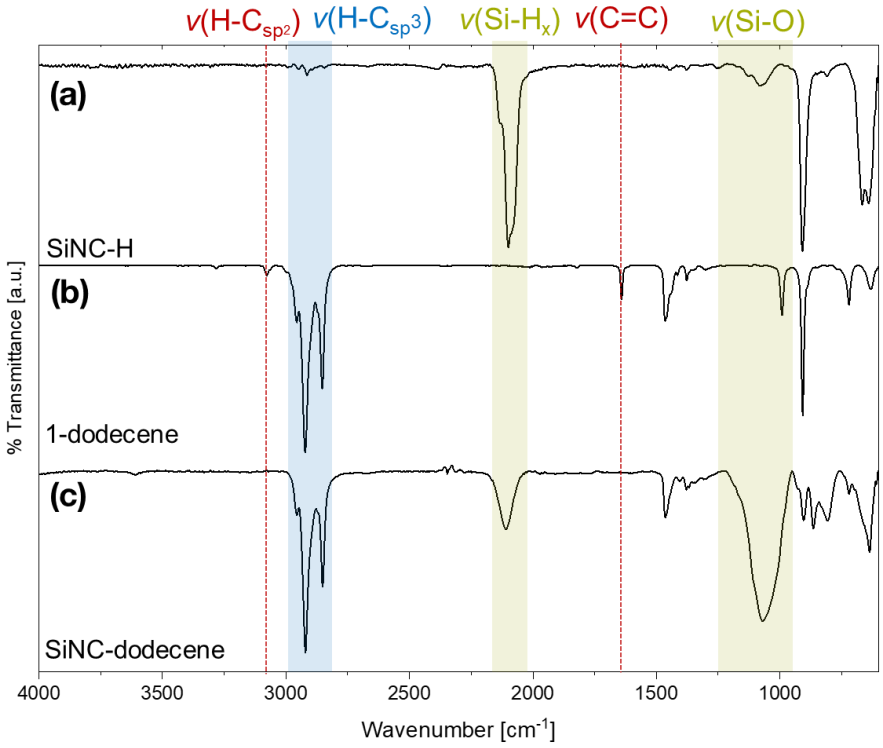

Figure 4.1–1. FTIR spectra of etched SiNCs (a), 1-dodecene (b) and SiNC-$C_{12}H_{25}$ obtained through trityl-initiated hydrosilylation of 1-dodecene (c)

The functionalization is confirmed with FTIR spectroscopy (**Figure 4.1–1**). In comparison with the original etched SiNCs (**Figure 4.1–1a**) the final sample exhibits a reduced ν(Si-H) band at around 2100 cm^{-1}, indicating its consumption during the reaction (**Figure 4.1–1c**). Spectral signatures corresponding to the dodecyl functionality are also clearly visible, exemplified by the strong ν(H-C$_{sp^3}$) and δ(H-C$_{sp^3}$) bands centered around 2900 cm^{-1} and 1460 cm^{-1}, respectively. Bands corresponding to unreacted 1-dodecene (i.e. ν(H-C$_{sp^2}$)

and ν(C=C), **Figure 4.1–1b**) are not observable after the functionalization, meaning that the substrate was consumed during the reaction and removed during purification. As is the case with most hydrosilylations of SiNCs, the obtained product also shows signs of oxidation (ν(Si-O), ~1100 cm^{-1}), likely arising from oxidation during the work-up procedure and lack of optimization. The observations during the reaction and the final IR analysis of the resulting product lead to the conclusion that trityl hexafluorophosphate does lead to functionalization, thus showing the viability of this method.

4.1.2.2 Optimizing Reaction Conditions

After establishing the proof of concept, the reaction with 1-dodecene was used to optimize the reaction conditions by comparing the mass losses observed in thermogravimetric analysis (TGA). TGA can give valuable insight on the degree of surface coverage by the organic groups, as these will decompose before the inorganic core of the SiNCs. While it does not determine absolute values of surface coverage, the relative comparison between samples is helpful to determine the conditions that yield the highest degree of functionalization. For each optimized parameter, a series of hydrosilylations were conducted, e.g. hydrosilylations with varying reaction times. For each of these series, the SiNCs were obtained from a single SiNC/SiO_2 composite and from the same HF acid etching batch. This was conducted in order to ensure a good comparability between the samples, the only differences being the one specified parameter.

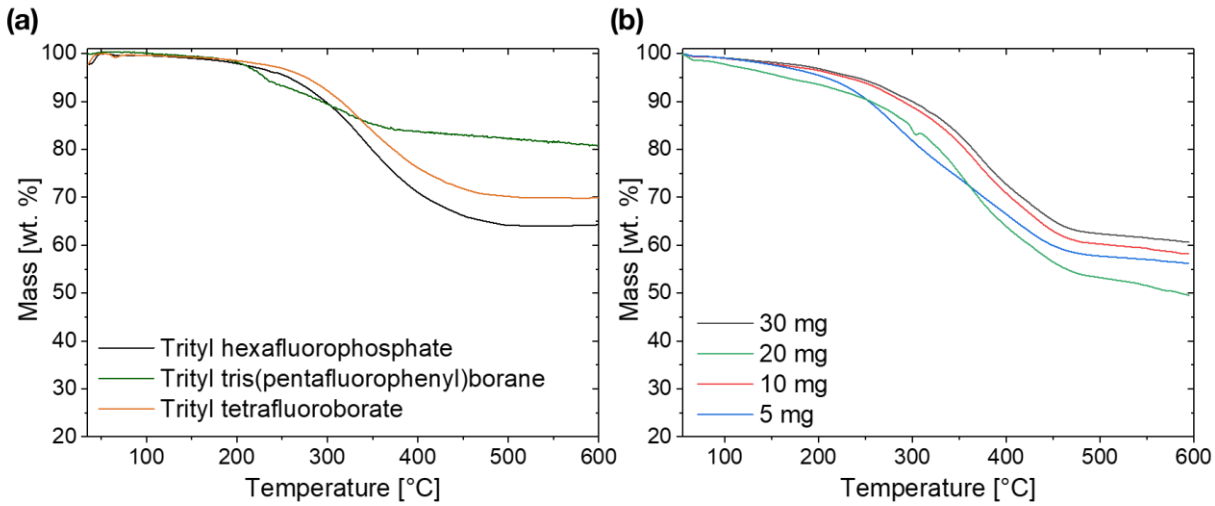

Figure 4.1–2. TGA traces of SiNC-$C_{12}H_{25}$ obtained through hydrosilylation with different (a) trityl salts and (b) with varying amounts of trityl hexafluorophosphate.

The impact that different counter anions have on the functionalization was explored first. From **Figure 4.1–2a** we see that trityl tris(pentafluorophenyl)borane (BCF) results in the lowest amount of surface coverage, while both trityl hexafluorophosphate and tetrafluoroborate only show a small difference of 5 % between each other. As such, trityl hexafluorophosphate was

chosen as the initiator for any further reactions. A series of experiments with varying amounts of the initiator was carried out and determined that an increased amount of initiator reaches a surface coverage maximum at about 10 mg, after which any more initiator leads to less overall coverage. Most likely, the additional initiator molecules are quench the reactive intermediate states during the reaction, resulting in less reaction with the desired substrate. The sweet spot of initiator, extracted from this data, is found to be 10 mg.

The choice of solvent was also considered. While unpolar high-boiling solvents such as toluene are generally preferred in SiNC hydrosilylation reactions, halogenated solvents are able to dissolve salts better. **Figure 4.1–3a** indicates that the reaction conducted in toluene results in higher surface coverage. As noted for molecular silane counterparts, the halogenated solvents react with the highly reactive trityl salt, lowering the amount of available initiator for the hydrosilylation and thus reducing the degree of functionalization.[224]

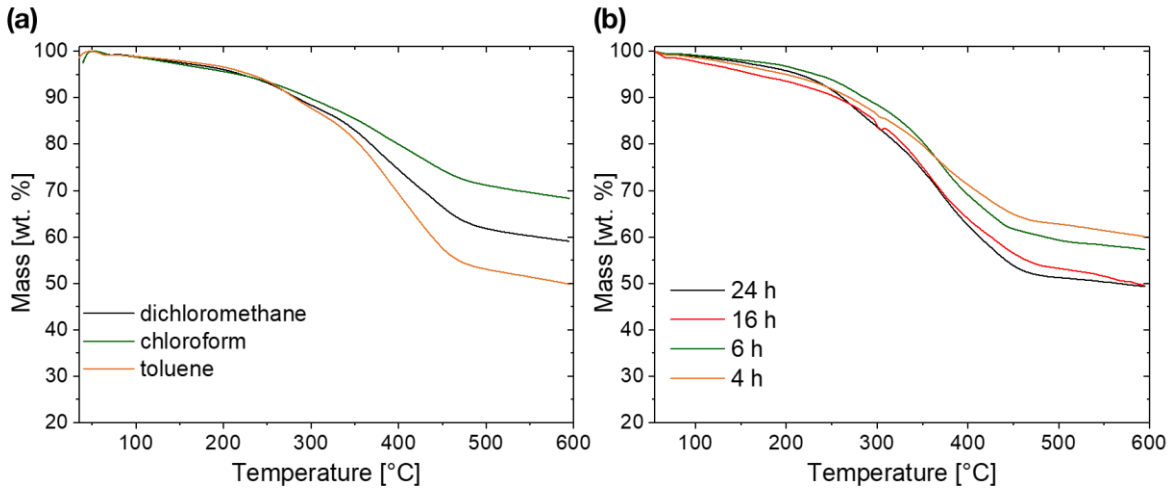

Figure 4.1–3. TGA traces of SiNC-$C_{12}H_{25}$ obtained through hydrosilylation with 1-dodecene using trityl hexafluorophosphate as the initiator in (a) different solvents and (b) with varying reaction times.

The most important metric to consider is reaction time. It was generally accepted with other hydrosilylation procedures that upon clearing of the turbid SiNC-dispersion, the reaction is considered complete. However, Kehrle *et al.* was able to demonstrate that the hydrosilylation takes considerably longer to reach maximum surface coverage, long after the suspension has turned clear.[60] This is the reason a clearing of the dispersion can only be regarded as a rough qualitative indicator for successful surface modification and not as an indicator for the completion of the reaction. Taking this into consideration, we performed the hydrosilylation of 1-dodecene with trityl hexafluorophosphate with varying reaction times ranging from 2 hours to 24 hours. Even though the dispersions turn clear after 1 hour, the TGA of the resulting products confirms that a prolonged reaction time leads to more surface coverage (**Figure 4.1–3b**). However, a maximum is reached after about 16 hours, after which

a continued reaction does not lead to more surface coverage. This is due to the increasing density of the organic layer on the SiNC surface, hindering the insertion of additional dodecyl groups. While the surface coverage does still increase slightly after 16 hours, the small difference does not warrant the extended reaction time, as this can have a negative effect on the final product, since there is more time for oxidation to occur.

Summarizing the results of this experimental series, the optimal reaction conditions for the hydrosilylation using trityl hexafluorophosphate as the initiator were found to be 10 mg of initiator with toluene as the solvent and a reaction time of 16 hours.

4.1.2.3 Substrate Scope

One of the key factors influencing the value of any given hydrosilylation method is the scope of possible substrates. For example, thermal hydrosilylation is only able to hydrosilylate high-boiling alkenes, but has a good functional group tolerance while diazonium- and iodonium initiated hydrosilylations are carried out in milder conditions, but have problems with substrates that have acidic protons, such as carboxyilic acids and alcohols, limiting their application.[69, 70] It is therefore vital to analyze the potential substrates that can be employed

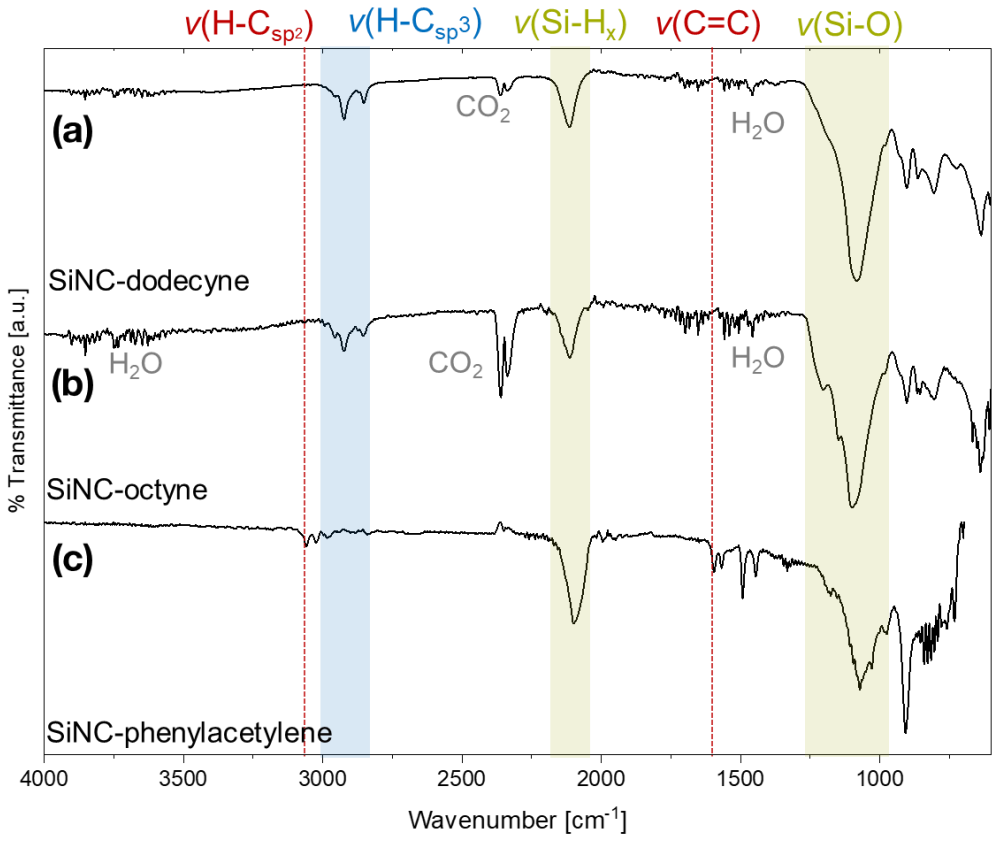

Figure 4.1–4. FTIR measurements of SiNCs functionalized with various alkynes: (a) 1-dodecyne, (b) 1-ocytne and (c) phenylacetylene. Due to atmosphere issues in the instrument, the infrared spectra exhibit bands corresponding to water and carbon dioxide.

in any given functionalization method. With the established reaction protocol in hand, various unsaturated substrates with different functional groups were screened. Among them alcohols, carboxylic acids, esters, acrylates, monomers of polymers and alkynes.

The triple bond containing substrates all did not show successful reactions (**Figure 4.1–4**). The dispersions did not turn clear and the corresponding infrared spectra do not indicate successful reactions. For both 1-dodecyne and 1-octyne functionalized SiNCs, the $\nu(H\text{-}C_{sp^3})$ bands are too weak when considering the long alkyl chains of the substrates. These two samples also do not exhibit any bands corresponding to the desired double bonds, i.e. $\nu(H\text{-}C_{sp^2})$ at 3050 cm^{-1} and $\nu(C{=}C)$ at 1605 cm^{-1}, which are expected if the triple bond were hydrosilylated. Phenylacetylene does show some characteristic double-bond-bands ($\nu(H\text{-}C_{sp^2})$, 3050 cm^{-1}; $\nu(C{=}C)$, 1605 cm^{-1}), however, taking the amount of double bonds of the substrate into account, more intense signals are expected. Furthermore, the lack of aromatic overtones ($\nu_{ov}(H\text{-}C_{Ar})$) between 2000 cm^{-1} and 1700 cm^{-1} indicates a low amount of phenyl rings in the SiNC sample. All samples exhibit significant oxidation, with the Si-O stretching band showing the highest intensity for all samples. Overall, the hydrosilylation of triple bonds using a trityl salt as an initiator, does not lead to any compelling results.

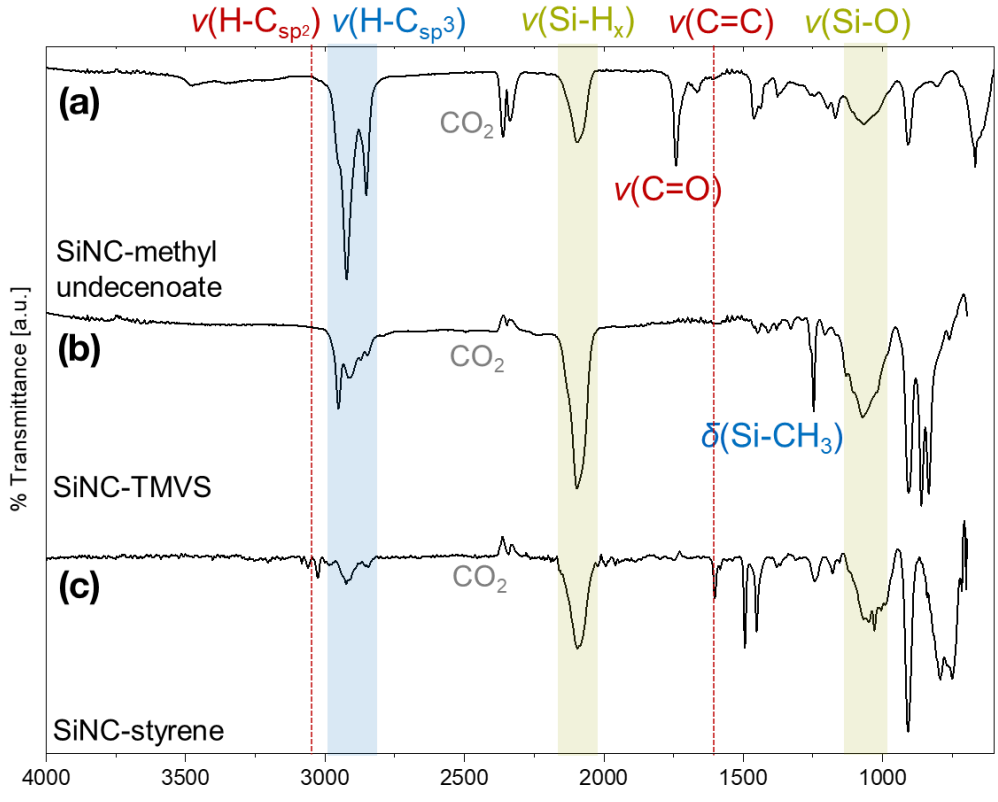

Figure 4.1–5. FTIR measurements of SiNCs functionalized with various alkenes: (a) methyl undecylenate, (b) trimethylvinylsilane and (c) styrene.

Hydrosilylation with substrates bearing relatively inert functional groups – methyl undecylenate, trimethylsilane and styrene – all lead to successful surface modifications, first indicated by the clearing of the dispersions. The IR spectra are consistent with the corresponding functional groups, as characteristic signals are visible: ν(C=O) at 1700 cm^{-1} in the case of methyl undecylenate, a δ(Si-CH_3) at 1260 cm^{-1} for TMVS and ν(C=C) at 1650 cm^{-1} for styrene (**Figure 4.1–5**). These signals fingerprint their respective substrate and the lack of alkenyl bands (ν(H-C_{sp^2}), ν(C=C)) for the ester and TMVS verifies the removal of unreacted substrates. The oxidation in these samples is minimal, especially when compared to the previous samples. Together with 1-dodecene, these substrates demonstrate the applicability of the trityl initiation method with substrates that do not bear a reactive functional group.

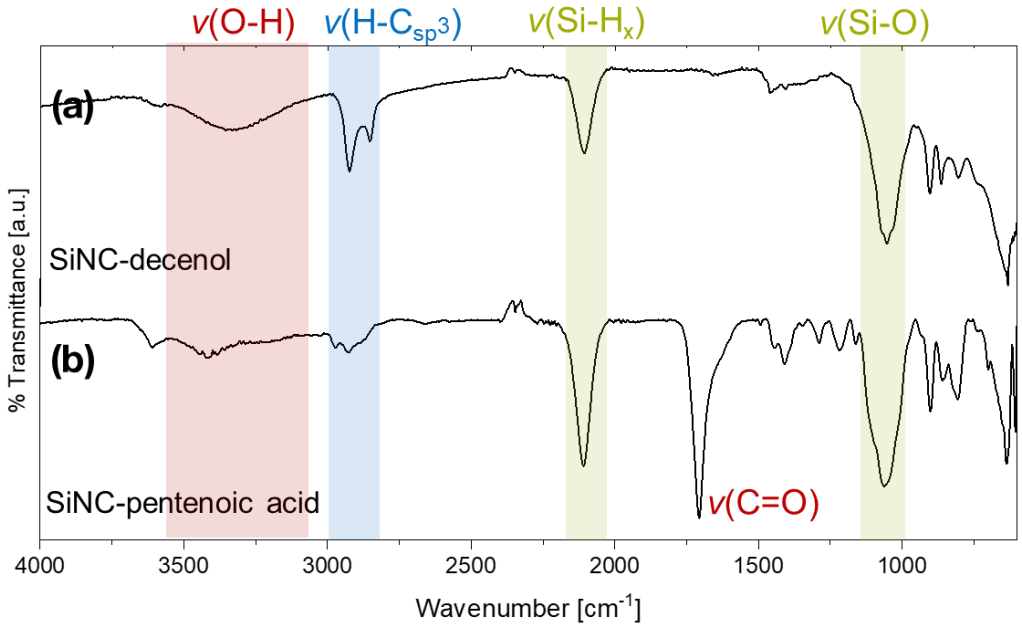

Figure 4.1–6. Infrared spectra of (a) SiNC-decenol and (b) SiNC-pentenoic acid.

The targeted substrates, alcohols and carboxylic acids, unfortunately did not exhibit a good reactivity with trityl salts and SiNCs. Only after a few attempts, usable samples of functionalized SiNCs could be isolated. While these samples never turned clear in solution, their infrared spectra indicate – at least to some degree – surface functionalization (**Figure 4.1–6**). The SiNCs functionalized with decenol exhibit a pronounced ν(O-H) band, as well as the expected ν(H-C_{sp^3}) at 2900 cm^{-1}. The acid sample bears the characteristic carbonyl stretch at 1700 cm^{-1}, however, the ν(H-C_{sp^3}) is fairly weak. In both cases, oxidation is clearly visible with the ν(Si-O) at 1100 cm^{-1}, however, some overlap with the ν(C-O) stretch at 1150 cm^{-1} is expected and may therefore have amplified the preexisting signal. Overall, the quality of the samples is lacking and given the fact that these are the best samples that were synthesized, the surface modification with alcohols and carboxylic acids is unsatisfactory. The results are similar to what we determined for the iodonium initiated functionalization.[70] Acidic protons

are detrimental to the reaction. A definitive reason for this remains unknown and also was not further explored in this work as this would take considerable effort and would not have led to any further advancements.

The substrates that were successful were analyzed with photoluminescence (PL) spectroscopy (**Figure 4.1–7**). The PL emission maxima of 710 nm indicates SiNCs with diameters of roughly 3.5 nm.[227] This is in agreement with the employed synthesis method, that was expected to produce sizes of around 3 nm. The discrepancy of 0.5 nm is within a tolerable margin, as exact size predictions are not possible due to minor influences, such as the employed oven, cooling- and etching time, which can vary between different batches.The spectra of the functionalized samples are all quite similar. The only major deviation is observed for SiNC-dodecene (**Figure 4.1–7**, green), which exhibits a shift of about 8 nm. However, the sample was obtained from a different etching-batch as the other samples, therefore such a shift can be expected and is not negative for the results. In total, the PL measurement leads to the conclusion that the optoelectronic properties of the silicon nanocrystals is not affected by the initiator trityl hexafluorophosphate and that the method is therefore viable to introduce functional groups to the silicon nanocrystal surface.

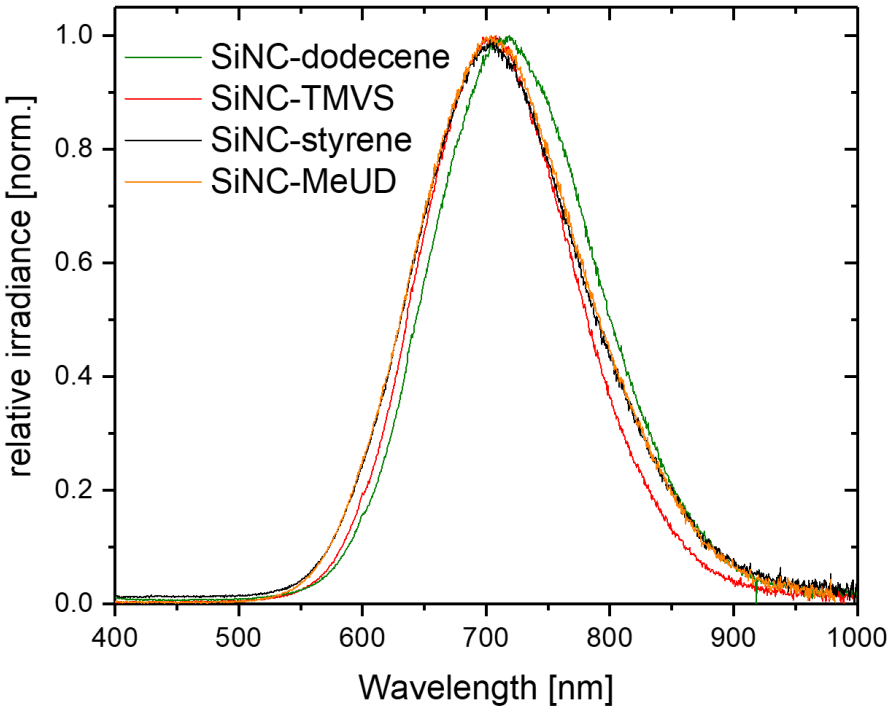

Figure 4.1–7. PL measurements taken of samples that were successfully functionalized using the trityl salt initiated hydrosilylation: 1-dodecene, trimethylvinyl silane, styrene, 10-methyl undecylenate.

4.1.3 Summary and Outlook

In this chapter, a new functionalization of silicon nanomaterials was developed using trityl salts as the initiator for hydrosilylations. The reaction conditions were optimized with 1-dodecene as the model substrate to obtain a maximum surface coverage of the organic groups, as determined by thermogravimetric analysis. Various potential unsaturated substrates with different functional groups were tested to determine the functional group tolerance of the method. Characterizations of these substrates revealed that this functionalization method only works for alkenes with functional groups that do not bear an acidic proton, i.e. it does not work for alcohols or carboxylic acids. Furthermore, contrary to expectations, the functionalization of alkynes also did not lead to any significant surface modification. For the substrates that did show successful incorporation, the photoluminescence showed no change in emission characteristics, meaning that the trityl salts do not affect the optoelectronic properties of the SiNCs. Unfortunately, this method does not offer any benefits over other established methods such as the use of AIBN or diazonium salts as initiators. Therefore, outside the scope of this work, this hydrosilylation method is not significantly relevant to the scientific community.

4.1.4 Experimental Procedures

4.1.4.1 General Information

The reagents employed in this work were purchased from *Sigma Aldrich* and stored under an inert atmosphere in a glove box. 4 Å molecular sieves were added to all reactants prior to storage. Details for the analytical techniques, procedures for solvent drying, as well as the synthesis of hydrogen-terminated silicon nanocrystals are found in chapter 6: *General Experimental Procedures,* p. 124.

4.1.4.2 General Procedure for the Hydrosilylation with Trityl Salt initiator

200 mg of SiNC/SiO_2 is etched according to the general procedure (6.1.3.7, p. 127). The SiNC-H are dispersed in 2 mL toluene and 2 mmol of the reaction substrate added. 10 mg of trityl tetrafluoroborate is added and the reaction mixture degassed three times using the freeze-pump-thaw method, after which the dispersion is stirred for 16 hours unless stated otherwise. The reaction mixture is precipitated in an anti-solvent (i.e. competing solubility, typically MeOH/EtOH 1:1) and centrifuged at 9000 rpm for 4 min. The supernatant is discarded and the residue redispersed in a minimal amount of solvent. Three-fold repetition of the precipitation/centrifugation/dispersion cycle yields purified functionalized SiNCs that are freeze-dried from benzene and stored for later use.

4.2 Dehydrogenative Coupling of Silanes with Silicon Nanosheets

4.2.1 Introduction

The dehydrogenative coupling of silanes describes the formation of Si-Si from silanes with the release of hydrogen (**Eq. 1**).

$$R_3Si{-}H \;+\; H{-}SiR_3 \longrightarrow R_3Si{-}SiR_3 \;+\; H_2 \qquad \textbf{Eq. 1}$$

For molecular silanes, this reaction only proceeds catalytically. However, using catalysts to perform this reaction with silicon nanocrystals results in the removal of the characteristic photoluminescence and therefore the method is not applicable as a functionalization method for SiNCs.[77] Sailor and coworkers were able to establish a working procedure for the thermal dehydrogenative coupling of molecular silanes with hydride-terminated silicon porous nanostructures without the use of a catalyst.[228]

Proper application of this method to zero- and two-dimensional silicon nanomaterials without a catalyst remains absent in literature. A reason for this may be that the reaction itself is not particularly interesting for silicon nanomaterials as it merely extends the silicon shell by one unit and introduces organic ligands that can already be introduced more easily via hydrosilylation (**Figure 4.2–1**). Essentially, hydrosilylation can produce the same particles that dehydrogenative coupling can produce.

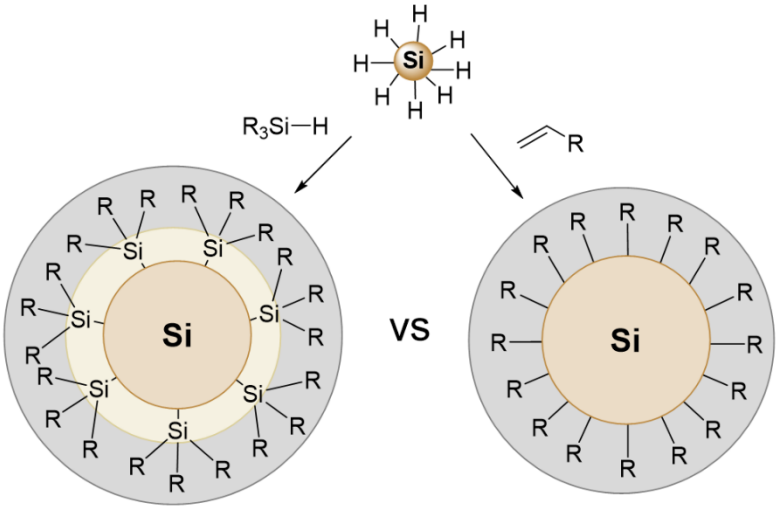

Figure 4.2–1. Schematic illustration of the minor difference between functionalized SiNCs obtained via dehydrogenative coupling and obtained via hydrosilylation. The relevant outer organic shell remains the same. Size differences are only due to the illustration.

One of the key advantages that dehydrogenative coupling may offer, is the formation of a Si-Si bond. While this does not entail any changes for silicon nanocrystals – because their properties are derived from the crystalline core – for silicon nanosheets this could be relevant, as many of the unique properties are derived from its Si-Si conjugated structure (see chapter 2.2.2: Properties *of Silicon Nanosheets*, p. 20) Dehydrogenative coupling with silanes could therefore enhance existing properties or could even lead to new unforeseen ones.

A very ambitious and slightly unrealistic idea is to use silanes to, in essence, repair structural defects in the nanosheet structure. The synthesis of the silicon nanosheets and subsequent treatment with HF acid can lead to holes in the nanosheet, which can have negative effects on the optoelectronic properties. Since the dehydrogenative coupling forms Si-Si bonds, the conjugated backbone is extended and the holes could be "filled-in" (**Figure 4.2–2**).

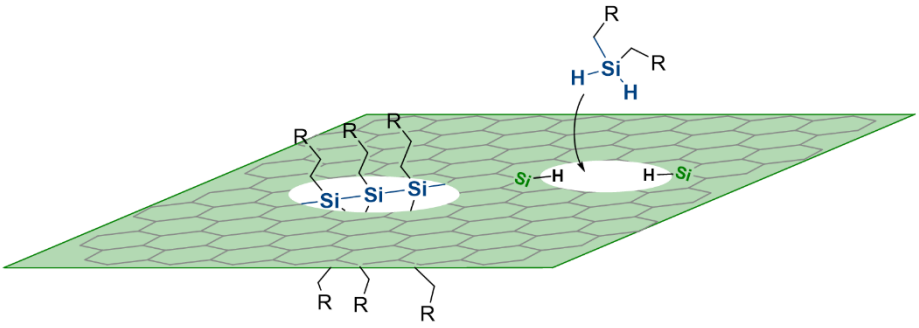

Figure 4.2–2. Illustration of how silanes could be used to "repair" holes that occur in the silicon nanosheet structure.

The "Holy Grail" of two-dimensional nanomaterials is the synthesis of large sheets, i.e. millimeters and upwards. The current synthesis method of silicon nanosheets – exfoliation from calcium disilicide – does not yield very large nanosheets (<500 µm). To obtain larger nanosheets, this method would require considerable changes. One limitation is the morphology of the $CaSi_2$ crystal, as a large and atomically flat single crystal is necessary to exfoliate one large silicon nanosheet; something that could only be accomplished with vapor deposition techniques, which themselves would require an atomically flat substrate. In essence, the synthesis of large two-dimensional nanomaterials remains the biggest challenge of 2D nanomaterial research. An alternative would be to connect the smaller nanosheets into one larger "supersheet". Crosslinking agents such as α,ω-dialkenes could be used to connect the nanosheets using hydrosilylation, however, the Si-Si conjugation – that is responsible for the nanosheets' unique properties – would be lost. Here, the dehydrogenative coupling could be the solution through the formation of a Si-Si conjugated polymer between the larger nanosheets.

4.2.2 Results and Discussion

4.2.2.1 Initial Reactions with Silicon Nanosheets

Certainly, the reparation and crosslinking of silicon nanosheets with molecular silanes are very ambitious and slightly unrealistic ideas. The first obstacle to overcome is to establish a proof of concept for the dehydrogenative coupling reaction and establish a working reaction protocol.

The first reaction with SiNS-H was carried out using toluene as solvent and octadecylsilane as the substrate. It should be noted that the temperatures described by Sailor *et al.*[228] cannot be used as silicon nanosheets will dehydrocouple with themselves at temperatures above 100 °C.[229] Therefore, the reaction was conducted at 80 °C for 16 hours. The sample exhibited significant bleaching, almost turning completely white from the initial yellow/green color. This is usually an indication of significant oxidation. Indeed, FTIR analysis shows a strong ν(Si-O) band at 1100 cm^{-1} (**Figure 4.2–3a**). Only minor evidence for surface functionalization is indicated by the band at 2900 cm^{-1} (ν(H-C_{sp^3})), which – due to the low intensity – might arise from surface impurities. The complete lack of a ν(Si-H_X) band – usually found at 2100 cm^{-1} – indicates that the entire Si-H surface of the sample was oxidized. Better results are achieved by increasing the temperature to 100 °C (**Figure 4.2–3b**). The ν(H-C_{sp^3}) and δ(H-C_{sp^3}) bands are more intense, signifying a higher degree of surface incorporation of the silane. The ν(Si-O) band is still very strong. However, the presence of remaining ν(Si-H_X) indicates that the organic groups are able to protect some of the surface from oxidation. If this were not the case, any remaining Si-H bonds would be oxidized during the work up procedure, as seen in the previous sample.

These initial reactions were able to show that the dehydrogenative coupling of silicon nanosheets with silanes is possible – it just isn't particularly efficient. The problem is exacerbated by oxidation, which competes with the reaction. Silicon – especially in the form of high-surface-area silicon nanosheets – is very prone to oxidation, which proceeds much faster than the desired reaction. Although air-free techniques are used, the complete exclusion of oxygen cannot be guaranteed. Any traces of oxygen will react with the silicon nanomaterial; aided by the elevated temperatures. To see whether improvements could be made by working more stringently, all solvents and reactants were dried and first degassed by sparging with argon, then subjected to three freeze-pump-thaw cycles and once everything was combined, the reaction mixture was degassed again. In addition, the reaction time was increased to 40 hours to allow more time for the slow reaction to proceed. Even with these strict conditions, only minor improvements could be achieved (**Figure 4.2–3c**).

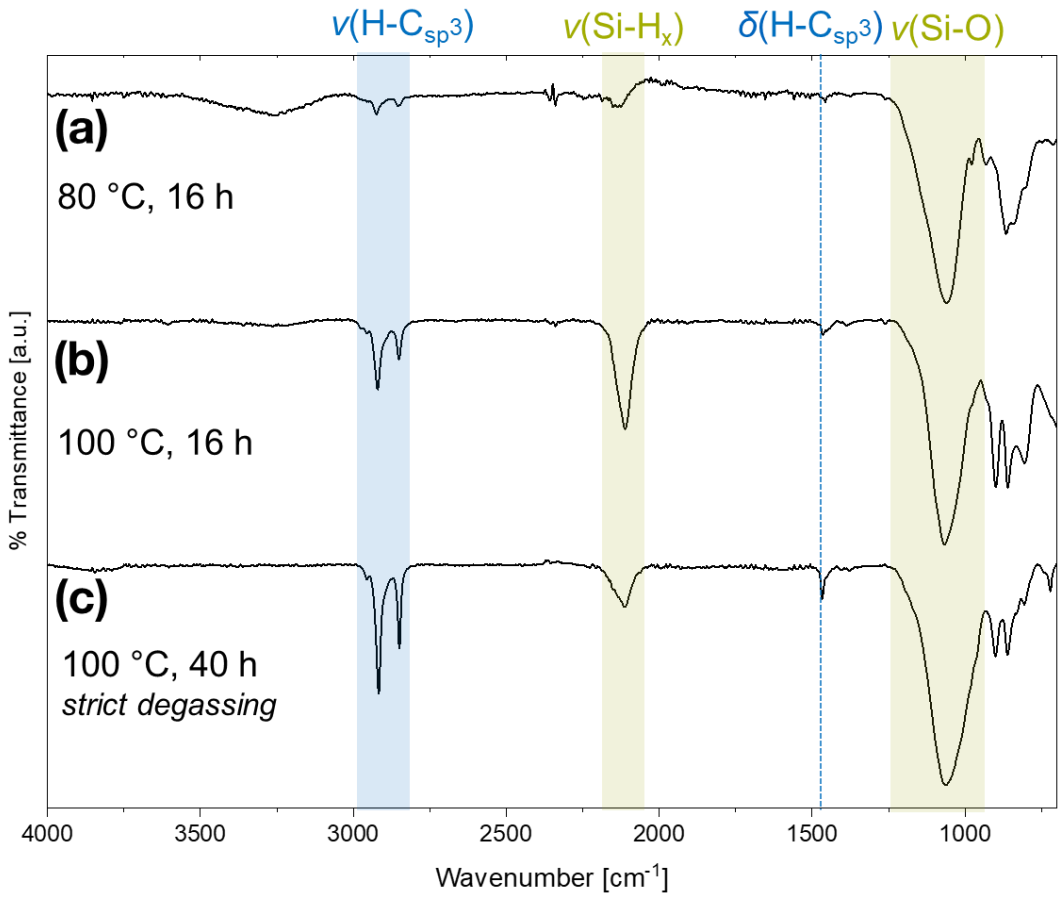

Figure 4.2–3. FTIR spectra of SiNSs obtained from the dehydrogenative coupling with octadecylsilane at (a) 80 °C for 16 h, (b) at 100 °C for 16 h and (c) at 100 °C for 40 h and with strict degassing protocols.

Compared to the previous sample, the IR spectrum only shows a slightly stronger ν(H-C_{sp^3}) band, a slightly diminished ν(Si-H_x) band and a still very significant oxidation band (ν(Si-O) at 1100 cm^{-1}). This oxidation might arise from the purification of the sample, which was not conducted in air-free, dry solvents. In hydrosilylation protocols, the oxidation that occurs during the purification is negligible, because the surface is protected by the organic groups that were introduced during the reaction. In this case however, the reaction proceeds so slowly that a sufficient surface coverage is not achieved to protect the nanoparticles. The results obtained in these initial tests are very disappointing. Considering that the reactant octadecylsilane possesses a large organic tail and three potential groups that can react with the surface (i.e. Oct-Si**H**$_3$), a much faster reaction and pronounced ν(H-C_{sp^3}) band in IR spectra were expected. In light of this and the fact that such painstaking conditions are required to gain only passable results, the application to other more desirable substrates, such as triethylsilane, was not pursued further.

4.2.2.2 Dehydrogenative Coupling of Silicon Nanosheets with Germanes

One of the possible reasons for the inefficiency of dehydrogenative coupling is the unfavorable formation of hydrogen. Because two hydrogen atoms of hydridic nature are forced to combine, the release of H_2 to form the Si-Si bond is slow. This is the reason why catalysis is often necessary to facilitate the reaction with molecular silanes. Coworkers *Asjad Hossain* and *Haoyang Yu* were able to successfully develop methods for the dehydrogenative coupling of silanes with germanium nanoparticles and germanium nanosheets.[230, 231] The combination of hydrides from different heteroatoms, i.e. Si-H and H-Ge, may be the reason for the increased reactivity. Therefore, the dehydrogenative coupling of silicon nanosheets was tested with di-*n*-butyl germane at 100 °C for 16 hours.

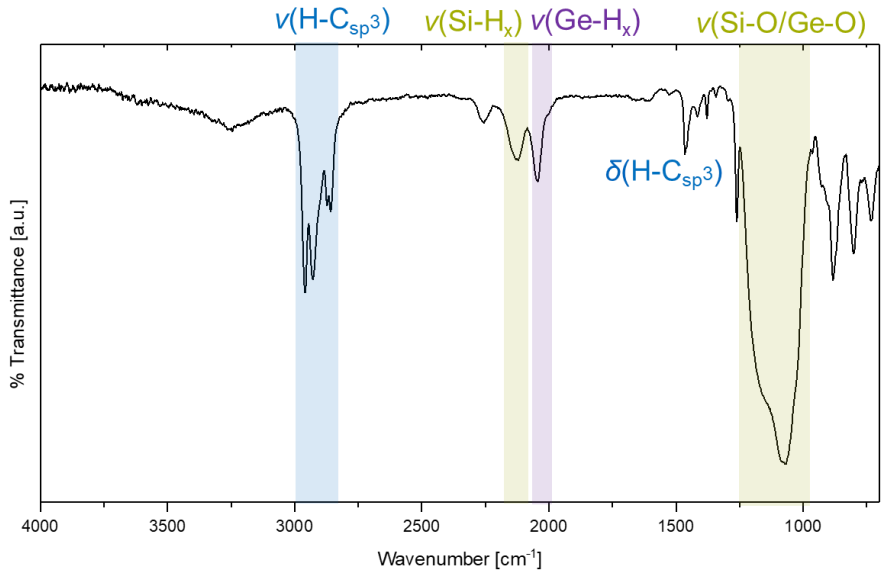

Figure 4.2–4. FTIR spectrum of SiNSs functionalized with di-*n*-butyl germane.

The reaction with the germane proceeded faster and did not exhibit bleaching of the SiNSs, as was observed for silanes. FTIR of the product shows bands consistent with functionalization (**Figure 4.2–4**). Both ν(Si-H_X) and ν(Ge-H_X) are visible at 2100 cm^{-1} and 2000 cm^{-1} respectively, indicating successful attachment of the germane functional group. A wide, intense band centered around 1100 cm^{-1} corresponds to the oxides of germanium and silicon. The relative intensity of the ν(H-C_{sp^3}) to the ν(Si-O) band is similar to that of the sample functionalized with octadecylsilane (**Figure 4.2–3c**). Since di-*n*-butyl germane possesses far less C-H moieties than octadecylsilane, a qualitative estimation can be made, that the dehydrogenative coupling with a germane produces a higher surface coverage, compared to silanes.

One of the initial reasons for pursuing this project was the potential of enhanced or new properties due to the formation of conjugated Si-Si (or Si-Ge) bonds. However, the characteristic photoluminescence of the SiNSs remains unaffected by the dehydrogenative coupling reaction – both with silanes and germanes. The visible brightness of the fluorescence remains unchanged and PL measurements (**Figure 4.2–5**) show that the emission maximum at around 510 nm does not significantly shift in comparison to a SiNS-$C_{12}H_{25}$ control sample. In total, the use of dehydrogenative coupling as a new reaction protocol to extend the functionalization possibilities for silicon nanosheets is not very lucrative.

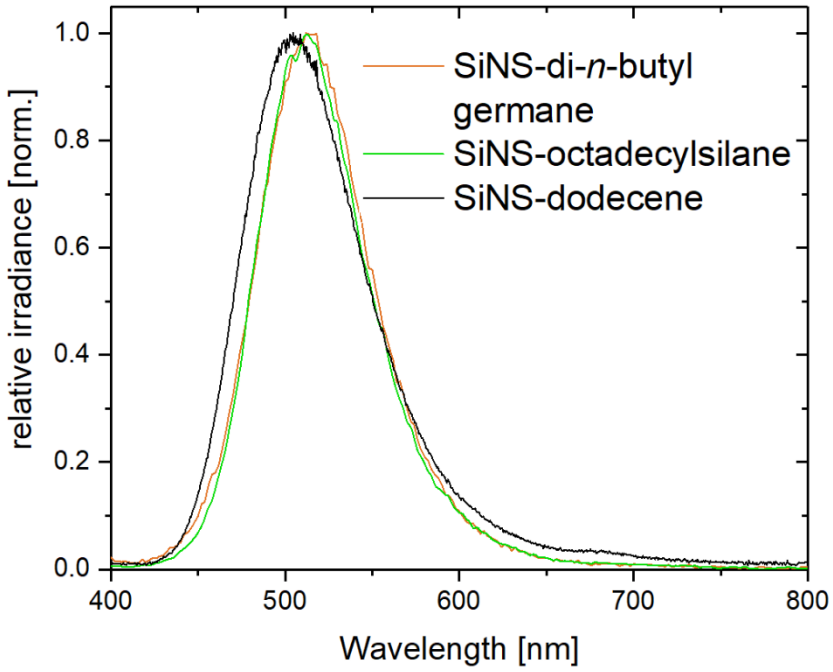

Figure 4.2–5. PL spectra of SiNS functionalized with a germane and a silane as well as a control sample, SiNS-dodecene.

4.2.2.3 Dehydrogenative Coupling between Silicon Nanosheets and Silicon Nanoparticles

Even though the reaction does not proceed effectively with silane or germane molecules, the dehydrogenative coupling could be used to combine different nanomaterials. Both silicon nanocrystals and silicon nanosheets possess a hydride-terminated surface, which could combine to form a new hybrid material. The reaction is aided by the adsorption of SiNCs on SiNSs that is caused by the van-der-Waals interaction of the two high-surface-area materials. Dehydrogenative coupling could then 'lock' the materials in place. In their research article, Haoyang Yu and colleagues demonstrated the attachment of silicon nanocrystals to germanium nanosheets using the dehydrogenative coupling reaction.[231] The extension of this method to silicon nanocrystals and silicon nanosheets should therefore also be possible.

A test reaction was carried out at 100 °C with freshly etched SiNCs and SiNSs. A small aliquot was taken after 16 hours for FTIR analysis (**Figure 4.2–6** top) and the reaction mixture was immediately subjected to thermal hydrosilylation with 1-dodecene to stabilize the resulting material for subsequent characterization. After centrifugation of the suspension, the supernatant still showed photoluminescence; consistent with free-standing (i.e. not on the surface of SiNSs) functionalized silicon nanocrystals.[231] The remaining residue exhibited a yellow/orange color – as expected of a SiNS and SiNC mixture. Most likely, not all SiNCs were deposited onto the SiNSs surface resulting in an excess of functionalized SiNCs that remain in solution. To remove these 'byproducts' the residue was washed and centrifuged in toluene several times.

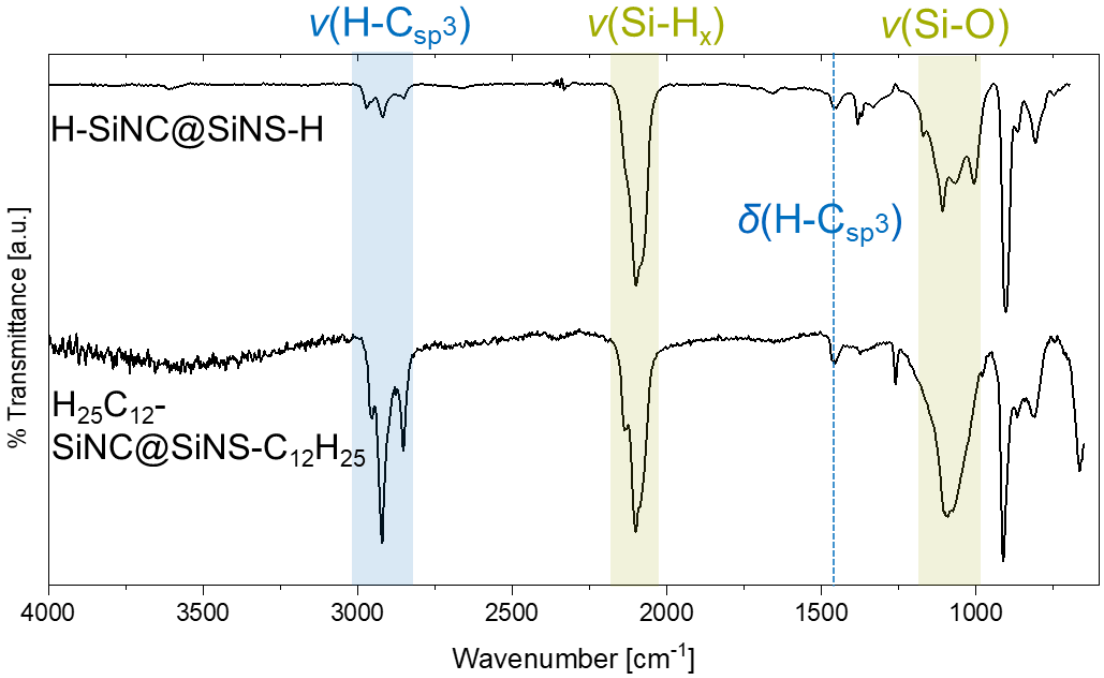

Figure 4.2–6. FTIR spectrum of SiNCs dehydrocoupled with SiNS, (top) before functionalization and (bottom) after functionalization with 1-dodecene.

FTIR of the aliquot taken after dehydrogenative coupling and after hydrosilylation shows bands corresponding to a Si-H terminated nanomaterial and a dodecyl-functionalized silicon nanomaterial respectively (**Figure 4.2–6**). The differentiation between silicon nanocrystals and silicon nanosheets is not possible with FTIR, however, the functionalization of the hybrid nanomaterial, denoted as $H_{25}C_{12}$-SiNC@SiNS-$C_{12}H_{25}$, can be confirmed.

The confirmation of silicon nanocrystals deposited on silicon nanosheets is given by images taken with TEM. Silicon nanocrystals with diameters around 3.5 nm can be seen 'sitting' on larger islands of silicon nanosheets (**Figure 4.4–7a, b**). Outside of the nanosheet domains, no free-standing nanocrystals are visible, a confirmation for the success of the reaction and the removal of excess SiNCs. The SiNCs are very densely packed on the surface.

Figure 4.4–7b shows some areas with seemingly no SiNC-deposition, however, the invisibility stems from the focus point of the microscope, as the particles sit lower than the focus plane. At higher magnification (**Figure 4.4–7c, d**) the lattice fringes of the crystalline domains of the SiNCs are visible. The distance of these is in agreement with diffraction patters observed for Si(111) planes (0.32 nm).[15] These observations indicate that one, the deposition of SiNCs on SiNSs by dehydrogenative coupling is possible and two, that the process does not alter the crystalline core of the silicon nanocrystals.

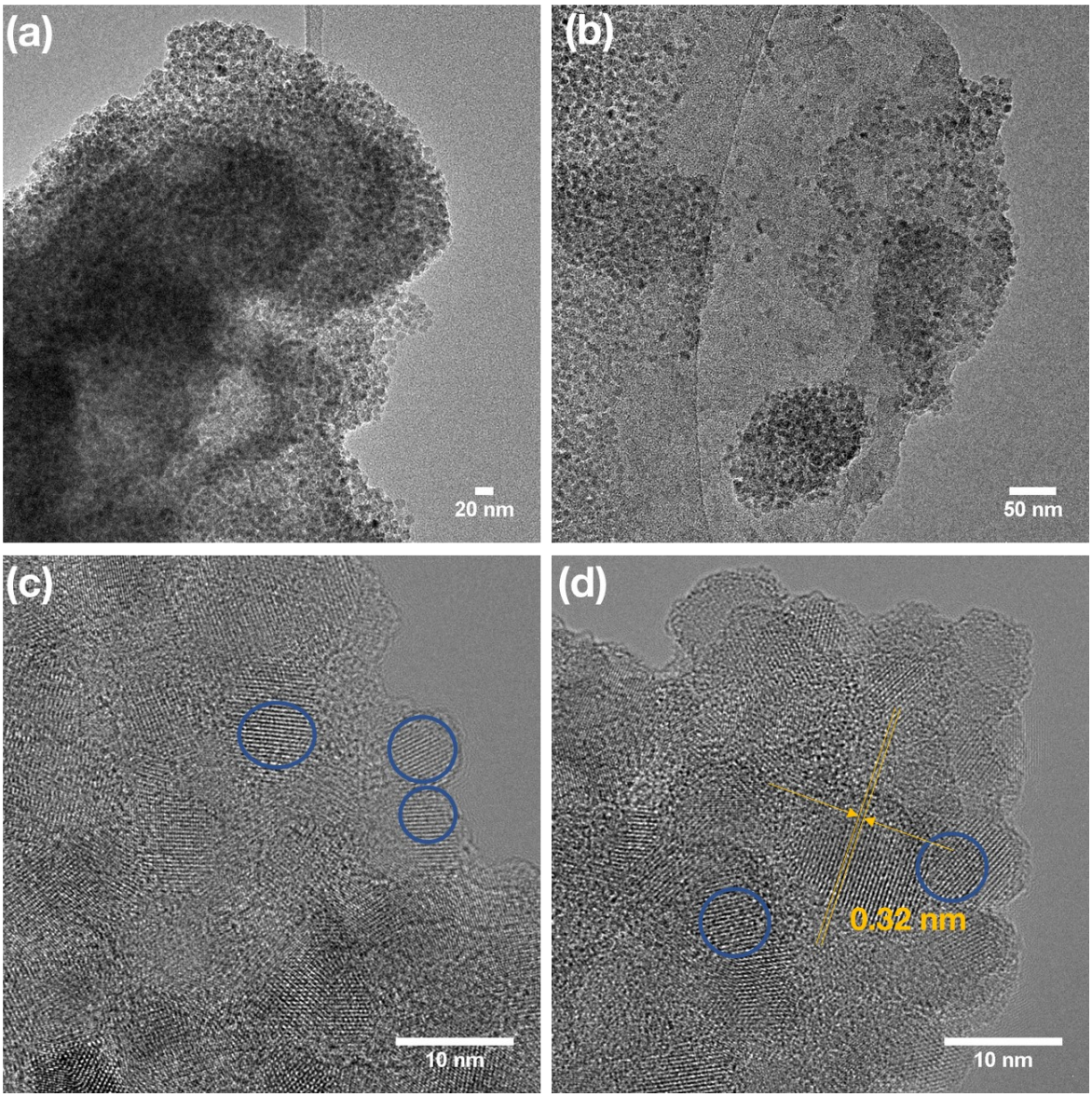

Figure 4.2–7. TEM images taken of the sample obtained by dehydrocoupling SiNCs with SiNSs at (a, b) lower magnification and (c, d) higher magnification. Blue circles in the high-magnification images estimate the diameter of silicon nanocrystals.

The sample, $H_{25}C_{12}$-SiNC@SiNS-$C_{12}H_{25}$, does not exhibit discernable visible photoluminescence – either of the silicon nanocrystals (orange/red) or the silicon nanosheets (green). Similar observations were made by Yu *et al.* with SiNCs bonded to germanium

nanosheets. Possible explanations given were charge-transfer processes between the two nanomaterials and scattering causing a lowered intensity.[231] A PL spectrum taken of $H_{25}C_{12}$-SiNC@SiNS-$C_{12}H_{25}$ indicates an overall low brightness of the PL, evident by the high noise of the measurement (**Figure 4.2–8**). While the PL of the silicon nanocrystals (at ~720 nm) is very weak, a slightly more intense PL of the silicon nanosheets is seen at ~515 nm. The low brightness of the nanosheets' PL can be explained by scattering in the turbid suspension, making detection of the already weak PL harder. Furthermore, since the SiNCs are assumed to 'sit' on the nanosheets; this additional layer could absorb and block any incoming or emitted light. For SiNCs, the almost complete lack of PL cannot be explained by scattering, especially considering that the remaining PL in the measurement could come from free-standing SiNCs that were not removed during purification. Charge transfer processes, described by Yu *et al.*, could explain these observations and have been established to take place between surface groups and the underlying silicon nanomaterial.[232] Another possibility is that the SiNCs are no longer quantum confined. Since the PL of SiNCs relies on the confinement of excitons to the small dimensions of the nanocrystals an extension of this framework could cause the PL to shift or diminish. Due to the formation of Si-Si bonds between the two materials such a phenomenon seems likely. In essence, this could be considered as a charge transfer process, as the exciton is now able to move between the silicon nanosheet and silicon nanocrystal structure.

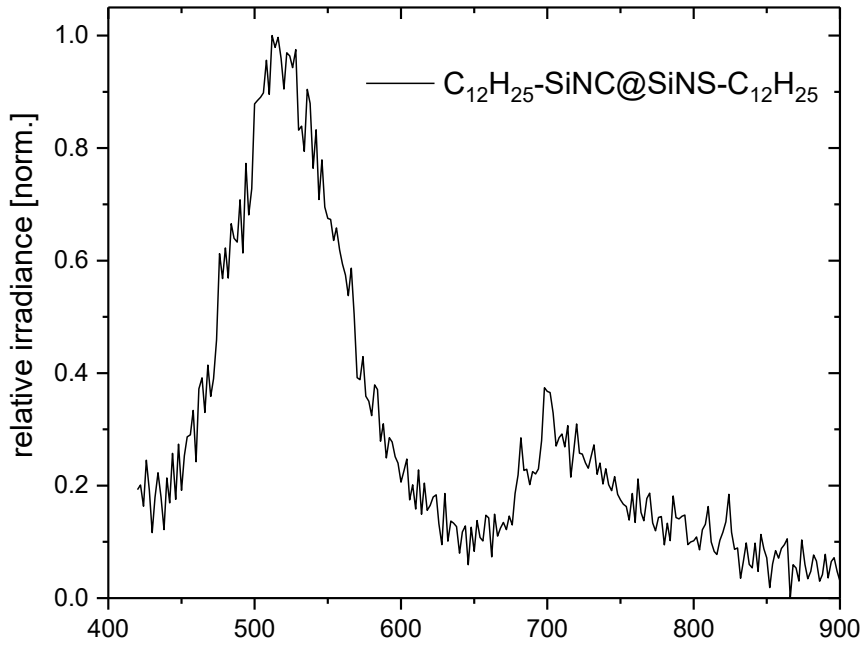

Figure 4.2–8. Photoluminescence spectrum of the sample obtained after dehydrocoupling of SiNCs onto SiNSs and subsequent functionalization with dodecane.

4.2.3 Summary and Outlook

Summarizing this short project, the dehydrogenative coupling of silicon nanosheets with silanes and germanes was explored. The reaction between the SiNS and silanes was found to proceed very slowly and led to strong oxidation during the purification of the samples. Minor improvements could be made by using germanes, as the reaction proceeds more efficiently due to the different character of the germanium- and silicon-bound hydrogen atoms. However, the SiNS-germane coupled sample also exhibited strong oxidation and did not show any improvement or change in the optoelectronic properties of the SiNSs. As such, the combination of silicon nanosheets with molecular silanes and germanes was not pursued any further, as the initial reactions for this reaction type failed to produce any positive results.

Promising results could, however, be achieved with the coupling of the two nanomaterials: silicon nanocrystals and silicon nanosheets. The dehydrogenative coupling was used to covalently bond these two materials, producing a new hybrid composite. TEM images reveal the SiNCs 'sitting' on the larger SiNSs and subsequent hydrosilylation could be used to functionalize any remaining Si-H groups. However, because this hybrid material did not exhibit any discernible, interesting properties, such as photoluminescence, no further work was conducted to characterize or test this material in any applications. Possible applications as an anode material or in microelectronics, and measurements such as cyclic voltammetry could be examined, but are outside of the scope of this thesis. Concerning the chemistry of this new hybrid material, one idea emerged during this project and is described in chapter 4.5: *Surface-Anisotropic Silicon Nanocrystals.*

4.2.4 Experimental Procedures

4.2.4.1 General Information

All of the reagents employed in this work were purchased from *Sigma Aldrich* and stored under an inert atmosphere in a glove box. Analytical techniques, procedures for solvent drying as well as the synthesis of hydrogen-terminated silicon nanocrystals and hydrogen-terminated silicon nanosheets are found in chapter 6: *General Experimental Procedures,* p. 124.

4.2.4.2 Dehydrogenative coupling of silicon nanosheets with a silane or germane

20 mg of SiNS-H (from etching 30 mg of SiNS) are dispersed in 2 mL dry toluene and 2 mmol of the substrate is added. The dispersion is degassed via three-freeze-pump thaw cycles and stirred at 100 °C (or indicated temperature) for 16 hours. The resulting reaction mixture is centrifuged (9000 rpm, 4 min). The supernatant is discarded, and the pellet re-

dispersed. The centrifugation/dispersion cycle is repeated two times to yield purified SiNS-Si-R.

4.2.4.3 Dehydrogenative coupling of silicon nanocrystals with silicon nanosheets (R-SiNC@SiNS-R)

10 mg of SiNS-H (from etching 15 mg SiNS) are dispersed in 3 mL dry, degassed toluene. Separately, 8 mg of SiNC-H (from etching 400 mg SiNC/SiO_2) are dispersed in 2 mL dry, degassed toluene. The dispersions are combined in a heat-dried Schlenk tube and subjected to three freeze-pump-thaw cycles (FPT). The reaction mixture is stirred at 100 °C for 20 hours after which 0.3 mL of dry 1-dodecene is added and the mixture is degassed again through three FPT cycles. The dispersion is heated to 130 °C and stirred for an additional 16 hours. After cooling to room temperature the mixture is transferred to a centrifuge tube and centrifuged at 9000 rpm for 4 min. The supernatant is discarded and the residue washed three times with toluene, yielding purified $H_{25}C_{12}$-SiNC@SiNS-$C_{12}H_{25}$.

4.3 Functionalization of Silicon Nanocrystals with Siliranes

4.3.1 Introduction

Silacyclopronaes, commonly referred to as *siliranes*, are a class of compounds that can be thought of as the silicon equivalent of cyclopropane. Because of the high ring strain and polarization of the Si-C bond, the ring moiety is easily removed, resulting in a *silylene* – the silicon equivalent of a carbene – a highly reactive substrate.[233] In essence, siliranes are protected silylenes. Compared to carbenes, silylenes have not gained much attention outside of fundamental chemistry.[234, 235] They are very unstable and require bulky and complex ligands for stabilization. Siliranes have emerged as stable alternatives as they offer the possibility of simple room-temperature-stable in-situ generators of silylenes (**Scheme 4.3-1**).

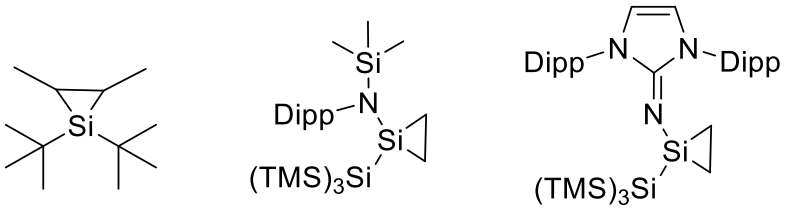

Scheme 4.3-1. Examples of room-temperature stable siliranes.

Within our research group, this reactivity was used to develop a cross-linking approach for the metal-free curing of silicones.[236] In their work Herz, Nobis and coworkers describe the insertion of the in-situ generated silylenes into Si-H bonds as the necessary step to induce crosslinking. In light of the parallels between carbenes and silylenes, and the hydride-terminated surface of the herein described nanomaterials, the application of siliranes as functionalization substrates was explored. Carbenes have been previously explored as functionalization substrates (see chapter 2.1.3.2, p. 11),[75] whereas the use of siliranes and silylenes remain absent in literature. The possible benefits of using siliranes as functionalization substrates are similar to the ones described in the chapter on dehydrogenative coupling. Since the insertion generates a silicon-silicon connection between the substrate (silirane) with the silicon nanomaterial, the extension of the silicon framework is the principal reason for the pursuit of the project. In addition, controlled design of the silirane substrate could directly introduce new hetero-atom linkages to the silicon surface (**Scheme 4.3-1**); this could impact the (opto)electronic properties of the underlying nanomaterial.

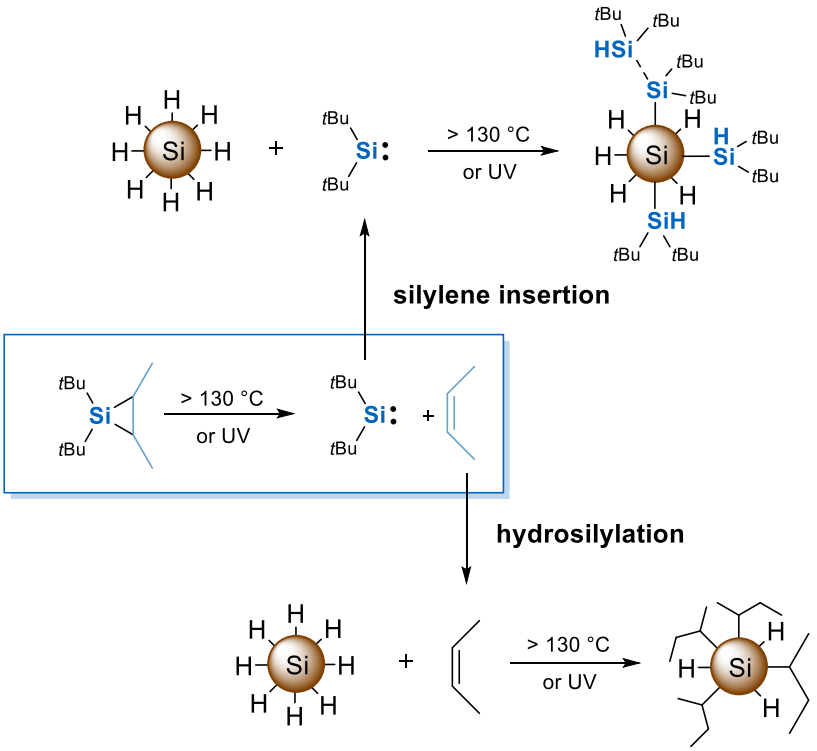

Scheme 4.3-2. Possible reaction pathways of siliranes with silicon nanomaterials, exemplified with silicon nanocrystals.

The possible reactions of the silirane with the silicon nanomaterial are depicted in **Scheme 4.3-2**. The high temperatures or the UV irradiation opens the silacyclopropane ring, resulting in a silylene and an alkene. Due to the extreme reaction conditions, both the silylene addition into the Si-H bond as well as the hydrosilylation can occur. It is likely that both of these reactions occur simultaneously. One of the key aspects of this project is therefore the elucidation of which reactions occur and how the silylene insertion can be favored.

4.3.2 Results and Discussion

The project focused on simple siliranes to avoid introducing complexity early on. It was previously determined that the coordinating olefin of the silirane is released at temperatures above 130 °C.[236] As such the inaugural reaction was carried out using di-*tert*-butyldimethylsilirane (DtBDMS) with silicon nanocrystals at 140 °C in *o*-xylene. The reaction turned clear overnight, a qualitative indication of successful surface modification. Indeed, the FTIR spectrum of the resulting product reveals bands corresponding to the initial silirane (**Figure 4.3–1**).

Since the introduced functional group is basically identical to the original substrate (**Figure 4.3–1a**), the observable bands suggest successful incorporation of the complete silirane. This means that both the silylene insertion as well as the alkene hydrosilylation take place. If only one of these reactions took place, the bands of the final IR spectrum should look different to the initial substrate, as only a part of the original molecule would be incorporated. Surprisingly, the sample exhibits almost no oxidation (ν(Si-O) at 1100 cm^{-1}) and a very diminished ν(Si-H_X) band at 2100 cm^{-1}. The ν(Si-H_X) is expected to be much stronger, as the actual amount of Si-H bonds is not decreased in the reaction, these are merely transferred to the silirane functional group (**Scheme 4.3-2**). When the reaction was conducted with silicon nanosheets, the ν(Si-O) and ν(Si-H_X) are much stronger. The reaction seems to proceed much more efficiently for SiNCs than for SiNSs.

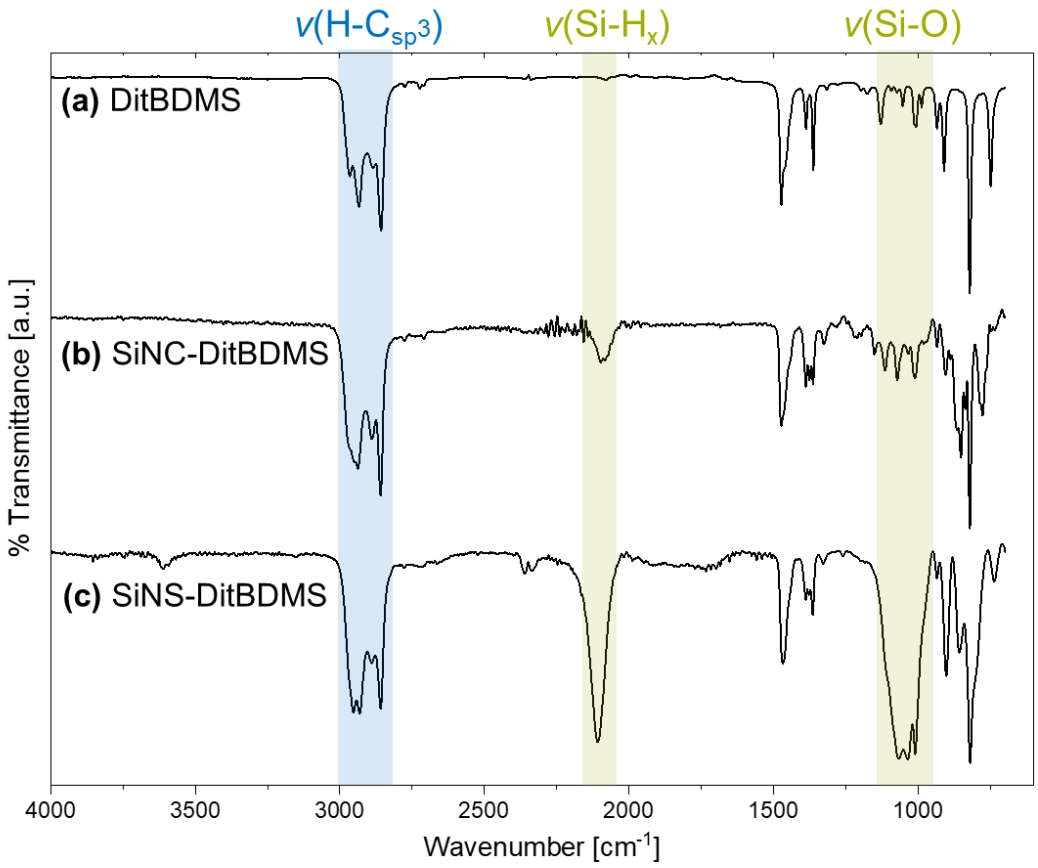

Figure 4.3–1. FTIR spectra of (a) di-*tert*-butyl-dimethylsilirane and correspondingly functionalized (b) silicon nanocrystals and (c) silicon nanosheets.

Subsequent TGA-measurements confirmed the differing functionalization behaviors between the two materials (**Figure 4.3–2**). The silicon nanocrystals show a significant mass loss of almost 80 %, which is only observed when a polymer is formed. This would also explain the low intensities of the characteristic bands of the SiNCs in the IR spectrum, i.e. ν(Si-H_X) and ν(Si-O), since the polymer dominates the spectral response. For the silicon nanosheets, TGA only shows a minor mass loss of around 20 %, indicative of very low

functionalization. This also explains the relatively high degree of oxidation observed for the SiNSs in FTIR, as there are no organic groups that protect the nanomaterial during the purification.

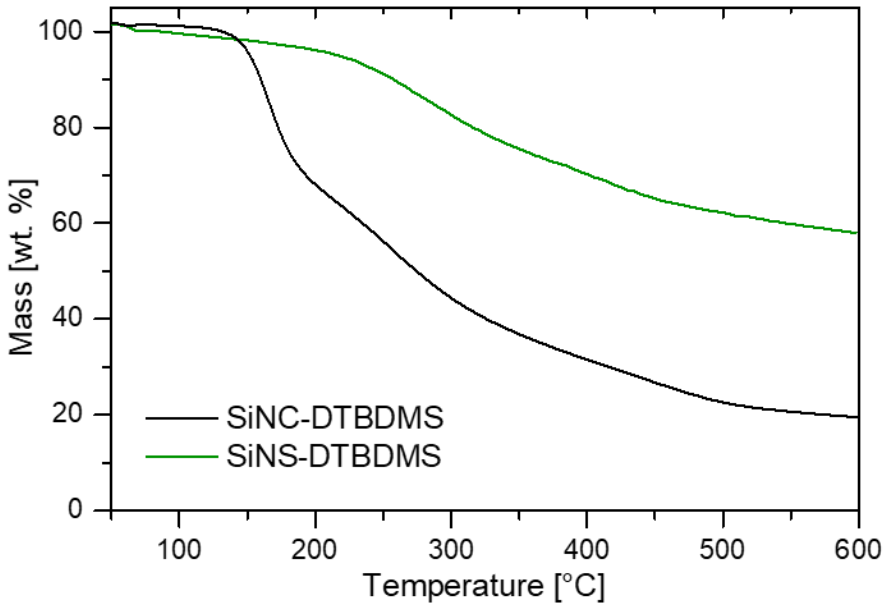

Figure 4.3–2. TGA measurements of silirane-functionalized silicon nanocrystals (black) and silicon nanosheets (green)

The reaction with silicon nanosheets was repeated several times, but did not show any improvement. At this stage of the project the use of siliranes as functionalization substrates for silicon nanosheets seemed unviable. As such, the research with silicon nanosheets was set aside in favor of development with silicon nanocrystals. Upon success, the silicon nanosheets would be explored again.

Since siliranes can also be activated with UV-light instead of thermal energy, the reaction was tested with SiNCs in a UV reactor. Just as in the previous reaction, the dispersion turned clear after about two hours. After purification, FTIR of the product shows the same spectral features, albeit with slightly more oxidation. This establishes the possibility of using either heat or UV light as the activator for the reaction, providing more flexibility to the method.

With FTIR it was determined that both the hydrosilylation as well as the silylene-incorporation seem to take place during the reaction of the silicon nanomaterials with siliranes (**Scheme 4.3-2**). Because only the silylene insertion is desired, reaction protocols were designed to suppress the alkene hydrosilylation. Performing the reaction at reduced pressure did not result in any noticeable change. The solubility of butene in organic solvents is too high to allow removal by reduced pressure of the surrounding atmosphere. The protocol was therefore adjusted to sparging Ar into the dispersion during the reaction, with the expectation that the generated butene is carried out of solution. This only lead to an increase

in oxidation, as shown by the more intense ν(Si-O) bands at 1100 cm^{-1} in later IR measurements (**Figure 4.3–3**). This strongly contradicts expectations, as a flow of Ar would continuously renew the surrounding atmosphere as well as saturate the reaction solution with an inert gas, removing oxygen in the process. The oxidation of the sample must therefore arise after the reaction, during the purification procedure.

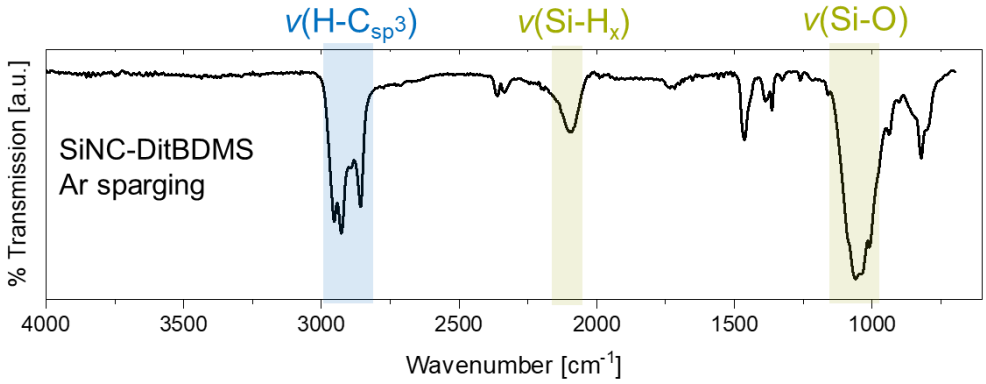

Figure 4.3–3. FTIR spectrum of SiNC-DitBDMS obtained while sparging with Ar.

In order to increase the efficiency of the hydrosilylation-suppression by Ar sparging, siliranes with smaller coordinating alkenes, i.e. propene or ethene, would be more desirable as these could be removed more easily from solution. However, the synthesis of siliranes requires the condensation of the alkene into liquid form. Propene and ethene would require very low temperatures and would pose an immense safety risk as the vapor pressure of these alkenes is very high. Therefore, the synthesis of siliranes with butene as the coordinating alkene, is the smallest unit feasible. Nevertheless, other available siliranes were tested as functionalization substrates to see whether any differences in reactivity can be observed. Next to siliranes – that incorporate an alkene – silirenes are related compounds that incorporate alkynes. It would therefore be interesting to see if this has an effect on the functionalization procedure, as the functionalization with alkynes usually proceeds much slower (chapter 4.1), which in turn could lead to more silylene insertion.[70] Two silirenes as well as an additional silirane were tested as functionalization substrates (**Scheme 4.3-3**).

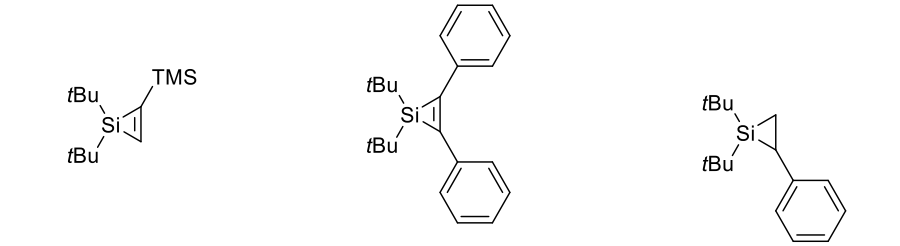

Scheme 4.3-3. Siliranes and silirenes tested as substrates for the functionalization of SiNCs.

Apart from di-*tert*-butylphenylsilirane (DtBPS), none of the substrates demonstrated a noticeable reaction. The dispersions did not turn clear and the corresponding FTIR spectra mainly denote strong oxidation (ν(Si-O) at 1100 cm^{-1}) due to the lack of protective organic groups, leading to oxidation during the purification (**Figure 4.3–4a, b**). An explanation for this is the stability of the silirenes; they do not undergo the reaction to the silylene and the alkenyl. The only substrate that worked is di-*tert*-butylphenylsilirane. The bands in the FTIR spectrum suggest a strong polymerization of the released styrene, as the usually weak aromatic overtones and weak ν(H-C_{sp^2}) bands are very intense. The lack of a discernible ν(Si-O) band indicates that the silicon nanomaterial is not the dominant component in the hybrid material (**Figure 4.3–4c**).

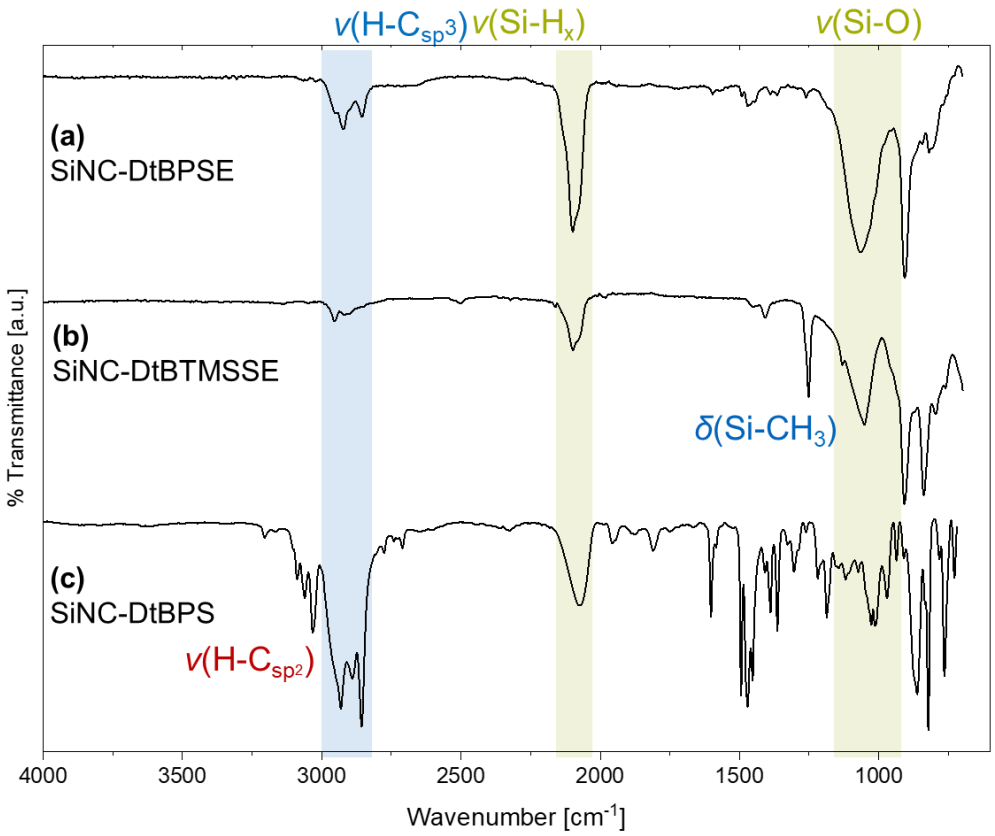

Figure 4.3–4. FTIR spectra of SiNCs reacted with various silirenes: (a) di-*tert*-butyldiphenylsilirene (b) di-*tert*-butyltrimethylsilylsilirene and (c) di-*tert*-butylphenylsilirane.

The results obtained for the reaction of silicon nanocrystals with di-*tert*-butylphenylsilirane revived concerns regarding the actual surface groups on the nanocrystal surface. Previous results suggested that the silylene insertion and hydrosilylation take place simultaneously, however, taking the intense bands of styrene (**Figure 4.3–4c**) into consideration, it is possible that the hydrosilylation is much more dominant, thus leading to polymer formation. In order to decisively elucidate the surface groups, the SiNCs need to be separated from the surrounding polymer matrix. Due to the similar chemical behavior of functionalized silicon nanocrystals and the corresponding polymer, precipitation – as it is

commonly employed for purification – is not applicable. For example, if the SiNCs are functionalized with styrene, i.e. SiNC-styrene, and the surrounding homopolymer is polystyrene, then both materials precipitate and dissolve in the same solvents. Therefore, the selective precipitation of one or the other is not possible. Previous reports established that ultracentrifugation can be used, because, even though both materials are dissolved, the SiNCs are much more dense and will form a pellet at very high rotational forces, while the polymer remains in solution.[237]

Di-*tert*-butylphenylsilirane was chosen as the silirane substrate, because the phenyl rings show a strong difference to the *tert*-butyl groups of the silylenes insertion product. The functionalized SiNC-DtBPS was dissolved in toluene and centrifuged at 200000 g for 4 hours. The supernatant was separated and the pellet redispersed in toluene. This centrifugation cycle was repeated a total of eight times for each sample. This many cycles are necessary to ensure the complete separation of the SiNCs and the homopolymer. Due to the functionalization of the SiNCs they quickly dissolve back into the supernatant. The supernatants of all fractions were combined and the solvent removed in vacuum. Unfortunately, no polymer-like material could be isolated (contrary to expectations), only small amounts of a viscous liquid; the FTIR shows signals corresponding to an alkane containing material (**Figure 4.3–5b**).

This could be due to a concentration of impurities resulting from the solvent, but the precise composition and origin of this substance remains unknown and was not characterized further. The FTIR measurement of the isolated SiNCs clearly shows signals corresponding to phenyl units (**Figure 4.3–5c**). The aromatic overtones (1950-1750 cm^{-1}), $\nu(H\text{-}C_{sp^2})$ at ~3050 cm^{-1} and $\nu(C{=}C)$ at 1605 cm^{-1} are all attributed to phenyl rings and are the dominant features in the spectrum. The alkyl stretching band ($\nu(H\text{-}C_{sp^3})$) at around 2900 cm^{-1} arises from the CH_2 groups of the phenyl units, but could also be attributed to potential *tert*-butyl groups of the silylene insertion product. However, if this were the case, the alkyl band would look different, as only *tert*-butyl groups would be present on the SiNC surface and these exhibit a different characteristic signal-shape in IR. An inset polystyrene standard shows almost identical bands to the isolated SiNCs (**Figure 4.3–5c**, inset).. The slightly more intense, $\nu(H\text{-}C_{sp^3})$ bands of the SiNCs as compared to the polystyrene standard are attributed to adventitious organic impurities.

The data obtained thus far concludes that the reaction of SiNCs with silirane does not lead to any insertion of the desired silylene units. In light of this, previous observations can be explained. The increased oxidation during the hydrosilylation suppression experiments are

explained by a lower degree of functionalization due to less available olefin, since it was carried out with the flow of Ar. This subsequently leads to oxidation during the purification procedure, as there are no protective organic groups on the surface.

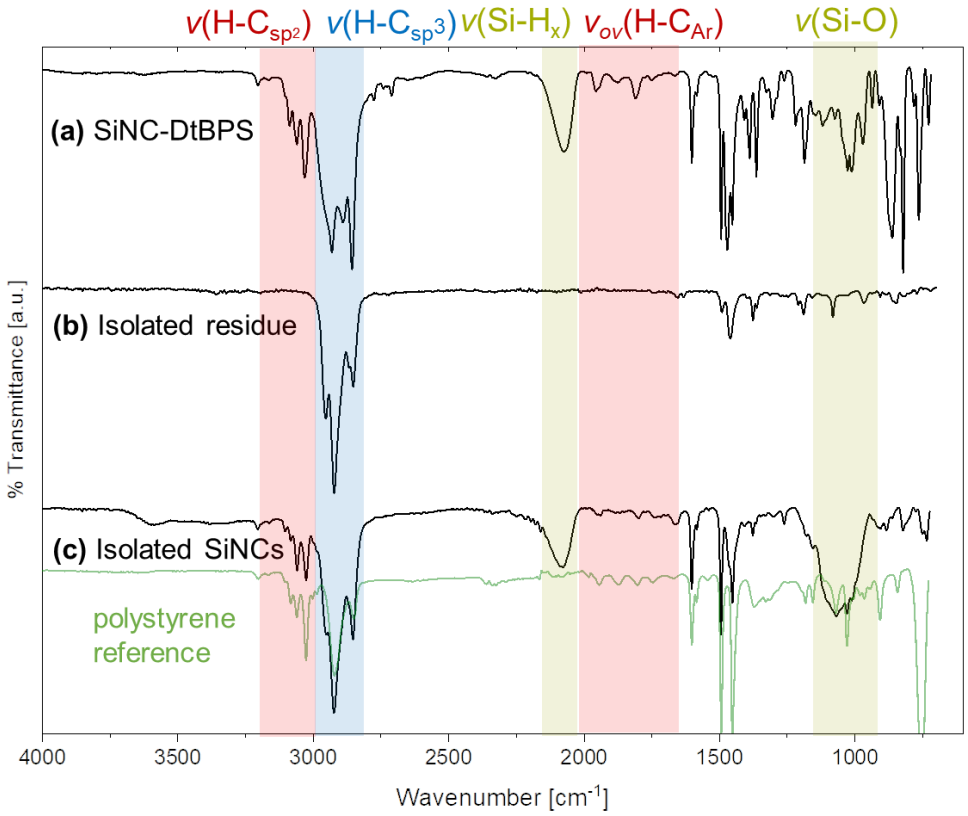

Figure 4.3–5. IR spectra of (a) sample obtained after reacting SiNCs with DtBPS, (b) the isolated residue after centrifugation and (c) the isolated SiNCs.

4.3.3 Summary and Conclusion

The use of siliranes as functionalization substrates for Si-H terminated silicon nanomaterials was explored. Initial reactions showed promising results, due to the high-reactivity and high quality of the sample as determined by infrared spectroscopy. The reaction can be initiated thermally or with UV-light and produces colloidally stable luminescent silicon nanocrystals. Considering that the activation of the silirane species results in a silylene and an alkene, the reaction was investigated as to whether silylene insertion, hydrosilylation or both occur. Through purification of the resulting silicon nanocrystals via ultracentrifugation and subsequent analysis, it was determined that only the undesired hydrosilylation takes place while the desired silylene insertion remains negligible, as no evidence for the insertion product could be found. Essentially, the employed silirane merely encompasses the most complex and expensive hydrosilylation substrate.

Some minor questions still remain open from this project: If the silylene does not insert, where does it go? Why could it not be isolated after the reaction? Why are the silicon

nanosheets less reactive? While these issues remain unanswered, because of the lack of any compelling results, this project was brought to a close and efforts were put into other more promising projects.

4.3.4 Experimental Procedures

4.3.4.1 General Information

Instrument information, analytical techniques, procedures for solvent drying, as well as the synthesis of hydrogen-terminated silicon nanocrystals and hydrogen-terminated silicon nanosheets are found in chapter 6: *General Experimental Procedures,* p. 124.

4.3.4.2 Synthesis of Siliranes

The siliranes presented in this work were synthesized by my colleague, *Matthias Nobis,* and were provided for my work.

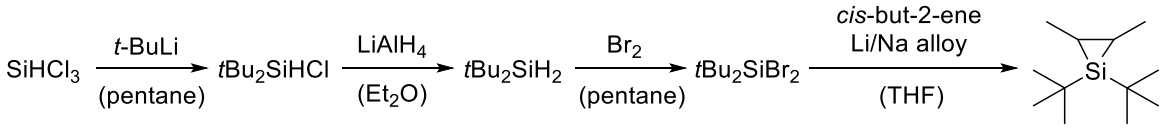

Scheme 4.3-4. Synthesis strategy to obtain siliranes.

The synthesis procedures up to $t\text{Bu}_2\text{SiH}_2$ are well known in the literature.[238, 239] Alternatively, $t\text{Bu}_2\text{SiH}_2$ can also be directly synthesized by reacting SiH_2Cl_2 with *t*BuLi.

$t\text{Bu}_2\text{SiBr}_2$ is obtained by brominating with Br_2 in pentane at 0 °C. The compound is distilled (60 °C, 10^{-2} mbar) and recrystallized from MeCN (-20 °C) prior to use.

4.3.4.2.1 Synthesis of *trans*-1,1-di-*tert*-butyl-2,3-dimethylsilirane (DTBDMS)

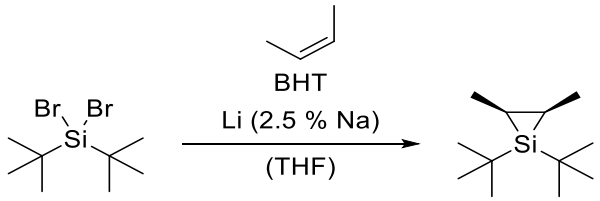

Scheme 4.3-5. Synthesis of cis-1,1-di-tert-butyl-2,3-dimethylsilirane.

A pressure-safe 500 mL Schlenk flask is charged with 30.0 g di-*tert*-butyldibromosilane (99.3 mmol, 1.0 eq.) and dissolved in 17.5 g THF (198.6 mmol, 2.0 eq.). 100 mg 3,5-Di-*tert*-butyl-4-hydroxytoluol (0.45 mmol, 0.005 eq.) are added to suppress radical reactions. The solution is cooled to -78 °C and the Ar removed in vacuum. 111.4 g *trans*-2-butene (1.9 mol, 20.0 eq.) are condensed into the reaction flask at 1.8 bar. The weight is determined by placing the flask on a scale. The flask is repressurized with Ar and the pressure carefully released by

opening the valve. 5.51 g Li/Na alloy (2.5 wt.% Na, 794.4 mmol, 8.0 eq., finely cut) is added und Ar flow. The flask is sealed and the solution is stirred and brought to room temperature over the course of 16 hours (*Caution!* The flask is now repressurized as butene is released from solution). The reaction dispersion is stirred for an additional 48 hours. The pressure is slowly released. THF is then removed *in vacuo*. The residue is extracted with dry pentane (5 x 100 mL) to remove LiBr. The oily residue is distilled at 40 °C at 10^{-2} mbar and the product condensed in a nitrogen-cooled receiving flask. The procedure yields 14.4 g (72.6 mmol, 73 %) *cis*-1,1-di-*tert*-butyl-2,3-dimethylsilirane as a clear oily liquid.

^{1}H-NMR: (297 K, 300 MHz, C_6D_6) δ = 1.06 (s, 2H, -Si-C*H*-), 1.09 (s, 18H, *t*Bu), 1.54–1.47 (m, 6H, -CH *Me*).

^{13}C-NMR: (300 K, 125 MHz, C_6D_6) δ = 10.0 (Si-*C*H-), 10.3 (Si-*C*H-), 18.6 (-CH-*Me*), 20.9 (-CH-*Me*), 30.0 (*t*Bu-Me), 31.6 (*t*Bu-Me).

^{29}Si-NMR: (300 K, 100 MHz, C_6D_6) δ = -53.2.

4.3.4.2.2 General Procedure for the Synthesis of Derivatized Siliranes

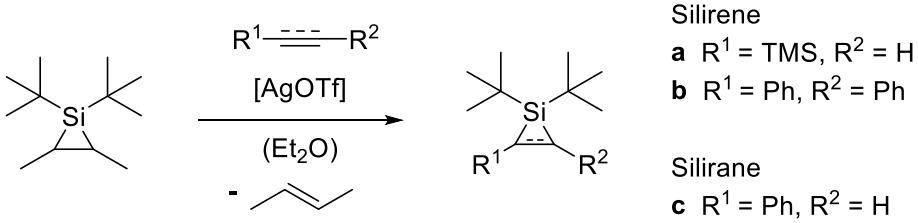

Scheme 4.3-6. Synthesis of derivatized siliranes and silirenes.

1,1-di-*tert*-butyl-2,3-dimethylsilirane (1.26 mmol, 1.0 eq.) are dissolved in 5 mL diethylether and transferred to a 25 mL Schlenk flask. The correexpsponding alkene/alkyne (1.26 mmol, 1.0 eq.) is added. The catalyst AgOTf (1.25 µmol, 0.001 eq.) is dissolved in diethyl ether (0.5 mL) and added to the solution. The solution is stirred for 24 h at room temperature. The reaction solution is filtered over heat-dried neutral alumina to remove the catalyst. The solvent is removed and the product distilled *in vacuo.*

4.3.4.3 General Reaction of Silicon Nanocrystals with Siliranes initiated thermally

In a heat-dried Schlenk tube, 4 mg of SiNC-H (from etching 200 mg SiNC/SiO_2) are dispersed in 2 mL dry, degassed *o*-xylene. 1 mmol of silirane is added and the solution degassed in three freeze-pump-thaw cycles. The dispersion is stirred for 16 hours at 150 °C. The resulting colloid is precipitated in MeOH and centrifuged for 4 minutes at 9000 rpm. The supernatant is discarded and the residue redissolved in toluene. This

precipitation/centrifugation/redispersion cycle is repeated two more times to yield functionalized SiNCs. The SiNCs are freeze-dried from benzene.

4.3.4.4 Reaction of Silicon Nanocrystals with Siliranes initiated with UV light

The reaction procedure is mainly the same as compared to the previous method. Instead of heating to 150 °C the Schlenk tube is placed in a home-made UV reactor system consisting of a single LED (360 nm) operating at 3W mounted on a water-cooled metal plate that is put on top of a magnetic stirrer. The Schlenk tube is irradiated and stirred for 16 hours. Final purification follows the same procedure as before.

4.3.4.5 Suppression of Hydrosilylation by sparging with argon

4 mg of SiNC-H (from etching 200 mg SiNC/SiO_2) are dispersed in 5 mL dry, degassed *o*-xylene and 1 mmol DTBDMS is added. The additional solvent is needed to account for losses during the reaction. The dispersion is transferred to a 3-neck flask equipped with a condenser and an air-tight glass tube that is connected to an Ar supply. The dispersion is degassed *via* three FPT cycles. The glass tube is submerged in the solution and Ar flow slowly increased. The reaction setup is opened at the top of the condenser to prevent over-pressurization. The Ar flow is kept to approximately 5 bubbles per second. The dispersion is heated to 150 °C and stirred for 16 hours. After cooling to room temperature and removal of Ar flow, the dispersion is purified according to 4.3.4.3.

4.3.4.6 Isolation of SiNCs from the polymer matrix by ultracentrifugation

5 mg of the sample are dispersed in 5 mL of toluene. The dispersion is separated into four ultracentrifugation vials and filled with solvent according to the manufacturers requirements. The samples are ultracentrifuged at 200 000 g for 4 hours. The vials are removed and the supernatant carefully removed with a pipette and stored for later. The pellets remaining in the vials are redispersed in toluene and transferred to new vials (one-time use only). The centrifugation/separation procedure is repeated for a total of 8 times resulting in SiNCs separated from the polymer matrix. The supernatants from the first three cycles are combined and the volume of solvent reduced under reduced pressure; the rest of the supernatants can be discarded. The supernatants are separated into four ultracentrifugation vials and ultracentrifuged to remove any residual SiNCs. This is repeated as necessary until the PL of the SiNCs is no longer visible in solution. Once complete, the solvent is completely removed in vacuum, to yield the separated homopolymer.

4.4 Functionalization of Silicon Nanocrystals with Dichalcogenides

4.4.1 Introduction

Most approaches for the functionalization of Si-H surfaces use hydrosilylation. This straightforward and versatile method is able to produce a variety of surface-modified SiNCs with different functional groups that can be used for a variety of applications.[25] While the hydrosilylation approach is robust and straightforward, it can only produce SiNC surfaces with Si-C linkages. Many reports have shown that the formation of heteroatom linkages on Si surfaces, i.e. Si-N, Si-P, has a strong effect on the underlying optoelectronic properties. In this fashion, *Dasog* and coworkers were able to tune the PL of SiNCs across the visible spectrum, only by using surface groups.[34] In terms of influencing the (opto)electronic properties, finding such alternate linkages may yield the most promising results.[240]

Korgel, Yu and coworkers were able to functionalize SiNCs with thiols by dispersing them in a high-boiling thiol (dodecanethiol) and heating to 190 °C.[241] They were able to show the formation of an Si-S bond through XPS and FTIR and noted the sensitivity of the sample to moisture. However, no changes in optoelectronic behavior were observed.[241] Looking to other nanostructured Si-H surfaces for inspiration, Buriak and co-workers developed methods for Si-chalcogen bond formation on hydride-terminated porous silicon and Si(111) surfaces, predicting that such a method is applicable to other Si-H materials.[242, 243] For the Si chalcogen bond, a change in work-function was predicted,[243, 240] however, UPS measurements by Hu *et al.* on moderately doped n-type Si(111) did not show any significant changes compared to the non-functionalized Si(111)-H sample.[244] As SiNCs are electronically different to the bulk Si(111) surface, the influence of the chalcogen group may manifest itself in a different way. Even small electronic changes of the surface head group could have strong effects on quantum confined particles. In fact, computational models on SiQDs predict tunable optical properties by varying the amount of incorporated sulfur.[240]

The use of dichalcogenides as substrates instead of the respective thiol or selenols offers some significant advantages. For one, the handling of dichalcogenides is much easier, since they are less reactive, less volatile, less malodorous and less toxic. In addition, both methods require high temperatures and dichalcogenides generally have higher boiling points. Mechanistically speaking, the dichalcogenides should exhibit a higher reactivity, since the mechanism involves the homolytic cleavage of the chalcogen-chalcogen bond, resulting in reactive radicals that react with the Si-H surface.[243] The proposed mechanisms for the thiol

reaction either rely on the cleavage of the Si-H bond or the in-situ formation of dichalcogenides.[241] Taking these insights into consideration the use of dichalcogenides as functionalization substrates for silicon nanocrystals was explored.

4.4.2 Results and Discussion

4.4.2.1 Functionalization

The initial reaction was carried out using 3 nm SiNCs-H dispersed in toluene and di-*n*-butyl disulfide at 130 °C in a sealed Schlenk flask. After 2 hours the dispersion exhibited a more intense red color – as compared to conventional functionalizations – and started to turn clear, although still slightly turbid. After 20 hours of reaction time, no further change was observed. As was noted by Korgel and coworkers, the Si-S bond is sensitive to moisture and requires purification under inert conditions.[241] As such, a centrifuge tube was sealed with a septum and the atmosphere exchanged with Ar. The reaction dispersion was precipitated in dry, degassed MeOH and purified via precipitation/centrifugation/dispersion cycles. Toluene was used as the solvent during the purification, but the SiNCs never formed a clear dispersion, as is usually the case for functionalized SiNCs. After testing various solvents, it was found that 1,4-dichlorobenzene is able to form a clear solution with the modified SiNCs and was mainly used from here onwards.

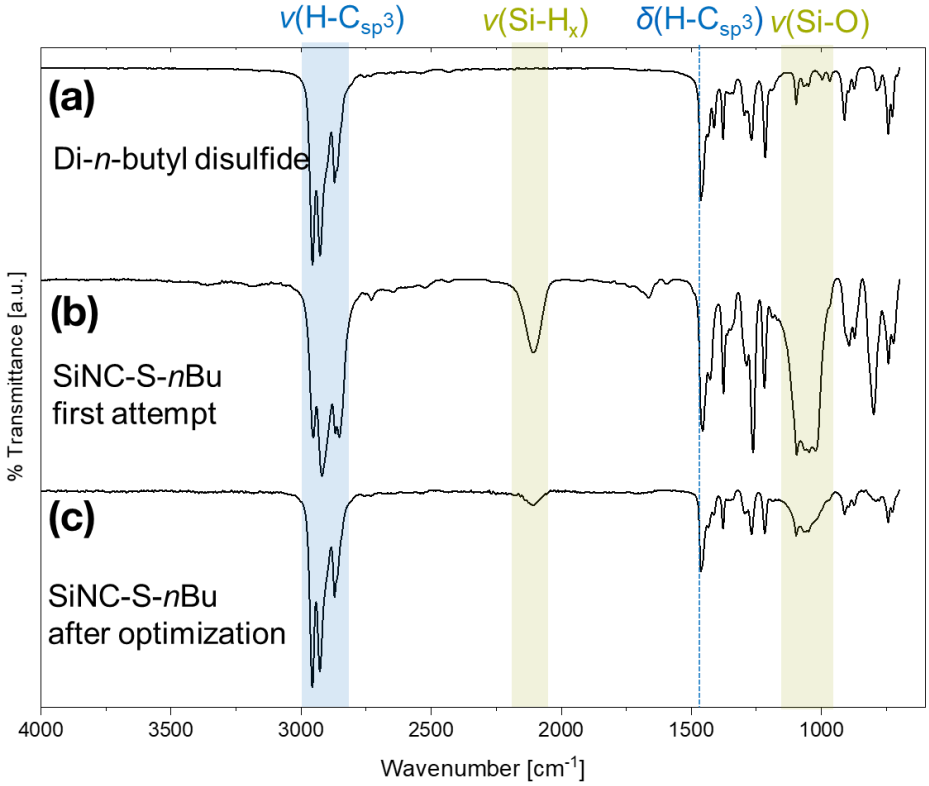

Figure 4.4–1. FTIR spectra of SiNCs functionalized with di-*n*-butyl disulfide. (a) Comparison spectrum of the substrate, (b) SiNCs obtained after the initial reaction and (c) after optimizing the reaction conditions.

FTIR of the product reveals bands corresponding to *n*-butyl-modifed SiNCs, exemplified by the strong ν(H-C_{sp^3}) and δ(H-C_{sp^3}) at 2900 cm^{-1} and 1460 cm^{-1} respectively (**Figure 4.4–1b**). Unfortunately, the sample still showed strong oxidation, indicated by the ν(Si-O) at 1100 cm^{-1}. This oxidation was attributed to an incomplete surface coverage due to the unoptimized reaction conditions. Repetition of the reaction with different parameters showed that the oxidation can be kept to a minimum by conducting the reaction at 150 °C and for a shorter 2 hour period (**Figure 4.4–1c**).

With the successful proof of concept in hand the initial reaction was repeated and extended to other dichalcogenides: diphenyl disulfide, diphenyl diselenide and diphenyl ditelluride. The dispersions all turned clear within 5 minutes of reaching the peak temperature of 150 °C except for the ditelluride reaction, which stayed turbid even after a 20 hour reaction period. During the reactions an increased brightness of the photoluminescence for the sulfur-containing reagents could be observed, while the PL brightness of the diselenide sample decreased (**Figure 4.4–2**[†]).

Figure 4.4–2. Pictures of SiNC samples reacted with (i) di-*n*-butyl disulfide (ii) diphenyl disulfide and (iii) diphenyl diselenide under visible light (left picture) and UV illumination (right picture).[†]

FTIR measurements of the purified products showed bands corresponding to the employed substrates, but also showed ν(H-C_{sp^3}) bands which were not expected, since no sp^3-hybridized carbon atoms are present in the in the final samples (**Figure 4.4–3a**). It is likely that this band arises from trace impurities that adsorb to the surface of the SiNCs. Usually, these are not as relevant as they are overlapped by the much more intense ν(H-C_{sp^3}) bands of substrates containing alkyl chains, such as for SiNC-S-*n*Bu (**Figure 4.4–1**). In this case however, the bands are disturbing for the measurements. Washing the samples with analytical grade, dry dichloromethane diminished this band, but was not able to remove it completely (**Figure 4.4–3b**). It turns out that the use of glass instead of polypropylene syringes is

[†] The diphenyldisulfide (ii) sample oxidized before taking the picture and therefore did not form a clear dispersion.

necessary to completely remove the disturbing ν(H-C_{sp^3}) bands (**Figure 4.4–3c**). Their presence comes from the dissolution of additives in the plastic syringes that can then adsorb onto the SiNCs.

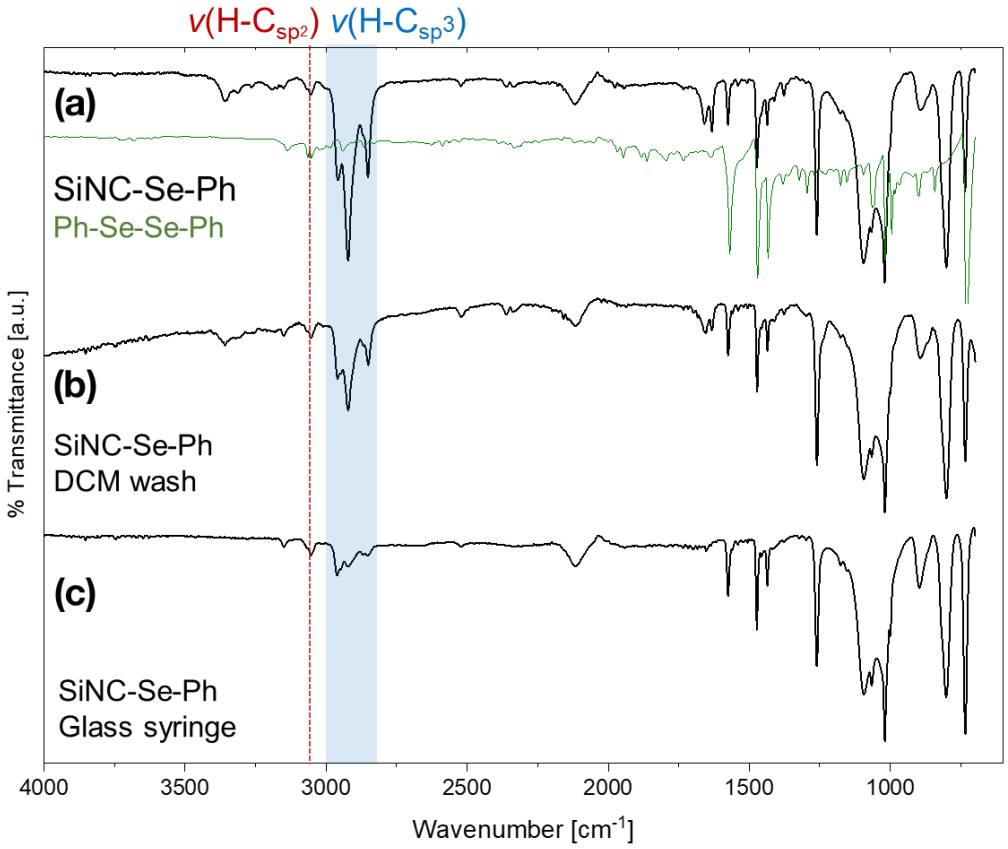

Figure 4.4–3. IR spectra of SiNC-Se-Ph showing the diminishing ν(H-C_{sp^3}) band upon washing with (b) DCM and (c) using a glass syringe. Green inset spectrum is the substrate diphenyl diselenide.

Accordingly, an additional dichloromethane washing step was included from hereon. The IR spectra obtained from the samples reacted with various dichalcogenides are shown in **Figure 4.4–4**. Even though the reactions and purification were conducted under inert conditions, some oxidation still occurred, evident by the ν(Si-O) features found for all substrates at 1100 cm^{-1}. ν(H-C_{sp^3}) bands at 2900 cm^{-1} and δ(H-C_{sp^3}) bands at 1460 cm^{-1} are found for the SiNC-S-*n*Bu sample corresponding to the expected aliphatic surface groups (**Figure 4.4–4a**). SiNC-S-Ph (**Figure 4.4–4b**) and SiNC-Se-Ph (**Figure 4.4–4c**) exhibit characteristic ν(H-C_{sp^2}) and ν(C=C) bands, centered at 3100 cm^{-1} and 1640 cm^{-1} respectively. The FTIR spectrum of SiNC-Te-Ph did not show any bands that suggest successful modification, merely oxidation occurred, demonstrated by the strong ν(Si-O) feature. Similar observations were made by Hu and coworkers, who also noted the lack of reactivity towards the Si-H surface.[244] This oxidation likely occurred during the transfer of the sample to the spectrometer, as the samples are exposed to air and the telluride sample does not have any protective organic groups. Overall, all samples exhibit bands that strongly overlap with the

bands produced by the original substrates (orange spectra) and thus the attachment of the functional groups can be confirmed.

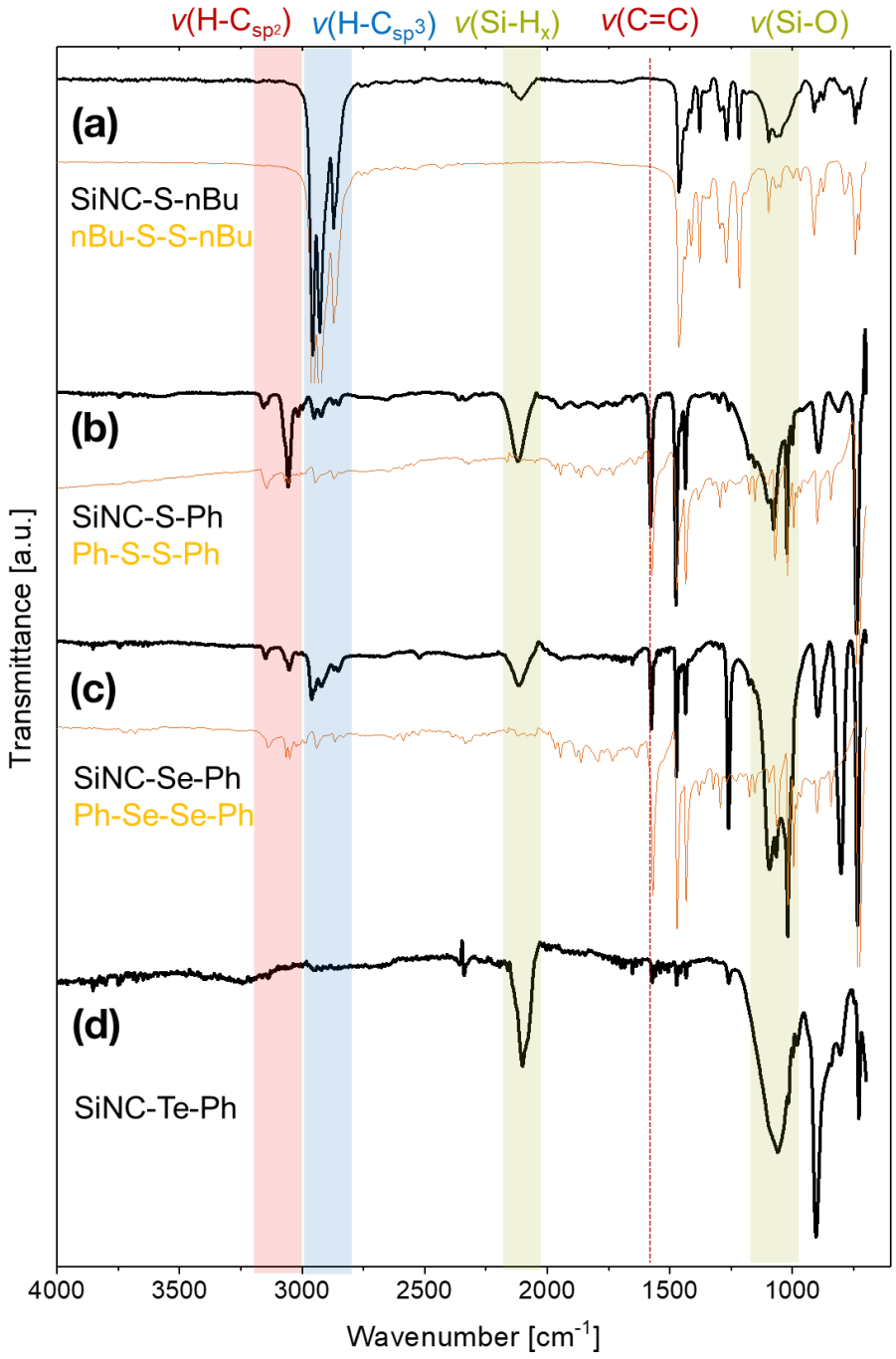

Figure 4.4–4. IR spectra of SiNCs functionalized with different organic dichalcogenides. The original substrate spectra are inset (orange). (a) SiNC-S-nBu, (b) SiNC-S-Ph, (c) SiNC-Se-Ph and (d) SiNC-Te-Ph.

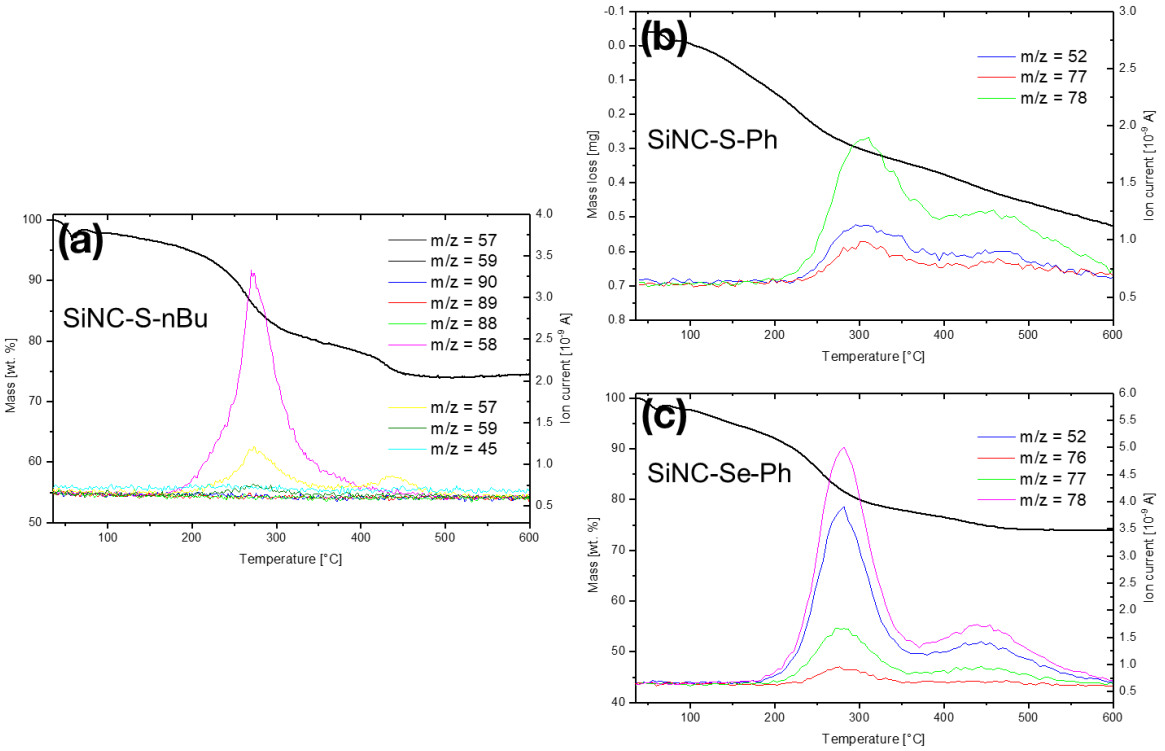

Figure 4.4–6. TGA-MS data obtained for the different samples: (a) SiNC-S-n-Bu, (b) SiNC-S-Ph and (c) SiNC-Se-Ph.

The mass losses observed with TGA-MS indicate organic groups on the surface of the SiNCs. In addition, the detection of specified mass to ionization ratios (m/z) allows the direct observation of characteristic groups. For phenyl sulfide and phenyl selenide, m/z of 78 were detected (**Figure 4.4–6b, c**), indicating the presence of phenyl groups, whereas for the SiNC-S-*n*Bu sample butyl groups with m/z of 58 can be seen (**Figure 4.4–6a**). Since only one weight loss event is visible for each sample it is assumed that only one surface bound species are present. The onset of the decomposition (~150 °C) is lower than that of hydrosilylated substrates and is explained by the lower decomposition temperature of the Si-chalcogen bond.

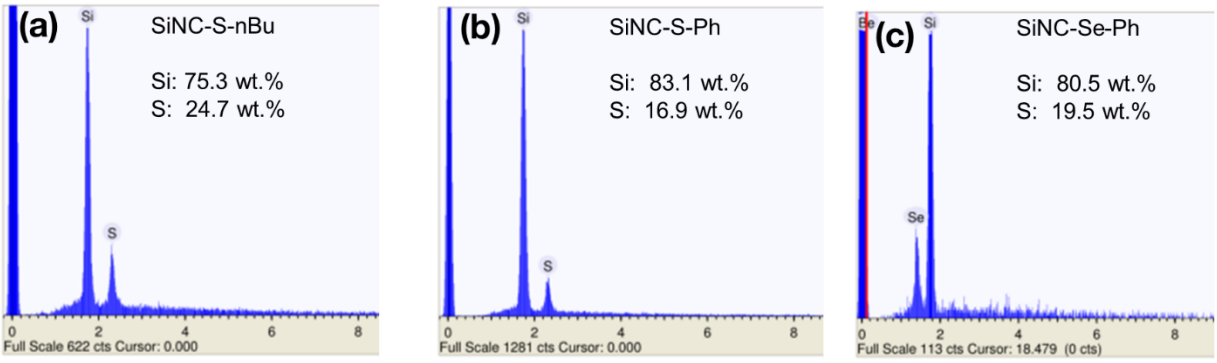

Figure 4.4–5. EDX measurements showing qualitative compositions for (a) SiNC-S-nBu, (b) SiNC-S-Ph and (c) SiNC-Se-Ph.

Data thus far was able to show the presence of organic groups, however, the presence of the chalcogens remains unverified. Energy dispersive X-ray spectroscopy is able to reveal the elemental presence of the respective chalcogens. However, the employed instrument is not able to detect elements smaller than sodium, therefore the obtained relative compositions cannot be regarded as absolute values but rather, the measurements serve as a qualitative indicator for the presence of the respective chalcogens. Indeed, all measurements are able to show the presence of the respective chalcogens (**Figure 4.4–5**).

TEM images of the samples show very large agglomerations of the functionalized SiNCs (**Figure 4.4–7a-c**). These large agglomerations and the close proximity of the SiNCs prevents accurate diameter measurements of the SiNCs. A size-distribution could therefore not be obtained for any of the samples. The large agglomerations are likely caused by the bad

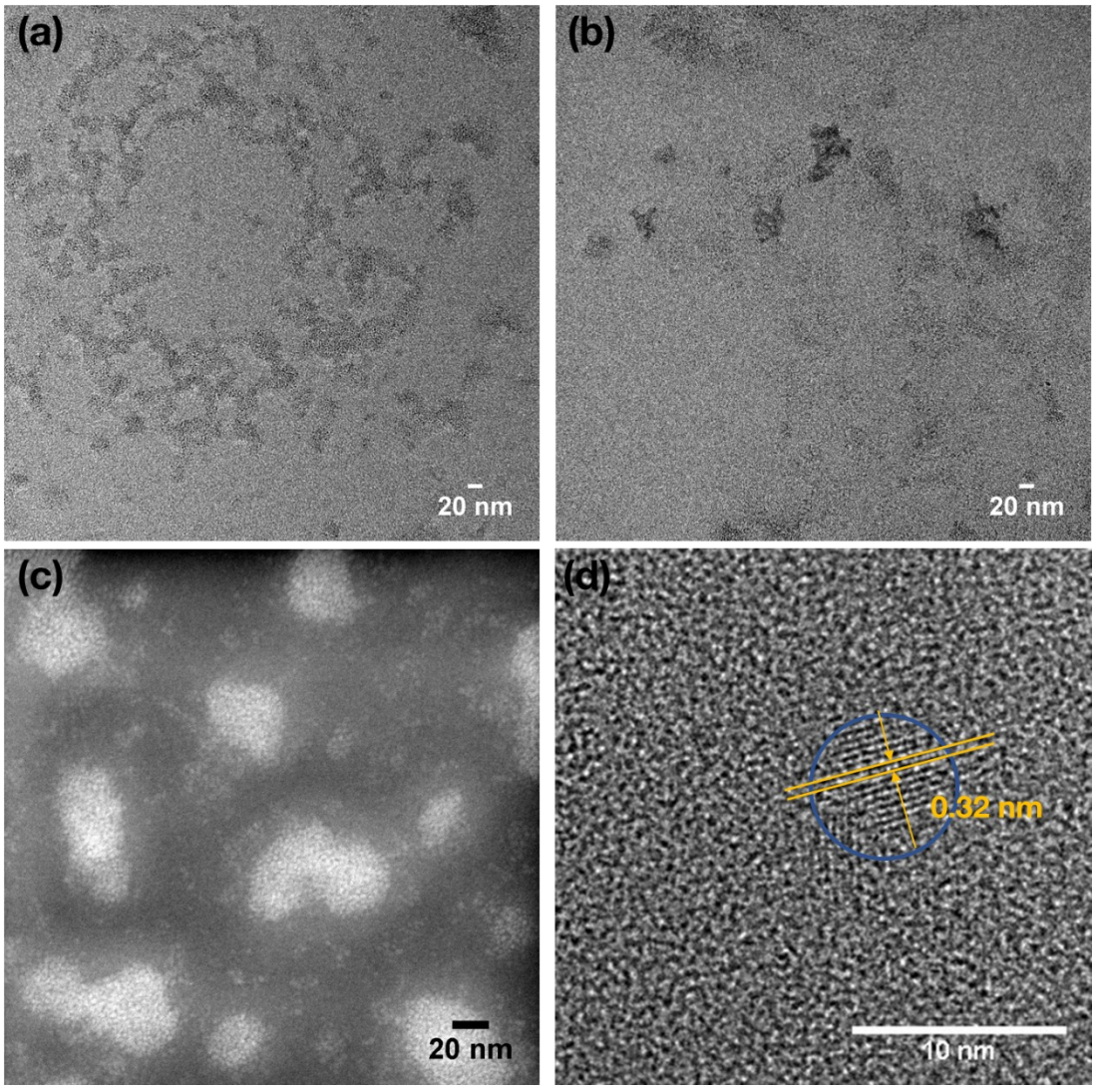

Figure 4.4–7. Selected TEM images of dichalcogenide samples. (a) Dark field image of SiNC-S-nBu, (b) dark field image of SiNC-S-Ph and (c) SiNC-Se-Ph. All samples show large agglomerations. (d) A cropped HR-TEM image of SiNC-S-Ph showing the lattice fringes of the Si(111) plane.

solubility of the functionalized samples in any given solvent. 1,4-dichlorobenzene was used to dissolve the SiNCs and prepare the TEM samples and the low volatility of 1,4-DCB causes the SiNCs to form highly concentrated regions during the slow drying process. For other TEM preparations, benzene was typically used, which has a much lower boiling point. For one of the samples a high quality HR-TEM image could be obtained, which is able to show the crystallinity of the SiNCs, evident by the lattice fringes of the Si(111) plane (**Figure 4.4–7c**). This confirms that the SiNCs remain crystalline throughout the reaction procedure.

4.4.2.2 Optoelectronic properties

As was mentioned earlier, the functionalization with organic dichalcogenides has a profound effect on the photoluminescence of the silicon nanocrystals. For the disulfides higher PL brightness was observed, while the selenides exhibited a lower one. In order to achieve comparable optical measurements of the differently functionalized SiNCs, a batch of hydride-terminated silicon nanocrystals were etched from the same SiNC/SiO_2 composite and subsequently functionalized with the organic dichalcogenides as well as 1-dodecene as a control sample. Subsequently, they were subjected to the same photoluminescence, and quantum yield measurements.

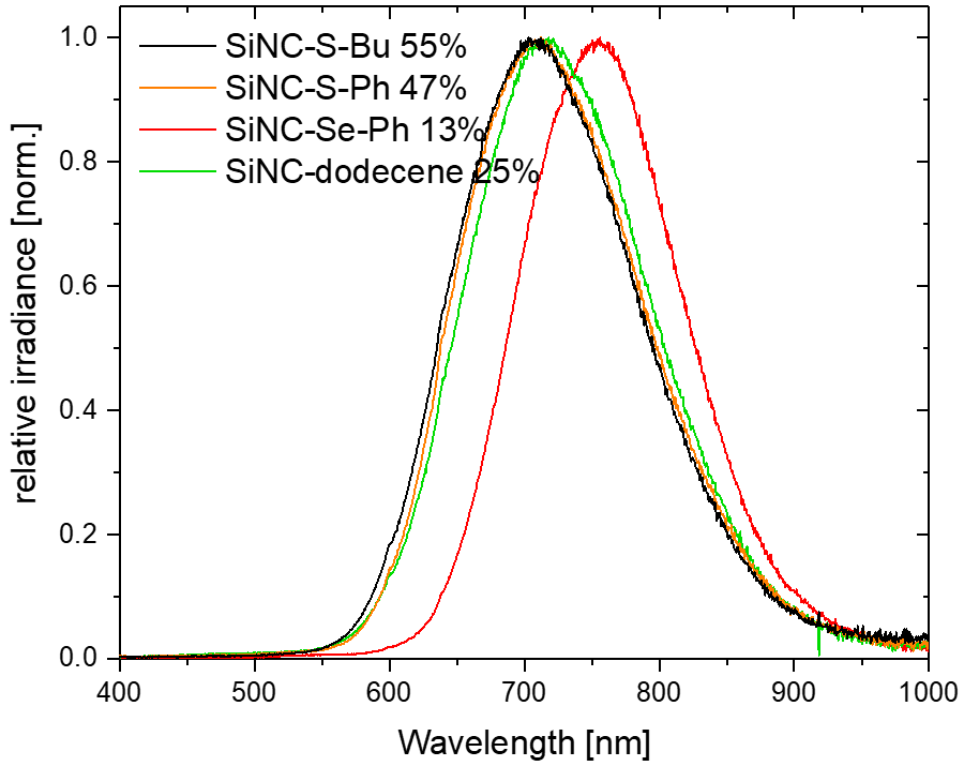

Figure 4.4–8. PL spectra of SiNCs functionalized with different dichalcogenides and a control sample, SiNC-dodecene. Percentages describe the quantum yield.

The control sample SiNC-dodecene has a PL maximum at 710 nm with a full-width-at-half-maximum (FWHM) of 122 nm. This suggests 3.5 nm diameter SiNCs,[43] which coincides

with rough estimations made with TEM. The sulfide samples SiNC-S-*n*Bu and SiNC-S-Ph exhibit nearly identical spectra to the control sample, with minimal deviations that can be attributed to minor concentration differences in the measurement solutions. Interestingly, the SiNC-Se-Ph sample shows a PL red-shift of 45 nm, exhibiting an emission maximum at 757 nm. The FWHM remains similar to the other samples at 125 nm. The unchanged FWHM between all samples and control are an indication that the quality of the SiNCs remain unaffected during the reaction procedure. Usually, oxidation of a sample is accompanied by a blue-shift of the PL maximum, as well as an increase of the FWHM due to the destruction of the crystal structure and increased size deviations between the oxidized SiNCs.

Quantum yield measurements also show that SiNC-Se-Ph exhibits a much lower QY of only 13 % compared to the baseline of 25 % determined for the control sample SiNC-dodecene. The disulfide samples, however, show an increased QY, nearly twice that of SiNC-dodecene with 55 % and 47 % for SiNC-S-*n*Bu and SiNC-S-Ph respectively, explaining the increased brightness observed during the reaction. Because there is almost no difference between the optoelectronic properties of SiNC-S-*n*Bu and SiNC-S-Ph, it is assumed that the increased QY stems from the chalcogen group and not the organic modifier (i.e. butyl vs. phenyl).

Further insight was gained by measuring the excited state lifetimes of the dichalcogenide samples. By measuring the time and intensity of detected photons, the excited state lifetimes can be determined by fitting the data to a stretched exponential decay.[245]

$$I(t) = I_0\, e^{-(\frac{t}{\tau})^{\beta}} \qquad \textbf{Eq. 2}$$

Equation 2 describes the decay rate where $I(t)$ and I_0 describe the PL intensity over time and at the start of the measurement, respectively and β is the dispersion factor related to the curvature of the decay. Solving for τ gives the decay time. The spectra for the dichalcogenide samples are shown in **Figure 4.4–9**. Lifetimes were calculated at 102 µs, 80 µs and 73 µs for SiNC-S-*n*Bu, SiNC-S-Ph and SiNC-Se-Ph respectively. For lifetime measurements the exact values are not as important as the magnitude of the values. For all samples microseconds lifetimes were found, which are in agreement with the lifetimes observed for hydrosilylated SiNCs and correspond to the core-emissions of the SiNCs.[246, 41] If a surface-defect or a surface-state is responsible for the changes in optoelectronic behavior, then lifetimes with nanoseconds are expected.[41]

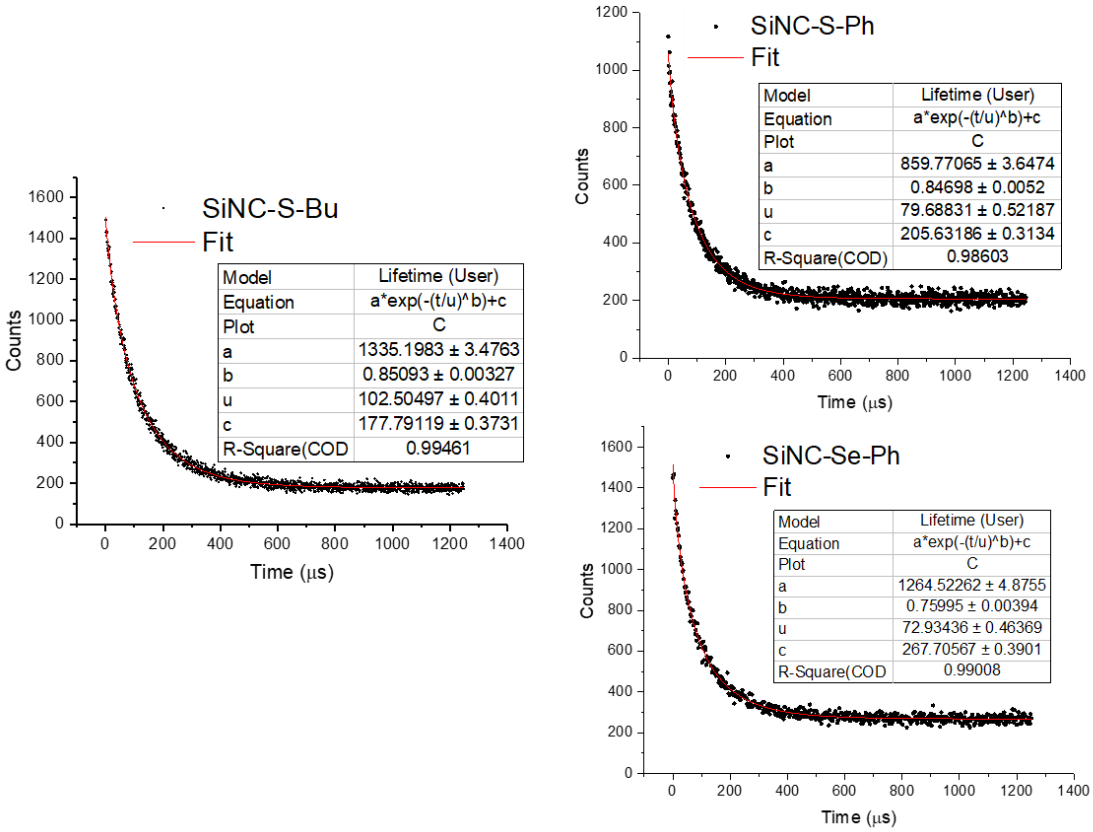

Figure 4.4–9. PL decays obtained for dichalcogenide samples.

Unfortunately, due to a misunderstanding only a microsecond pulsed laser was used for the measurements and thus only the microsecond components of the lifetime decays were obtained. In order to comprehensively determine the nanosecond component of the excited state lifetimes, additional measurements with a nanosecond pulsed laser are required. Unfortunately, due to logistical reasons these measurements could not be performed, before the end of this thesis.‡

However, in light of the consistent microsecond lifetimes and red emission of all dichalcogenide samples it is reasonable to assume that the photoluminescence stems from the core-emission of the silicon nanocrystals and is not due to any defects or surface states caused by the functionalization.[247, 103] Yu and coworkers determined very similar excited state lifetimes, consistent with the data provided here.[241]

4.4.2.3 Alternative reaction protocols

Up to now only the thermal activation of organic dichalcogenides was considered. Reports in the literature also show other possibilities of obtaining chalcogen-functionalized

‡ Unfortunately, CoVid-19 prevented an exchange with the University of Alberta, where the measurements would have been performed.

particles. For one, the homolytic cleavage of the dichalcogenides can also be activated by UV-irradiation.[244] Yu and coworkers were also able to functionalize SiNCs using dodecanethiol, resulting in SiNC-S-$C_{12}H_{25}$.[241] They, however, did not report any changes or significant observations about the optoelectronic behavior of the sample. Since this is the unique selling point of this method, these methods were also analyzed and compared, to see whether the method affects the properties.

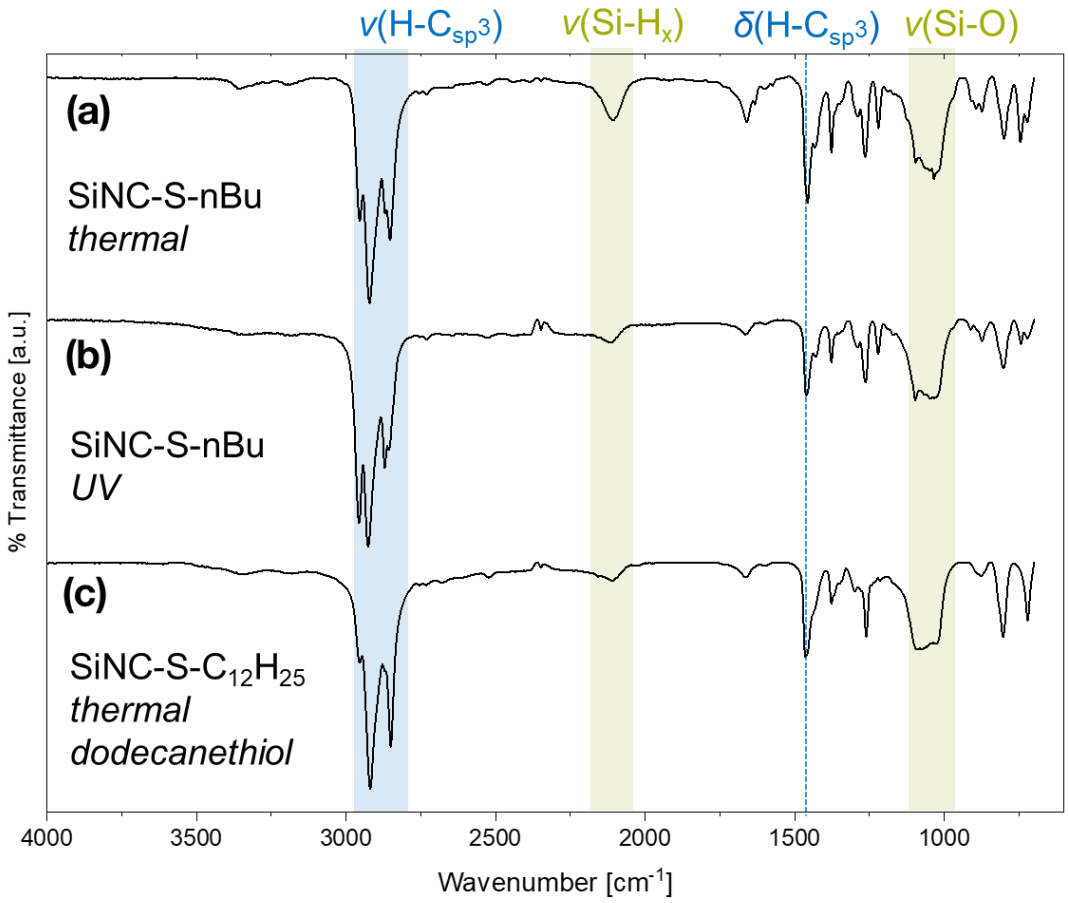

Figure 4.4–10. IR spectra of SiNCs functionalized with thiol groups obtained from di-*n*-butyl disulfide initiated (a) thermally, (b) with UV irradiation and (c) SiNCs thermally functionalized with dodecanethiol.

The SiNCs-H for these reactions were liberated form the same SiNC/SiO_2 composite, di-*n*-butyl disulfide was used as the substrate, and a thermal control reaction was included as well. For the UV reaction, instead of heating the reaction mixture to 150 °C, the Schlenk tube was placed in a UV reactor and irradiated for 2 hours. For the thiol-method, the reaction was conducted with dodecanethiol as described in the literature.[241] In all cases, the reaction mixture turned clear within the reaction time and a noticeable increase in PL intensity was noted. FTIR spectroscopy revealed successful functionalization for all samples, as shown by the expected ν(H-C_{sp^3}) bands at 2900 cm^{-1} (**Figure 4.4–10**). The samples show nearly identical bands with only minor oxidation (ν(Si-O), 1100 cm^{-1}). The ν(Si-H_X) are diminished in all cases, indicating its consumption during the reaction.

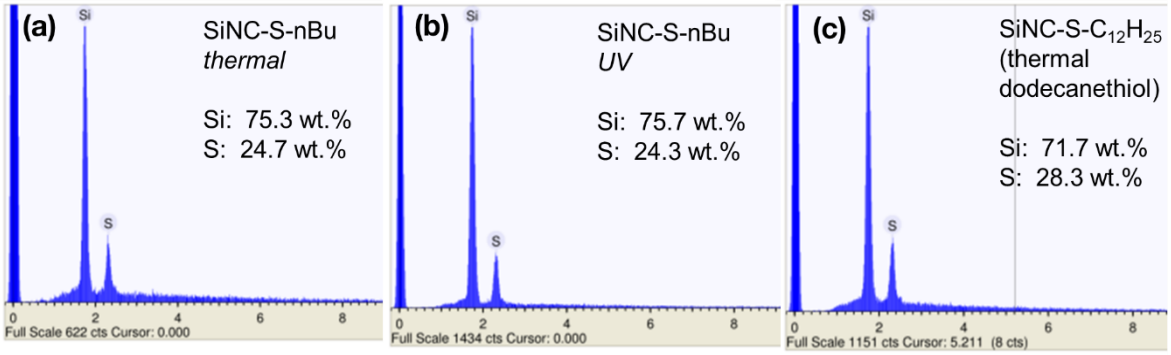

Figure 4.4–11. EDX spectra of thio-functionalized SiNCs obtained from different methods. (a) Thermal initiation with di-*n*-butyl disulfide, (b) using UV irradiation and (d) reaction of SiNC-H with dodecanethiol.

Similar to the previous results, EDX measurements confirmed the presence of sulfur in the samples (**Figure 4.4–11**). The calculated content is similar between the thermal, UV and thiol samples, all showing around 24 wt.%. As stated before, these EDX measurements merely serve as qualitative indicators for the presence of the thiol group. The combined results of EDX and FTIR indicate successful functionalization of SiNCs with the respective thio-groups, showing that the alternative pathways are just as viable as the thermal reaction with dichalcogenides.

The optoelectronic properties of the samples show almost identical behavior. The PL emission maxima are essentially identical at 712 nm between all samples and a FWHM of 125 nm is seen for all products (**Figure 4.4–12**).

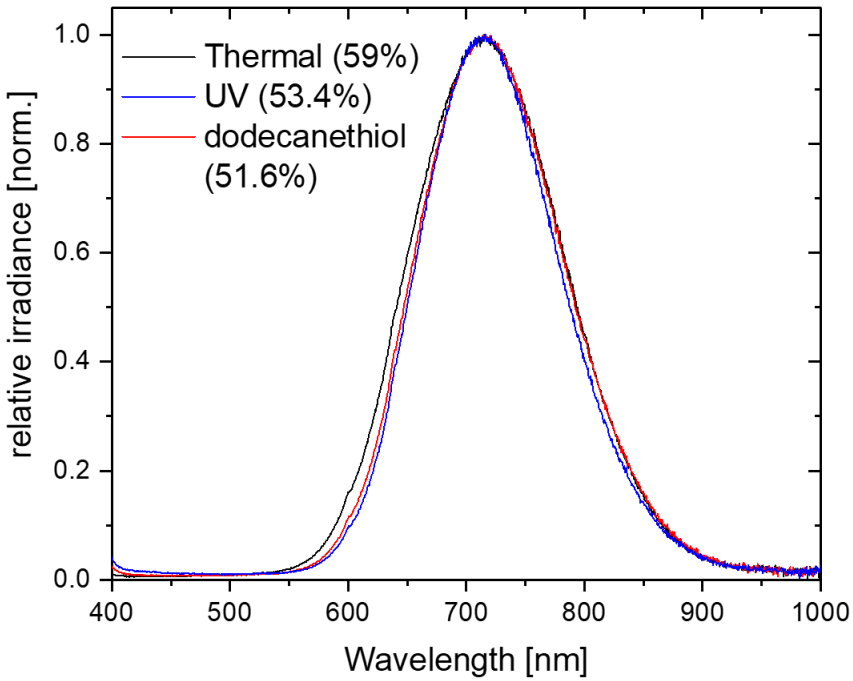

Figure 4.4–12. PL spectra of SiNC-chalcogenides obtained via different reaction pathways. Values in parentheses are absolute quantum yields.

The QYs were also analyzed and all samples exhibit a quantum yield above 50 %, consistent with the observations made previously. These results are a clear indicator that for chalcogen-functionalized SiNCs, the method is not what affects the emission characteristics, but the effects are rather due to the intrinsic effect of the chalcogen-silicon bond. The increased quantum yield for the dodecanethiol functionalized sample was not observed – or at least noted – by Yu and coworkers. The reason why no differences in the PL of the SiNCs was observed may be due to the weak kinetic stability of the Si-S bond. The reported IR spectrum exhibits significant oxidation, which changes the optoelectronic characteristics of the sample and may have negated any observable increases in brightness.[241]

4.4.3 Conclusion and Outlook

In this chapter, the functionalization of silicon nanocrystals with organic dichalcogenides is described. The reaction is conducted at elevated temperatures to homolytically cleave the dichalcogen bond, which produces radicals that can react with the Si-H surface.[242] This reaction was tested with di-*n*-butyl disulfide, diphenyl disulfide, diphenyl diselenide and diphenyl ditelluride. For the ditelluride, no reaction was observed. Interestingly, the diselenide sample exhibited a PL red-shift of 45 nm along with a reduced quantum yield of 13 % while the disulfide samples both exhibited a significantly higher quantum yield of around 50 % as compared to the reference SiNC-dodecene sample (25 %). Through excited state lifetime measurements it was determined that the PL emission stems from core emission states rather than surface- or defect-states introduced by the functionalization. In comparison, for chalcogen-functionalized Si(111) wafers, Hu *et al.* predicted a change in work function, but no changes were observed with UPS measurements.[242, 244] The given explanation is the low coverage of chalcogenide, relative to the amount of silicon. In this case, the functionalization leads to a much higher relative surface coverage due to the high surface area of the silicon nanocrystals as compared to a Si(111) wafer. The effect of the chalcogenide group is therefore much more pronounced. While theoretical models predicted a change in properties for SiQDs,[240] the exact mechanisms behind the observed changes in optoelectronic characteristics remain unknown and are beyond the scope of this thesis. Possible clarification could be gained with more extensive measurements such as UPS, and more precise PL instrumentation (temperature-dependent PL, time-resolved PL).

The pathway to obtain chalcogen-functionalized SiNCs was also analyzed. Apart from thermal initiation, UV light can also be used to initiate the reaction with dichalcogenides. Yu *et al.* also showed the possibility of directly functionalizing SiNCs with thiols, but did not note any changes in optoelectronic properties.[241] Upon repetition in this work, an increased PL

brightness was observed regardless of functionalization method. This indicates that the changes are indeed due to the heteroatom linkage and are not dependent on the employed method. Mechanistically, *Yu* and coworkers suggest the in-situ formation of the disulfide during the reaction of SiNCs with thiols, explaining the similarities. The use of dichalcogenides offers some significant advantages over their thiol and selenol counterparts. They are less reactive, less toxic and less odorous and are thus much easier to handle.[248] In addition, the flexibility of using UV initiation instead, permits the use of low-boiling substrates. This is not possible when reacting with thiols at 190 °C.

Overall, the results obtained here are very promising for increasing the performance of optoelectronic devices that utilize silicon nanocrystals. One of the major obstacles that still needs addressing however, is the stability of the samples. The weak stability of the Si-S and Si-Se bonds currently prohibits their use in any meaningful way.[248] Costly and elaborate techniques are required to exclude oxygen and moisture from reacting with the sample and as such, the fabrication of optoelectronic devices is severely hindered. Future work on this topic should address this problem. One possible idea is to produce a bifunctional particle with one half of the functional groups comprising Si-Se/S, while the other is composed of robust Si-C linkages obtained from hydrosilylation. This could, in theory, provide enhanced optoelectronic characteristics while increasing the stability of the sample.

4.4.4 Experimental Procedures

4.4.4.1 General Information

Instrument information, analytical techniques, procedures for solvent drying, as well as the synthesis of hydrogen-terminated silicon nanocrystals are found in chapter 6: *General Experimental Procedures,* p. 124.

All reactants used in this project were purchased from *Sigma-Aldrich* and immediately stored in a glove box prior to use. No additional purification or drying was performed. Unless stated otherwise all solvents were dried and degassed prior to use.

4.4.4.2 Thermal Functionalization of Silicon Nanocrystals with Dichalcogenides

SiNC-H obtained from etching 200 mg SiNC/SiO_2 composite are dispersed in 1 mL dry 1,4-dichlorobenzene (DCB) and transferred to a heat-dried Schlenk flask. 2 mmol of the desired dichalcogenide are dissolved in 0.5 mL dry DCB and added to the flask. After three FPT cycles, the reaction mixture is heated to 150 °C and stirred for one hour. The deep red dispersion is reduced to approximately 0.5 mL volume to facilitate subsequent purification.

4.4.4.3 UV Functionalization of Silicon Nanocrystals with Dichalcogenides

SiNC-H obtained from etching 200 mg SiNC/SiO_2 composite are dispersed in 1 mL dry 1,4-dichlorobenzene (DCB) and transferred to a heat-dried Schlenk flask. 2 mmol of the desired dichalcogenide are dissolved in 0.5 mL dry DCB and added to the flask. After three FPT cycles, the reaction mixture is transferred to a UV reactor and illuminated for two hours. The deep red dispersion is reduced in vacuum to approximately 0.5 mL volume to facilitate subsequent purification.

4.4.4.4 Thermal Functionalization of Silicon Nanocrystals with Dodecanethiol

SiNC-H obtained from etching 200 mg SiNC/SiO_2 composite are dispersed in 2 mL dodecanethiol, degassed *via* three FPT cycles and heated to 180 °C for 12 hours. Subsequent purification of the dark red suspension yields purified SiNC-S-$C_{12}H_{25}$.

4.4.4.5 Purification of Organic chalcogenide Functionalized Silicon Nanocrystals

An FEP centrifuge tube is sealed with a rubber septum and the atmosphere exchanged with Ar using a canula connected to an Ar line. 15 mL acetonitrile (MeCN) are added to the tube. The reaction mixture is transferred and precipitated in the centrifuge tube. The Ar canula is removed and the mixture centrifuged at 9000 rpm for 4 minutes. The centrifuge tube is connected to the Ar line and the supernatant carefully removed using a syringe. The residue is dispersed in a minimal amount of DCB and MeCN (10 mL) used to precipitate the colloidal suspension. This centrifugation cycle is repeated three times. After the last cycle, the remaining residue is washed with dichloromethane that was transferred using only heat-dried glass syringe and stainless steel canula (no polymers!). Centrifugation yields purified SiNC-E-R.

Alternatively, the procedure can be conducted with dry degassed solvents and a centrifuge in a glove box. This was not performed in this case as chalcogens, thiols and selenols are detrimental to the glove box catalyst.

4.5 Surface-Anisotropic Silicon Nanocrystals

4.5.1 Introduction

The projects outlined in the previous chapters were concerned with various functionalization methods of both silicon nanocrystals and silicon nanosheets. For the silicon nanocrystals, all methods produce uniformly functionalized particles, meaning that the functional groups are homogenously distributed on the particle. This also applies to all published functionalization methods concerning silicon nanocrystals; no one has yet produced silicon nanocrystals where the functional groups are localized to specific areas on the surface. This type of particle, i.e. one side of the particle possesses a different functional group than the other, is known as a *Janus particle* (for more details see chapter 2.3: *Janus Particles*, p. 25).

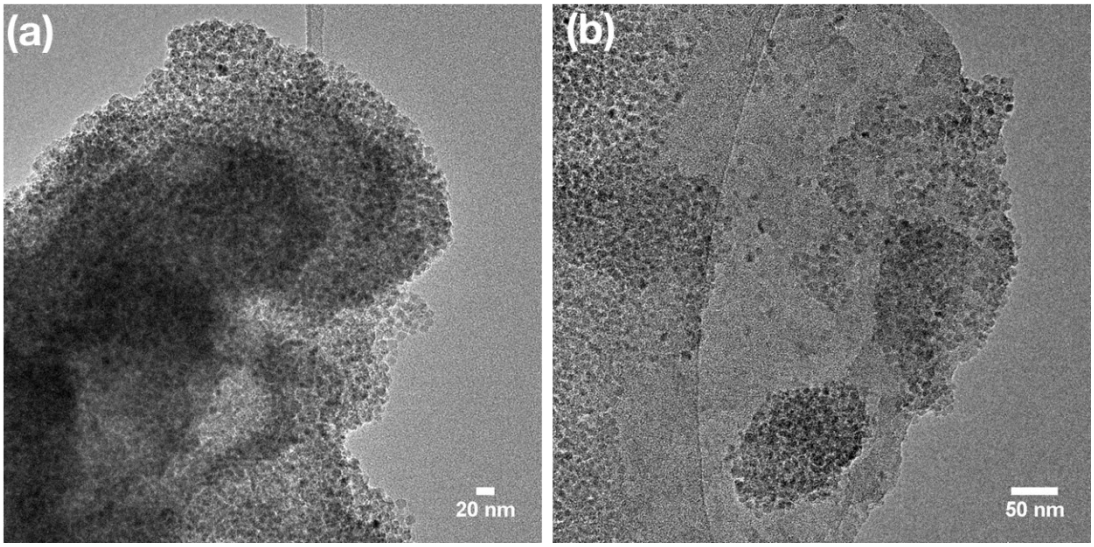

Figure 4.5–1. TEM image of SiNC deposited on SiNS as shown in chapter 4.2.

In chapter 4.2, the dehydrogenative coupling of silanes as a functionalization method for silicon nanosheets was explored and discussed; the results of which were shown to be fairly unpromising. However, it was established that the two silicon-based nanomaterials, silicon nanosheets and silicon nanocrystals, can be bonded together using this reaction, forming a new hybrid material. The remaining Si-H groups were subsequently thermally hydrosilylated with 1-dodecene to stabilize the sample and facilitate characterization. This material is denoted as $H_{25}C_{12}$-SiNC@SiNS-$C_{12}H_{25}$ (see 4.5.5.2: *Nomenclature of Silicon Nanocrystals*, p. 116). FTIR of the sample confirmed the functionalization with 1-dodecene and transmission electron microscopy images show the bound silicon nanocrystals on the surface of the larger two-dimensional material (**Figure 4.5–1**). This material, at first, did not offer any immediately discernable interesting applications, as the attractive properties of both nanomaterials –

namely the (opto)electronic properties, such as photoluminescence – disappeared; likely caused by scattering and charge-transfer processes.

However, an interesting idea emerged: Since silicane is UV-sensitive (see chapter 2.2.2: *Properties of Silicon Nanosheets*, p. 20),[149] while SiNCs can be functionalized using UV-irradiation,[62, 61] would it be possible to simultaneously destroy the underlying nanosheets and functionalize the SiNCs in the presence of an alkene (**Scheme 4.5-1**)? Because one side of the silicon nanocrystal was protected by the silicon nanosheets, their destruction should re-expose the protected side and the second alkene should react with exactly this newly exposed side, resulting in a two-sided nanoparticle (**Scheme 4.5-1**). Similar processes have been developed to produce other Janus particles and is commonly referred to as “masking” (chapter 2.3.1).[249, 174]

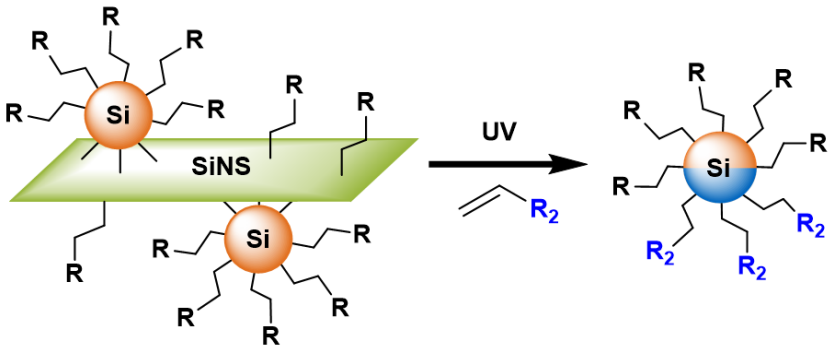

Scheme 4.5-1. Synthetic strategy to obtain Janus particles after deposition of silicon nanocrystals on silicon nanosheets. UV irradiation simultaneously destroys the SiNSs and functionalizes the SiNCs.

4.5.2 Results and Discussion

4.5.2.1 Proof of Concept

To test this hypothesis, $H_{25}C_{12}$-SiNC@SiNS-$C_{12}H_{25}$ – synthesized as described in chapter 4.2 – was dispersed in toluene and ethyl undecylenate was added to the dispersion. The dispersion was irradiated with UV-light for two hours, but after only five minutes of exposure, the previously non-luminescent sample showed the characteristic strong photoluminescence of the silicon nanocrystals (**Figure 4.5–2**). Pictures of the samples reveal that the turbid dispersion becomes much clearer after the irradiation and comparing the pictures under UV-light shows that the non-luminescent dispersion of $H_{25}C_{12}$-SiNC@SiNS-$C_{12}H_{25}$ (**Figure 4.5–2**, left) shows photoluminescence after the irradiation process (**Figure 4.5–2**, right). These observations are indications that the SiNCs were liberated from the SiNS-mask. As the sample is irradiated, the silicon nanosheets are destroyed and the SiNCs are released from the surface. Simultaneously, the newly exposed side of the nanocrystals is functionalized with the available alkene (here, ethyl undecylenate), the particle is stabilized and able to form a

clear colloidal dispersion. Since the SiNCs are no longer connected to the silicon framework of the nanosheets, no charge transfer processes and scattering occur, resulting in the re-emergence of photoluminescence, which can then be seen under UV illumination (**Figure 4.5–2**, right).

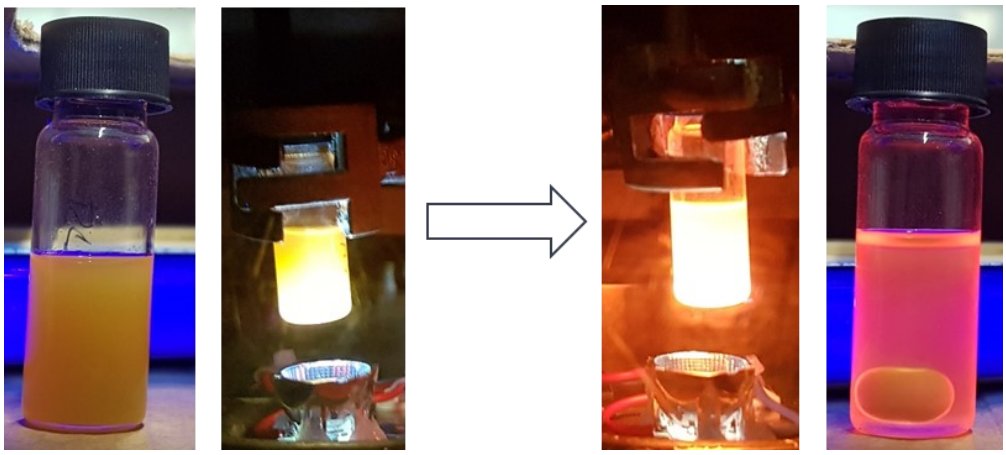

Figure 4.5–2. Pictures of $H_{25}C_{12}$-SiNC@SiNS-$C_{12}H_{25}$ irradiated in a UV reactor in the presence of ethyl undecylenate. Left pictures show the sample at the start of the reaction and pictures on the right depict the sample after one hour of irradiation.

The free-standing SiNCs are purified through centrifugation. The non-luminescent precipitate is separated from the solution after centrifugation and washed with toluene. The separated supernatant contains the liberated SiNCs and is purified according to procedures as performed for common hydrosilylation protocols. Briefly, the SiNCs are precipitated in an anti-solvent, centrifuged and redispersed. Repetition of this dispersion/precipitation/centrifugation cycle yields purified SiNCs (for details see 4.5.5.5, p. 117).

IR spectroscopy was used to monitor the functional groups of the materials during the reaction. The initial material, $H_{25}C_{12}$-SiNC@SiNS-$C_{12}H_{25}$, shows features corresponding to a dodecyl functionalized silicon nanomaterial (**Figure 4.5–3**a). The isolated residue/precipitate mainly shows signs of a strongly oxidized Si-species confirmed by the ν(Si-O) band at ~1100 cm^{-1} dominating the spectrum. Some traces of organic residue are also discernible through the ν(H-C_{sp^3}) at 2900 cm^{-1} (**Figure 4.5–3b**), which indicates that the residue comprises the decomposition products of the silicon nanosheets that were functionalized in the first step, explaining the ν(H-C_{sp^3}) band. The spectrum of the isolated SiNCs (from the supernatant) is very different (**Figure 4.5–3c**). Next to the typical signals of a silicon nanomaterial (ν(Si-H_x) at 2100 cm^{-1} and ν(Si-O) at ~1000 cm^{-1}), bands corresponding to the ester functionality are also visible: ν(C=O) at ~1700 cm^{-1} and ν(H-C_{sp^3}) at ~2900 cm^{-1}, indicating successful attachment of ethyl undecylenate. Of course, both dodecyl and ethyl undecenoyl groups are

expected in the final sample, however, IR spectroscopy is not able differentiate between the two organic groups, because the dodecyl functionality does not possess a unique identifier; at least in FTIR.

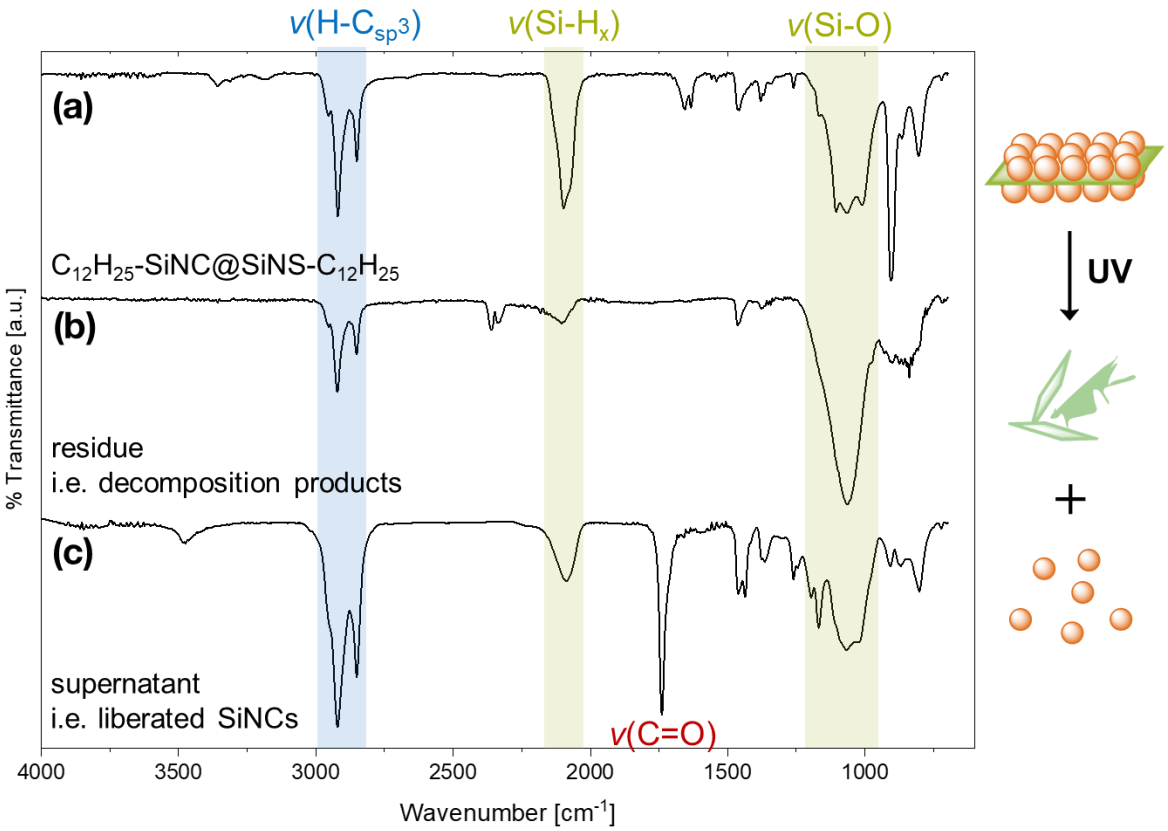

Figure 4.5–3. FTIR spectra of the (a) SiNCs deposited on SiNSs with dodecyl functionalization, (b) the residue obtained after UV irradiation and centrifugation and (c) the purified supernatant containing liberated SiNCs.

To confirm the suspected liberation of the silicon nanocrystals from the silicon nanosheets, TEM images were taken of the final sample. The images reveal that there were still unwanted silicon nanosheets in the sample (**Figure 4.5–4a**) but some areas also showed agglomerations of free-standing silicon nanocrystals (**Figure 4.5–4b**), explaining the observed emergence of PL and clear colloidal dispersion. Improvements to the liberation were made by extending the irradiation time to 4 hours and purifying more carefully, after which no more silicon nanosheets could be found in the sample (**Figure 4.5–4c**).

The observations and results from the TEM and IR measurements show promising first results for the synthesis of two-sided Janus silicon nanocrystals. With the proof of concept established, the project was pursued further.

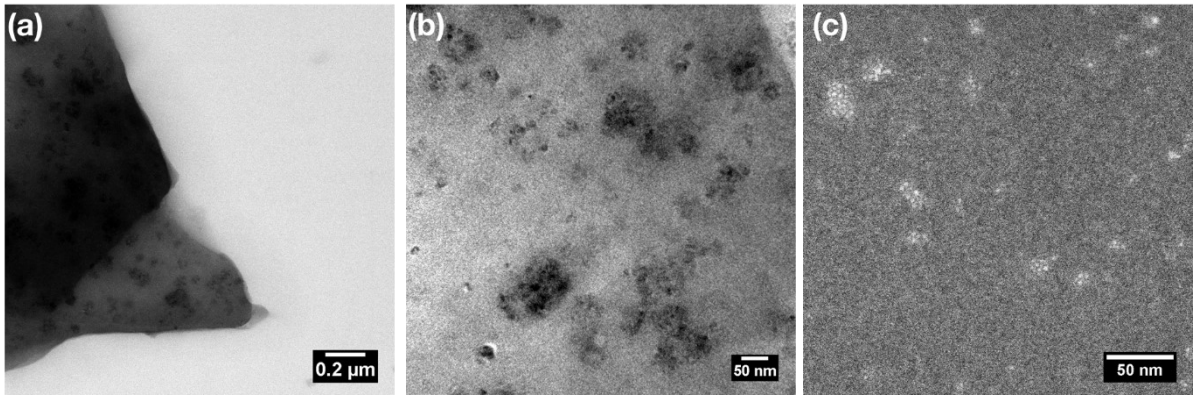

Figure 4.5–4. Bright field TEM images depicting the samples obtained after irradiation for two hours: (a) and (b). Dark field TEM image of samples obtained after 4 hours of UV irradiation: (c).

4.5.2.2 Verifying Bi-Functionality

In order to determine if the synthesis strategy results in a Janus particle, the attachment of two different functional groups needs to be confirmed. The previous characterization of the liberated particles with FTIR merely suggested the presence two functional groups, but did not offer a clear confirmation.

As such, a strategy was designed, wherein energy dispersive X-ray (EDX) spectroscopy would show the presence of two elemental markers – chlorine and bromine. For this, SiNCs were once again deposited on SiNSs through dehydrogenative coupling and the exposed Si-H groups thermally functionalized with 1-chlorohexene. In the irradiation step, bromoundecene was used as the reactive alkene, resulting in the bifunctional $ClH_{12}C_6$-SiNC-$C_{11}H_{22}Br$. The initial H-SiNC@SiNS-H sample shows a small chlorine content of

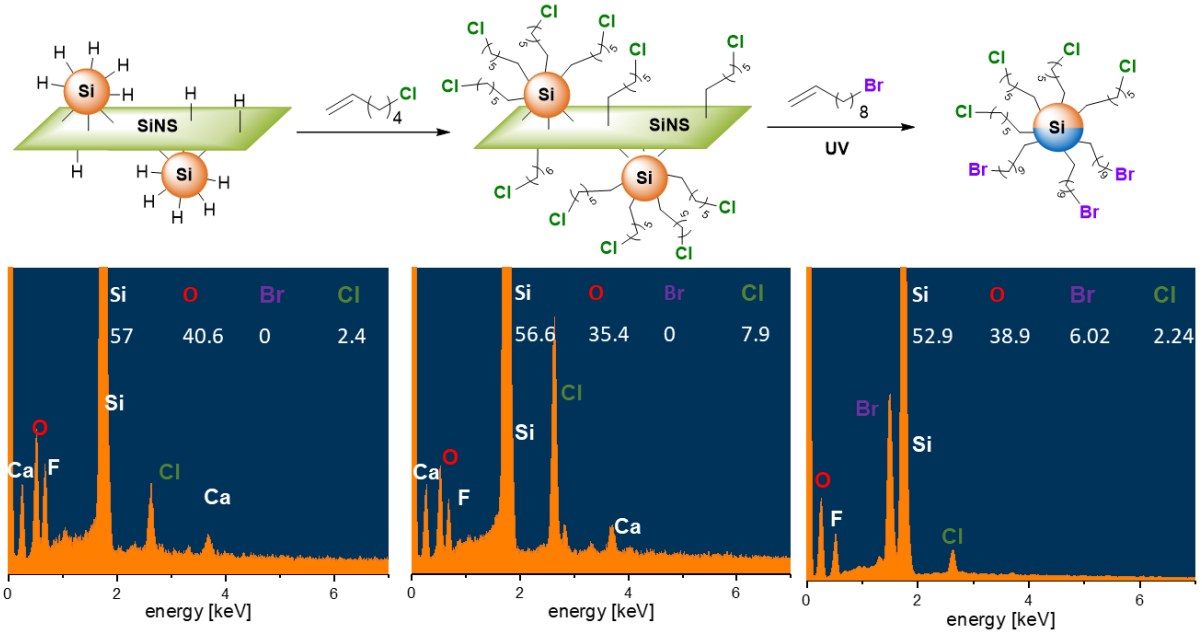

Figure 4.5–5. Top row: Synthesis strategy for Janus SiNCs with halogen elemental markers. Bottom row: EDX spectra of the corresponding samples. Only Si, O, Br, Cl are part of the total calculation, in order to ensure comparability. All ratios are given in atomic-%.

2.4 at.%, which is expected, as the silicon nanosheets are synthesized in hydrochloric acid, during which chlorine incorporation cannot be prevented. In addition, a calcium signal is also visible in the EDX spectrum, attributed to residual $CaSi_2$. After the functionalization with 1-chlororhexene a significant increase in the chlorine content is seen (7.9 at.%). Up to this point, no bromine was detected in any of the samples. The sample is functionalized with 1-bromoundecene under four hours of UV irradiation, after which no calcium signal is seen, indicating removal of SiNSs. EDX measurements of the sample shows a strong increase of the bromine content (6 at.%), but a lower chlorine content than the sample before (2.2 at.%). This explained by the removal of the decomposed SiNSs during the purification. Because the nanosheets were also functionalized with 1-chlorohexene in the previous step, a relatively large amount of chlorine is removed from the sample, resulting in a lower overall chlorine content. However, the initial chlorine that resulted from the silicon nanosheet synthesis is now removed, meaning that the detected elements are only localized to the silicon nanocrystals. Critically, the final sample shows both chlorine and bromine, confirming the attachment of two different alkenes. Mapping the locations of the elements with secondary electron microscopy (SEM) and EDX showed that all of the relevant elements (Si, C, O, Cl, Br) are distributed evenly throughout the two measured areas (**Figure 4.5–6**), excluding the possibility that the two hydrosilylations only proceeded on 'patches' of SiNCs, instead of the same particle.

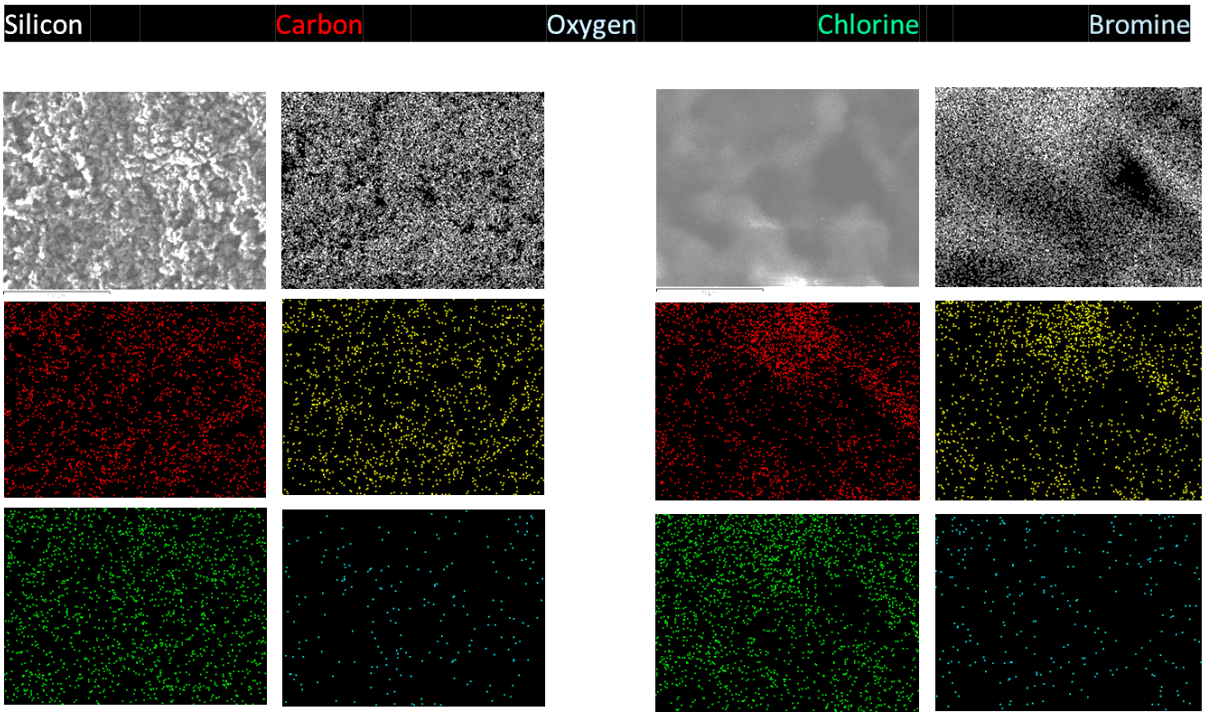

Figure 4.5–6. EDX mapping of two areas of the halogenated Janus SiNCs ($ClH_{12}C_6$-SiNC-$C_{11}H_{22}Br$) showing a homogeneous dispersion of all elements.

The obtained data through this EDX mapping does suggest the synthesis of bifunctional particles, however, some ambiguity still remains. The pre-existing chlorine from the synthesis of the SiNSs, leaves doubts to the incorporation of chlorine in the final SiNC sample, as the atomic ratios are very similar. Replacement of the elemental marker, 1-chlorohexene, with an alternative could not be achieved. A fluorinated marker would be even more uncertain, as both the SiNSs and the SiNCs are etched with hydrofluoric acid, resulting in an preexisting fluorine content (the fluorine signal can also be seen in the EDX spectra, **Figure 4.5–5**). The use of 1-iodohexene showed no promising results, as the functionalization proceeded much slower and the intermediate showed almost no iodine incorporation. This is likely due to the instability of the iodine species, which easily decomposes during the reaction or purification. Using alkenes that contain other heteroatoms such as nitrogen, sulfur or other chalcogenides also did not result in successful surface modifications in SiNC control reactions.

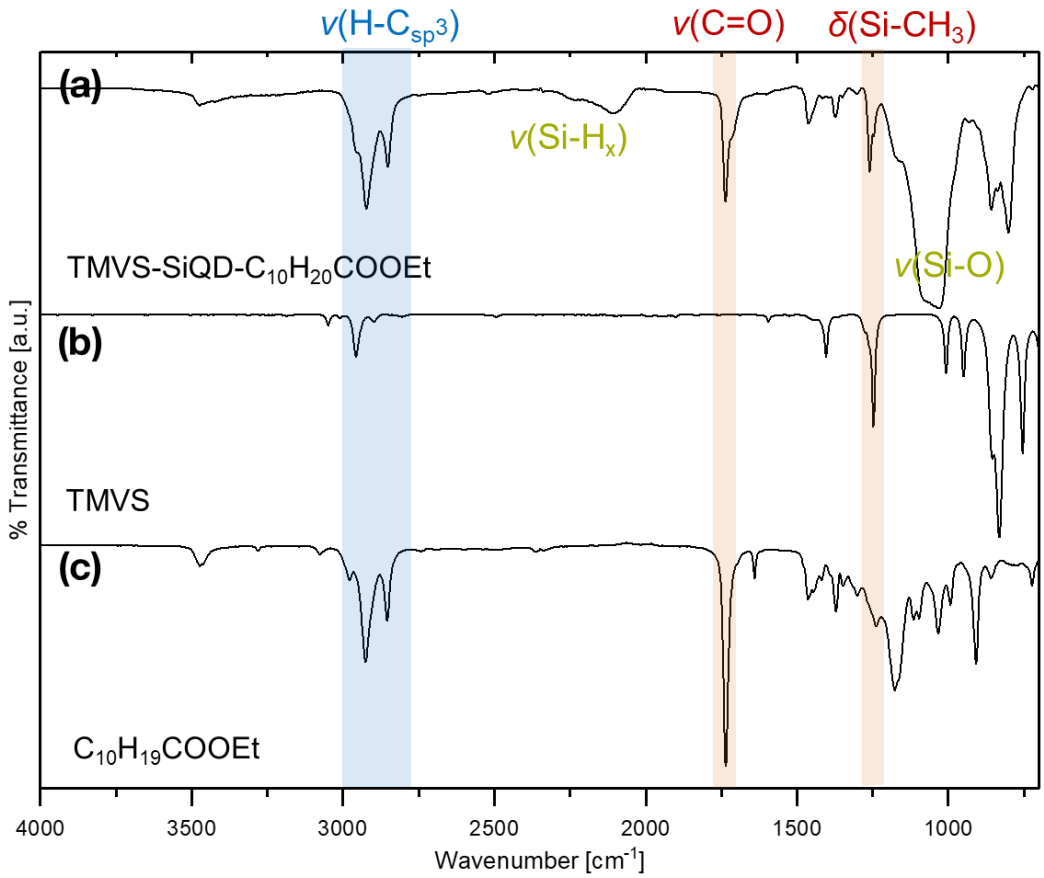

Figure 4.5–7. FTIR spectra of (a) the Janus sample (b) and (c) control substrates. The unique identifying bands are marked in red.

For these reasons, an additional approach was designed to show the bifunctionality of the silicon nanocrystals. Instead of relying on EDX spectroscopy to show both functional groups, the SiNCs were functionalized with two alkenes that show characteristic bands in IR spectroscopy: trimethylvinylsilane (TMVS) and ethyl undecylenate. While the TMVS exhibits a unique δ(Si-CH$_3$) at 1260 cm^{-1} (**Figure 4.5–7b**), the ester group is identifiable through its

ν(C=O) band at 1700 cm^{-1} (**Figure 4.5–7c**). After the deposition of the SiNCs on the SiNSs, the sample was hydrosilylated with trimethylvinylsilane (TMVS). Remaining freestanding SiNCs were removed through centrifugation in toluene and the TMVS-SiNC@SiNS-TMVS sample was irradiated with UV-light in the presence of ethyl undecylenate. Just as before, the dispersion exhibits bright photoluminescence shortly after the start of the reaction. After purification of the resulting SiNCs (denoted TMVS-SiNC-$C_{10}H_{20}COOEt$), an FTIR spectrum was recorded. Indeed, the TMVS-SiNC-$C_{10}H_{20}COOEt$ sample exhibits both of the characteristic signals (**Figure 4.5–7a**), implying that both functional groups are incorporated onto the silicon nanocrystal surface. Control spectra of the corresponding substrates are also included (**Figure 4.5–7b**, **c**) and shows that TMVS-SiNC-$C_{10}H_{20}COOEt$ exhibits nearly identical bands to both.

TGA-MS is also able to confirm both of these functional groups through their unique m/z ratios (**Figure 4.5–8b**). During the decomposition of the ester group CO_2 is released which possesses an m/z ratio of 43, while the TMVS functionality is identified through an m/z of 59, corresponding to a dimethylsiliane group. Control experiments with mono-functional SiNCs were conducted and were able to verify the uniqueness of the m/z ratios (**Figure 4.5–8b**, **c**).

The evidence provided by the characterization techniques EDX, FTIR and TGA-MS confirm the bifunctionality of the SiNCs obtained from the silicon nanosheet masking procedure. Therefore, the project progressed into the next step: identifying the localization of the two functional groups.

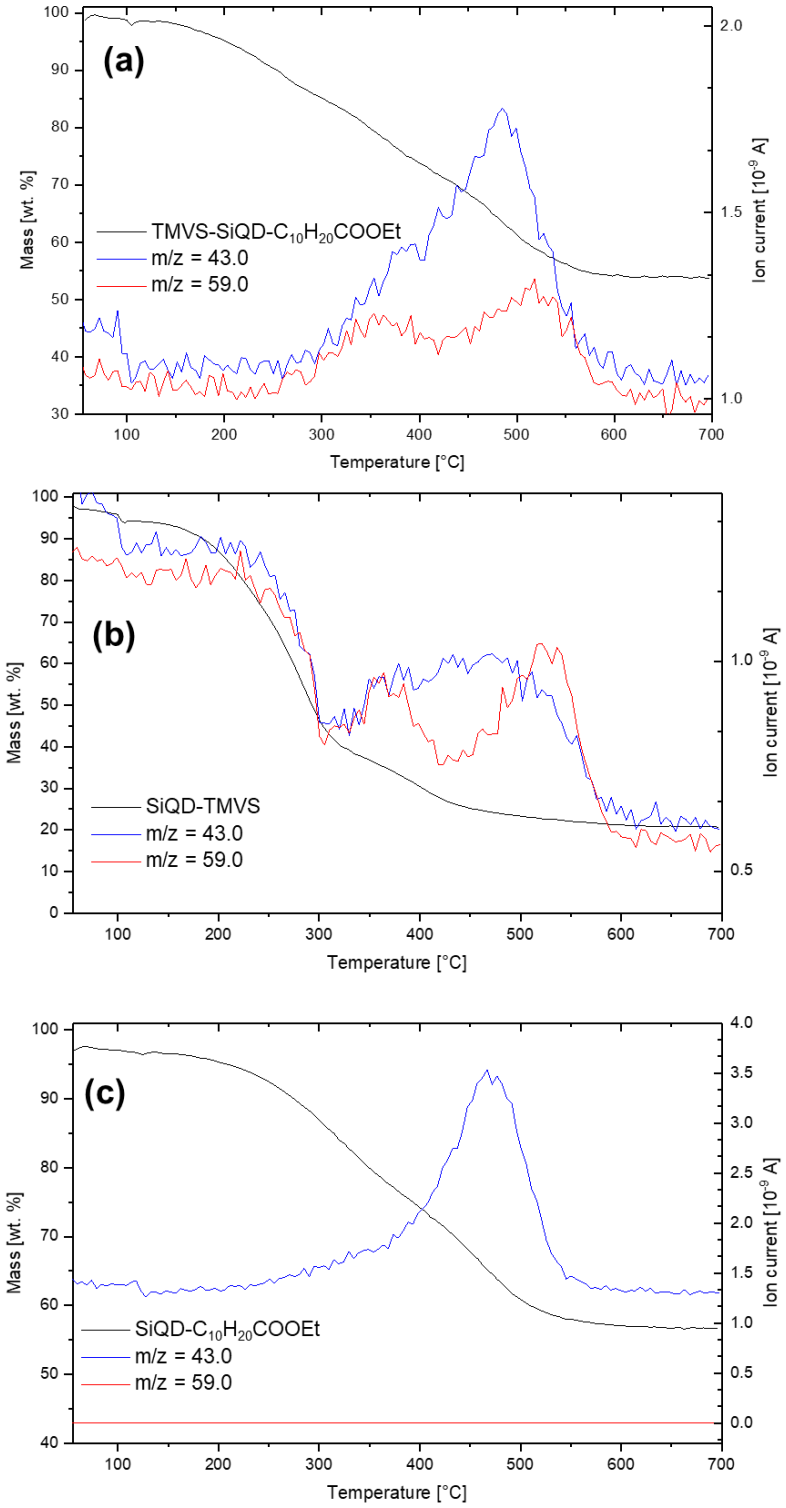

Figure 4.5–8. TGA-MS spectra of (a) the Janus sample TMVS-SiNC-$C_{10}H_{20}$COOEt and TGA-MS spectra of monofunctional isotropic control samples: (b) SiNC-TMVS and (c) SiNC-$C_{10}H_{20}$COOEt.

4.5.2.3 Verifying Anisotropy

The data presented thus far is consistent with bifunctional silicon nanocrystals. However, this constitutes only one part of the overall goal in synthesizing surface-anisotropic silicon nanocrystals. The challenge is showing that the resulting particles are indeed functionalized

with different groups on either side of the particle. The previous analytical techniques were only able to show the bifunctionality, but not the anisotropy.

In chapter 2.3.2 (p. 33) the various strategies found in literature that are used to analyze the anisotropy of Janus particles are described in detail. In summary, the main techniques rely on using microscopy (TEM, SEM, AFM, etc.) to show the different compositions of the particles' sides. However, these techniques are not easily applicable to nanoscale particles, as the resolution of such techniques is often not good enough. To further complicate the matter, silicon nanomaterials are notoriously difficult to image with electron-microscopy techniques due to their low electron density and therefore low contrast. Going one step further, the anisotropy in our case stems from the organic surface groups that have an even lower contrast than the silicon core of the nanoparticles, making the use of microscopy nearly impossible. In similar cases, authors infer the anisotropic nature of the nanoparticles through observation of their behavior, chemical or physical. For example, if the nanoparticles possess a hydrophilic and a hydrophobic side, the particles will preferentially agglomerate at the interface of two immiscible solvents, similar to molecular amphiphiles (tensides, detergents, etc.).[167, 208, 215, 213] Other strategies include modifying the nanomaterial with surface groups that preferentially interface with a larger nanomaterial and subsequently imaging the resulting structures, which cannot be achieved with non-Janus particles. From the agglomeration patterns the anisotropy is thus confirmed.[167, 213]

The first employed strategy involved using the previously synthesized $ClH_{12}C_6$-SiNC-$C_{11}H_{22}Br$. With high-resolution TEM (HR-TEM) as well as electron energy loss spectroscopy (EELS) mapping, the localization of the halogen groups would be determined to a single silicon nanocrystal. Essentially, it is a higher resolution version of the previous method using SEM/EDX (**Figure 4.5–6**). This method, however, turned out to be unsuccessful.

Before using high resolution transmission electron microscopy (HR-TEM) and electron energy loss spectroscopy mapping (EELS) the sample was subjected to the simpler and less cost-intensive TEM-EDX method (**Figure 4.5–9**); basically a pre-analysis. Unfortunately, due to the low concentration of the halogen atoms, their locations are difficult to map and their detection was only slightly above the margin of error of the employed EDX instrument. Since imaging with TEM and EDX proved challenging on its own, the application to HR-TEM/EELS seems impractical, as it is a more complicated method and requires a pristine sample. Additionally, this strategy relies on the coincidental correct orientation of the particles to show both faces. Therefore, the strategy of using elemental markers and atomic detection was abandoned in favor of other strategies.

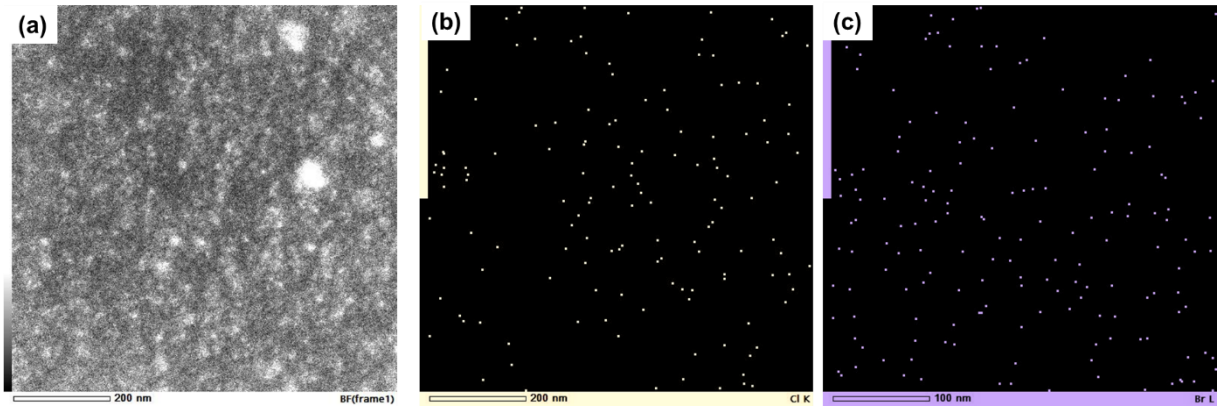

Figure 4.5–9. (a) BF-TEM image of a selected area of $ClH_{12}C_6$-SiNC-$C_{11}H_{22}Br$. Corresponding elemental mapping of (b) chlorine and (c) bromine.

Amphiphilic Janus Silicon Nanocrystals

Another method that is frequently employed to show the anisotropy of Janus particles is to look at the agglomeration behavior of amphiphilic particles in a mixture of immiscible solvents.[167, 208, 215, 213] When particles are modified with hydrophobic and hydrophilic groups at the same time, they will preferentially orient at the interface of two immiscible phases, since each functional group prefers their respective solvent. This behavior mimics how molecular amphiphiles, such as soaps and detergents, behave in solvent mixtures. In order for this to work, the particles need to be rendered visible, as the small size of nanoparticles precludes their visualization. This can be accomplished through the use of dyes (**Figure 2.3–9**),[208] but in this case silicon nanocrystals offer a key advantage: photoluminescence; making the use of dyes unnecessary.

The synthesis of amphiphilic Janus SiNCs presented a unique challenge. The functionalization with hydrophilic groups such as pentenoic or hexenoic acid did not produce any usable samples, as either there was not enough surface coverage or the removal of the byproducts was not possible (more in chapter 4.5.2.5: Limitations of the Procedure and Substrate Scope). Good results were achieved by functionalizing with allyloxy(polyethylene oxide) in the hydrosilylation step and with 1-dodecene in the UV irradiation step. This produced Janus SiNCs with hydrophilic polyethylene glycol units and hydrophobic dodecyl ligands (PEG-SiNC-$C_{12}H_{25}$). The obtained product was not soluble in any solvent (**Figure 4.5–10b**) and could only be separated from byproducts through differential centrifugation. The insolubility is somewhat expected, as there are not enough functional groups of either type to sufficiently stabilize the particles in any particular solvent. However, this did not hinder further use. The FTIR spectrum of the sample is consistent with SiNCs bearing both dodecyl and allyloxy(polyethelene oxide) groups (**Figure 4.5–10a**). The strong ν(H-C_{sp^3}) band at 2900 cm^{-1} confirms dodecyl incorporation, while ν(O-H) is indicative of hydroxyl groups end groups. The

sample also exhibits a significant band at 1100 cm^{-1} caused by the overlap of both ν(Si-O) and ν(C-O) bands; assessment of oxidation is therefore not possible, but in this case the quality of the sample is not as relevant as the subsequent agglomeration behavior.

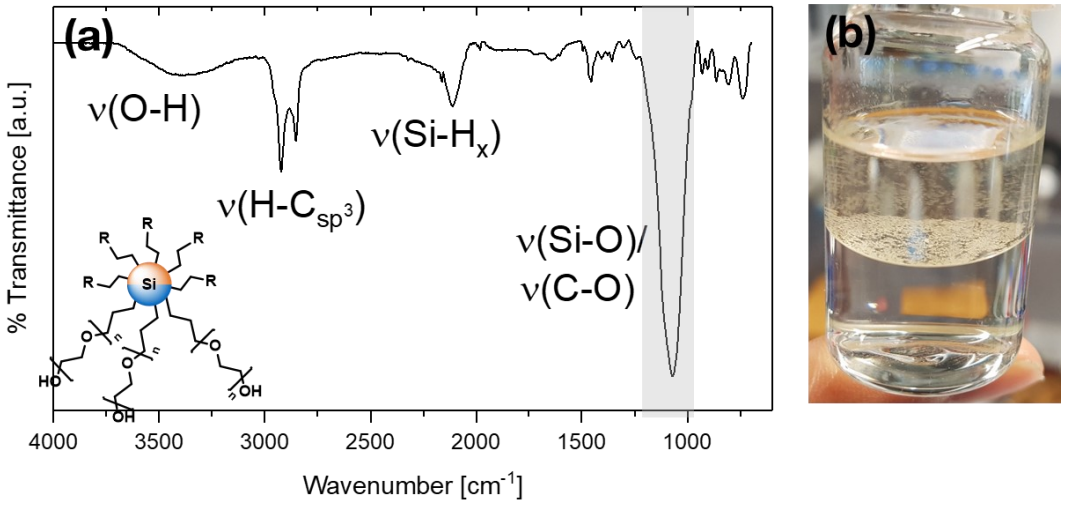

Figure 4.5–10. (a) FTIR spectrum of PEG-SiNC-$C_{12}H_{25}$ and (b) picture of sample in water/hexane.

Pictures of the Janus sample in water/hexane as well as corresponding control samples reveal the anisotropic nature (**Figure 4.5–11**). While the isotropic control samples partition into their respective solvents – visualized by photoluminescence – the anisotropic sample prefers agglomeration at the interface. The Janus SiNCs even seem to "walk" up the polar glass and unpolar hexane interface. This self-arranging behavior is a very strong indicator of anisotropic particles, especially considering that the isotropic control samples do not behave similarly.

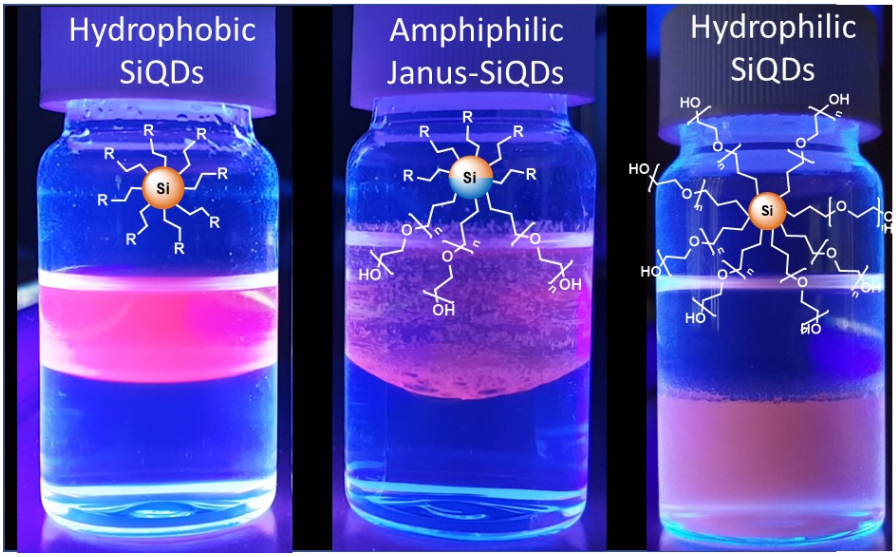

Figure 4.5–11. Pictures of silicon nanocrystal samples in a solvent mixture of hexane and water. (left) Isotropic dodecyl-functionalized SiNCs, (middle) anisotropic amphiphilic Janus SiNCs and (right) hydrophilic SiNCs.

Interfacing Janus SiNCs with Gold Nanoparticles

While the amphiphilic method was able to strongly substantiate the claim of anisotropic particles, some doubts still remain. The IR spectrum of the synthesized particles showed strong oxidation and the photographic images do not constitute enough conclusive evidence. Therefore additional methods for demonstrating anisotropy were pursued. One of the devised methods to show the anisotropy exploits the preferential orientation of Janus silicon nanocrystals when connected to other nanomaterials. The idea is that the anisotropic SiNCs will show a different arrangement pattern compared to their isotropic counterparts.[167, 213]

Gold is known to readily react with thiols to form a stable Au-S bond. This behavior is frequently used to produce self-assembled monolayers on gold surfaces. Using this reactivity, thiol-capped SiNCs could form superstructures with gold surfaces. The predicted superstructures of thiol end-capped anisotropic and isotropic SiNCs with gold nanoparticles (AuNPs) are illustrated in **Figure 4.5–12**. Isotropic hydrophobic SiNCs with no thiol group to interface with the AuNPs should show a random distribution of the both particles in TEM images (**Figure 4.5–12a**), while an isotropic particle with thiol end-caps would act as a crosslinker and large agglomerates of gold nanoparticles would be visible (**Figure 4.5–12b**). If the particles are anisotropically functionalized with thiol groups on one side only, then the particles should form so-called raspberries with the gold particles, arranging themselves around the AuNPs; essentially functionalizing the AuNP surface with SiNCs (**Figure 4.5–12c**).

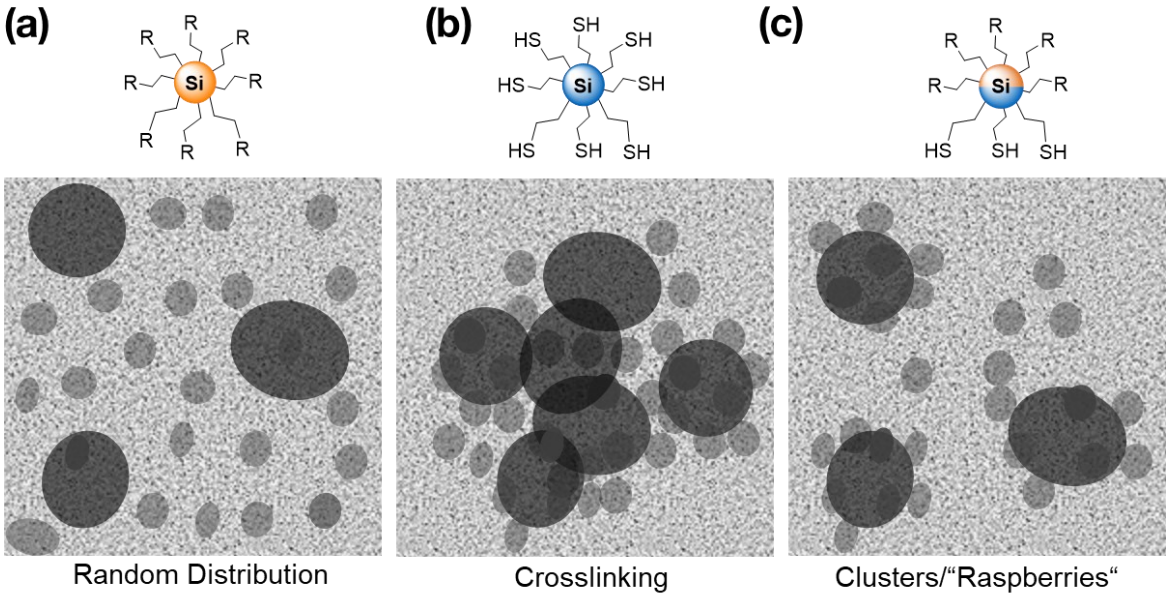

Figure 4.5–12. Approximation of TEM images resulting from interfacing silicon nanocrystals of different isotropy with gold nanoparticles (AuNP). Larger, darker circles represent the AuNP and the smaller lighter ones SiNCs.

In order to attempt this strategy, the SiNCs need to be functionalized with α,ω-alkenyl thiols; substrates that have not been previously reported in silicon nanomaterial literature. Therefore, the functionalization method needed to be developed prior to any AuNP interfacing. In general, alkenyl thiols need to be handled with care, as they are prone to polymerization through the thiol-ene reaction. Unfortunately, this undesired reaction is aided by radicals, which are part of nearly every hydrosilylation procedure. Nevertheless, the hydrosilylation of thioundecene with SiNCs was tested with thermal activation and AIBN initiation. This only resulted in polymer formation, which could be seen through the flocculation of the reaction mixture. The corresponding FTIR spectra show bands indicative of functionalization, but these are only due to the large polymer matrix (**Figure 4.5–13**). In theory, grafted oligomers or polymers are not detrimental to the procedure, as long as they have thiol end groups. These, however, do not seem to be present as the expected thiol bands (ν(S-H)) at ~2600 cm^{-1} are not visible in the IR spectrum.

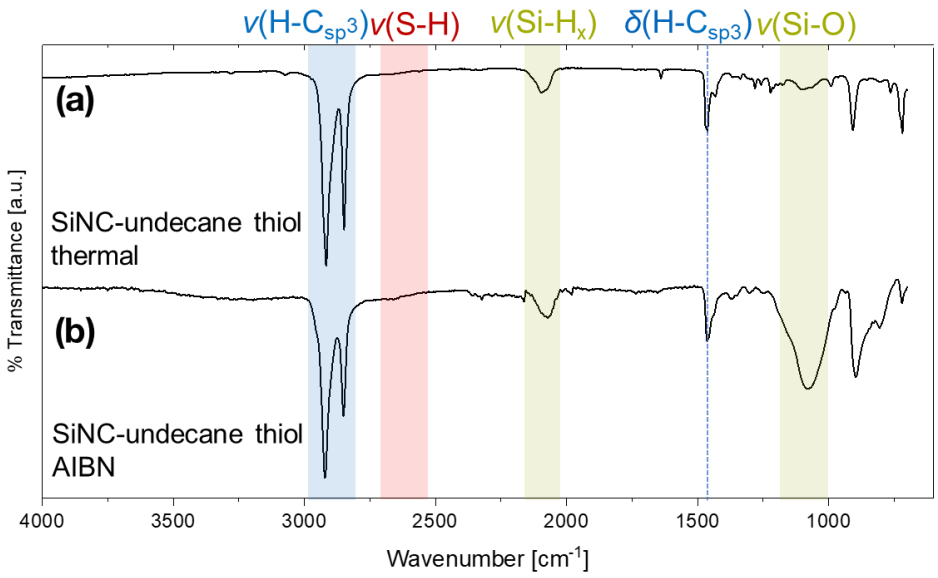

Figure 4.5–13. FTIR spectrum of SiNCs functionalized with thioundecene activated by (a) elevated temperatures and (b) AIBN.

Due to the unpredictability of the polymerization, the thiol end caps of the polymer cannot be ensured and therefore the subsequent immobilization with AuNPs cannot be guaranteed. A temporary removal of the thiol moiety through a protecting group would solve the polymerization issue. A reaction of thioundecene with trityl chloride was tested, but thin layer chromatography still revealed the presence of unreacted thiol, even after chromatography. Since the functionalization of the Si-H groups is conducted with a large excess of substrate, these traces of unprotected thiol can still lead to polymer formation during the reaction. The problem is exacerbated by the large steric demand of the protecting group, which hampers functionalization and results in kinetic favorability of the unprotected alkenyl thiol, resulting in

the preferential functionalization of SiNCs by the unprotected thiol. Even if a quantitative protection were possible, the deprotection does not proceed quantitatively and the large steric demand could hinder the interfacing with the AuNPs. Here, a less sterically demanding protecting group – such as a methyl thioether – would be favorable, but the deprotection requires aqueous basic conditions, which would destroy the silicon nanomaterial.

Basically, in order for the interface strategy with AuNP strategy to work, a pristine SiNC surface with thiol end groups is required. The methods for directly producing terminal thiols on silicon nanocrystals is too uncertain and therefore, a completely different functionalization strategy was devised. Instead of using thiol end groups on the surface of the SiNCs to interact with the AuNPs, the AuNPs are pre-functionalized with a monolayer of thioethanol. SiNCs functionalized with chloro(dimethyl)vinylsilane (ClDMVS)[71] can then react with the hydroxyl end-group, forming the SiNC-AuNP superstructures (**Scheme 4.5-2**).

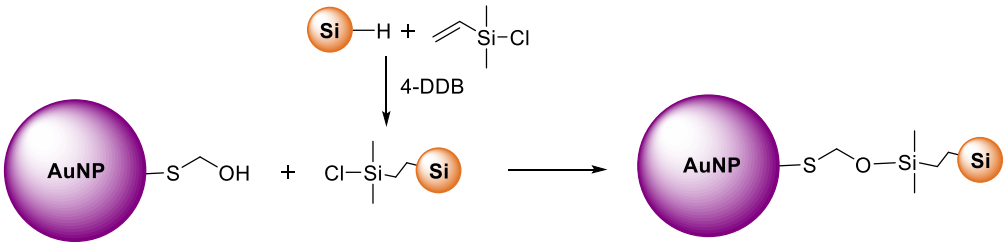

Scheme 4.5-2. Synthesis strategy to interface silicon nanocrystals with gold nanoparticles.

The formed superstructures (**Figure 4.5–12**) should not be affected by the new synthesis strategy. In addition, the functionalization of SiNCs with ClDMVS is also well established.[71] While the surface-modification of AuNPs with thioethanol is not specifically mentioned, there are many reports concerned with the stabilization of AuNPs with different thiols.[250] The methods should be applicable to this case.

The AuNPs (10 nm) were purchased from *Sigma Aldrich* and come dispersed in water, stabilized by a citrate buffer. Unlike thiol-stabilized AuNPs – that are typically dispersed in an organic solvent – the citrate buffer is easily substituted by more strongly bonding ligands, such as thiols. A typical problem associated with AuNPs is their agglomeration. When insufficiently stabilized, AuNPs form large agglomerations that are subsequently difficult to disperse. This is easily monitored through the color of the solution. Well dispersed solutions of AuNPs have a red-purple color and turn dark/black when the AuNPs agglomerate – providing a straightforward indicator for the quality of a dispersion.[251]

The received AuNPs were centrifuged and washed with water and THF. Upon addition of a 2 M thioethanol in EtOH solution, the color of the dispersion turned from red to purple, indicating the formation of agglomerates. After stirring overnight, the solution turned grey, suggesting complete agglomeration of the particles. FTIR measurements of the product do not show any desired ν(O-H) bands at 3600 cm^{-1} (**Figure 4.5–14a**). The challenges of the ligand-exchange method are the competing solubilities of the starting citrate stabilized AuNPs (water soluble) and the resulting thioethanol functionalized AuNPs (polar organic solubility). Going from one solubility to another results in the agglomeration of the particles, which is difficult to reverse. In addition, thioethanol is not as good of a stabilizer, as the much more commonly used dodecanethiol.

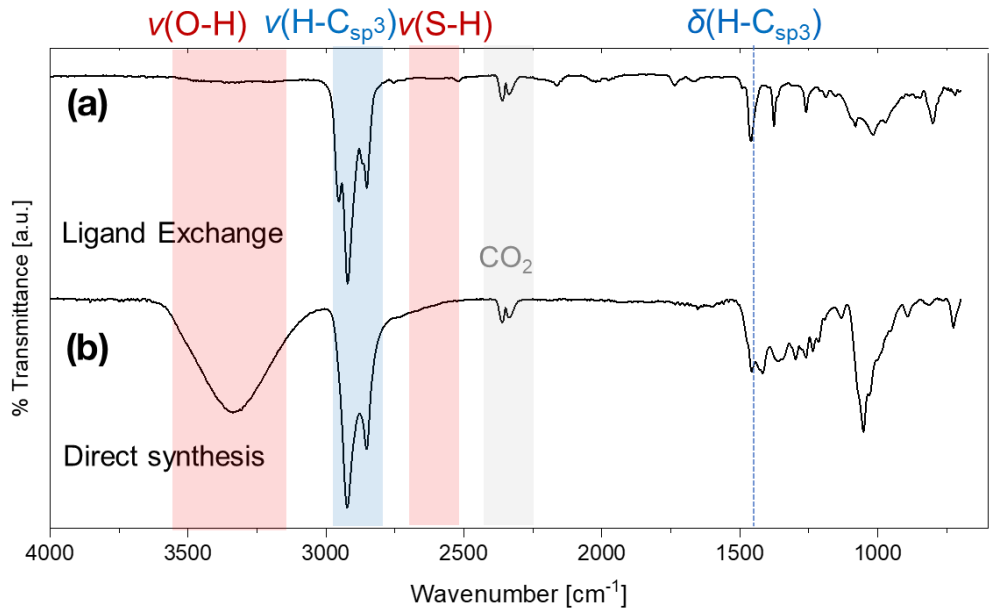

Figure 4.5–14. FTIR spectra of AuNPs functionalized with thioethanol through (a) ligand-exchange and (b) through direct synthesis using the Brust-Schiffrin method and thioethanol as the stabilizer.

In order to overcome these issues, the direct synthesis of thioethanol stabilized AuNPs from chloroauric acid was pursued. The Brust-Schiffrin method was used to produce particles with predicted sizes of 5 – 10 nm (for experimental details see 4.5.5.16, p. 121).[252] Upon completion of the reaction, the AuNPs were extracted from the water phase with toluene. Final drying and dispersion in nmP yields thioethanol AuNPs. Unfortunately, the color of the AuNP dispersion was dark purple, again indicating strong agglomeration. FTIR analysis, however, shows promising results as there is a strong ν(O-H), band at 3400 cm^{-1}, indicating successful hydroxy-termination of the AuNPs (**Figure 4.5–14b**).

Both AuNP batches – ligand-exchange and direct synthesis – were dispersed with Janus SiNCs ($H_{25}C_{12}$-SiNC-ClDMVS) in THF and stirred overnight. After purification *via* centrifugation, the resulting sample is dispersed in benzene and prepared for TEM.

The TEM images of the ligand-exchange AuNPs with SiNCs (**Figure 4.5–15 a – d**) shows the expected large agglomerations of AuNPs. The AuNPs strongly overlap, making identification of any AuNP-SiNC superstructures extremely difficult. At closer magnification, at the edges of the AuNP agglomerates, SiNCs are more visible (**Figure 4.5–15c**) in close proximity with AuNPs. However, discerning any regular structures is nearly impossible. The images obtained from the direct synthesis are much more promising (**Figure 4.5–15 d-f**). Less agglomerates of AuNPs are visible and the AuNPs can be seen interacting with the SiNCs. However, the SiNCs seem to form agglomerations with themselves, once again making identification of any regular, repeating (super)structures difficult. Some raspberry-like superstructures of AuNPs and SiNCs are visible in all images; best seen in **Figure 4.5–15f**. However, these AuNPs are integrated into a larger agglomeration of SiNCs and therefore, the superstructure could have been formed randomly. Additionally, there are some free-standing AuNPs visible **Figure 4.5–15d**, which is the expected pattern, if the SiNCs only have dodecyl ligands.

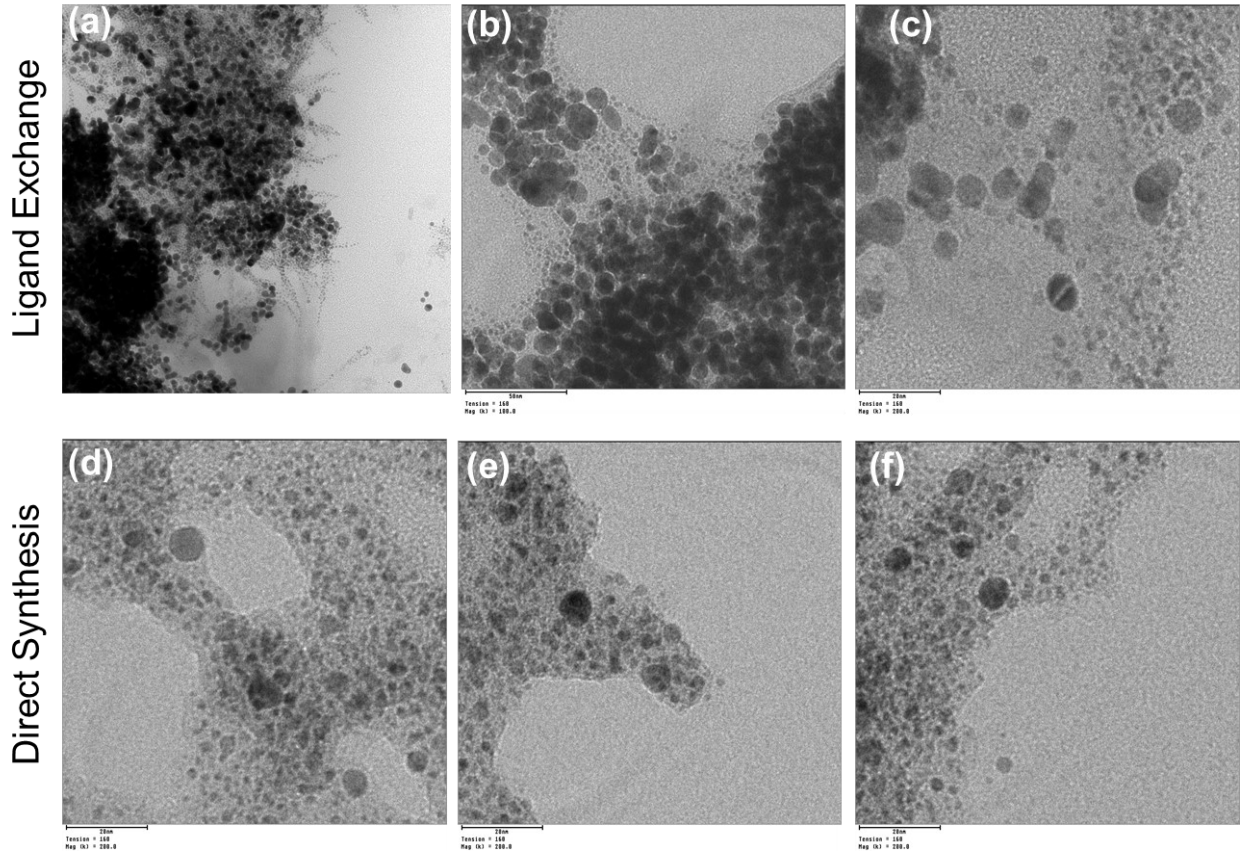

Figure 4.5–15. TEM images of Janus SiNCs interfaced with AuNPs. Top row depicts AuNPs obtained via ligand exchange and bottom row obtained through direct synthesis.

Overall, the interfacing of SiNCs with AuNPs is unviable as a reliable proof for anisotropic SiNCs. The tendency of both NPs to agglomerate prevents proper interaction between them. This problem was slightly mitigated through the direct synthesis of thioethanol capped AuNPs, but here the SiNCs formed agglomerations. Due to the reactive Si-Cl bond of the SiNC ligand, crosslinking could easily occur through involvement of moisture or oxidation. The complexities of the sample preparation and the requirement of water during the AuNP synthesis, makes ensuring an inert atmosphere extremely difficult, which in turn is detrimental to the SiNC samples, since they possess a labile chlorsilane moiety. Separation of the excess SiNCs from the SiNC/AuNP superstructures is also very challenging, since the sizes and solubility of the nanomaterials is very similar. But even if high quality samples can be synthesized, the serendipity of obtained TEM images needs to be taken into account. During the drying of the samples on the TEM grid, many random agglomerations can be formed and thus results could still remain unreliable. A much more controlled formation of a silicon nanocrystal gold surface interaction is necessary.

Immobilizing Anisotropic Janus Silicon Nanocrystals on Gold Wafers

In favor of using AuNPs as the "interaction interface" and TEM images as the final proof, a different strategy using gold wafers was developed. In a similar reaction pathway, isotropic and anisotropic SiNCs are interfaced with a thioethanol-coated gold wafer, and the contact angle of the resulting samples is used to show the different exposed surface groups (**Figure 4.5–16**). In order to differentiate the ClDMVS groups from the hydrophobic dodecyl groups, all samples are washed with ethylene glycol, rendering any remaining ClDMVS groups hydrophilic.

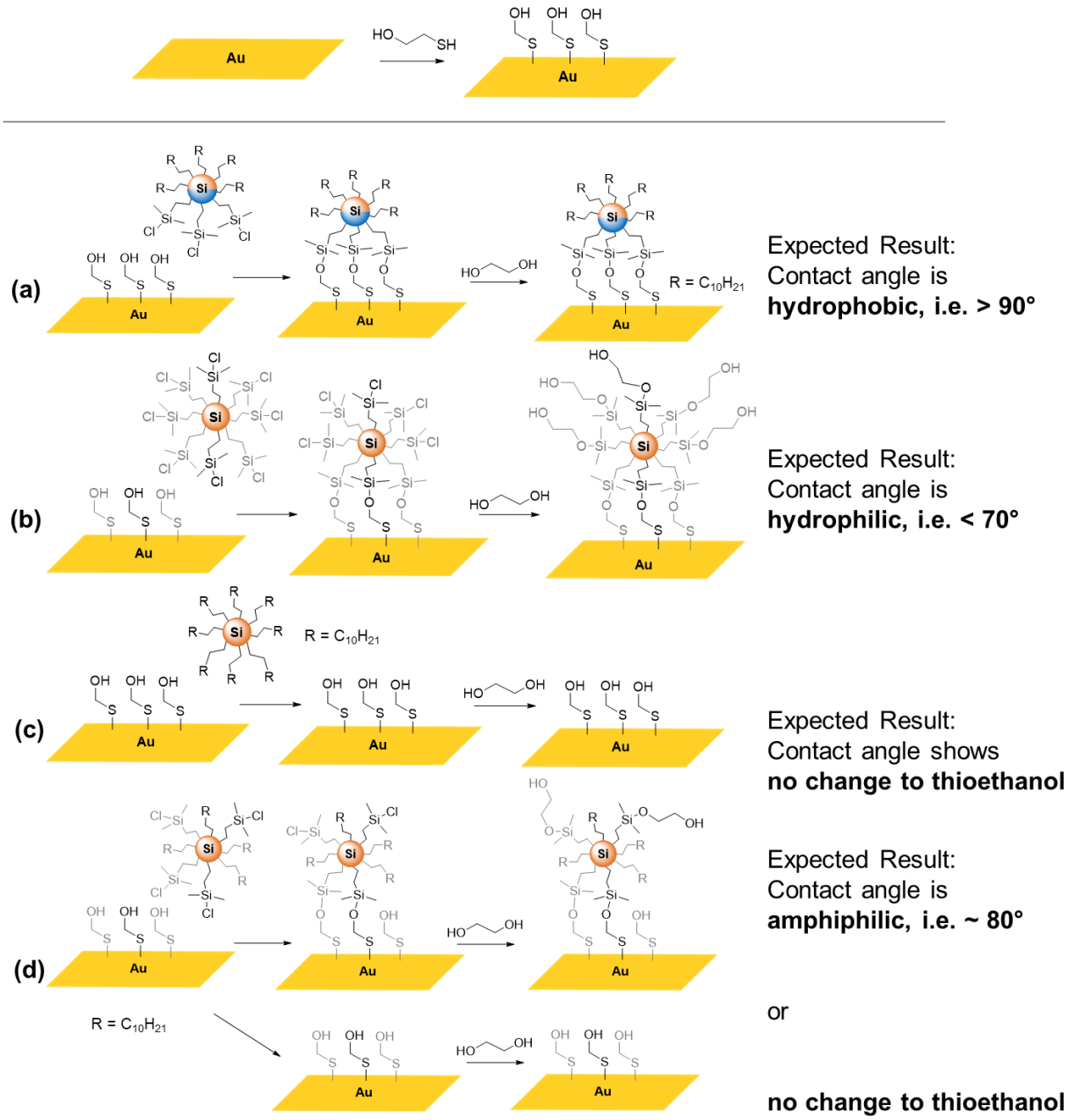

Figure 4.5–16. Assembly strategies of different SiNCs on gold wafers. The gold wafer is pre-functionalized with thioethanol and the silicon nanocrystals are deposited on the surface.

In the case of Janus $H_{25}C_{12}$-SiNC-ClDMVS a very hydrophobic contact angle is expected as the Janus particles will rotate to assemble onto the gold wafer – as only the ClDMVS shows the selective reactivity. The dodecyl groups are thus exposed, practically forming a monolayer on the surface of the wafer (**Figure 4.5–16a**). If the particles are isotropic and only have ClDMVS groups, then the resulting contact angle should be hydrophilic, since the remaining ClDMVS groups are rendered hydrophilic with ethylene glycol (**Figure 4.5–16b**). For purely dodecyl-functionalized particles, no deposition is expected, because there are no groups that can react with the gold surface and remaining SiNCs are washed away in the purification step. Thus the contact angle remains unchanged (**Figure 4.5–16c**). A SiNC particle that contains both ClDMVS groups and dodecyl groups (**Figure 4.5–16d**), but distributed randomly instead of anisotropically should either show no change – because the dodecyl groups sterically prevent interaction – or show an amphiphilic contact angle due to the mixed hydrophilic, hydrophobic surface.

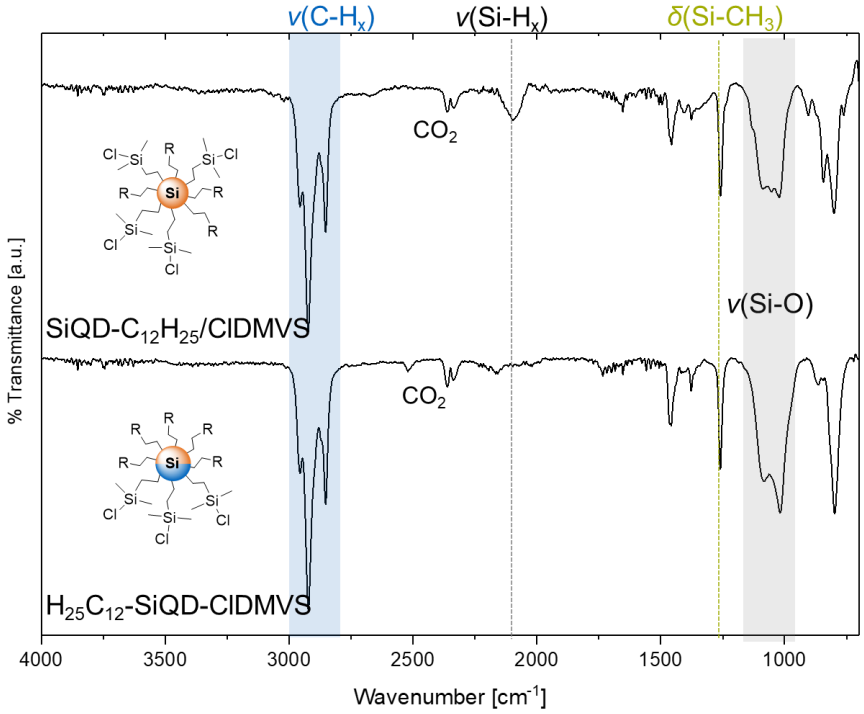

Figure 4.5–17. FTIR SiNCs functionalized with 1-dodecene and ClDMVS, but with different localizations. (a) The functional groups are distributed randomly and (b) the functional groups are located on either side, i.e. Janus.

The synthesis of the particles was performed as previously described. For the mixed particle, equal amounts of both substrates were added to the reaction mixture. The resulting FTIR spectrum is virtually indistinguishable from the Janus SiNCs. This is expected, since both samples contain the same functional groups (**Figure 4.5–17**); their only difference is the surface group localization (i.e. the location of these groups), which IR is not able to distinguish.

For the deposition of the SiNCs, small pieces of gold wafers are submerged in a 2 M solution of thioethanol in ethanol overnight to produce the SAM. The gold wafers are washed with dry toluene and submerged in a solution of the respective SiNCs overnight. The wafers are washed with and submerged in ethylene glycol. After washing with ethanol, contact angles of the samples are measured.

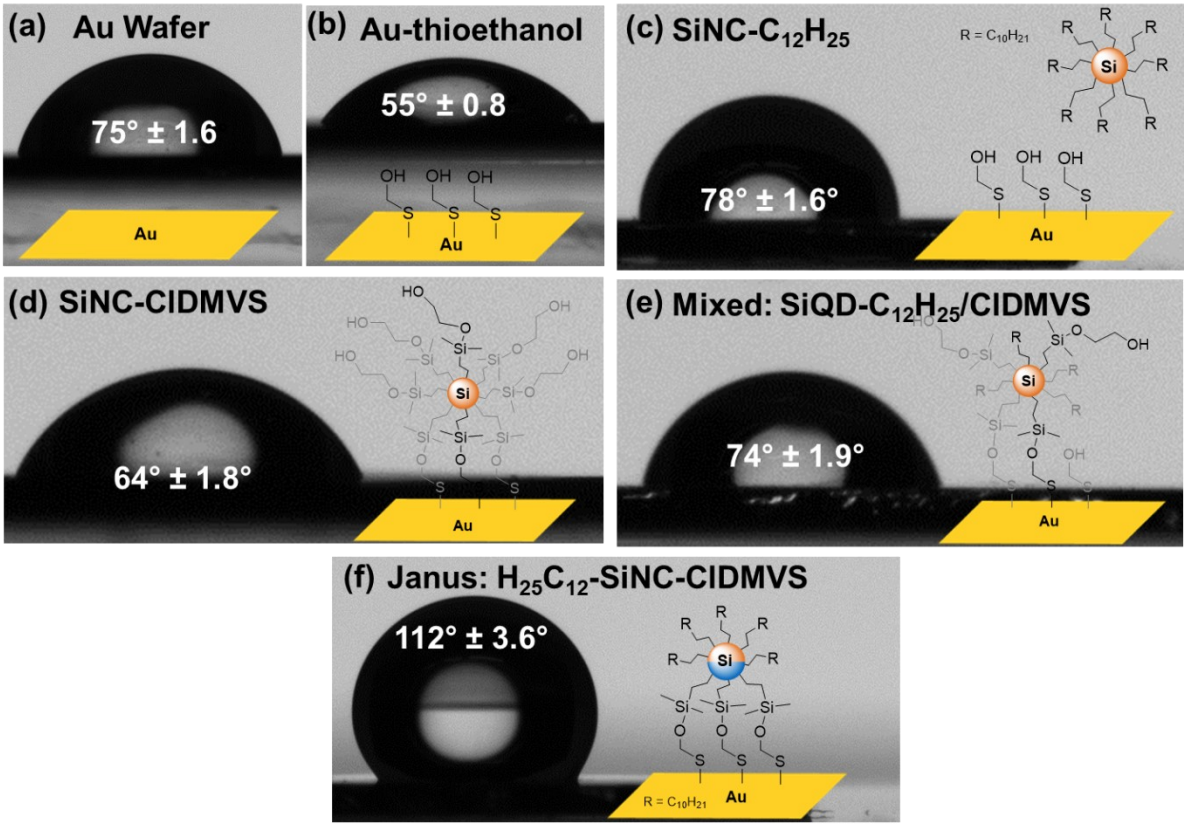

Figure 4.5–18. Contact angles of silicon nanocrystals deposited on gold wafers coated with a SAM of thioethanol.

The results are summarized in (**Figure 4.5–18**). After the self-assembly of thioethanol the contact angle of the gold wafer decreases from 75° to 55° (**Figure 4.5–18a, b**). After the deposition process with dodecyl-functionalized SiNCs, the contact angle increases to 78° (**Figure 4.5–18c**). Contrary to expectations, this indicates a change on the surface. However, a value of 78° seems too low to suggest any deposition of SiNC-$C_{12}H_{25}$, since a much more hydrophobic contact angle would be expected (> 90°). The steps involved in the deposition process may have removed the thioethanol monolayer, reverting the contact angle back to the original gold wafer. Another possibility is the adsorption of traces of impurities, which are challenging to fully exclude in the multi-step process. More information on this is gained later. The deposition of the control sample SiNC-ClDMVS shows a contact angle of 64°, in line with the prediction of a hydrophilic contact angle. Both the thioethanol SAM and the SiNC-ClDMVS predict an exposure of hydroxy groups, resulting in the hydrophilic contact angle. The

increased hydrophobicity of SiNC-ClDMVS compared to the thioethanol SAM is caused by the ethylene glycol chains that can freely move and expose the hydrophobic carbon links. The control sample with mixed surface ligands (i.e. dodecyl and ClDMVS groups) also exhibits an anticipated contact angle: 74°. Due to the incorporation of additional dodecyl groups – compared to SiNC-ClDMVS – a more hydrophobic surface is generated. However, the hydrophilicity of the ethylene glycol units keeps the contact angle lower than a conventional hydrophobic surface (i.e. < 90°). Critically, the Janus sample with ClDMVS- and dodecyl ligands on either side of the particle exhibits a very hydrophobic contact angle of 112°, suggesting exposure of the dodecyl groups. This is only possible if the particles are able to rotate, bonding the ClDMVS groups on one side to the gold wafer thus orienting the dodecyl groups outward. Especially when comparing the results of control samples, it is evident that the particles are in fact surface-anisotropic. The contact angle even exceeds expectations, as 112° is considered very hydrophobic and is typically only achievable in a controlled manner. For comparison, dodecanethiol SAMs on gold exhibit contact angles of 100 – 110° and here it needs to be taken into account that the self-assembly of small molecules allows for more dense packing of the alkyl chains.[253, 254] The high contact angle of the Janus particles suggest the generation of a densely packed layer of SiNCs on the gold wafer surface.

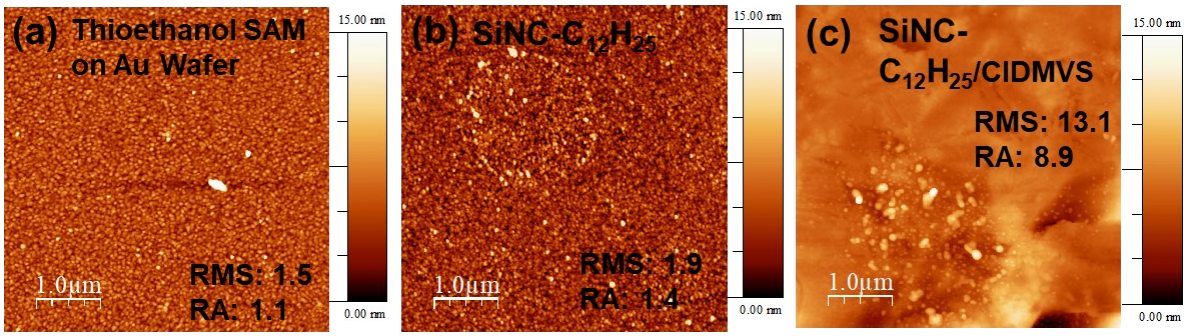

Figure 4.5–19. AFM images and calculated roughness of (a) gold wafer and (b) SiNC-$C_{12}H_{25}$ deposited on a gold wafer and (c) mixed SiNC-$C_{12}H_{25}$/ClDMVS deposited on a gold wafer.

To take a closer look at the surface of the gold wafers, AFM measurements were conducted for each sample. The gold wafer submerged in the SiNC-dodecyl solution shows no evidence for any nanoparticles (**Figure 4.5–19b**). The calculated surface roughness is similar to that of the original thioethanol coated wafer (**Figure 4.5–19a**). In the case of the SiNC-ClDMVS sample, a much higher surface roughness was determined, suggesting a thick layer of particles. Looking at the micrographs, large agglomerations (heights up to 300 nm) are distributed homogenously throughout the mapped area (**Figure 4.5–20d, e**). As predicted, the SiNC-ClDMVS were able to bond to the thioethanol coated surface, forming a thick layer. The mixed particles, SiNC-$C_{12}H_{25}$/ClDMVS, exhibits similar results. Large agglomerations are

visible (up to 150 nm), however, these are not as homogeneously distributed as SiNC-ClDMVS (**Figure 4.5–19c**). This is due to the random insertion of the functional groups, which may result in patches of single functional groups on the surface, making interactions with the gold surface or other SiNCs more random.

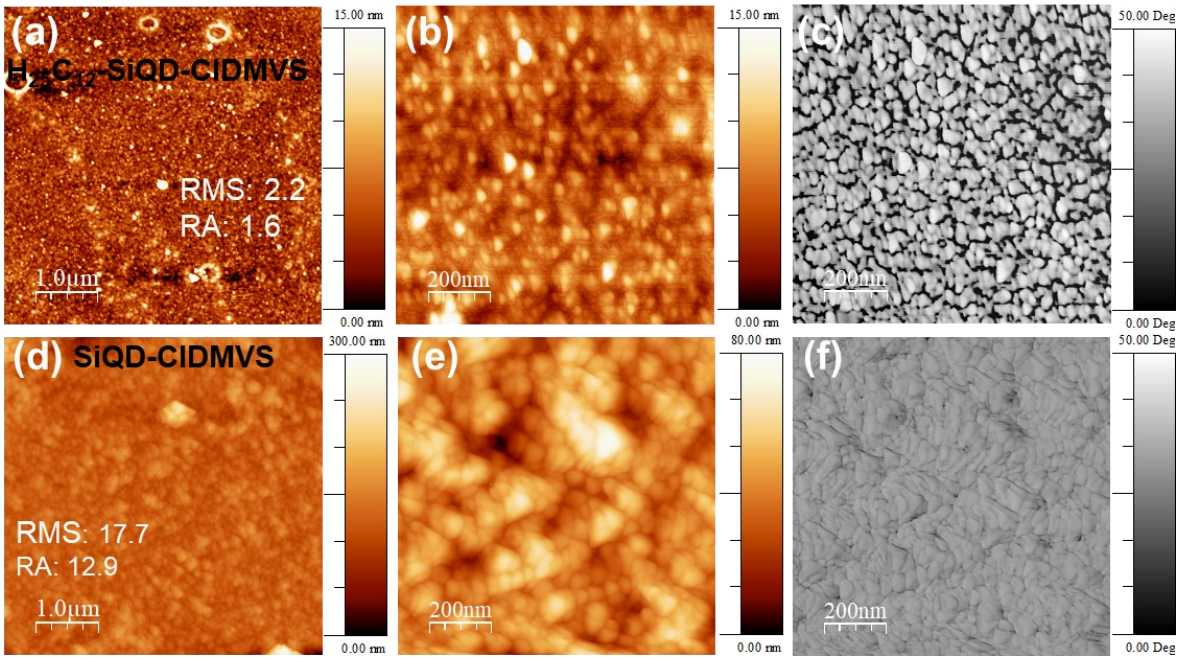

Figure 4.5–20. AFM micrographs of Janus SiNCs on a gold wafer (a,b) as well as the corresponding phase diagram (c). (d, e) AFM micrographs of the control sample SiNC-ClDMVS as well as a corresponding phase diagram (f).

The Janus sample shows a more regular grain structure (**Figure 4.5–20a, b**). The roughness is slightly higher than the reference wafer, which would be expected if only a monolayer of SiNCs is present, as was predicted. The micrograph also shows circular agglomerations, which could be micellar formations that formed during the drying process, supporting the claim of surface anisotropic particles, as micelles can only be formed by two-sided substances. The micrograph with larger magnification shows isolated particles or agglomerations and exhibits an overall very low height profile (up to 15 nm) corroborating the evidence for a monolayer.

Looking closely, artifacts – that look like worms – are visible at the grain boundaries of the aforementioned particles (**Figure 4.5–20b**). These are accompanied by a change in phase space. The phase diagram of the same area reveals the existence of a monolayer (**Figure 4.5–20c**). Dark and light areas contrast the differences between phases, which themselves indicate differences of adhesion forces between the AFM cantilever and the sample. Therefore, phase changes occur when the sample exhibits stark differences in hydrophobicity

and hydrophilicity, as is the case here, where the underlying substrate (hydrophilic gold wafer) is exposed under a monolayer of the hydrophobic SiNCs. In the case of SiNC-ClDMVS no phase differences are visible in the respective phase diagram (**Figure 4.5–20f**). Since SiNC-ClDMVS formed such a dense layer, no substrate (i.e. gold wafer) is able to "look" past the grain boundaries. Even if the underlaying substrate is theoretically exposed, the dimensions of the AFM tip and the thick particle layer prevents any contact with the substrate (**Figure 4.5–21**). As such, it is very reasonable that in the case of $H_{25}C_{12}$-SiNC-ClDMVS a monolayer was formed on the surface of the gold wafer; a phenomenon that is only achievable if the particles were indeed Janus in nature.

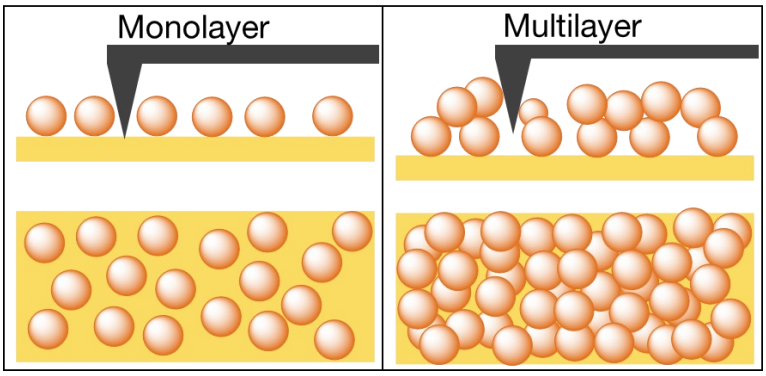

Figure 4.5–21. Schematic illustration of the AFM measurements of monolayers and multilayers. In a monolayer the AFM cantilever is able to penetrate to the underlying substrate, while a multilayer prohibits any connection.

4.5.2.4 Integrity of the Janus Silicon Nanocrystals

Having established the viability of the silicon nanosheet masking method, the integrity of the nanoparticles needed to be analyzed. Since the nanoparticles are deposited on a substrate and subsequently removed, these bonding/debonding processes could have adverse effects on the integrity of the SiNCs.

Therefore, a batch of SiNCs-H were liberated from a SiNC/SiO_2 composite, one part of which was kept as a control sample, while the rest was subjected to the silicon nanosheet masking procedure. Control sample and Janus sample were obtained from the same batch in order to ensure good comparable results – because even minute differences in etching time and functionalization can lead to differences later on. The control SiNCs were functionalized with trimethylvinylsilane (SiNC-TMVS), while the Janus sample were functionalized with TMVS as well as ethyl undecylenate.

The characteristic photoluminescence spectra of the Janus SiNCs and control SiNCs, exhibit nearly identical characteristics (**Figure 4.5–22a**). This is a clear indication that the optoelectronic properties and the particle size remain unchanged during the masking

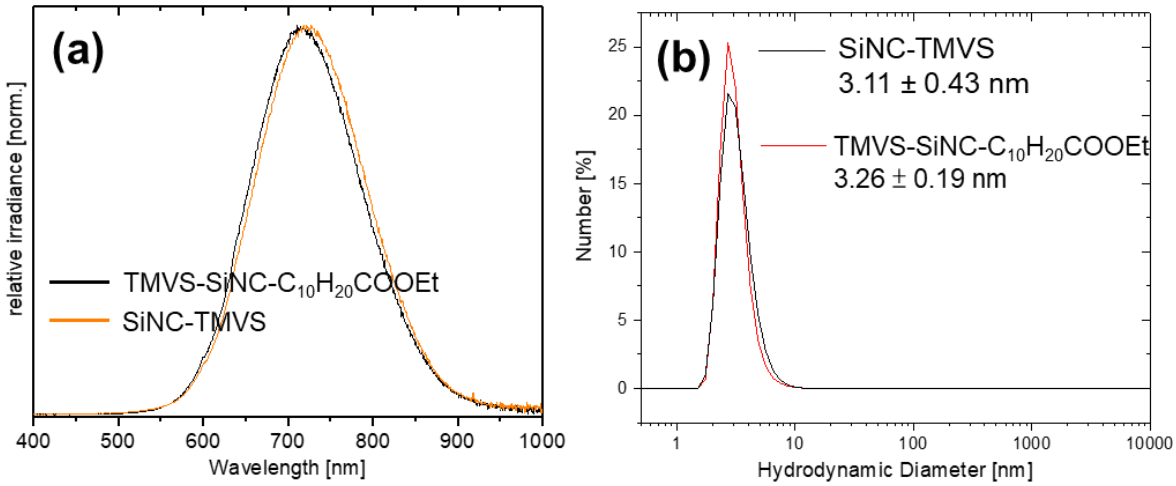

Figure 4.5–22. (a) Photoluminescence spectrum and (b) DLS histogram of SiNCs obtained via the silicon nanosheet masking procedure and control sample obtained through conventional hydrosilylation.

procedure. The corresponding spectra overlap and show the same emission maximum at around 710 nm, consistent with particles with diameters around 3.2 nm.[43] Dynamic light scattering (DLS) measurements are able to corroborate this result, as both samples exhibit hydrodynamic radii of 3.1 – 3.2 nm; exhibiting sizes that are within their respective margins of errors, indicating that the size of the particles is unchanged through the masking procedure (**Figure 4.5–22b**).

Measuring the size-distribution with TEM is able to give the most reliable results. The images obtained from the two samples are very similar. As before, the removal of the SiNSs was reaffirmed with these measurements, as no structures resembling silicon nanosheets could be found within the imaged areas. The Janus sample $H_{25}C_{12}$-SiNC-TMVS exhibits a size distribution of 3.40 nm (**Figure 4.5–23a**), while the control samples' size distribution is very close with 3.38 nm; within the margin of error of the measurement (**Figure 4.5–23b**). The size distributions can essentially be regarded as the same, which is expected if the SiNCs are not

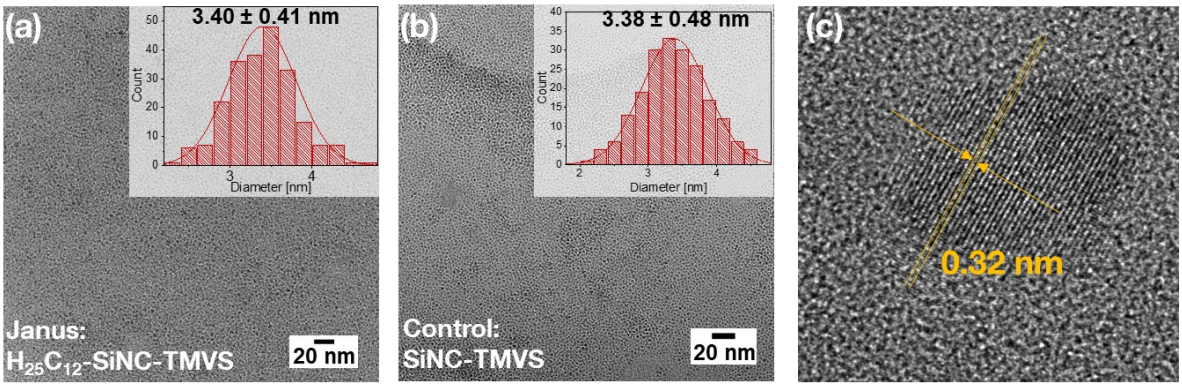

Figure 4.5–23. TEM images of (a) Janus SiNCs $H_{25}C_{12}$-SiNC-TMVS and (b) the control sample SiNC-TMVS obtained from the same synthesis. Histograms of the size-distributions inset into the images.

affected by the masking procedure. High-resolution transmission electron microscopy is able to confirm the crystallinity of the sample, as the lattice spacing coincides with the diffraction pattern of the crystalline Si(111) plane.[15] These data are clear indications that the quality and integrity of the silicon nanocrystals remains unaffected throughout the silicon nanosheet masking procedure.

4.5.2.5 Limitations of the Procedure and Substrate Scope

As with any method, there are some limitations to the described method of masking the silicon nanocrystals with silicon nanosheets. These are mostly derived from the functionalization techniques used in the method and the actual laboratory procedures. To clarify the overall procedure an illustration is given in **Figure 4.5–24**.

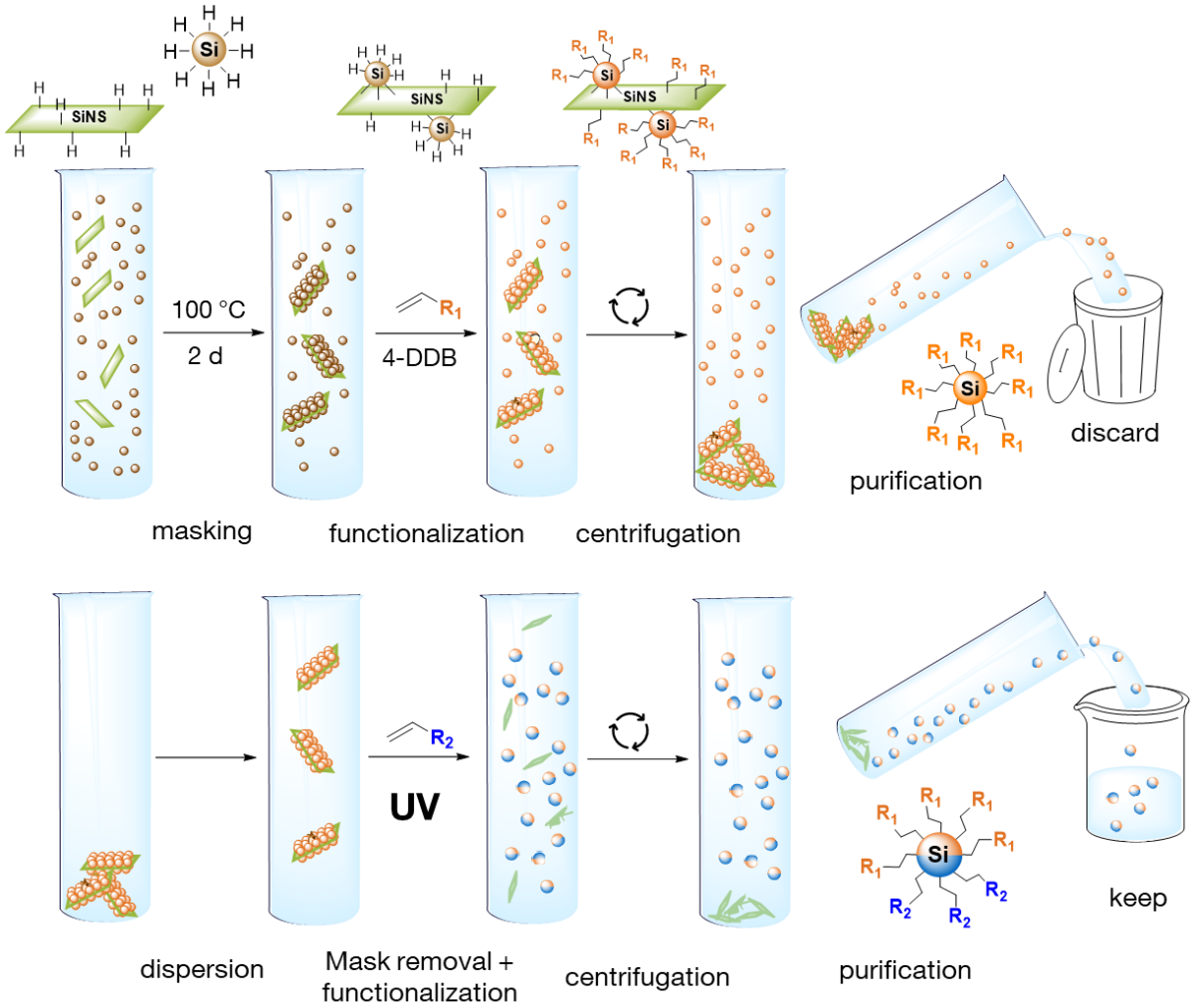

Figure 4.5–24. Illustration of the masking procedure as it proceeds in solution. Work up steps and the different types of dispersions are shown.

A dispersion of SiNC-H and SiNS-H is subjected to the dehydrogenative coupling procedure, after which most of the SiNCs will be bonded to the SiNSs, but some free-standing

SiNC-H will remain. A functionalization method can then be directly applied to the dispersion (here any preferred hydrosilylation method can be used), resulting in functionalized SiNCs on SiNSs (i.e. R-SiNC@SiNS-R) as well as functionalized, free-standing, isotropic SiNCs (SiNC-R). At this stage, the separation of the isotropic SiNCs is absolutely critical, as later on these cannot be differentiated from the anisotropic Janus silicon nanocrystals. Since the R-SiNC@SiNS-R are much more dense than the SiNC-R and do not dissolve, centrifugation of the dispersion leaves the SiNC-R in solution, while the desired R-SiNC@SiNS-R are forced to the bottom. This way the isotropic SiNC-R can be removed and discarded by decanting. Here is where the first limitation is found: The isotropic SiNCs need to be soluble and therefore need to be smaller than 8 nm in diameter and functionalized in a manner that a clear stable colloidal dispersion is produced. If not, separation is only possible through much more complex differential velocity centrifugation.

Once purification is complete, the residue is re-dispersed and the UV functionalization performed. This destroys the nanosheet mask while simultaneously liberating and rendering the Janus silicon nanocrystals. Again, these two materials are separated by centrifugation; the Janus SiNCs remain in solution, while the decomposition products are sedimented. Unlike in the previous centrifugation, this time the supernatant is kept while the residue is discarded. Note that this supernatant still contains unreacted substrate (i.e. alkene) and the Janus SiNCs need to be purified according to the commonly used dispersion/precipitation cycles found in other functionalization techniques. Instead of using centrifugation as a means to separate the Janus SiNCs from the decomposition products, filtration can also be used. However, this can lead to lower yields, because SiNCs are known to agglomerate into larger structures that can be unwillingly filtered as well. This technique should be reserved for when centrifugation is not possible, e.g. when the Janus SiNCs do not dissolve properly.

To summarize the previous paragraph, one of the main drawbacks is the separation of the isotropic and anisotropic SiNCs that is mainly accomplished through centrifugation. As such, a difference in density needs to be guaranteed, i.e. the functionalized SiNCs and the Janus SiNCs need to be soluble and SiNC particle size needs to remain under 7 nm. If this is not the case, the problem can be resolved through differential centrifugation; this however, significantly increases complexity.

The second major limitation lies within de-masking/functionalization step: the UV-functionalization method. The photoinitiated hydrosilylation is size dependent and can only be conducted with particles with sizes up to 5 nm.[61] Therefore, huge Janus particles cannot be obtained with this method. However, while this work describes the use of UV irradiation

as a means to simultaneously de-mask and functionalize, it should also be possible to separate these two steps, i.e. first de-mask with UV irradiation and functionalize in a second step. This should, in theory, circumvent the size limitation imposed by the photoinitiated functionalization. Furthermore, instead of relying on UV-irradiation other sacrificial methods could be used (see 4.5.4: *Outlook*, p. 112 for details).

Throughout this work, various substrates were used for the synthesis of different Janus SiNC samples. Not all substrates can be hydrosilylated using same methods or be used in the photoinitiated hydrosilylation. In addition, while some substrates may undergo hydrosilylation, they do not always render clear dispersions, which is crucial for purification. As such each substrate was tested in a control reaction with isotropic SiNCs first, prior to their use in the Janus SiNC synthesis. A summary of these control reactions and substrates is given in **Table 1** and may provide some valuable information to you, the reader.

Table 1. Summary of employed substrates and methods used for the synthesis of Janus SiNCs. All reactions were tested with isotropic SiNCs first, prior to Janus SiNC synthesis.

Substrate	Hydrosilylation methods	clear dispersion?	UV hydrosilyl.	clear dispersion?
1-dodecene	4-DDB	yes	works	yes
	Thermal	yes		
	AIBN	yes		
bromo-undecene	4-DDB	yes	works	yes
chlorohexene	4-DDB	yes	works	yes
methyl undecylenate	4-DDB	yes	works	yes
	AIBN	yes		
ethyl undecylenate	4-DDB	yes	works	yes
	AIBN	yes		
TMVS	4-DDB	yes	does not work	no
	AIBN	yes		
ClDMVS	4-DDB	yes	does not work	no
	AIBN	no		
allyloxy(PO)	Thermal	no	works a little	no
allyloxy(PO) + methyl undecylenate	Thermal	yes	does not work	no
	AIBN	no		
pentenoic acid	AIBN	yes	does not work	no
hexenoic acid	AIBN	yes	does not work	no

4.5.3 Summary

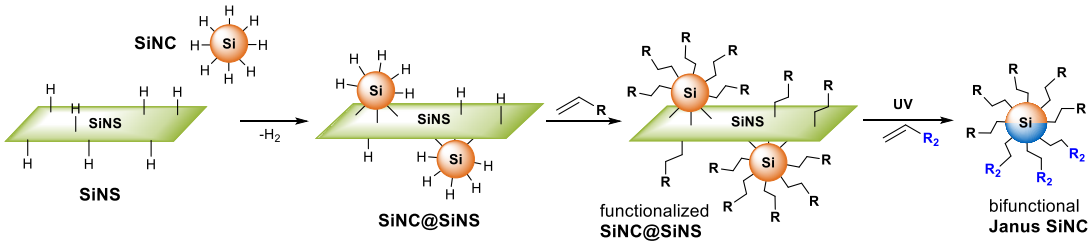

Scheme 4.5-3. Reaction procedure to produce Janus silicon nanocrystals using silicon nanosheets as a protective substrate.

This project – *Surface Anisotropic Janus Silicon Nanocrystals* – describes the use of two-dimensional silicon nanosheets as a masking substrate to produce two-sided, surface anisotropic silicon nanocrystals. The silicon nanosheets act as a flat, solid-state substrate onto which silicon nanocrystals can be deposited and bonded (4.2.2.3: *Dehydrogenative Coupling between Silicon Nanosheets and Silicon* Nanoparticles*, pp. 51-55*). In this state, the exposed side of the SiNCs are functionalized using common hydrosilylation procedures. The silicon nanocrystals are subsequently released from the substrate by UV-irradiation, which destroys the UV-sensitive silicon nanosheets. This has the synergistic effect of simultaneously functionalizing the newly-exposed side of the silicon nanocrystals when a different alkene is present, due to the *photoinitiated hydrosilylation* – thus rendering a bi-functional, two-sided silicon nanocrystal; known as a Janus particle (**Scheme 4.5-3**).

While the proof of concept and reaction protocol were established relatively quickly, the challenges of this project were mainly associated with proving the two-sided, anisotropic nature of the resulting SiNCs. The bifunctionality was demonstrated straightforwardly with EDX, FTIR and TGA-MS measurements, but revealing the localization of the two functional groups remained difficult. For other types of Janus particles, microscopy is frequently used to show anisotropy (see 2.3.2: *Proving Anisotropy* , p. 33), this however, could not be employed for the Janus silicon nanocrystals due to the low contrast of silicon and low contrast of the organic functional groups in electron imaging techniques (SEM, TEM). Therefore, various strategies were developed that use the unique chemical behavior of the two-sided particles to demonstrate the surface-anisotropic character. After failed attempts to use TEM/EELS mapping, the aggregation of amphiphilically modified Janus SiNCs at the interface of a hexane/water mixture was able to sufficiently indicate the two-sided nature, providing the necessary affirmation to continue the project.

Specially modified Janus SiNCs were synthesized that were supposed to form characteristic patterns with gold nanoparticles (AuNP). However, difficulties with the synthesis

and agglomeration of the AuNPs prevented their controlled use. In favor of using AuNPs as an interaction interface for the Janus SiNCs, gold wafers were used instead. Finally, the surface-anisotropic nature of the SiNCs could be assuredly demonstrated by the comparison of the self-assembly behavior of anisotropic and isotropic SiNCs onto the gold wafers. The exposed surface groups were determined by contact angle measurements and showed that the two-sided Janus SiNCs favorably rotate and orient themselves to expose only one specific surface group, thus demonstrating the anisotropic character. Subsequent AFM measurements determined that the Janus SiNCs formed a monolayer on the surface, a phenomenon only achievable if the particles are indeed anisotropic.

In light of the excellent results achieved in this project, the results were drafted into a manuscript and submitted for publication (January 2021). At the time of final submission of this thesis, the manuscript been published online:[255]

Kloberg, M. J.; Yu, H.; Groß, E.; Eckmann, F.; Restle, T. M. F.; Fässler, T. F.; Veinot, J. G. C.; Rieger, B. Surface-Anisotropic Janus Silicon Quantum Dots via Masking on 2D Silicon Nanosheets. *Advanced materials* **2021**, *33* (38), e2100288. DOI: 10.1002/adma.202100288

4.5.4 Outlook

Having established the *silicon nanosheet masking* procedure as a viable method to produce surface-anisotropic Janus silicon nanocrystals, many new research opportunities arise. Some of these ideas and opportunities are outlined in this chapter.

New Janus SiNCs and Their Properties

With a vast library of functionalization methods for silicon nanocrystals, this new concept provides the possibility of synthesizing a wide variety of modified SiNCs with unknown unique behavior. For example, SiNCs modified with alkenes on one side and amines on the other could show interesting optoelectronic properties, due to the differing luminescence behavior of the surface groups.[34] Or, one side could be modified with an inert, stabilizing group (e.g. 1-dodecene) while the other side is left to form a passivating SiO_2 layer, forming a unique half core-shell quantum dot. The possibilities are only limited by the available surface groups.

The amphiphilic SiNCs described in this work were only briefly used to demonstrate the aggregation behavior. Quantifying the surface activity of these amphiphilic Janus SiNCs could provide useful information about their use as surface-active materials or for their use in biological applications. Improvements to the amphiphilic SiNCs synthesized in this work could be made by using the surface groups described by Islam *et al.*[88]

Monolayers

More or less serendipitously, monolayers of Janus SiNCs were self-assembled onto gold wafers and represent one of the first controlled monolayers of SiNCs. The controlled synthesis of monolayers could have a profound impact on the characterization of silicon nanocrystals.

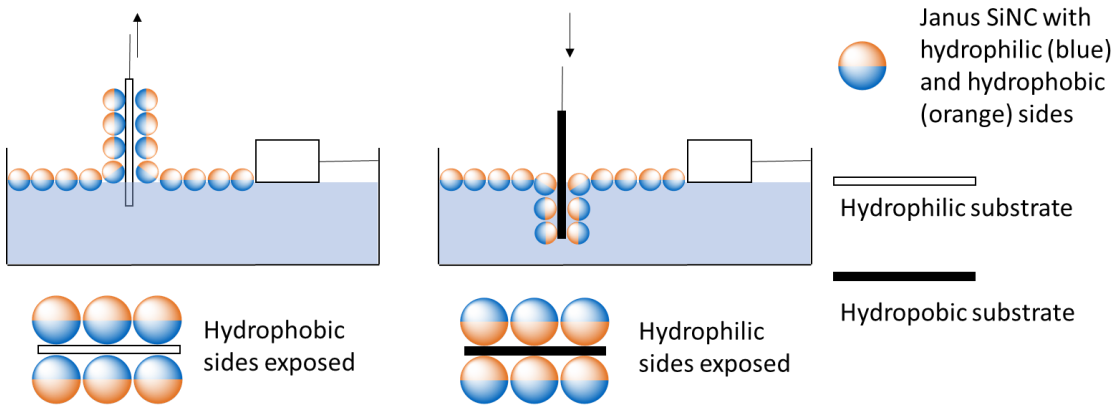

Figure 4.5–25. Illustration of the *Langmuir-Blodgett* technique to produce controlled monolayers of amphiphilic Janus SiNCs. A monolayer of SiNCs is formed at the interface of water and air. The monolayer is compressed with a barrier until maximal packing is achieved. At this point a substrate is dipped into the layer to transfer the SiNC monolayer onto the substrate. Depending on the substrate a hydrophilic or hydrophobic monolayer is formed.

As only a single layer is formed – which is easily visualized with AFM or STM – single nanocrystals (or at least few-SiNC-agglomerates) could be targeted for direct characterization. Conductive AFM measurements or tip-enhanced characterization techniques, such as TERS (tip-enhanced Raman spectroscopy) come to mind.

In addition, improvements to monolayer-formation could be made by using the *Langmuir-Blodgett* technique. The described method of kinetically self-assembling Janus SiNCs onto a gold wafer, only produces a 'random' monolayer, i.e. the SiNCs deposit in random locations. The LB technique first compresses a monolayer of amphiphilic Janus SiNCs before depositing on a substrate. This produces a very controlled and densely packed monolayer. Such SiNC monolayers could prove very useful for fundamental characterizations and applications that require thin layers (e.g. photovoltaics).

Alternative Janus Methods

The method described in this work centers around using UV light to simultaneously liberate and functionalize the silicon nanocrystals. This has some inherent limitations, as only SiNCs with sizes up to 5 nm can be used and some substrates cannot be hydrosilylated with this method (see 4.5.2.5: *Limitations of the Procedure and Substrate Scope ,* p. 108). Alternative reaction protocols could circumvent these issues. For one, the "mask-destruction" and the functionalization step could be separated, i.e. liberate the SiNCs with UV irradiation and

functionalize in a second step using other hydrosilylation procedures (**Scheme 4.5-4**). Other size-independent 'sacrificial' functionalization methods could also be used instead of the photoinitiated functionalization. Hydrosilylations using XeF_2 or PCl_5 are known to etch the surface of silicon nanocrystals during the reaction.[68, 67] This could be used to simultaneously etch away the nanosheets, while hydrosilylating the SiNCs. An added benefit of using XeF_2, is that the etching byproduct, SiF_4, is gaseous and is thus easily removed, not requiring purification *via* centrifugation.

The functionalization of silicon nanocrystals using organolithium reagents relies on the cleavage of a Si-Si bond to modify the surface.[256] This could be enough to remove the atomically thin silicon nanosheet layer, while introducing a new functional group. In addition, the organolithium method is able to incorporate photoluminescence-altering groups.[247] This begs the questions: *What are the optoelectronic properties of such "dual-luminescent" Janus particles? Could the rotation of the particles be visualized in a fluorescence microscope?*

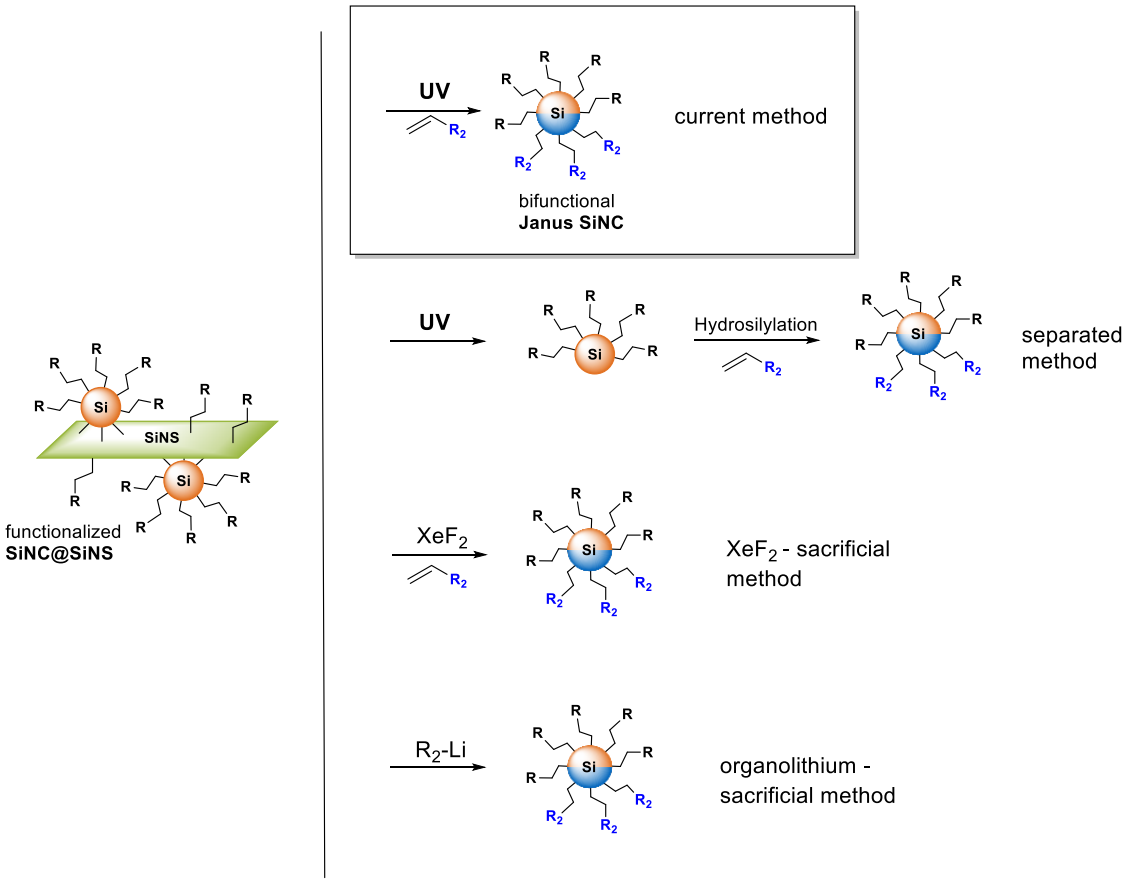

Scheme 4.5-4. Alternative reaction protocols to synthesize Janus Silicon Nanocrystals.

The *silicon nanosheet masking* method is not necessarily limited to silicon nanocrystals. The only requirement is that the nanoparticles can be deposited onto the nanosheet surface. Various publications have shown that noble metal particles can be directly grown on the

surface of silicon nanosheets.[159, 158] Therefore, the silicon nanosheet masking procedure could be extended to produce other surface-anisotropic metal nanoparticles.

Potential Applications of Janus SiNCs

Since Janus SiNCs were synthesized for the first time, the application of this new type of material remains completely unknown. Some ideas and concepts that rely on pre-existing data are presented.

Significant progress with Janus particles has been made in the field of self-assembly. Janus particles are known to self-assemble into larger structures, inaccessible to their isotropic counterparts.[178, 174] For example, "supermicelles" of amphiphilic Janus particles were reported that behave similarly to multilamellar vesicles.[174] Micelle formation was already observed with the herein reported Janus SiNCs and could provide a stepping-stone for further investigations. In addition, the fuel-driven reaction field developed by *Groetsch, Angi* and coworkers for silicon nanocrystals[257] could be combined with the Janus nature to develop the fuel-driven self-assembly of hierarchical superstructures.

Going one step further in terms of self-assembly, combining anisotropic and isotropic SiNCs with complementary functional groups could produce interesting superstructures. For example, an isotropic SiNC could be surrounded by a sphere of anisotropic SiNCs when functionalized with corresponding complementary functional groups – similar to the suggested "raspberries" in chapter 4.5.2.3. Parameters such as size, isotropic to anisotropic ratio and concentration will define the structure that is formed. Such SiNC superstructures have already been suggested and are predicted to show very interesting properties (Mie resonance).[258]

One of the fields where Janus SiNCs could be a promising material is in *biological imaging.* Both Janus particles and silicon nanocrystals have shown potential in biological applications on their own. Janus particles due to their favorable interaction behavior (mimicking biological amphiphiles) and silicon nanocrystals due to their optoelectronic properties – making them viable contrast agents in biological imaging (see 2.1.4: *Applications of Silicon Nanocrystals*, p. 14). The Janus nature could provide the necessary targeting and physiological behavior, while the nanocrystal core provides favorable optoelectronic characteristics. Undoubtedly, the combination of these two could progress the adoption of these materials in the future.

4.5.5 Experimental Procedures

4.5.5.1 General

All of the reagents used in this project were purchased from Sigma Aldrich and stored under an inert atmosphere in a glove box unless stated otherwise. AuNPs (10 nm, stabilized in citrate buffer, ~6.0E+12 particles/mL), purchased form Sigma Aldrich, were stored in a fridge at 7 °C. Allyloxyethanol (PEG-allyl) was passed over heat-dried basic silica and stored over 4 Å molecular sieves prior to use.

For analytical techniques, procedures for solvent drying, as well as the synthesis of hydrogen-terminated silicon nanocrystals and hydrogen-terminated silicon nanosheets see chapter 6: *General Experimental Procedures,* p. 124.

4.5.5.2 Nomenclature of Silicon Nanocrystals

This project uses many different abbreviations for various synthesized silicon nanocrystals. Because two functional groups are introduced and may cause confusion, some clarification is provided:

Abbreviation	Description
SiNC	silicon nanocrystal
SiNC-**R**	silicon nanocrystal functionalized with organic group **R**
H-SiNC@SiNS-H	silicon nanocrystals bonded to silicon nanosheets (unfunctionalized)
R-SiNC@SiNS-**R**	H-SiNC@SiNS-H that were functionalized with organic group **R**
R-SiNC-**R²**	Janus silicon nanocrystals with group **R** on one side and group **R²** on the other
SiNC-**R**/**R²**	bifunctional silicon nanocrystal with groups **R** and **R²** randomly distributed

4.5.5.3 Dehydrogenative Coupling of SiNCs and SiNSs to produce H-SiNC@SiNS-H

10 mg of SiNC-H (obtained from 500 mg SiNC/SiO_2) are dispersed in 3 mL dry toluene. 15 mg SiNS-H (obtained from etching 20 mg silicane) are dispersed in 1.5 mL dry toluene. Both dispersions are transferred to a heat-dried 20 mL Schlenk tube. The mixture is degassed *via* three FPT cycles and stirred at 100 °C for two days. The dispersion (H-SiNC@-SiNS-H) is directly used in the next step or freeze-dried from benzene for storage.

4.5.5.4 General Procedure to Functionalize H-SiNC@SiNS-H to produce R-SiNC@SiNS-R

2 mmol of substrate (alkene) is added to the H-SiNC@SiNS-H dispersion obtained from the previous step. 7 mg 4-DDB are added and the dispersion is degassed three times via freeze-pump-thaw. The mixture is stirred at room temperature for 16 hours to yield R-SiNC@SiNS-R. Purification of the product is performed *via* centrifugation. The dispersion

is centrifuged in the reaction solvent (9000 rpm, 5 min). The supernatant may exhibit photoluminescence due to residual free-standing SiNCs. This is discarded. The residue is dispersed in 10 mL toluene and centrifuged (9000 rpm, 5 min). The cycle is repeated two more times to yield purified R-SiNC@SiNS-R.

4.5.5.5 General Synthesis of Janus R-SiNC-R^2 from R-SiNC@SiNS-R

R-SiNC@SiNS-R from the previous procedure is dispersed in 2 mL dry reaction solvent (typically toluene) and transferred to a heat-dried Schlenk tube. 2 mmol of desired substrate is added and the mixture degassed *via* three FPT cycles. The vessel is placed in a UV reactor (see 6.1.2: *Instrument Information*, p. 124) and stirred under irradiation for 4 hours. To remove the non-soluble byproducts of the SiNS-destruction, the reaction mixture is centrifuged in 3 mL of the reaction solvent (9000 rpm, 5 min). The residue contains the undesired byproduct while the luminescent supernatant contains desired Janus SiNCs. The supernatant is set aside and the residue redispersed in reaction solvent and centrifuged (9000 rpm, 5 min) two more times. Alternatively, the byproducts can be removed by filtration of the reaction mixture through a 0.45 µm PTFE syringe filter. This, however, leads to a lower yield. The combined luminescent supernatants are reduced to 1 mL under vacuum. The purification of the Janus SiNCs is conducted similarly to hydrosilylation procedures. The dispersion is precipitated in an anti-solvent (5 mL) and centrifuged (9000 rpm, 5 min). The supernatant is discarded and the residue redispersed in a minimal amount of solvent. The precipitation/centrifugation/dispersion cycle is repeated three times to yield purified Janus SiNCs (R-SiNC-R^2).

4.5.5.6 Initial Reaction of $H_{25}C_{12}$SiNC@SiNS-$C_{12}H_{25}$ with ethyl undecylenate

In a glove box, 1.5 mg $H_{25}C_{12}$SiNC@SiNS-$C_{12}H_{25}$ (obtained from 4.2.4.3) are dispersed in 2 mL dry toluene and transferred to a heat-dried vial with a stir bar. 0.3 mL ethyl undecylenate (1.24 mmol) are added and the vial brought to a UV reactor (see 6.1.2: *Instrument Information*, p. 124). Under UV irradiation the sample is stirred for two hours. An intense orange photoluminescence is observed after 5 minutes. The dispersion is transferred to a centrifuge tube with 2 mL toluene. After centrifugation (9000 rpm, 5 min), the supernatant (desired liberated SiNCs) is transferred to a clean flask. The residue is washed with toluene and centrifuged (9000 rpm, 5 min). The supernatant is added to the clean flask. This is repeated one more time. The combined supernatant fractions are reduced in vacuum to approximately 0.5 mL to facilitate precipitation. The red suspension is precipitated in MeOH/EtOH (1:1) and centrifuged (9000 rpm, 5 min). The supernatant is discarded and the residue subjected to three further redispersion/precipitation/centrifugation cycles to yield purified $H_{25}C_{12}$-SiNC-$C_{10}H_{20}$COOEt Janus SiNCs.

4.5.5.7 Synthesis of $ClH_{12}C_6$-SiNC-$C_{11}H_{22}Br$

0.26 mL 6-chloro-1-hexene (2 mmol) is added to a dispersion of H-SiNC@SiNS-H, obtained from 4.5.5.3. The mixture is degassed *via* three FPT cycles and stirred at 130 °C for 16 h. The dispersion is centrifuged in 10 mL toluene (9000 rpm, 5 min), the supernatant discarded and the residue redispersed in 10 mL toluene. The cycle is repeated twice to yield $ClH_{12}C_6$-SiNC@SiNS-$C_6H_{12}Cl$. The product is dispersed in 2 mL dry toluene and transferred to a heat-dried Schlenk tube. 0.44 mL 11-bromo-1-undecene (2 mmol) is added and the mixture degassed three times *via* FPT. The Schlenk tube is placed in a UV reactor and the dispersion stirred for 4 h under UV irradiation. The luminescent dispersion is centrifuged in 2 mL toluene (9000 rpm, 5 min) and the supernatant set aside (contains desired SiNCs). The residue is washed twice with 3 mL toluene *via* centrifugation (9000 rpm, 5 min). The supernatants are combined and the volume reduced to 1 mL in vacuum. The dispersion should exhibit significant photoluminescence. The dispersion is precipitated in MeCN/Et_2O (2:1) and centrifuged (9000 rpm, 5 min). The supernatant is discarded and the residue redispersed in a minimal amount of toluene (~0.2 mL). The precipitation/centrifugation/dispersion cycle is repeated twice to yield Janus $ClH_{12}C_6$-SiNC-$C_{11}H_{22}Br$.

4.5.5.8 Synthesis of TMVS-SiNC-$C_{10}H_{20}COOEt$

The synthesis of TMVS-SiNC-$C_{10}H_{20}COOEt$ is conducted as described in procedures 4.5.5.3 to 4.5.5.5. Trimethylvinylsilane was used in the hydrosilylation step and ethyl undecylenate in the UV irradiation step. Toluene was used as the reaction solvent and a mixture of MeOH/EtOH as the anti-solvent during purification of the Janus SiNCs.

4.5.5.9 Synthesis of Amphiphilic PEG-SiNC-$C_{12}H_{25}$

Synthesis of amphiphilic PEG-SiNC-$C_{12}H_{25}$ requires special care due to the bad solubility of the product.

H-SiNC@SiNS-H, obtained from 6.6.5.2, are dispersed in 1 mL dry allyloxy ethanol. The dispersion is degassed *via* three FPT cycles and stirred at 150 °C for 1 h. The purification requires special care, as the freestanding SiNC byproduct (SiNC-PEG) and the PEG-SiNC@SiNS-PEG are both insoluble, making separation difficult. The reaction mixture is mildly centrifuged (1000 rpm, 2 min), the supernatant removed and the residue dispersed in 10 mL methanol. The dispersion is left to settle for 15 minutes, after which the supernatant is carefully removed with a pipette. The sediment contains desired PEG-SiNC@SiNS-PEG while the supernatant contains most of the SiNC-PEG. The dispersion/decanting cycle is repeated five times to yield purified PEG-SiNC@SiNS-PEG.

PEG-SiNC@SiNS-PEG are dispersed in 2 mL dry toluene, transferred to a heat-dried Schlenk tube and 2 mmol 1-dodecene is added. The dispersion is degassed and the mixture irradiated for 4 hours in a UV reactor while stirring. Purification of the product, PEG-SiNC-$C_{12}H_{25}$, is conducted *via* sedimentation. The reaction dispersion is transferred to a vial and dichloromethane (10 mL) is added. The dispersion is left to settle for 15 min. The byproduct settles, while the PEG-SiNC-$C_{12}H_{25}$ remain suspended (they can be easily tracked with PL). The supernatant is decanted and set aside (not all). Care needs to be taken that no non-luminescent byproduct is transferred along with the desired Janus SiNCs. Dichloromethane is added to the vial and the suspension ultrasonicated. After sedimentation for 15 min, the supernatant is separated. This cycle is repeated an additional time. The combined supernatants are reduced to a volume of 1 mL and MeOH/EtOH (1:1) added to facilitate precipitation. The dispersion is centrifuged (9000 rpm, 5 min), the supernatant discarded, the residue redispersed and precipitated. The cycle is repeated twice to yield purified PEG-SiNC-$C_{12}H_{25}$.

4.5.5.10 Interface Testing of Amphiphilic Janus SiNCs

3 mg of PEG-SiNC-$C_{12}H_{25}$ is added to a mixture of hexane (~5 mL) and water (~5 mL). The vial is shaken and left to equilibrate.

4.5.5.11 Hydrosilylation of SiNCs with Thioundecene (Control Reaction)

Thioundecene is synthesized according to a published literature procedure.[259] 4 mg SiNC-H (obtained from etching 200 mg SiNC/SiO_2) is dispersed in 2 mL dry toluene and transferred to a heat dried Schlenk tube. 0.42 mL thioundecene (2 mmol, 372 mg) and 6 mg AIBN are added and the dispersion degassed *via* three FPT cycles. The dispersion is stirred at 75 °C for 16 h. Flocculation (polymer formation) is observed and the reaction product is purified *via* precipitation/centrifugation/dispersion cycles using toluene as the solvent and MeOH/EtOH (1:1) as an antisolvent.

4.5.5.12 Hydrosilylation of SiNCs with ClDMVS (Control Reaction)

SiNC-ClDMVS are synthesized according to a published procedure.[71] 4 mg SiNC H (obtained from etching 200 mg SiNC/SiO_2) are dispersed in 2 mL dry toluene and transferred to a heat-dried Schlenk tube. 0.28 mL chlorodimethylvinylsilane (2 mmol) and 4 mg 4-DDB are added and the dispersion degassed *via* three FPT cycles. The reaction mixture is stirred at room temperature for 16 hours. Due to the sensitivity of SiNC-ClDMVS toward nucleophiles the purification is conducted in a glove box. SiNC-ClDMVS are precipitated in dry, degassed MeCN and centrifuged (6000 rpm, 5 min). The supernatant is discarded and the residue

dispersed in a minimal amount of dry, degassed dichloromethane. The precipitation/centrifugation/dispersion cycle is repeated twice to yield SiNC-ClDMVS.

4.5.5.13 Synthesis of mixed functional SiNC: SiNC-ClDMVS/$C_{12}H_{25}$

4 mg SiNC-H (obtained from etching 200 mg SiNC/SiO_2) are dispersed in 2 mL dry toluene and transferred to a heat-dried Schlenk tube. 0.14 mL chlorodimethylvinylsilane (1 mmol), 0.22 mL 1-dodecene (1 mmol) and 4 mg 4-DDB are added and the dispersion degassed *via* three FPT cycles. The reaction mixture is stirred at room temperature for 16 hours. Due to the sensitivity of SiNC-ClDMVS toward hydrolysis the purification is conducted in a glove box. SiNC-ClDMVS/$C_{12}H_{25}$ are precipitated in dry, degassed MeCN and centrifuged (6000 rpm, 5 min). The supernatant is discarded and the residue dispersed in a minimal amount of dry, degassed dichloromethane. The precipitation/centrifugation/dispersion cycle is repeated twice to yield SiNC-ClDMVS/$C_{12}H_{25}$

4.5.5.14 Synthesis of Janus ClDMVS-SiNC-$C_{12}H_{25}$ for Gold Interfacing

H-SiNC@SiNS-H, obtained from 6.6.5.2, are dispersed in 2 mL dry toluene and transferred to a heat-dried Schlenk tube. 0.28 mL chlorodimethylvinylsilane (2 mmol) and 4 mg 4-DDB are added and the dispersion degassed *via* three FPT cycles. The reaction mixture is stirred for 16 h. Under Ar atmosphere the dispersion is transferred to a centrifuge tube flushed with Ar and sealed with a septum. After centrifugation (9000 rpm, 5 min) the supernatant is discarded and the residue redispersed in dry toluene. Two further centrifugation cycles yield purified ClDMVS-SiNC@SiNS-ClDMVS.

The ClDMVS-SiNC@SiNS-ClDMVS are dispersed in 2 mL dry toluene and transferred to a heat-dried Schlenk tube. 2 mmol 1-dodecene is added and the dispersion degassed and transferred to a UV reactor. After 4 hours of irradiation the dispersion is transferred to a sealed centrifuged tube flushed with Ar. The dispersion is centrifuged (9000 rpm, 5 min), the supernatant set aside and the residue redispersed and centrifuged two more times in dry toluene (under Ar atmosphere). The combined supernatants are reduced to approximately 1 mL and precipitated in dry MeCN (Et_2O can be added in case there are two phases). After centrifugation (9000 rpm, 5 min), the residue is dispersed in dry toluene. The precipitation/centrifugation/dispersion cycles is repeated twice to yield purified Janus ClDMVS-SiNC-$C_{12}H_{25}$. **AuNP Ligand Exchange with Thioethanol**

1.5 mL of AuNP solution are centrifuged and washed twice with water (1.5 mL). After centrifugation the residue is dispersed in 1.5 mL thioethanol solution (2 M in EtOH). The sample is stirred overnight and centrifuged. Washing with dry THF yields thioethanol functionalized AuNPs.

4.5.5.16 AuNP-Thioethanol Synthesis – Brust Schiffrin method

The synthesis of AuNP with thioethanol ligands is performed according to a modified procedure published by Brust and Schiffrin.[252]

177.2 mg $HAuCl_4 \cdot H_2O$ (0.5 mmol) are dissolved in 15 mL H_2O. A solution of 1.09 g TOAB (2 mmol) in 40 mL toluene is added and the mixture vigorously stirred until the all of the $HAuCl_4$ is transferred to the organic phase. 62 µL thioethanol (0.9 mmol) is added. 189.5 mg $NaBH_4$ in 25 mL H_2O is slowly added to the solution and stirred for 3 h.

Contrary to the literature description, the AuNPs partitioned into the water phase. Toluene is completely removed in vacuum and the water phase is extracted with dichloromethane (3 times). The dichloromethane phase is then washed and extracted three times with water. The solvent is completely removed in a rotatory evaporator and the final AuNP-thioethanol dispersed in EtOH.

4.5.5.17 SiNC-AuNP Interfacing

0.8 mg of SiNC-R or R-SiNC-R[2] are dispersed in 1 mL dry THF. The functionalized AuNPs are added to the dispersion and stirred overnight.

4.5.5.18 Gold Wafer Deposition

Gold wafers were prepared from a silicon <100> wafer by thermally evaporating a 3 nm thick titanium layer, followed by a 50 nm gold layer at speeds of roughly 1 Å/s. Before evaporation the chamber held a vacuum of at least 10^{-6} mbar. The gold wafer is cleaved into small pieces (roughly 5 x 5 mm) and clean with water, isopropanol and acetone in an ultrasonication bath for 5 minutes (CA 76°). The gold wafer is subsequently submerged in a 2 M solution of thioethanol in ethanol for 16 h. The wafer is washed with dry ethanol and dried with an Ar stream to yield a SAM of thioethanol on gold (CA 55°).

3 mg SiNCs are dispersed in 2 mL dry toluene and the SAM gold wafer piece submerged in the colloid overnight. The wafer is carefully washed with dry toluene and dried using an Ar stream. The wafer piece is then submerged in dry ethylene glycol for 16 h. Subsequently, the wafer is washed with dry ethylene glycol, dry ethanol and dried under Ar to yield SiNCs deposited on the gold wafer.

5 Summary and Conclusion

Since each research project features a conclusion and outlook of its own, this final chapter only briefly summarizes the advances and key results achieved in the discussed research projects.

In the first research project, a new initiator for the hydrosilylation with silicon nanocrystals – *trityl salts* – was investigated. It was found that the reaction proceeds straightforwardly and quickly, but detailed examination of the substrate scope revealed limitations in the tolerance toward certain functional groups. Without key benefits, such as a higher surface coverage, simpler reaction procedure or easier handling, this method does not offer any significant advantage to already established hydrosilylation procedures.[69, 70]

Moving away from simple hydrosilylation reactions, the use of the *dehydrogenative coupling of silanes* was explored as a method to extend the framework of Si-Si linkages in silicon nanosheets. However, due to the slow proceeding reaction and the oxophilicity of the material, mainly oxidation was observed with only minor incorporation of the desired substrates. Major advances were made when silicon nanosheets were coupled with silicon nanocrystals, based on the procedures established by Yu *et al.* for silicon nanocrystals and germanium nanosheets.[231] The reaction produces a new hybrid material, dubbed SiNC@SiNS, which, at first, did not exhibit interesting properties, but proved to be a crucial component for the subsequent research project, *Surface-Anisotropic Silicon Nanocrystals.*

Following the dehydrogenative coupling, the functionalization of silicon nanomaterials using *siliranes* was explored. At elevated temperatures siliranes decompose into a silylene and an alkene, both of which were predicted to react with the Si-H surface of silicon nanomaterials. At first, the reaction seemed to proceed successfully, with both the desired silylene insertion and undesired hydrosilylation taking place. However, extensive investigations revealed that only the hydrosilylation of the undesired alkene occurs, while the desired silylene remained elusive. In essence, this method constituted the most elaborate and expensive hydrosilylation procedure.

Major advances were finally achieved by using *dichalcogenides* as functionalization substrates. At elevated temperatures or with UV-irradiation, the dichalcogenides form reactive radicals that can react with the Si-H surface. The reaction produces Si-chalcogen bonds that were found to have profound effects on the optoelectronic properties. When diselenides were used, the photoluminescence maximum shifts by 45 nm while the quantum yield decreases. When disulfides are employed, the absolute quantum yield of the photoluminescence is

doubled, when compared to hydrosilylated counterparts (24 % vs 50 %). Previous reports have predicted an effect of chalcogen doping on Si-surfaces but no experimental evidence has yet been published.[240] The newly developed method establishes a new reaction concept that could improve the performance of optoelectronic devices and applications that rely on the bright emission of silicon nanocrystals.

The titular research project, *Surface-Anisotropic Silicon Nanocrystals*, establishes a new reaction protocol to temporarily mask silicon nanocrystals on silicon nanosheets using the procedures developed in the *dehydrogenative coupling* project. Silicon nanocrystals are bonded to the silicon nanosheet surface, thereby protecting one-side of the nanocrystals. The exposed side is then functionalized with common hydrosilylation procedures. Upon irradiation with UV light and in the presence of another substrate, the silicon nanosheet mask decomposes while simultaneously introducing the second functional group to the other side of the silicon nanocrystals. This produces never before synthesized two-sided *Janus silicon nanocrystals.* The main challenge of the research project was to conclusively prove the two-sided nature of the synthesized material. Common analytical techniques, such as FTIR, EDX, TGA, etc., are only able to show the composition of the nanocrystals as a whole and thus differentiation of the two sides is not possible. Various Janus silicon nanocrystals were synthesized and the anisotropic character could be demonstrated with amphiphilic Janus particles — i.e. one side hydrophilic, the other hydrophobic — by observing the agglomeration behavior at the interface of a water/hexane mixture. Final conclusive evidence was given through the self-assembly behavior of anisotropic Janus SiNCs on a gold wafer. In contrast to isotropic control samples, the Janus particles formed a self-assembled monolayer on the gold surface, which represents one of the first examples of a controlled monolayer of SiNCs. This could have great implications for fundamental characterizations of silicon nanocrystals, as single nanocrystals can be isolated and studied. This newly established class of materials opens many possibilities for future research. With a vast library of functionalization substrates, a wide range of two-sided silicon nanocrystals with distinct properties are conceivable. Applications in biological imaging, fundamental research and self-assembly are only some of the opportunities that could arise from this new and exciting material.

6 General Experimental Procedures

6.1.1 Chemical and Solvent Preparations

A Labmaster 130 glove box by *Bruker* was used for storing samples, preparing samples in an inert atmosphere and general handling of solid substances that are sensitive to oxidation and moisture. Purchased reagents were used without further purification and were stored under inert gas prior to use in air-sensitive reactions.

Acetonitrile, toluene, benzene, dichloromethane, diethyl ether and pentane were dried with an *MBraun* solvent purification system, MB SPS-800, using argon 5.0 (99.999%, *Westfalen AG*) as the working gas. Other solvents were dried by passing over a column with heat-dried basic silica. Molecular sieves (4 Å) were used when storing solvents for longer periods of time. Acetone was not kept over molecular sieves due to side reactions. For methanol and ethanol pore sizes of 3 Å were used. After drying all solvents are degassed by sparging with argon for at least 15 minutes.

6.1.2 Instrument Information

FTIR spectra were recorded on a Vertex 70 FTIR using a Platinum ATR from *Bruker.* For solutions, the analyte is drop cast onto the ATR crystal and dried in a N_2 stream.

The **TGA-MS** measurements were performed in a glove box on a *Netzsch* TG 209 F 1 Libra coupled with a QMS 403 Aëolos Quadro mass spectrometer. A typical measurement is conducted by heating at least 1 mg of a sample to 700 °C at a rate of 10 K/min and an Ar flow of 10 mL/min.

Photoluminescence spectra were measured with an AVA-Spec 2048 from *Avantes* using a Prizmatix (LED) light source. An appropriate solvent needs to be used in order to avoid scattering in turbid dispersions. Typical concentration of a silicon nanocrystal sample is 1 mg/mL.

Absolute quantum yield values were obtained using a *Hamamatsu* Absolute PL Quantum yield C11347 spectrometer and taking the values calculated by the supplied software.

Solvodynamic radii were determined by **dynamic light scattering** experiments using a *Malvern* Zetasizer Nano ZS with a laser wavelength of 633 nm. Each measurement consisted of at least 10 acquisitions with an acquisition time of 15 s.

Energy-dispersive X-ray spectroscopy (EDX) was performed on a *Hitachi* TM-1000 tabletop microscope.

Secondary electron microscopy was conducted on a FE-SEM JSM 7500F from *Jeol* at an accelerating voltage of 1 kV. An INCA system by *Oxford Instruments* with an accelerating voltage of 10 kV was used for element mapping and EDX measurements.

A *Krüss* DSA25 goniometer was used to measure **contact angles** by averaging the results of at least 5 droplets (volume of deionized water droplet was 5 µL).

Transmission electron microscopy images were recorded with a Ruby CCD camera on a JEM 1400 plus microscope by *Jeol* with an accelerating voltage of 120 kV. Size distributions were determined by measuring a minimum of 150 nanoparticles using ImageJ software. Additional **transmission electron microscopy (TEM)** images were taken with a *JEOL* JEM-ARM200CF S/TEM electron microscope at an accelerating voltage of 200 kV. The HRTEM images were processed using Gatan Digital Micrograph software (Version 3.4.1). TEM samples were prepared by depositing a droplet of diluted suspensions in toluene onto a holey or ultra-thin carbon coated copper grid (obtained from Electron Microscopy Inc.). The grid was kept in a vacuum chamber for at least 24 h prior to data collection.

Atomic force microscopy was measured in tapping mode with a *Bruker* Multimode AFM using NSG30 tips by measuring over 5 x 5 µm or 1 x 1 µm areas.

A homemade UV reactor system is used for **UV reactions**. The reactor consists of a single near-UV LED light (360 nm), operating at 3W and mounted on a water-cooled metal plate that sits on a magnetic stirrer. Reaction vessels are clamped above the light source.

6.1.3 Experimental Information

6.1.3.1 Synthesis of 4-decyldiazobenzene tetrafluoroborate (4 DDB)

The synthesis of 4-DDB follows a known literature procedure and was mainly used as an established method for the hydrosilylation of silicon nanocrystals and silicon nanosheets.[69, 152]

1.17 g of 4-decylaniline (5 mmol, 1 eq.) is added to a mixture of acetic acid (9 ml), propionic acid (9 ml) and HBF_4 (50 wt%, 6 mL). After the mixture is cooled to 0 °C, 0.52 g of $NaNO_2$ (7.5 mmol, 1.5 eq.) is slowly added over 30 minutes and the suspension stirred for an additional 30 minutes. The suspension is precipitated in ice water, the red solid filtered off,

washed with ice water and dried in a reduced atmosphere. The red product, 4-decyldiazobenzene tetrafluoroborate (1.33 g, 4 mmol, 82%), is stored in a fridge.

^{1}H-NMR (400 MHz, $CHCl_3$-*d,* δ): 8.56-8.50 (m, 2 H), 7.61 (m, 2H), 2.86-2.77 (m, 2 H), 1.72-1.58 (m, 2 H) 1.35-1.18 (m, 14 H), 0.85 (m, 3 H).

6.1.3.2 Synthesis of $CaSi_2$

A pellet of stoichiometric amounts of calcium and silicon is pressed. The pellet is melted with an arc-furnaced in a glove box. The silver regulus is ground in an agate mortar and pressed into a pellet. After a two-time repetition, $CaSi_2$ is formed, which is ground for further use.

6.1.3.3 Synthesis of Silicane / Silicon Nanosheets

1 g of $CaSi_2$ is added to 100 mL of concentrated hydrochloric acid (37 %aq.) and cooled to -30 °C. To aid the exfoliation, the flask is occasionally stirred. The exfoliation is completed after 7 days, after which the yellow flakes are filtered using a Schlenk frit. The flakes are washed with dry acetone or dry alcohol (ethanol, methanol) to remove any residual calcium dichloride. The flakes are dried in vacuum and stored in a glove box. A typical yield from 1 g of $CaSi_2$ is 550 mg.

6.1.3.4 Etching of Silicane with HF

40 mg of SiNSs are dispersed in 2 mL dry and degassed ethanol and ultrasonicated for 5 min to break up large agglomerates. The dispersion is transferred to an FEP container and 1 mL of water and 0.25 mL of HF (48% aq.) are added. After 5 seconds, dichloromethane is added (~5 mL) and the container gently shaken. Once etched, the SiNS-H will partition into the organic phase. Using a polypropylene pipette the SiNS-H are extracted and transferred into an FEP centrifuge tube. This process is repeated until all nanosheets are extracted. The tube is filled with toluene to aid subsequent centrifugation. If the amount of dichloromethane exceeds the amount of toluene, the dispersion is split into two tubes and the tubes filled up with toluene. After centrifugation of the centrifuge tubes (9000 rpm, 4 min) the SiNS-H pellet is dispersed in dry acetone, centrifuged (9000 rpm, 4 min), redispersed in dry toluene and centrifuged again (9000 rpm, 4 min). The SiNS-H are now dispersed in dry reaction solvent or in dry benzene for freeze-drying. The etching procedure typically yields 30 mg of SiNS-H.

6.1.3.5 Synthesis of SiNC/SiO_2 composite

A detailed description of the synthesis of the 3 nm SiNC in SiO_2 composite is found in the literature.[30] A quartz reaction boat is filled with 7.00 g polymeric HSQ, placed into a quartz working tube and transferred to an oven (*Nabertherm* RD 30/200/11). Under a reducing

atmosphere of H_2/N_2 (5/95 %), the tube is heated to 1100 °C over one hour and and the temperature maintained for an additional hour. After cooling to room temperature the resulting amber solid is ground to a powder using an agate mortar and shaken in ethanol with borosilicate beads (d ≈ 3 mm) for 24 h in a *WAB* Turbula mixer. The composite is dried in a vacuum oven at 80 °C to obtain the SiNC/SiO_2 composite as a fine brown powder.

6.1.3.6 Determination of etching time for the SiNC/SiO_2 composite

In a polypropylene beaker charged with a Teflon-coated stir bar, 300 mg of SiNC/SiO_2 composite is dispersed in 3 mL ethanol, 3 mL water and 3 mL HF. After 20 minutes of stirring, every 2 minutes aliquots of the dispersion are taken and extracted in a vial with toluene. A small amount of the SiNC/toluene dispersion is taken for FTIR measurements. The etching time is complete when the Si-O stretching band (ν(Si-O); ~1000 cm^{-1}) is no longer visible. This process is conducted for every batch of SiNC/SiO_2 composite that is synthesized.

6.1.3.7 Liberation of SiNC-H from SiNC/SiO_2 composite with HF

In a polypropylene beaker charged with a Teflon-coated stir bar, per 100 mg of SiNC/SiO_2 composite 1 mL ethanol, 1 mL water and 1 mL HF acid (48% aq.) is added and the dispersion stirred for the previously determined amount of time. The etched silicon nanocrystals (SiNC-H) are extracted with toluene (3 × 10 mL) and centrifuged (9000 rpm; 5 min). The supernatant is discarded, and the residue washed and centrifuged once with dry acetone and once with dry toluene. The resulting SiNC-H is used directly for reactions or freeze-dried from benzene for storage in a glove box. Typically, per 100 mg of etched SiNC/SiO_2 composite, 2 mg of SiNC-H are obtained.

6.1.3.8 General procedure for the hydrosilylation of a given alkene with SiNCs

4 mg SiNC-H (obtained from etching 200 mg SiNC/SiO_2) are dispersed in 2 ml dry toluene. 2 mmol of alkene and 15 mmol of initiator (AIBN, 4-DDB, BIP) is added. The dispersion is degassed *via* three freeze-pump-thaw cycles and stirred for 16 h at room temperature. The dispersion is precipitated in an anti-solvent (10 mL) and centrifuged (9000 rpm, 5 min). Note that the solvent/anti-solvent mix must be able to dissolve the alkene. The residue is dispersed in a minimal amount of solvent (0.5 mL), anti-solvent is added (10 mL) and the dispersion centrifuged. This cycle is repeated an additional two times to yield functionalized silicon nanocrystals (SiNC-R).

7 References

[1] X. The Bakerian Lecture. —Experimental relations of gold (and other metals) to light. *Phil. Trans. R. Soc.* **1857,** *147*, 145–181. DOI: 10.1098/rstl.1857.0011.

[2] Tans, S. J.; Devoret, M. H.; Dai, H.; Thess, A.; Smalley, R. E.; Geerligs, L. J.; Dekker, C. Individual single-wall carbon nanotubes as quantum wires. *Nature* **1997,** *386* (6624), 474–477. DOI: 10.1038/386474a0.

[3] Canham, L. T. Silicon quantum wire array fabrication by electrochemical and chemical dissolution of wafers. *Appl. Phys. Lett.* **1990,** *57* (10), 1046–1048. DOI: 10.1063/1.103561.

[4] Cullis, A. G.; Canham, L. T. Visible light emission due to quantum size effects in highly porous crystalline silicon. *Nature* **1991,** *353* (6342), 335–338. DOI: 10.1038/353335a0.

[5] Heinrich, J. L.; Curtis, C. L.; Credo, G. M.; Sailor, M. J.; Kavanagh, K. L. Luminescent colloidal silicon suspensions from porous silicon. *Science* **1992,** *255* (5040), 66–68. DOI: 10.1126/science.255.5040.66.

[6] Bley, R. A.; Kauzlarich, S. M.; Davis, J. E.; Lee, H. W. H. Characterization of Silicon Nanoparticles Prepared from Porous Silicon. *Chem. Mater.* **1996,** *8* (8), 1881–1888. DOI: 10.1021/cm950608k.

[7] Seraphin, A. A.; Ngiam, S.-T.; Kolenbrander, K. D. Surface control of luminescence in silicon nanoparticles. *Journal of Applied Physics* **1996,** *80* (11), 6429–6433. DOI: 10.1063/1.363662.

[8] Lam, C.; Zhang, Y.; Tang, Y.; Lee, C.; Bello, I.; Lee, S. Large-scale synthesis of ultrafine Si nanoparticles by ball milling. *Journal of Crystal Growth* **2000,** *220* (4), 466–470. DOI: 10.1016/S0022-0248(00)00882-4.

[9] Heintz, A. S.; Fink, M. J.; Mitchell, B. S. Mechanochemical Synthesis of Blue Luminescent Alkyl/Alkenyl-Passivated Silicon Nanoparticles. *Advanced materials (Deerfield Beach, Fla.)* **2007,** *19* (22), 3984–3988. DOI: 10.1002/adma.200602752.

[10] Mangolini, L. Synthesis, properties, and applications of silicon nanocrystals. *Journal of Vacuum Science & Technology B, Nanotechnology and Microelectronics: Materials, Processing, Measurement, and Phenomena* **2013,** *31* (2), 20801. DOI: 10.1116/1.4794789.

[11] Veinot, J. G. C. Synthesis, surface functionalization, and properties of freestanding silicon nanocrystals. *Chemical communications (Cambridge, England)* **2006,** No. 40, 4160–4168.

[12] Wu, J. J.; Flagan, R. C. Onset of runaway nucleation in aerosol reactors. *Journal of Applied Physics* **1987,** *61* (4), 1365–1371. DOI: 10.1063/1.338115.

[13] Ehbrecht, M.; Ferkel, H.; Huisken, F.; Holz, L.; Polivanov, Y. N.; Smirnov, V. V.; Stelmakh, O. M.; Schmidt, R. Deposition and analysis of silicon clusters generated by laser-induced gas phase reaction. *Journal of Applied Physics* **1995,** *78* (9), 5302–5306. DOI: 10.1063/1.360737.

[14] Kortshagen, U. Nonthermal plasma synthesis of semiconductor nanocrystals. *J. Phys. D: Appl. Phys.* **2009,** *42* (11), 113001. DOI: 10.1088/0022-3727/42/11/113001.

[15] Ledoux, G.; Guillois, O.; Porterat, D.; Reynaud, C.; Huisken, F.; Kohn, B.; Paillard, V. Photoluminescence properties of silicon nanocrystals as a function of their size. *Phys. Rev. B* **2000,** *62* (23), 15942–15951. DOI: 10.1103/PhysRevB.62.15942.

[16] Ledoux, G.; Gong, J.; Huisken, F.; Guillois, O.; Reynaud, C. Photoluminescence of size-separated silicon nanocrystals: Confirmation of quantum confinement. *Appl. Phys. Lett.* **2002,** *80* (25), 4834–4836. DOI: 10.1063/1.1485302.

[17] Mangolini, L.; Kortshagen, U. Plasma-Assisted Synthesis of Silicon Nanocrystal Inks. *Advanced materials (Deerfield Beach, Fla.)* **2007,** *19* (18), 2513–2519. DOI: 10.1002/adma.200700595.

[18] Li, Z.; Kortshagen, U. R. Aerosol-Phase Synthesis and Processing of Luminescent Silicon Nanocrystals. *Chem. Mater.* **2019,** *31* (20), 8451–8458. DOI: 10.1021/acs.chemmater.9b02743.

[19] Murray, C. B.; Norris, D. J.; Bawendi, M. G. Synthesis and characterization of nearly monodisperse CdE (E = sulfur, selenium, tellurium) semiconductor nanocrystallites. *J. Am. Chem. Soc.* **1993,** *115* (19), 8706–8715. DOI: 10.1021/ja00072a025.

[20] McVey, B. F. P.; Tilley, R. D. Solution synthesis, optical properties, and bioimaging applications of silicon nanocrystals. *Acc. Chem. Res.* **2014,** *47* (10), 3045–3051. DOI: 10.1021/ar500215v.

[21] Bley, R. A.; Kauzlarich, S. M. A Low-Temperature Solution Phase Route for the Synthesis of Silicon Nanoclusters. *J. Am. Chem. Soc.* **1996,** *118* (49), 12461–12462. DOI: 10.1021/ja962787s.

[22] Zou, J.; Baldwin, R. K.; Pettigrew, K. A.; Kauzlarich, S. M. Solution Synthesis of Ultrastable Luminescent Siloxane-Coated Silicon Nanoparticles. *Nano Lett.* **2004,** *4* (7), 1181–1186. DOI: 10.1021/nl0497373.

[23] Atkins, T. M.; Louie, A. Y.; Kauzlarich, S. M. An efficient microwave-assisted synthesis method for the production of water soluble amine-terminated Si nanoparticles. *Nanotechnology* **2012,** *23* (29), 294006. DOI: 10.1088/0957-4484/23/29/294006.

[24] Holmes, J. D.; Ziegler, K. J.; Doty, R. C.; Pell, L. E.; Johnston, K. P.; Korgel, B. A. Highly luminescent silicon nanocrystals with discrete optical transitions. *J. Am. Chem. Soc.* **2001,** *123* (16), 3743–3748. DOI: 10.1021/ja002956f.

[25] Dasog, M.; Kehrle, J.; Rieger, B.; Veinot, J. G. C. Silicon nanocrystals and silicon-polymer hybrids: Synthesis, surface engineering, and applications. *Angewandte Chemie - International Edition* **2016,** *55* (7), 2322–2339. DOI: 10.1002/anie.201506065.

[26] Hayashi, S.; Nagareda, T.; Kanzawa, Y.; Yamamoto, K. Photoluminescence of Si-Rich SiO 2 Films: Si Clusters as Luminescent Centers. *Jpn. J. Appl. Phys.* **1993,** *32* (Part 1, No. 9A), 3840–3845. DOI: 10.1143/JJAP.32.3840.

[27] Hessel, C. M.; Henderson, E. J.; Veinot, J. G. C. Hydrogen Silsesquioxane: A Molecular Precursor for Nanocrystalline Si–SiO 2 Composites and Freestanding Hydride-Surface-Terminated Silicon Nanoparticles. *Chem. Mater.* **2006,** *18* (26), 6139–6146. DOI: 10.1021/cm0602803.

[28] Hessel, C. M.; Henderson, E. J.; Veinot, J. G. C. An Investigation of the Formation and Growth of Oxide-Embedded Silicon Nanocrystals in Hydrogen Silsesquioxane-Derived Nanocomposites. *J. Phys. Chem. C* **2007,** *111* (19), 6956–6961. DOI: 10.1021/jp070908c.

[29] Henderson, E. J.; Kelly, J. A.; Veinot, J. G. C. Influence of HSiO 1.5 Sol–Gel Polymer Structure and Composition on the Size and Luminescent Properties of Silicon Nanocrystals. *Chem. Mater.* **2009,** *21* (22), 5426–5434. DOI: 10.1021/cm902028q.

[30] Clark, R. J.; Aghajamali, M.; Gonzalez, C. M.; Hadidi, L.; Islam, M. A.; Javadi, M.; Mobarok, M. H.; Purkait, T. K.; Robidillo, C. J. T.; Sinelnikov, R.; Thiessen, A. N.; Washington, J.; Yu, H.; Veinot, J. G. C. From Hydrogen Silsesquioxane to Functionalized Silicon Nanocrystals. *Chem. Mater.* **2017,** *29* (1), 80–89. DOI: 10.1021/acs.chemmater.6b02667.

[31] Cullis, A. G.; Canham, L. T.; Calcott, P. D. J. The structural and luminescence properties of porous silicon. *Journal of Applied Physics* **1997,** *82* (3), 909–965. DOI: 10.1063/1.366536.

[32] Wang, Y.; Herron, N. Nanometer-sized semiconductor clusters: materials synthesis, quantum size effects, and photophysical properties. *J. Phys. Chem.* **1991,** *95* (2), 525–532. DOI: 10.1021/j100155a009.

[33] Brus, L. E. A simple model for the ionization potential, electron affinity, and aqueous redox potentials of small semiconductor crystallites. *The Journal of chemical physics* **1983,** *79* (11), 5566–5571. DOI: 10.1063/1.445676.

[34] Dasog, M.; los Reyes, G. B. de; Titova, L. V.; Hegmann, F. A.; Veinot, J. G. C. Size vs surface: Tuning the photoluminescence of freestanding silicon nanocrystals across the visible spectrum via surface groups. *ACS Nano* **2014,** *8* (9), 9636–9648. DOI: 10.1021/nn504109a.

[35] Wolkin, M. V.; Jorne, J.; Fauchet, P. M.; Allan, G.; Delerue, C. Electronic States and Luminescence in Porous Silicon Quantum Dots: The Role of Oxygen. *Phys. Rev. Lett.* **1999,** *82* (1), 197–200. DOI: 10.1103/PhysRevLett.82.197.

[36] English, D. S.; Pell, L. E.; Yu, Z.; Barbara, P. F.; Korgel, B. A. Size Tunable Visible Luminescence from Individual Organic Monolayer Stabilized Silicon Nanocrystal Quantum Dots. *Nano Lett.* **2002,** *2* (7), 681–685. DOI: 10.1021/nl025538c.

[37] Garcia, C.; Garrido, B.; Pellegrino, P.; Ferre, R.; Moreno, J. A.; Morante, J. R.; Pavesi, L.; Cazzanelli, M. Size dependence of lifetime and absorption cross section of Si nanocrystals embedded in SiO2. *Appl. Phys. Lett.* **2003,** *82* (10), 1595–1597. DOI: 10.1063/1.1558894.

[38] Hannah, D. C.; Yang, J.; Podsiadlo, P.; Chan, M. K. Y.; Demortière, A.; Gosztola, D. J.; Prakapenka, V. B.; Schatz, G. C.; Kortshagen, U.; Schaller, R. D. On the origin of

photoluminescence in silicon nanocrystals: pressure-dependent structural and optical studies. *Nano Lett.* **2012,** *12* (8), 4200–4205. DOI: 10.1021/nl301787g.

[39] Hartel, A. M.; Gutsch, S.; Hiller, D.; Zacharias, M. Fundamental temperature-dependent properties of the Si nanocrystal band gap. *Phys. Rev. B* **2012,** *85* (16). DOI: 10.1103/PhysRevB.85.165306.

[40] los Reyes, G. B. de; Dasog, M.; Na, M.; Titova, L. V.; Veinot, J. G. C.; Hegmann, F. A. Charge transfer state emission dynamics in blue-emitting functionalized silicon nanocrystals. *Physical chemistry chemical physics : PCCP* **2015,** *17* (44), 30125–30133. DOI: 10.1039/c5cp04819b.

[41] Sinelnikov, R.; Dasog, M.; Beamish, J.; Meldrum, A.; Veinot, J. G. C. Revisiting an Ongoing Debate: What Role Do Surface Groups Play in Silicon Nanocrystal Photoluminescence? *ACS Photonics* **2017,** *4* (8), 1920–1929. DOI: 10.1021/acsphotonics.7b00102.

[42] Yang, Z.; los Reyes, G. B. de; Titova, L. V.; Sychugov, I.; Dasog, M.; Linnros, J.; Hegmann, F. A.; Veinot, J. G. C. Evolution of the Ultrafast Photoluminescence of Colloidal Silicon Nanocrystals with Changing Surface Chemistry. *ACS Photonics* **2015,** *2* (5), 595–605. DOI: 10.1021/acsphotonics.5b00143.

[43] Thiessen, A. N.; Zhang, L.; Oliynyk, A. O.; Yu, H.; O'Connor, K. M.; Meldrum, A.; Veinot, J. G. C. A Tale of Seemingly "Identical" Silicon Quantum Dot Families: Structural Insight into Silicon Quantum Dot Photoluminescence. *Chem. Mater.* **2020,** *32* (16), 6838–6846. DOI: 10.1021/acs.chemmater.0c00650.

[44] Wheeler, L. M.; Anderson, N. C.; Palomaki, P. K. B.; Blackburn, J. L.; Johnson, J. C.; Neale, N. R. Silyl Radical Abstraction in the Functionalization of Plasma-Synthesized Silicon Nanocrystals. *Chem. Mater.* **2015,** *27* (19), 6869–6878. DOI: 10.1021/acs.chemmater.5b03309.

[45] Mazzaro, R.; Romano, F.; Ceroni, P. Long-lived luminescence of silicon nanocrystals: from principles to applications. *Physical chemistry chemical physics : PCCP* **2017,** *19* (39), 26507–26526. DOI: 10.1039/c7cp05208a.

[46] Yu, Y.; Fan, G.; Fermi, A.; Mazzaro, R.; Morandi, V.; Ceroni, P.; Smilgies, D.-M.; Korgel, B. A. Size-Dependent Photoluminescence Efficiency of Silicon Nanocrystal Quantum Dots. *J. Phys. Chem. C* **2017,** *121* (41), 23240–23248. DOI: 10.1021/acs.jpcc.7b08054.

[47] Niquet, Y. M.; Delerue, C.; Allan, G.; Lannoo, M. Method for tight-binding parametrization: Application to silicon nanostructures. *Physical review. B, Condensed matter* **2000,** *62* (8), 5109–5116. DOI: 10.1103/PhysRevB.62.5109.

[48] Hessel, C. M.; Reid, D.; Panthani, M. G.; Rasch, M. R.; Goodfellow, B. W.; Wei, J.; Fujii, H.; Akhavan, V.; Korgel, B. A. Synthesis of Ligand-Stabilized Silicon Nanocrystals with Size-Dependent Photoluminescence Spanning Visible to Near-Infrared Wavelengths. *Chem. Mater.* **2012,** *24* (2), 393–401. DOI: 10.1021/cm2032866.

[49] Li, X.; He, Y.; Talukdar, S. S.; Swihart, M. T. Process for Preparing Macroscopic Quantities of Brightly Photoluminescent Silicon Nanoparticles with Emission Spanning the Visible Spectrum. *Langmuir* **2003,** *19* (20), 8490–8496. DOI: 10.1021/la034487b.

[50] Thiessen, A. N.; Ha, M.; Hooper, R. W.; Yu, H.; Oliynyk, A. O.; Veinot, J. G. C.; Michaelis, V. K. Silicon Nanoparticles: Are They Crystalline from the Core to the Surface? *Chem. Mater.* **2019,** *31* (3), 678–688. DOI: 10.1021/acs.chemmater.8b03074.

[51] Buriak, J. M. Organometallic chemistry on silicon and germanium surfaces. *Chemical Reviews* **2002,** *102* (5), 1271–1308. DOI: 10.1021/cr000064s.

[52] Sailor, M. J. *Porous silicon in practice*. *Preparation, characterization and applications* / *Michael J. Sailor;* Wiley-VCH: Weinheim, 2012.

[53] Linford, M. R.; Chidsey, C. E. D. Alkyl monolayers covalently bonded to silicon surfaces. *J. Am. Chem. Soc.* **1993,** *115* (26), 12631–12632. DOI: 10.1021/ja00079a071.

[54] Linford, M. R.; Fenter, P.; Eisenberger, P. M.; Chidsey, C. E. D. Alkyl Monolayers on Silicon Prepared from 1-Alkenes and Hydrogen-Terminated Silicon. *J. Am. Chem. Soc.* **1995,** *117* (11), 3145–3155. DOI: 10.1021/ja00116a019.

[55] Cheng, X.; Lowe, S. B.; Reece, P. J.; Gooding, J. J. Colloidal silicon quantum dots: from preparation to the modification of self-assembled monolayers (SAMs) for bio-applications. *Chemical Society reviews* **2014,** *43* (8), 2680–2700. DOI: 10.1039/c3cs60353a.

[56] Rogozhina, E.; Belomoin, G.; Smith, A.; Abuhassan, L.; Barry, N.; Akcakir, O.; Braun, P. V.; Nayfeh, M. H. Si–N linkage in ultrabright, ultrasmall Si nanoparticles. *Appl. Phys. Lett.* **2001,** *78* (23), 3711–3713. DOI: 10.1063/1.1377619.

[57] Yang, C.-S.; Bley, R. A.; Kauzlarich, S. M.; Lee, H. W. H.; Delgado, G. R. Synthesis of Alkyl-Terminated Silicon Nanoclusters by a Solution Route. *J. Am. Chem. Soc.* **1999,** *121* (22), 5191–5195. DOI: 10.1021/ja9828509.

[58] Mayeri, D.; Phillips, B. L.; Augustine, M. P.; Kauzlarich, S. M. NMR Study of the Synthesis of Alkyl-Terminated Silicon Nanoparticles from the Reaction of SiCl 4 with the Zintl Salt, NaSi. *Chem. Mater.* **2001,** *13* (3), 765–770. DOI: 10.1021/cm000418w.

[59] Dasog, M.; Bader, K.; Veinot, J. G. C. Influence of Halides on the Optical Properties of Silicon Quantum Dots. *Chem. Mater.* **2015,** *27* (4), 1153–1156. DOI: 10.1021/acs.chemmater.5b00115.

[60] Kehrle, J.; Kaiser, S.; Purkait, T. K.; Winnacker, M.; Helbich, T.; Vagin, S.; Veinot, J. G. C.; Rieger, B. In situ IR-spectroscopy as a tool for monitoring the radical hydrosilylation process on silicon nanocrystal surfaces. *Nanoscale* **2017,** *9* (24), 8489–8495. DOI: 10.1039/c7nr02265d.

[61] Kelly, J. A.; Shukaliak, A. M.; Fleischauer, M. D.; Veinot, J. G. C. Size-dependent reactivity in hydrosilylation of silicon nanocrystals. *Journal of the American Chemical Society* **2011,** *133* (24), 9564–9571. DOI: 10.1021/ja2025189.

[62] Kelly, J. A.; Veinot, J. G. C. An investigation into near-UV hydrosilylation of freestanding silicon nanocrystals. *ACS Nano* **2010,** *4* (8), 4645–4656. DOI: 10.1021/nn101022b.

[63] Stewart, M. P.; Buriak, J. M. Exciton-mediated hydrosilylation on photoluminescent nanocrystalline silicon. *J. Am. Chem. Soc.* **2001,** *123* (32), 7821–7830. DOI: 10.1021/ja011116d.

[64] Yu, Y.; Hessel, C. M.; Bogart, T. D.; Panthani, M. G.; Rasch, M. R.; Korgel, B. A. Room temperature hydrosilylation of silicon nanocrystals with bifunctional terminal alkenes. *Langmuir : the ACS journal of surfaces and colloids* **2013,** *29* (5), 1533–1540. DOI: 10.1021/la304874y.

[65] Purkait, T. K.; Iqbal, M.; Wahl, M. H.; Gottschling, K.; Gonzalez, C. M.; Islam, M. A.; Veinot, J. G. C. Borane-catalyzed room-temperature hydrosilylation of alkenes/alkynes on silicon nanocrystal surfaces. *J. Am. Chem. Soc.* **2014,** *136* (52), 17914–17917. DOI: 10.1021/ja510120e.

[66] Yang, Z.; Gonzalez, C. M.; Purkait, T. K.; Iqbal, M.; Meldrum, A.; Veinot, J. G. C. Radical Initiated Hydrosilylation on Silicon Nanocrystal Surfaces: An Evaluation of Functional Group Tolerance and Mechanistic Study. *Langmuir : the ACS journal of surfaces and colloids* **2015,** *31* (38), 10540–10548. DOI: 10.1021/acs.langmuir.5b02307.

[67] Islam, M. A.; Mobarok, M. H.; Sinelnikov, R.; Purkait, T. K.; Veinot, J. G. C. Phosphorus Pentachloride Initiated Functionalization of Silicon Nanocrystals. *Langmuir : the ACS journal of surfaces and colloids* **2017,** *33* (35), 8766–8773. DOI: 10.1021/acs.langmuir.7b00518.

[68] Mobarok, M. H.; Purkait, T. K.; Islam, M. A.; Miskolzie, M.; Veinot, J. G. C. Instantaneous Functionalization of Chemically Etched Silicon Nanocrystal Surfaces. *Angew. Chem.* **2017,** *129* (22), 6169–6173. DOI: 10.1002/ange.201609651.

[69] Höhlein, I. M. D.; Kehrle, J.; Helbich, T.; Yang, Z.; Veinot, J. G. C.; Rieger, B. Diazonium salts as grafting agents and efficient radical-hydrosilylation initiators for freestanding photoluminescent silicon nanocrystals. *Chemistry (Weinheim an der Bergstrasse, Germany)* **2014,** *20* (15), 4212–4216. DOI: 10.1002/chem.201400114.

[70] Helbich, T.; Kloberg, M. J.; Sinelnikov, R.; Lyuleeva, A.; Veinot, J. G. C.; Rieger, B. Diaryliodonium salts as hydrosilylation initiators for the surface functionalization of silicon nanomaterials and their collaborative effect as ring opening polymerization initiators. *Nanoscale* **2017,** *9* (23), 7739–7744. DOI: 10.1039/c7nr01559c.

[71] Höhlein, I. M. D.; Kehrle, J.; Purkait, T. K.; Veinot, J. G. C.; Rieger, B. Photoluminescent silicon nanocrystals with chlorosilane surfaces--synthesis and reactivity. *Nanoscale* **2015,** *7* (3), 914–918. DOI: 10.1039/c4nr05888g.

[72] Morselli, G.; Romano, F.; Ceroni, P. Amine functionalised silicon nanocrystals with bright red and long-lived emission. *Faraday discussions* **2020,** *222* (0), 108–121. DOI: 10.1039/c9fd00089e.

[73] Romano, F.; Angeloni, S.; Morselli, G.; Mazzaro, R.; Morandi, V.; Shell, J. R.; Cao, X.; Pogue, B. W.; Ceroni, P. Water-soluble silicon nanocrystals as NIR luminescent probes for time-gated biomedical imaging. *Nanoscale* **2020,** *12* (14), 7921–7926. DOI: 10.1039/d0nr00814a.

[74] Shiohara, A.; Hanada, S.; Prabakar, S.; Fujioka, K.; Lim, T. H.; Yamamoto, K.; Northcote, P. T.; Tilley, R. D. Chemical reactions on surface molecules attached to silicon quantum dots. *J. Am. Chem. Soc.* **2010,** *132* (1), 248–253. DOI: 10.1021/ja906501v.

[75] Zhukhovitskiy, A. V.; Mavros, M. G.; Queeney, K. T.; Wu, T.; van Voorhis, T.; Johnson, J. A. Reactions of Persistent Carbenes with Hydrogen-Terminated Silicon Surfaces. *Journal of the American Chemical Society* **2016,** *138* (27), 8639–8652. DOI: 10.1021/jacs.6b04962.

[76] Saghatelian, A.; Buriak, J.; Lin, V. S.; Reza Ghadiri, M. Transition metal mediated surface modification of porous silicon. *Tetrahedron* **2001,** *57* (24), 5131–5136. DOI: 10.1016/S0040-4020(01)00366-0.

[77] Yang, Z.; Wahl, M. H.; Veinot, J. G. Size-independent organosilane functionalization of silicon nanocrystals using Wilkinson's catalyst. *Can. J. Chem.* **2014,** *92* (10), 951–957. DOI: 10.1139/cjc-2014-0048.

[78] Kehrle, J.; Höhlein, I. M. D.; Yang, Z.; Jochem, A.-R.; Helbich, T.; Kraus, T.; Veinot, J. G. C.; Rieger, B. Thermoresponsive and photoluminescent hybrid silicon nanoparticles by surface-initiated group transfer polymerization of diethyl vinylphosphonate. *Angewandte Chemie - International Edition* **2014,** *53* (46), 12494–12497. DOI: 10.1002/anie.201405946.

[79] Thiessen, A. N.; Purkait, T. K.; Faramus, A.; Veinot, J. G. C. Lewis Acid Protection: A Method Toward Synthesizing Phase Transferable Luminescent Silicon Nanocrystals. *Phys. Status Solidi A* **2018,** *215* (7), 1700620. DOI: 10.1002/pssa.201700620.

[80] Lin, S.-W.; Chen, D.-H. Synthesis of water-soluble blue photoluminescent silicon nanocrystals with oxide surface passivation. *Small (Weinheim an der Bergstrasse, Germany)* **2009,** *5* (1), 72–76. DOI: 10.1002/smll.200800677.

[81] Švrček, V.; Sasaki, T.; Shimizu, Y.; Koshizaki, N. Blue luminescent silicon nanocrystals prepared by ns pulsed laser ablation in water. *Appl. Phys. Lett.* **2006,** *89* (21), 213113. DOI: 10.1063/1.2397014.

[82] Warner, J. H.; Hoshino, A.; Yamamoto, K.; Tilley, R. D. Water-soluble photoluminescent silicon quantum dots. *Angewandte Chemie (International ed. in English)* **2005,** *44* (29), 4550–4554. DOI: 10.1002/anie.200501256.

[83] Cheng, X.; Hinde, E.; Owen, D. M.; Lowe, S. B.; Reece, P. J.; Gaus, K.; Gooding, J. J. Enhancing Quantum Dots for Bioimaging using Advanced Surface Chemistry and Advanced Optical Microscopy: Application to Silicon Quantum Dots (SiQDs). *Advanced materials (Deerfield Beach, Fla.)* **2015,** *27* (40), 6144–6150. DOI: 10.1002/adma.201503223.

[84] Pujari, S. P.; Driss, H.; Bannani, F.; van Lagen, B.; Zuilhof, H. One-Pot Gram-Scale Synthesis of Hydrogen-Terminated Silicon Nanoparticles. *Chem. Mater.* **2018,** *30* (18), 6503–6512. DOI: 10.1021/acs.chemmater.8b03113.

[85] Zhai, Y.; Dasog, M.; Snitynsky, R. B.; Purkait, T. K.; Aghajamali, M.; Hahn, A. H.; Sturdy, C. B.; Lowary, T. L.; Veinot, J. G. C. Water-soluble photoluminescent d-mannose and l-alanine functionalized silicon nanocrystals and their application to cancer cell imaging. *Journal of materials chemistry. B* **2014,** *2* (47), 8427–8433. DOI: 10.1039/C4TB01161A.

[86] Li, Z. F.; Ruckenstein, E. Water-Soluble Poly(acrylic acid) Grafted Luminescent Silicon Nanoparticles and Their Use as Fluorescent Biological Staining Labels. *Nano Lett.* **2004,** *4* (8), 1463–1467. DOI: 10.1021/nl0492436.

[87] Clark, R. J.; Dang, M. K. M.; Veinot, J. G. C. Exploration of organic acid chain length on water-soluble silicon quantum dot surfaces. *Langmuir : the ACS journal of surfaces and colloids* **2010,** *26* (19), 15657–15664. DOI: 10.1021/la102983c.

[88] Islam, M. A.; Sinelnikov, R.; Howlader, M. A.; Faramus, A.; Veinot, J. G. C. Mixed Surface Chemistry: An Approach to Highly Luminescent Biocompatible Amphiphilic Silicon Nanocrystals. *Chem. Mater.* **2018,** *30* (24), 8925–8931. DOI: 10.1021/acs.chemmater.8b04227.

[89] Ni, Z.; Zhou, S.; Zhao, S.; Peng, W.; Yang, D.; Pi, X. Silicon nanocrystals: unfading silicon materials for optoelectronics. *Materials Science and Engineering: R: Reports* **2019,** *138*, 85–117. DOI: 10.1016/j.mser.2019.06.001.

[90] *Restriction of the Use of Certain Hazardous Substances in Electrical and Electronic Equipment,"*. *2002/95/EC*, 2003.

[91] Bhattacharjee, S.; Rietjens, I. M. C. M.; Singh, M. P.; Atkins, T. M.; Purkait, T. K.; Xu, Z.; Regli, S.; Shukaliak, A.; Clark, R. J.; Mitchell, B. S.; Alink, G. M.; Marcelis, A. T. M.; Fink, M. J.; Veinot, J. G. C.; Kauzlarich, S. M.; Zuilhof, H. Cytotoxicity of surface-functionalized silicon and germanium nanoparticles: the dominant role of surface charges. *Nanoscale* **2013,** *5* (11), 4870–4883. DOI: 10.1039/c3nr34266b.

[92] Angı, A.; Loch, M.; Sinelnikov, R.; Veinot, J. G. C.; Becherer, M.; Lugli, P.; Rieger, B. The influence of surface functionalization methods on the performance of silicon nanocrystal LEDs. *Nanoscale* **2018,** *10* (22), 10337–10342. DOI: 10.1039/c7nr09525b.

[93] Maier-Flaig, F.; Rinck, J.; Stephan, M.; Bocksrocker, T.; Bruns, M.; Kübel, C.; Powell, A. K.; Ozin, G. A.; Lemmer, U. Multicolor silicon light-emitting diodes (SiLEDs). *Nano Lett.* **2013,** *13* (2), 475–480. DOI: 10.1021/nl3038689.

[94] Fukata, N.; Subramani, T.; Jevasuwan, W.; Dutta, M.; Bando, Y. Functionalization of Silicon Nanostructures for Energy-Related Applications. *Small (Weinheim an der Bergstrasse, Germany)* **2017,** *13* (45). DOI: 10.1002/smll.201701713.

[95] Kasavajjula, U.; Wang, C.; Appleby, A. J. Nano- and bulk-silicon-based insertion anodes for lithium-ion secondary cells. *Journal of Power Sources* **2007,** *163* (2), 1003–1039. DOI: 10.1016/j.jpowsour.2006.09.084.

[96] Son, I. H.; Hwan Park, J.; Kwon, S.; Park, S.; Rümmeli, M. H.; Bachmatiuk, A.; Song, H. J.; Ku, J.; Choi, J. W.; Choi, J.-M.; Doo, S.-G.; Chang, H. Silicon carbide-free graphene growth on silicon for lithium-ion battery with high volumetric energy density. *Nature Communications* **2015,** *6*, 7393. DOI: 10.1038/ncomms8393.

[97] Aghajamali, M.; Xie, H.; Javadi, M.; Kalisvaart, W. P.; Buriak, J. M.; Veinot, J. G. C. Size and Surface Effects of Silicon Nanocrystals in Graphene Aerogel Composite Anodes for Lithium Ion Batteries. *Chem. Mater.* **2018,** *30* (21), 7782–7792. DOI: 10.1021/acs.chemmater.8b03198.

[98] Hill, S. K. E.; Connell, R.; Peterson, C.; Hollinger, J.; Hillmyer, M. A.; Kortshagen, U.; Ferry, V. E. Silicon Quantum Dot–Poly(methyl methacrylate) Nanocomposites with Reduced Light Scattering for Luminescent Solar Concentrators. *ACS Photonics* **2019,** *6* (1), 170–180. DOI: 10.1021/acsphotonics.8b01346.

[99] Mazzaro, R.; Gradone, A.; Angeloni, S.; Morselli, G.; Cozzi, P. G.; Romano, F.; Vomiero, A.; Ceroni, P. Hybrid Silicon Nanocrystals for Color-Neutral and Transparent Luminescent Solar Concentrators. *ACS Photonics* **2019,** *6* (9), 2303–2311. DOI: 10.1021/acsphotonics.9b00802.

[100] Gonzalez, C. M.; Iqbal, M.; Dasog, M.; Piercey, D. G.; Lockwood, R.; Klapötke, T. M.; Veinot, J. G. C. Detection of high-energy compounds using photoluminescent silicon nanocrystal paper based sensors. *Nanoscale* **2014,** *6* (5), 2608–2612. DOI: 10.1039/C3NR06271F.

[101] Gonzalez, C. M.; Veinot, J. G. C. Silicon nanocrystals for the development of sensing platforms. *J. Mater. Chem. C* **2016,** *4* (22), 4836–4846. DOI: 10.1039/C6TC01159D.

[102] Alsharif, N. H.; Berger, C. E. M.; Varanasi, S. S.; Chao, Y.; Horrocks, B. R.; Datta, H. K. Alkyl-capped silicon nanocrystals lack cytotoxicity and have enhanced intracellular accumulation in malignant cells via cholesterol-dependent endocytosis. *Small (Weinheim an der Bergstrasse, Germany)* **2009,** *5* (2), 221–228. DOI: 10.1002/smll.200800903.

[103] Belyakov, V. A.; Burdov, V. A.; Lockwood, R.; Meldrum, A. Silicon Nanocrystals: Fundamental Theory and Implications for Stimulated Emission. *Advances in Optical Technologies* **2008,** *2008*, 1–32. DOI: 10.1155/2008/279502.

[104] Weissleder, R. A clearer vision for in vivo imaging. *Nature biotechnology* **2001,** *19* (4), 316–317. DOI: 10.1038/86684.

[105] Furey, B. J.; Silbaugh, D. A.; Yu, Y.; Guillaussier, A. C.; Estrada, A. D.; Stevens, C.; Maynard, J. A.; Korgel, B. A.; Downer, M. C. Measurement of Two-Photon Absorption of Silicon Nanocrystals in Colloidal Suspension for Bio-Imaging Applications. *Phys. Status Solidi B* **2018,** *255* (4), 1700501. DOI: 10.1002/pssb.201700501.

[106] Henderson, E. J.; Shuhendler, A. J.; Prasad, P.; Baumann, V.; Maier-Flaig, F.; Faulkner, D. O.; Lemmer, U.; Wu, X. Y.; Ozin, G. A. Colloidally stable silicon nanocrystals with near-infrared photoluminescence for biological fluorescence imaging. *Small (Weinheim an der Bergstrasse, Germany)* **2011,** *7* (17), 2507–2516. DOI: 10.1002/smll.201100845.

[107] Chandra, S.; Ghosh, B.; Beaune, G.; Nagarajan, U.; Yasui, T.; Nakamura, J.; Tsuruoka, T.; Baba, Y.; Shirahata, N.; Winnik, F. M. Functional double-shelled silicon nanocrystals for two-photon fluorescence cell imaging: spectral evolution and tuning. *Nanoscale* **2016,** *8* (16), 9009–9019. DOI: 10.1039/C6NR01437B.

[108] Billinton, N.; Knight, A. W. Seeing the wood through the trees: a review of techniques for distinguishing green fluorescent protein from endogenous autofluorescence. *Analytical biochemistry* **2001,** *291* (2), 175–197. DOI: 10.1006/abio.2000.5006.

[109] Mastronardi, M. L.; Henderson, E. J.; Puzzo, D. P.; Ozin, G. A. Small silicon, big opportunities: the development and future of colloidally-stable monodisperse silicon nanocrystals. *Advanced materials (Deerfield Beach, Fla.)* **2012,** *24* (43), 5890–5898. DOI: 10.1002/adma.201202846.

[110] Hessel, C. M.; Rasch, M. R.; Hueso, J. L.; Goodfellow, B. W.; Akhavan, V. A.; Puvanakrishnan, P.; Tunnel, J. W.; Korgel, B. A. Alkyl passivation and amphiphilic polymer coating of silicon nanocrystals for diagnostic imaging. *Small (Weinheim an der Bergstrasse, Germany)* **2010,** *6* (18), 2026–2034. DOI: 10.1002/smll.201000825.

[111] Erogbogbo, F.; Yong, K.-T.; Roy, I.; Xu, G.; Prasad, P. N.; Swihart, M. T. Biocompatible luminescent silicon quantum dots for imaging of cancer cells. *ACS Nano* **2008,** *2* (5), 873–878. DOI: 10.1021/nn700319z.

[112] Erogbogbo, F.; Yong, K.-T.; Roy, I.; Hu, R.; Law, W.-C.; Zhao, W.; Ding, H.; Wu, F.; Kumar, R.; Swihart, M. T.; Prasad, P. N. In vivo targeted cancer imaging, sentinel lymph node mapping and multi-channel imaging with biocompatible silicon nanocrystals. *ACS Nano* **2011,** *5* (1), 413–423. DOI: 10.1021/nn1018945.

[113] Robidillo, C. J. T.; Aghajamali, M.; Faramus, A.; Sinelnikov, R.; Veinot, J. G. C. Interfacing enzymes with silicon nanocrystals through the thiol-ene reaction. *Nanoscale* **2018,** *10* (39), 18706–18719. DOI: 10.1039/c8nr05368e.

[114] Robidillo, C. J. T.; Islam, M. A.; Aghajamali, M.; Faramus, A.; Sinelnikov, R.; Zhang, X.; Boekhoven, J.; Veinot, J. G. C. Functional Bioinorganic Hybrids from Enzymes and Luminescent Silicon-Based Nanoparticles. *Langmuir : the ACS journal of surfaces and colloids* **2018,** *34* (22), 6556–6569. DOI: 10.1021/acs.langmuir.8b01119.

[115] Nishimura, H.; Ritchie, K.; Kasai, R. S.; Goto, M.; Morone, N.; Sugimura, H.; Tanaka, K.; Sase, I.; Yoshimura, A.; Nakano, Y.; Fujiwara, T. K.; Kusumi, A. Biocompatible fluorescent silicon nanocrystals for single-molecule tracking and fluorescence imaging. *The Journal of cell biology* **2013,** *202* (6), 967–983. DOI: 10.1083/jcb.201301053.

[116] McVey, B. F. P.; Prabakar, S.; Gooding, J. J.; Tilley, R. D. Solution Synthesis, Surface Passivation, Optical Properties, Biomedical Applications, and Cytotoxicity of Silicon and Germanium Nanocrystals. *ChemPlusChem* **2017,** *82* (1), 60–73. DOI: 10.1002/cplu.201600207.

[117] Huey, W. L. B.; Goldberger, J. E. Covalent functionalization of two-dimensional group 14 graphane analogues. *Chemical Society reviews* **2018**.

[118] Okamoto, H.; Kumai, Y.; Sugiyama, Y.; Mitsuoka, T.; Nakanishi, K.; Ohta, T.; Nozaki, H.; Yamaguchi, S.; Shirai, S.; Nakano, H. Silicon nanosheets and their self-assembled regular stacking structure. *Journal of the American Chemical Society* **2010,** *132* (8), 2710–2718. DOI: 10.1021/ja908827z.

[119] Molle, A.; Goldberger, J.; Houssa, M.; Xu, Y.; Zhang, S.-C.; Akinwande, D. Buckled two-dimensional Xene sheets. *Nature materials* **2017,** *16* (2), 163–169. DOI: 10.1038/nmat4802.

[120] Butler, S. Z.; Hollen, S. M.; Cao, L.; Cui, Y.; Gupta, J. A.; Gutiérrez, H. R.; Heinz, T. F.; Hong, S. S.; Huang, J.; Ismach, A. F.; Johnston-Halperin, E.; Kuno, M.; Plashnitsa, V. V.; Robinson, R. D.; Ruoff, R. S.; Salahuddin, S.; Shan, J.; Shi, L.; Spencer, M. G.; Terrones, M.; Windl, W.; Goldberger, J. E. Progress, challenges, and opportunities in two-dimensional materials beyond graphene. *ACS Nano* **2013,** *7* (4), 2898–2926. DOI: 10.1021/nn400280c.

[121] Balendhran, S.; Walia, S.; Nili, H.; Sriram, S.; Bhaskaran, M. Elemental analogues of graphene: silicene, germanene, stanene, and phosphorene. *Small (Weinheim an der Bergstrasse, Germany)* **2015,** *11* (6), 640–652. DOI: 10.1002/smll.201402041.

[122] Sugiyama, Y.; Okamoto, H.; Mitsuoka, T.; Morikawa, T.; Nakanishi, K.; Ohta, T.; Nakano, H. Synthesis and optical properties of monolayer organosilicon nanosheets. *J. Am. Chem. Soc.* **2010,** *132* (17), 5946–5947. DOI: 10.1021/ja100919d.

[123] Tan, C.; Cao, X.; Wu, X.-J.; He, Q.; Yang, J.; Zhang, X.; Chen, J.; Zhao, W.; Han, S.; Nam, G.-H.; Sindoro, M.; Zhang, H. Recent Advances in Ultrathin Two-Dimensional Nanomaterials. *Chemical Reviews* **2017,** *117* (9), 6225–6331. DOI: 10.1021/acs.chemrev.6b00558.

[124] Cinquanta, E.; Scalise, E.; Chiappe, D.; Grazianetti, C.; van den Broek, B.; Houssa, M.; Fanciulli, M.; Molle, A. Getting through the Nature of Silicene: An sp 2 –sp 3 Two-Dimensional Silicon Nanosheet. *J. Phys. Chem. C* **2013,** *117* (32), 16719–16724. DOI: 10.1021/jp405642g.

[125] Takeda; Shiraishi. Theoretical possibility of stage corrugation in Si and Ge analogs of graphite. *Physical review. B, Condensed matter* **1994,** *50* (20), 14916–14922. DOI: 10.1103/PhysRevB.50.14916.

[126] Grazianetti, C.; Cinquanta, E.; Molle, A. Two-dimensional silicon: the advent of silicene. *2D Mater.* **2016,** *3* (1), 12001. DOI: 10.1088/2053-1583/3/1/012001.

[127] Cahangirov, S.; Topsakal, M.; Aktürk, E.; Sahin, H.; Ciraci, S. Two- and one-dimensional honeycomb structures of silicon and germanium. *Physical review letters* **2009,** *102* (23), 236804. DOI: 10.1103/PhysRevLett.102.236804.

[128] Takeda; Shiraishi. Theoretical possibility of stage corrugation in Si and Ge analogs of graphite. *Physical review. B, Condensed matter* **1994,** *50* (20), 14916–14922. DOI: 10.1103/PhysRevB.50.14916.

[129] Wöhler, F. Ueber Verbindungen des Siliciums mit Sauerstoff und Wasserstoff. *Ann. Chem. Pharm.* **1863,** *127* (3), 257–274. DOI: 10.1002/jlac.18631270302.

[130] Kautzky, H.; Herzberg, G. Über die Konstitution des Siloxens. *Ber. dtsch. Chem. Ges. A/B* **1924,** *57* (9), 1665–1670. DOI: 10.1002/cber.19240570907.

[131] Weiss, A.; Beil, G.; Meyer, H. The Topochemical Reaction of CaSi2 to a Two-Dimensional Subsiliceous Acid Si6H3(OH)3 (= Kautskys' Siloxene). *Zeitschrift für Naturforschung B* **1980,** *35* (1), 25–30. DOI: 10.1515/znb-1980-0108.

[132] Kurmaev, E. Z.; Shamin, S. N.; Ederer, D. L.; Dettlaff-Weglikowska, U.; Weber, J. Local and Electronic Structure of Siloxene. *J. Mater. Res.* **1999,** *14* (4), 1235–1237. DOI: 10.1557/JMR.1999.0168.

[133] Dahn; Way; Fuller; Tse. Structure of siloxene and layered polysilane (Si6H6). *Physical review. B, Condensed matter* **1993,** *48* (24), 17872–17877. DOI: 10.1103/PhysRevB.48.17872.

[134] Nishimura, K.; Nagao, Y.; Yamanaka, S.; Matsu-ura, H. Characterization of Layered Polysilane. *Jpn. J. Appl. Phys.* **1996,** *35* (Part 2, No. 3A), L293-L296. DOI: 10.1143/JJAP.35.L293.

[135] Yamanaka, S.; Matsu-ura, H.; Ishikawa, M. New deintercalation reaction of calcium from calcium disilicide. Synthesis of layered polysilane. *Materials Research Bulletin* **1996,** *31* (3), 307–316. DOI: 10.1016/0025-5408(95)00195-6.

[136] Brandt, M. S.; Fuchs, H. D.; Stutzmann, M.; Weber, J.; Cardona, M. The origin of visible luminescencefrom "porous silicon": A new interpretation. *Solid State Communications* **1992,** *81* (4), 307–312. DOI: 10.1016/0038-1098(92)90815-Q.

[137] Dahn, J. R.; Way, B. M.; Fuller, E. W.; Weydanz, W. J.; Tse, J. S.; Klug, D. D.; van Buuren, T.; Tiedje, T. X-ray diffraction and x-ray absorption studies of porous silicon, siloxene, heat-treated siloxene, and layered polysilane. *Journal of Applied Physics* **1994,** *75* (4), 1946–1951. DOI: 10.1063/1.356342.

[138] Fuchs; Stutzmann; Brandt; Rosenbauer; Weber; Breitschwerdt; Deák; Cardona. Porous silicon and siloxene: Vibrational and structural properties. *Physical review. B, Condensed matter* **1993,** *48* (11), 8172–8189. DOI: 10.1103/PhysRevB.48.8172.

[139] Ohshita, J.; Yamamoto, K.; Tanaka, D.; Nakashima, M.; Kunugi, Y.; Ohashi, M.; Nakano, H. Preparation and Photocurrent Generation of Silicon Nanosheets with Aromatic Substituents on the Surface. *Journal of Physical Chemistry C* **2016,** *120* (20), 10991–10996. DOI: 10.1021/acs.jpcc.6b03014.

[140] Kuritka, I.; Schauer, F.; Saha, P.; Zemek, J.; Jiricek, P.; Nespurek, S. UV degradability of polysilanes for nanoresists examined by electron spectroscopies and photoluminescence. *Czech J Phys* **2006,** *56* (1), 41–50. DOI: 10.1007/s10582-006-0064-z.

[141] Lew Yan Voon, L. C.; Sandberg, E.; Aga, R. S.; Farajian, A. A. Hydrogen compounds of group-IV nanosheets. *Appl. Phys. Lett.* **2010,** *97* (16), 163114. DOI: 10.1063/1.3495786.

[142] Schauer, F.; Kuritka, I.; Dokoupil, N.; Horvath, P. Nanostructural effects in plasmatically prepared polysilylenes. *Physica E: Low-dimensional Systems and Nanostructures* **2002,** *14* (1-2), 272–276. DOI: 10.1016/S1386-9477(02)00394-6.

[143] Ryan, B. J.; Hanrahan, M. P.; Wang, Y.; Ramesh, U.; Nyamekye, C. K. A.; Nelson, R. D.; Liu, Z.; Huang, C.; Whitehead, B.; Wang, J.; Roling, L. T.; Smith, E. A.; Rossini, A. J.; Panthani, M. G. Silicene, Siloxene, or Silicane?: Revealing the Structure and Optical Properties of Silicon Nanosheets Derived from Calcium Disilicide. *Chem. Mater.* **2019**.

[144] Lauerhaas, J. M.; Sailor, M. J. Chemical modification of the photoluminescence quenching of porous silicon. *Science* **1993,** *261* (5128), 1567–1568. DOI: 10.1126/science.261.5128.1567.

[145] Hengge, E. Siloxen und schichtförmig gebaute Siliciumsubverbindungen. *Silicium-Chemie*; Fortschritte der Chemischen Forschung; Springer-Verlag: Berlin/Heidelberg, 1967; pp 145–164.

[146] Hengge, E. Properties and preparations of Si-Si linkages**,** *51*, 1–127. DOI: 10.1007/3-540-06722-1_4.

[147] Staebler, D. L.; Wronski, C. R. Reversible conductivity changes in discharge-produced amorphous Si. *Appl. Phys. Lett.* **1977,** *31* (4), 292–294. DOI: 10.1063/1.89674.

[148] Shimizu, T. Staebler-Wronski Effect in Hydrogenated Amorphous Silicon and Related Alloy Films. *Jpn. J. Appl. Phys.* **2004,** *43* (6A), 3257–3268. DOI: 10.1143/JJAP.43.3257.

[149] Helbich, T.; Lyuleeva, A.; Ludwig, T.; Scherf, L. M.; Fässler, T. F.; Lugli, P.; Rieger, B. One-Step Synthesis of Photoluminescent Covalent Polymeric Nanocomposites from 2D Silicon Nanosheets. *Adv. Funct. Mater.* **2016,** *26* (37), 6711–6718. DOI: 10.1002/adfm.201602137.

[150] Lyuleeva, A.; Holzmüller, P.; Helbich, T.; Stutzmann, M.; Brandt, M. S.; Becherer, M.; Lugli, P.; Rieger, B. Charge transfer doping in functionalized silicon nanosheets/P3HT hybrid material for applications in electrolyte-gated field-effect transistors. *J. Mater. Chem. C* **2018,** *6* (27), 7343–7352. DOI: 10.1039/C8TC01484A.

[151] Helbich, T.; Lyuleeva, A.; Marx, P.; Scherf, L. M.; Purkait, T. K.; Fässler, T. F.; Lugli, P.; Veinot, J. G. C.; Rieger, B. Lewis Acid Induced Functionalization of Photoluminescent 2D Silicon Nanosheets for the Fabrication of Functional Hybrid Films. *Adv. Funct. Mater.* **2017,** *27* (21), 1606764. DOI: 10.1002/adfm.201606764.

[152] Helbich, T.; Lyuleeva, A.; Höhlein, I. M. D.; Marx, P.; Scherf, L. M.; Kehrle, J.; Fässler, T. F.; Lugli, P.; Rieger, B. Radical-Induced Hydrosilylation Reactions for the Functionalization of Two-Dimensional Hydride Terminated Silicon Nanosheets. *Chemistry (Weinheim an der Bergstrasse, Germany)* **2016,** *22* (18), 6194–6198. DOI: 10.1002/chem.201505134.

[153] Nakano, H. Synthesis and modification of two-dimensional crystalline silicon nanosheets. *Journal of the Ceramic Society of Japan* **2014,** *122* (1429), 748–754. DOI: 10.2109/jcersj2.122.748.

[154] Jiang, S.; Butler, S.; Bianco, E.; Restrepo, O. D.; Windl, W.; Goldberger, J. E. Improving the stability and optical properties of germanane via one-step covalent methyl-termination. *Nature Communications* **2014,** *5*, 3389. DOI: 10.1038/ncomms4389.

[155] Tao, L.; Cinquanta, E.; Chiappe, D.; Grazianetti, C.; Fanciulli, M.; Dubey, M.; Molle, A.; Akinwande, D. Silicene field-effect transistors operating at room temperature. *Nature nanotechnology* **2015,** *10* (3), 227–231. DOI: 10.1038/nnano.2014.325.

[156] Okamoto, H.; Sugiyama, Y.; Nakano, H. Synthesis and modification of silicon nanosheets and other silicon nanomaterials. *Chemistry - A European Journal* **2011,** *17* (36), 9864–9887. DOI: 10.1002/chem.201100641.

[157] Lyuleeva, A.; Helbich, T.; Rieger, B.; Lugli, P. Polymer-silicon nanosheet composites: bridging the way to optoelectronic applications. *J. Phys. D: Appl. Phys.* **2017,** *50* (13), 135106. DOI: 10.1088/1361-6463/aa5005.

[158] Qian, C.; Sun, W.; Hung, D. L. H.; Qiu, C.; Makaremi, M.; Hari Kumar, S. G.; Wan, L.; Ghoussoub, M.; Wood, T. E.; Xia, M.; Tountas, A. A.; Li, Y. F.; Wang, L.; Dong, Y.; Gourevich, I.; Singh, C. V.; Ozin, G. A. Catalytic CO2 reduction by palladium-decorated silicon–hydride nanosheets. *Nat Catal* **2019,** *2* (1), 46–54. DOI: 10.1038/s41929-018-0199-x.

[159] Ohashi, M.; Yaokawa, R.; Takatani, Y.; Nakano, H. Versatile Reducing Reaction Field within Layered Polysilane for Efficient One-Pot Synthesis of Metal Nanoparticles. *ChemNanoMat* **2017,** *3* (8), 534–537. DOI: 10.1002/cnma.201700102.

[160] Xu, K.; Ben, L.; Li, H.; Huang, X. Silicon-based nanosheets synthesized by a topochemical reaction for use as anodes for lithium ion batteries. *Nano Res.* **2015,** *8* (8), 2654–2662. DOI: 10.1007/s12274-015-0772-4.

[161] Yu, X.; Xue, F.; Huang, H.; Liu, C.; Yu, J.; Sun, Y.; Dong, X.; Cao, G.; Jung, Y. Synthesis and electrochemical properties of silicon nanosheets by DC arc discharge for lithium-ion batteries. *Nanoscale* **2014,** *6* (12), 6860–6865. DOI: 10.1039/c3nr06418b.

[162] Wang, H.; Tang, W.; Ni, L.; Ma, W.; Chen, G.; Zhang, N.; Liu, X.; Ma, R. Synthesis of silicon nanosheets from kaolinite as a high-performance anode material for lithium-ion batteries. *Journal of Physics and Chemistry of Solids* **2020,** *137*, 109227. DOI: 10.1016/j.jpcs.2019.109227.

[163] Chen, S.; Chen, Z.; Xu, X.; Cao, C.; Xia, M.; Luo, Y. Scalable 2D Mesoporous Silicon Nanosheets for High-Performance Lithium-Ion Battery Anode. *Small (Weinheim an der Bergstrasse, Germany)* **2018,** *14* (12), e1703361. DOI: 10.1002/smll.201703361.

[164] Ryu, J.; Hong, D.; Choi, S.; Park, S. Synthesis of Ultrathin Si Nanosheets from Natural Clays for Lithium-Ion Battery Anodes. *ACS Nano* **2016,** *10* (2), 2843–2851. DOI: 10.1021/acsnano.5b07977.

[165] Kim, W.-S.; Hwa, Y.; Shin, J.-H.; Yang, M.; Sohn, H.-J.; Hong, S.-H. Scalable synthesis of silicon nanosheets from sand as an anode for Li-ion batteries. *Nanoscale* **2014,** *6* (8), 4297. DOI: 10.1039/c3nr05354g.

[166] Gennes, P.-G. de. Soft Matter (Nobel Lecture). *Angewandte Chemie - International Edition* **1992,** *31* (7), 842–845. DOI: 10.1002/anie.199208421.

[167] Takahara, Y. K.; Ikeda, S.; Ishino, S.; Tachi, K.; Ikeue, K.; Sakata, T.; Hasegawa, T.; Mori, H.; Matsumura, M.; Ohtani, B. Asymmetrically modified silica particles: A simple particulate surfactant for stabilization of oil droplets in water. *Journal of the American Chemical Society* **2005,** *127* (17), 6271–6275. DOI: 10.1021/ja043581r.

[168] Valadares, L. F.; Tao, Y.-G.; Zacharia, N. S.; Kitaev, V.; Galembeck, F.; Kapral, R.; Ozin, G. A. Catalytic nanomotors: Self-propelled sphere dimers. *Small (Weinheim an der Bergstrasse, Germany)* **2010,** *6* (4), 565–572. DOI: 10.1002/smll.200901976.

[169] Yi, C.; Zhang, S.; Webb, K. T.; Nie, Z. Anisotropic Self-Assembly of Hairy Inorganic Nanoparticles. *Accounts of Chemical Research* **2017,** *50* (1), 12–21. DOI: 10.1021/acs.accounts.6b00343.

[170] Glotzer, S. C. Materials science. Some Assembly Required. *Science (New York, N.Y.)* **2004,** *306* (5695), 419–420. DOI: 10.1126/science.1099988.

[171] Cho, I.; Jung, H.; Jeong, B. G.; Hahm, D.; Chang, J. H.; Lee, T.; Char, K.; Lee, D. C.; Lim, J.; Lee, C.; Cho, J.; Bae, W. K. Ligand-Asymmetric Janus Quantum Dots for Efficient Blue-Quantum Dot Light-Emitting Diodes. *ACS applied materials & interfaces* **2018,** *10* (26), 22453–22459. DOI: 10.1021/acsami.8b08300.

[172] Sotiriou, G. A.; Hirt, A. M.; Lozach, P.-Y.; Teleki, A.; Krumeich, F.; Pratsinis, S. E. Hybrid, silica-coated, Janus-like plasmonic-magnetic nanoparticles. *Chem. Mater.* **2011,** *23* (7), 1985–1992. DOI: 10.1021/cm200399t.

[173] Synytska, A.; Khanum, R.; Ionov, L.; Cherif, C.; Bellmann, C. Water-repellent textile via decorating fibers with amphiphilic Janus particles. *ACS applied materials & interfaces* **2011,** *3* (4), 1216–1220. DOI: 10.1021/am200033u.

[174] Walther, A.; Müller, A. H. E. Janus particles. *Soft Matter* **2008,** *4* (4), 663. DOI: 10.1039/b718131k.

[175] Poggi, E.; Gohy, J.-F. Janus particles: From synthesis to application. *Colloid Polym Sci* **2017,** *295* (11), 2083–2108. DOI: 10.1007/s00396-017-4192-8.

[176] Liang, F.; Zhang, C.; Yang, Z. Rational design and synthesis of Janus composites. *Advanced materials (Deerfield Beach, Fla.)* **2014,** *26* (40), 6944–6949. DOI: 10.1002/adma.201305415.

[177] Zhang, J.; Grzybowski, B. A.; Granick, S. Janus Particle Synthesis, Assembly, and Application. *Langmuir : the ACS journal of surfaces and colloids* **2017,** *33* (28), 6964–6977. DOI: 10.1021/acs.langmuir.7b01123.

[178] Moffitt, M. G. Self-Assembly of Polymer Brush-Functionalized Inorganic Nanoparticles: From Hairy Balls to Smart Molecular Mimics. *J. Phys. Chem. Lett.* **2013,** *4* (21), 3654–3666. DOI: 10.1021/jz401814s.

[179] Saito, N.; Nakatsuru, R.; Kagari, Y.; Okubo, M. Formation of "snowmanlike" polystyrene/poly(methyl methacrylate)/toluene droplets dispersed in an aqueous solution of a nonionic surfactant at thermodynamic equilibrium. *Langmuir* **2007,** *23* (23), 11506–11512. DOI: 10.1021/la701388w.

[180] Nie, Z.; Li, W.; Seo, M.; Xu, S.; Kumacheva, E. Janus and ternary particles generated by microfluidic synthesis: design, synthesis, and self-assembly. *J. Am. Chem. Soc.* **2006,** *128* (29), 9408–9412. DOI: 10.1021/ja060882n.

[181] Roh, K.; Martin, D. C.; Lahann, J. Biphasic Janus particles with nanoscale anisotropy. *Nature materials* **2005,** *4* (10), 759–763. DOI: 10.1038/nmat1486.

[182] Zhao, N.; Gao, M. Magnetic Janus Particles Prepared by a Flame Synthetic Approach: Synthesis, Characterizations and Properties. *Advanced materials (Deerfield Beach, Fla.)* **2009,** *21* (2), 184–187. DOI: 10.1002/adma.200800570.

[183] Wang, C.; Yin, H.; Dai, S.; Sun, S. A General Approach to Noble Metal−Metal Oxide Dumbbell Nanoparticles and Their Catalytic Application for CO Oxidation. *Chem. Mater.* **2010,** *22* (10), 3277–3282. DOI: 10.1021/cm100603r.

[184] Casavola, M.; Buonsanti, R.; Caputo, G.; Cozzoli, P. D. Colloidal Strategies for Preparing Oxide-Based Hybrid Nanocrystals. *Eur. J. Inorg. Chem.* **2008,** *2008* (6), 837–854. DOI: 10.1002/ejic.200701047.

[185] Cho, I.; Lee, K.-W. Morphology of latex particles formed by poly(methyl methacrylate)-seeded emulsion polymerization of styrene. *J. Appl. Polym. Sci.* **1985,** *30* (5), 1903–1926. DOI: 10.1002/app.1985.070300510.

[186] Tang, C.; Zhang, C.; Liu, J.; Qu, X.; Li, J.; Yang, Z. Large Scale Synthesis of Janus Submicrometer Sized Colloids by Seeded Emulsion Polymerization. *Macromolecules* **2010,** *43* (11), 5114–5120. DOI: 10.1021/ma100437t.

[187] Misra, A.; Urban, M. W. Acorn-shape polymeric nano-colloids: synthesis and self-assembled films. *Macromol. Rapid Commun.* **2010,** *31* (2), 119–127. DOI: 10.1002/marc.200900233.

[188] Staff, R. H.; Willersinn, J.; Musyanovych, A.; Landfester, K.; Crespy, D. Janus nanoparticles with both faces selectively functionalized for click chemistry. *Polym. Chem.* **2014,** *5* (13), 4097. DOI: 10.1039/C4PY00085D.

[189] Li, B.; Wang, M.; Chen, K.; Cheng, Z.; Chen, G.; Zhang, Z. Synthesis of Biofunctional Janus Particles. *Macromol. Rapid Commun.* **2015,** *36* (12), 1200–1204. DOI: 10.1002/marc.201500063.

[190] Chen, T.; Yang, M.; Wang, X.; Tan, L. H.; Chen, H. Controlled assembly of eccentrically encapsulated gold nanoparticles. *J. Am. Chem. Soc.* **2008,** *130* (36), 11858–11859. DOI: 10.1021/ja8040288.

[191] Ohnuma, A.; Cho, E. C.; Camargo, P. H. C.; Au, L.; Ohtani, B.; Xia, Y. A facile synthesis of asymmetric hybrid colloidal particles. *J. Am. Chem. Soc.* **2009,** *131* (4), 1352–1353. DOI: 10.1021/ja8079934.

[192] Gröschel, A. H.; Walther, A.; Löbling, T. I.; Schmelz, J.; Hanisch, A.; Schmalz, H.; Müller, A. H. E. Facile, solution-based synthesis of soft, nanoscale Janus particles with tunable Janus balance. *J. Am. Chem. Soc.* **2012,** *134* (33), 13850–13860. DOI: 10.1021/ja305903u.

[193] Erhardt, R.; Zhang, M.; Böker, A.; Zettl, H.; Abetz, C.; Frederik, P.; Krausch, G.; Abetz, V.; Müller, A. H. E. Amphiphilic Janus micelles with polystyrene and poly(methacrylic acid) hemispheres. *J. Am. Chem. Soc.* **2003,** *125* (11), 3260–3267. DOI: 10.1021/ja028982q.

[194] Walther, A.; André, X.; Drechsler, M.; Abetz, V.; Müller, A. H. E. Janus discs. *J. Am. Chem. Soc.* **2007,** *129* (19), 6187–6198. DOI: 10.1021/ja068153v.

[195] Liu; Abetz, V.; Müller, A. H. E. Janus Cylinders. *Macromolecules* **2003,** *36* (21), 7894–7898. DOI: 10.1021/ma0345551.

[196] Casagrande, C.; Fabre, P.; Raphaël, E.; Veyssié, M. “Janus Beads”: Realization and Behaviour at Water/Oil Interfaces. *Europhys. Lett.* **1989,** *9* (3), 251–255. DOI: 10.1209/0295-5075/9/3/011.

[197] Nakahama, K.; Kawaguchi, H.; Fujimoto, K. A Novel Preparation of Nonsymmetrical Microspheres Using the Langmuir–Blodgett Technique. *Langmuir* **2000,** *16* (21), 7882–7886. DOI: 10.1021/la000684o.

[198] Gu, H.; Yang, Z.; Gao, J.; Chang, C. K.; Xu, B. Heterodimers of nanoparticles: formation at a liquid-liquid interface and particle-specific surface modification by functional molecules. *J. Am. Chem. Soc.* **2005,** *127* (1), 34–35. DOI: 10.1021/ja045220h.

[199] Takei, H.; Shimizu, N. Gradient Sensitive Microscopic Probes Prepared by Gold Evaporation and Chemisorption on Latex Spheres. *Langmuir* **1997,** *13* (7), 1865–1868. DOI: 10.1021/la9621067.

[200] Hong, L.; Jiang, S.; Granick, S. Simple method to produce Janus colloidal particles in large quantity. *Langmuir : the ACS journal of surfaces and colloids* **2006,** *22* (23), 9495–9499. DOI: 10.1021/la062716z.

[201] Ye, S.; Carroll, R. L. Design and fabrication of bimetallic colloidal "Janus" particles. *ACS applied materials & interfaces* **2010,** *2* (3), 616–620. DOI: 10.1021/am900839w.

[202] McConnell, M. D.; Kraeutler, M. J.; Yang, S.; Composto, R. J. Patchy and multiregion janus particles with tunable optical properties. *Nano Lett.* **2010,** *10* (2), 603–609. DOI: 10.1021/nl903636r.

[203] Cha, B. G.; Piao, Y.; Kim, J. Asymmetric nanoparticle assembly via simple mechanical pressing using relative hardness of materials. *Materials Research Bulletin* **2015,** *70*, 424–429. DOI: 10.1016/j.materresbull.2015.05.011.

[204] Lin, C.-C.; Liao, C.-W.; Chao, Y.-C.; Kuo, C. Fabrication and characterization of asymmetric Janus and ternary particles. *ACS applied materials & interfaces* **2010,** *2* (11), 3185–3191. DOI: 10.1021/am1006589.

[205] Chao, Y.-C.; Huang, W.-H.; Cheng, K.-M.; Kuo, C. Assembly and manipulation of Fe(3)O(4)/coumarin bifunctionalized submicrometer Janus particles. *ACS applied materials & interfaces* **2014,** *6* (6), 4338–4345. DOI: 10.1021/am5000189.

[206] Ling, X. Y.; Phang, I. Y.; Acikgoz, C.; Yilmaz, M. D.; Hempenius, M. A.; Vancso, G. J.; Huskens, J. Janus particles with controllable patchiness and their chemical functionalization and supramolecular assembly. *Angewandte Chemie (International ed. in English)* **2009,** *48* (41), 7677–7682. DOI: 10.1002/anie.200903579.

[207] Liu, B.; Wei, W.; Qu, X.; Yang, Z. Janus Colloids Formed by Biphasic Grafting at a Pickering Emulsion Interface. *Angew. Chem.* **2008,** *120* (21), 4037–4039. DOI: 10.1002/ange.200705103.

[208] Jiang, S.; Schultz, M. J.; Chen, Q.; Moore, J. S.; Granick, S. Solvent-free synthesis of Janus colloidal particles. *Langmuir : the ACS journal of surfaces and colloids* **2008,** *24* (18), 10073–10077. DOI: 10.1021/la800895g.

[209] Zahn, N.; Kickelbick, G. Synthesis and aggregation behavior of hybrid amphiphilic titania Janus nanoparticles via surface-functionalization in Pickering emulsions. *Colloids and Surfaces A: Physicochemical and Engineering Aspects* **2014,** *461*, 142–150. DOI: 10.1016/j.colsurfa.2014.07.039.

[210] Mendez-Gonzalez, D.; Alonso-Cristobal, P.; Lopez-Cabarcos, E.; Rubio-Retama, J. Multi-responsive hybrid Janus nanoparticles: Surface functionalization through solvent physisorption. *European Polymer Journal* **2016,** *75*, 363–370. DOI: 10.1016/j.eurpolymj.2016.01.013.

[211] Aveyard, R.; Binks, B. P.; Clint, J. H. Emulsions stabilised solely by colloidal particles. *Advances in Colloid and Interface Science* **2003,** *100-102*, 503–546. DOI: 10.1016/S0001-8686(02)00069-6.

[212] Jiang, S.; Granick, S. Controlling the geometry (Janus balance) of amphiphilic colloidal particles. *Langmuir* **2008,** *24* (6), 2438–2445. DOI: 10.1021/la703274a.

[213] Perro, A.; Meunier, F.; Schmitt, V.; Ravaine, S. Production of large quantities of “Janus” nanoparticles using wax-in-water emulsions. *Colloids and Surfaces A: Physicochemical and Engineering Aspects* **2009,** *332* (1), 57–62. DOI: 10.1016/j.colsurfa.2008.08.027.

[214] Li, W.; Cai, X.; Ma, S.; Zhan, X.; Lan, F.; Wu, Y.; Gu, Z. Synthesis of amphipathic superparamagnetic Fe 3 O 4 Janus nanoparticles via a moderate strategy and their controllable self-assembly. *RSC Adv.* **2016,** *6* (46), 40450–40458. DOI: 10.1039/C6RA04648G.

[215] Sharifzadeh, E.; Salami-Kalajahi, M.; Hosseini, M. S.; Aghjeh, M. K. R. A temperature-controlled method to produce Janus nanoparticles using high internal interface systems: Experimental and theoretical approaches. *Colloids and Surfaces A: Physicochemical and Engineering Aspects* **2016,** *506*, 56–62. DOI: 10.1016/j.colsurfa.2016.06.006.

[216] Love, J. C.; Gates, B. D.; Wolfe, D. B.; Paul, K. E.; Whitesides, G. M. Fabrication and Wetting Properties of Metallic Half-Shells with Submicron Diameters. *Nano Letters* **2002,** *2* (8), 891–894. DOI: 10.1021/nl025633l.

[217] Sardar, R.; Heap, T. B.; Shumaker-Parry, J. S. Versatile solid phase synthesis of gold nanoparticle dimers using an asymmetric functionalization approach. *Journal of the American Chemical Society* **2007,** *129* (17), 5356–5357. DOI: 10.1021/ja070933w.

[218] Wang, B.; Li, B.; Ferrier, R. C. M.; Li, C. Y. Polymer single crystal templated janus nanoparticles. *Macromolecular rapid communications* **2010,** *31* (2), 169–175. DOI: 10.1002/marc.200900735.

[219] Li, B.; Li, C. Y. Immobilizing au nanoparticles with polymer single crystals, patterning and asymmetric functionalization. *Journal of the American Chemical Society* **2007,** *129* (1), 12–13. DOI: 10.1021/ja0668318.

[220] Zhou, T.; Wang, B.; Dong, B.; Li, C. Y. Thermoresponsive Amphiphilic Janus Silica Nanoparticles via Combining “Polymer Single-Crystal Templating” and “Grafting-from” Methods. *Macromolecules* **2012,** *45* (21), 8780–8789. DOI: 10.1021/ma3019987.

[221] Wang, B.; Li, B.; Zhao, B.; Li, C. Y. Amphiphilic Janus gold nanoparticles via combining "solid-state grafting-to" and "grafting-from" methods. *Journal of the American Chemical Society* **2008,** *130* (35), 11594–11595. DOI: 10.1021/ja804192e.

[222] Cui, J.-Q.; Kretzschmar, I. Surface-anisotropic polystyrene spheres by electroless deposition. *Langmuir* **2006,** *22* (20), 8281–8284. DOI: 10.1021/la061742u.

[223] Müller, T. Silylium Ions: Cham. In *Functional Molecular Silicon Compounds I*; Scheschkewitz, D., Ed.; Structure and Bonding; Springer International Publishing, 2014; pp 107–162.

[224] Reed, C. A. The Silylium Ion Problem, R 3 Si + . Bridging Organic and Inorganic Chemistry. *Acc. Chem. Res.* **1998,** *31* (6), 325–332. DOI: 10.1021/ar960132q.

[225] Lambert, J. B.; Zhao, Y.; Wu, H. beta-Silyl and beta-Germyl Carbocations Stable at Room Temperature. *The Journal of Organic Chemistry* **1999,** *64* (8), 2729–2736. DOI: 10.1021/jo982146a.

[226] Schmeltzer, J. M.; Porter, L. A.; Stewart, M. P.; Buriak, J. M. Hydride Abstraction Initiated Hydrosilylation of Terminal Alkenes and Alkynes on Porous Silicon. *Langmuir* **2002,** *18* (8), 2971–2974. DOI: 10.1021/la0156560.

[227] Jakob, M.; Javadi, M.; Veinot, J. G. C.; Meldrum, A.; Kartouzian, A.; Heiz, U. Ensemble Effects in the Temperature-Dependent Photoluminescence of Silicon Nanocrystals. *Chemistry - A European Journal* **2019,** *25* (12), 3061–3067. DOI: 10.1002/chem.201804986.

[228] Kim, D.; Joo, J.; Pan, Y.; Boarino, A.; Jun, Y. W.; Ahn, K. H.; Arkles, B.; Sailor, M. J. Thermally Induced Silane Dehydrocoupling on Silicon Nanostructures. *Angew. Chem.* **2016,** *128* (22), 6533–6537. DOI: 10.1002/ange.201601010.

[229] He, J.; Tse, J. S.; Klug, D. D.; Preston, K. F. Layered polysilane: Thermolysis and photoluminescence. *J. Mater. Chem.* **1998,** *8* (3), 705–710. DOI: 10.1039/A703992A.

[230] Hossain, M. A.; Javadi, M.; Yu, H.; Thiessen, A. N.; Ikpo, N.; Oliynyk, A. O.; Veinot, J. G. C. Dehydrocoupling - an alternative approach to functionalizing germanium nanoparticle surfaces. *Nanoscale* **2020,** *12* (11), 6271–6278. DOI: 10.1039/c9nr10837h.

[231] Yu, H.; Thiessen, A. N.; Hossain, M. A.; Kloberg, M. J.; Rieger, B.; Veinot, J. G. C. Thermally Induced Dehydrogenative Coupling of Organosilanes and H-Terminated Silicon Quantum Dots onto Germanane Surfaces. *Chem. Mater.* **2020,** *32* (11), 4536–4543. DOI: 10.1021/acs.chemmater.0c00482.

[232] los Reyes, G. B. de; Dasog, M.; Na, M.; Titova, L. V.; Veinot, J. G. C.; Hegmann, F. A. Charge transfer state emission dynamics in blue-emitting functionalized silicon nanocrystals. *Physical chemistry chemical physics : PCCP* **2015,** *17* (44), 30125–30133. DOI: 10.1039/c5cp04819b.

[233] Wendel, D.; Eisenreich, W.; Jandl, C.; Pöthig, A.; Rieger, B. Reactivity of an Acyclic Silylsilylene toward Ethylene: Migratory Insertion into the Si–Si Bond. *Organometallics* **2016,** *35* (1), 1–4. DOI: 10.1021/acs.organomet.5b00797.

[234] Wendel, D.; Szilvási, T.; Henschel, D.; Altmann, P. J.; Jandl, C.; Inoue, S.; Rieger, B. Precise Activation of Ammonia and Carbon Dioxide by an Iminodisilene. *Angew. Chem.* **2018,** *130* (44), 14783–14787. DOI: 10.1002/ange.201804472.

[235] Wendel, D.; Szilvási, T.; Jandl, C.; Inoue, S.; Rieger, B. Twist of a Silicon-Silicon Double Bond: Selective Anti-Addition of Hydrogen to an Iminodisilene. *J. Am. Chem. Soc.* **2017,** *139* (27), 9156–9159. DOI: 10.1021/jacs.7b05335.

[236] Herz, F. A. D.; Nobis, M.; Wendel, D.; Pahl, P.; Altmann, P. J.; Tillmann, J.; Weidner, R.; Inoue, S.; Rieger, B. Application of multifunctional silylenes and siliranes as universal crosslinkers for metal-free curing of silicones. *Green Chem.* **2020,** *22* (14), 4489–4497. DOI: 10.1039/d0gc00272k.

[237] Höhlein, I. M. D.; Werz, P. D. L.; Veinot, J. G. C.; Rieger, B. Photoluminescent silicon nanocrystal-polymer hybrid materials via surface initiated reversible addition-fragmentation chain transfer (RAFT) polymerization. *Nanoscale* **2015,** *7* (17), 7811–7818. DOI: 10.1039/C5NR00561B.

[238] Wiberg, N.; Amelunxen, K.; Lerner, H.-W.; Schuster, H.; Nöth, H.; Krossing, I.; Schmidt-Amelunxen, M.; Seifert, T. Donorfreie und donorhaltige supersilylalkalimetalle tBu3SiM1: Synthesen, charakterisierung, strukturen. *Journal of Organometallic Chemistry* **1997,** *542* (1), 1–18. DOI: 10.1016/S0022-328X(97)00306-9.

[239] Weidenbruch, M.; Schäfer, A.; Rankers, R. Silicium-verbindungen mit starken intramolekularen sterischen wechselwirkungen. *Journal of Organometallic Chemistry* **1980,** *195* (2), 171–184. DOI: 10.1016/S0022-328X(00)90001-9.

[240] Li, Q. S.; Zhang, R. Q.; Lee, S. T.; Niehaus, T. A.; Frauenheim, T. Optimal surface functionalization of silicon quantum dots. *The Journal of chemical physics* **2008,** *128* (24), 244714. DOI: 10.1063/1.2940735.

[241] Yu, Y.; Rowland, C. E.; Schaller, R. D.; Korgel, B. A. Synthesis and Ligand Exchange of Thiol-Capped Silicon Nanocrystals. *Langmuir : the ACS journal of surfaces and colloids* **2015,** *31* (24), 6886–6893. DOI: 10.1021/acs.langmuir.5b01246.

[242] Hu, M.; Liu, F.; Buriak, J. M. Expanding the Repertoire of Molecular Linkages to Silicon: Si-S, Si-Se, and Si-Te Bonds. *ACS applied materials & interfaces* **2016,** *8* (17), 11091–11099. DOI: 10.1021/acsami.6b00784.

[243] Buriak, J. M.; Sikder, M. D. H. From Molecules to Surfaces: Radical-Based Mechanisms of Si-S and Si-Se Bond Formation on Silicon. *Journal of the American Chemical Society* **2015,** *137* (30), 9730–9738. DOI: 10.1021/jacs.5b05738.

[244] Hu, M.; Hauger, T. C.; Olsen, B. C.; Luber, E. J.; Buriak, J. M. UV-Initiated Si–S, Si–Se, and Si–Te Bond Formation on Si(111): Coverage, Mechanism, and Electronics. *J. Phys. Chem. C* **2017,** *122* (25), 13803–13814. DOI: 10.1021/acs.jpcc.8b00910.

[245] Linnros, J.; Lalic, N.; Galeckas, A.; Grivickas, V. Analysis of the stretched exponential photoluminescence decay from nanometer-sized silicon crystals in SiO2. *Journal of Applied Physics* **1999,** *86* (11), 6128–6134. DOI: 10.1063/1.371663.

[246] Dasog, M.; Yang, Z.; Regli, S.; Atkins, T. M.; Faramus, A.; Singh, M. P.; Muthuswamy, E.; Kauzlarich, S. M.; Tilley, R. D.; Veinot, J. G. C. Chemical insight into the origin of red and blue photoluminescence arising from freestanding silicon nanocrystals. *ACS Nano* **2013,** *7* (3), 2676–2685. DOI: 10.1021/nn4000644.

[247] Angı, A.; Sinelnikov, R.; Meldrum, A.; Veinot, J. G. C.; Balberg, I.; Azulay, D.; Millo, O.; Rieger, B. Photoluminescence through in-gap states in phenylacetylene functionalized silicon nanocrystals. *Nanoscale* **2016,** *8* (15), 7849–7853. DOI: 10.1039/c6nr01435f.

[248] Armitage, D. A. Chemistry of compounds with silicon-sulphur, silicon-selenium and silicon-tellurium bonds: Chichester. In *The chemistry of organic silicon compounds*; Patai, S., Rappoport, Z., Eds.; The chemistry of functional groups; Wiley, 1989; pp 213–232.

[249] Yang, Y.; Webb, K.; Liu, Y.; Liu, K.; Nie, Z. Synthesis, Self-Assembly, and Applications of Amphiphilic Janus and Triblock Janus Nanoparticle Analogs **2017**, 233–275.

[250] Woehrle, G. H.; Brown, L. O.; Hutchison, J. E. Thiol-functionalized, 1.5-nm gold nanoparticles through ligand exchange reactions: scope and mechanism of ligand exchange. *J. Am. Chem. Soc.* **2005,** *127* (7), 2172–2183. DOI: 10.1021/ja0457718.

[251] Voliani, V. Gold Nanoparticles **2020**.

[252] Brust, M.; Walker, M.; Bethell, D.; Schiffrin, D. J.; Whyman, R. Synthesis of thiol-derivatised gold nanoparticles in a two-phase Liquid–Liquid system. *J. Chem. Soc., Chem. Commun.* **1994,** *0* (7), 801–802. DOI: 10.1039/C39940000801.

[253] GUO, Y. A.; CHEN, M.; HE, H. U. ALKYL CHAIN DEPENDENT ALKANETHIOL SELF-ASSEMBLED ADSORPTION DYNAMICS. *Surf. Rev. Lett.* **2015,** *22* (01), 1550004. DOI: 10.1142/S0218625X15500043.

[254] Debono, R. F.; Loucks, G. D.; Della Manna, D.; Krull, U. J. Self-assembly of short and long-chain n -alkyl thiols onto gold surfaces: A real-time study using surface plasmon resonance techniques. *Can. J. Chem.* **1996,** *74* (5), 677–688. DOI: 10.1139/v96-073.

[255] Kloberg, M. J.; Yu, H.; Groß, E.; Eckmann, F.; Restle, T. M. F.; Fässler, T. F.; Veinot, J. G. C.; Rieger, B. Surface-Anisotropic Janus Silicon Quantum Dots via Masking on 2D Silicon Nanosheets. *Advanced materials (Deerfield Beach, Fla.)* **2021,** *33* (38), e2100288. DOI: 10.1002/adma.202100288.

[256] Höhlein, I. M. D.; Angı, A.; Sinelnikov, R.; Veinot, J. G. C.; Rieger, B. Functionalization of hydride-terminated photoluminescent silicon nanocrystals with organolithium reagents. *Chemistry (Weinheim an der Bergstrasse, Germany)* **2015,** *21* (7), 2755–2758. DOI: 10.1002/chem.201405555.

[257] Grötsch, R. K.; Angı, A.; Mideksa, Y. G.; Wanzke, C.; Tena-Solsona, M.; Feige, M. J.; Rieger, B.; Boekhoven, J. Dissipative Self-Assembly of Photoluminescent Silicon Nanocrystals. *Angewandte Chemie (International ed. in English)* **2018,** *57* (44), 14608–14612. DOI: 10.1002/anie.201807937.

[258] Capretti, A.; Lesage, A.; Gregorkiewicz, T. Integrating Quantum Dots and Dielectric Mie Resonators: A Hierarchical Metamaterial Inheriting the Best of Both. *ACS Photonics* **2017,** *4* (9), 2187–2196. DOI: 10.1021/acsphotonics.7b00320.

[259] Yamanoi, Y.; Shirahata, N.; Yonezawa, T.; Terasaki, N.; Yamamoto, N.; Matsui, Y.; Nishio, K.; Masuda, H.; Ikuhara, Y.; Nishihara, H. Detailed structural examinations of covalently immobilized

gold nanoparticles onto hydrogen-terminated silicon surfaces. *Chemistry (Weinheim an der Bergstrasse, Germany)* **2005,** *12* (1), 314–323. DOI: 10.1002/chem.200500455.